Decadal Ocean Water Mass Changes: Global Observations and Interpretation

Kieran Patrick Helm
BEng (Hons.)
BSc (Hons.)

Submitted in fulfilment of the requirements for the degree of Doctor of Philosophy.

School of Mathematics and Physics and the Institute of Antarctic and Southern Ocean Studies,
University of Tasmania, Australia
October 2008

Statement of Declaration

I declare that this thesis contains no material which has been accepted for a degree or diploma by the University or any other institution, except by way of background information and duly acknowledged in the thesis, and to the best of my knowledge and belief no material previously published or written by another person except where due acknowledgement is made in the text of the thesis, nor does the thesis contain any material that infringes copyright.

This thesis may be made available for loan and limited copying in accordance with the *Copywright Act of 1968*

Kieran Patrick Helm

Abstract

Using a combination of three quality controlled oceanographic datasets, changes in temperature, salinity, and oxygen were interpolated to neutral density surfaces and investigated on a global scale. The analysis was broken into two comparisons, where 759,713 profiles (1940-1988 with a mean year of 1970) and then 242,087 Argo profiles (mean year of 2005), were objectively mapped to the locations of 38,463 full-depth WOCE profiles (mean year of 1992).

The largest water property changes along neutral density surfaces (1970-1992) occurred in the upper 1500 m, with a near-global cooling and freshening on density surfaces around the salinity minimum in both hemispheres (AAIW, NPIW), warming and salinity increases at the shallow salinity-maximum, freshening of NADW in the North Atlantic and salinity increases further south, and coherent salinity increases in CDW in the Southern Ocean for this period. Mid and high-latitude density surfaces all deepened, while there was shoaling in the equatorial low-latitudes. The pattern of water mass changes from 1992 to 2005 was generally consistent with the 1970-1992 observations on a global scale. However some regional decadal variability in the South Indian and the North Atlantic Oceans occurred, with the cooling and freshening pattern switching to warming and salinity increases on density surfaces from 1992 to 2005. Oxygen concentration levels in the upper-1500 m have reduced across all ocean basins at an average 1.82 μmol l^{-1} (1970-1992), with changes being strongest in mode, intermediate, and deep water ventilation regions. Less than 15% of the oxygen decreases can be attributed to temperature increases. The pattern of oxygen change poleward of 25° is correlated with upper-ocean stratification increases in both hemispheres.

Integrating changes along density layers from the equator to the surface outcrop of the layer highlights the importance of high-latitude regions to global budgets, with 117% of apparent heat flux increases, 116% of apparent freshwater flux increases, and 94% of oxygen flux decreases occurring in density surfaces that outcrop poleward of 40°. Statistically significant heat flux increases were evident at all latitudes, but the largest apparent heat and freshwater flux increases occurred around 50°N and 55°S (1970-1992). Precipitation-minus-evaporation decreases of up to 10

mm yr^{-1} have occurred in the low latitudes. Using the pure warming, freshening, and heave modes of subduction (Bindoff and McDougall, 1994), changes in salinity appear to have had relatively little contribution to density and hence to steric sea-level change. Instead pure warming and pure heave appear as the dominant subduction scenarios with both explaining the observed density changes with equal skill.

Both of these subduction mechanisms are the basis for a proposed physical model of a shift in the poleward boundaries of the subtropical gyres. The observed water mass changes imply an enhanced global hydrological cycle, and increased surface warming. Together these changes have lead to increased upper-ocean stratification, consistent with a reduced renewal rate of all water masses. Our observations compare well with the patterns of ocean change produced by model simulations of increasing carbon dioxide.

Acknowledgements

Firstly I would like to thank both my supervisors, Nathan Bindoff and John Church. Their guidance, passion for the subject, and wealth of knowledge has been the driving force behind this project. The effort they have both put in has gone beyond what could have reasonably been expected, and this has been much appreciated.

Secondly I'd like to acknowledge the financial support and staff of the Antarctic, Climate and Ecosystems CRC. Special thanks goes to Ben Joseph and Jason Roberts for helping with seemingly constant computing and programming issues, and to Helen Phillips for her assistance with Argo profiles. The analysis of the large datasets in this thesis was made possible through the use of the APAC computing facilities.

Throughout this project I have been surrounded by a number of post-graduate students, and have appreciated the chance to discuss problems, resolve computing issues, and bounce ideas off them. In this respect, my particular thanks goes to Stephanie Downes, whom I have been fortunate enough to have shared an office with for the past three years. Outside of university, I am grateful to my housemate Tim Moroney, who offered me a place to stay and over the past year has quietly helped out in many practical ways.

Finally on a personal level I'd like to thank my parents, Pat and Terri. Their moral support, practical advice, and constant encouragement will always be appreciated. Without this support I would not have been able to begin, let alone complete, this project.

Contents

List of Figures

List of Tables

Abbreviations and acronyms

AABW	Antarctic Bottom Water
AAIW	Antarctic Intermediate Water
ACC	Antarctic Circumpolar Current
CFC	Chlorofluorocarbons
CLIVAR	Climate Variability and Predictability (program)
CSIRO	Commonwealth Scientific And Industrial Research Organisation
CTD	Conductivity, Temperature and Depth
ECCO	Estimating the Circulation and Climate of the Ocean (program)
ENSO	El Niño Southern Oscillation
IPCC	Intergovernmental Panel on Climate Change
LCDW	Lower Circumpolar Deep Water
LSW	Labrador Sea Water
NADW	North Atlantic Deep Water
NAO	North Atlantic Oscillation
NCEP	National Centers for Environmental Prediction
NPI	North Pacific Index
NPIW	North Pacific Intermediate Water
P-E	Precipitation minus evaporation
PDO	Pacific Decadal Oscillation
SAF	Subantarctic Front
SAM	Southern Annular Mode
SAMW	Subantarctic Mode Water
SODA	Simple Ocean Data Assimilation
SPMW	Subpolar Mode Water
SST	Sea Surface Temperature
STF	Subtropical Front
UCDW	Upper Circumpolar Deep Water
WOCE	World Ocean Circulation Experiment
XBT	Expendable Bathythermograph

Chapter 1 Introduction and context of thesis

Over the last decade there has been an increasing political and public desire to understand, predict and address the causes of global climate change. Central to the science behind this is the need to quantify past changes in the atmospheric heat and freshwater distribution. As an integrated record of atmospheric variability, the ocean is a good diagnostic tool to achieve this quantification. In this thesis the observed changes in ocean water mass properties are explored using spatially well-distributed research-quality data, and the documented global patterns of change in the ocean are directly related to the changing energy balance of the earth.

The oceans cover 71% of the earth's surface area, and have the ability to store the vast majority of water and heat in the climate system. Compared with the land surface, relatively little is known about the oceans, and it is only in the last forty years that scientific surveys have been undertaken on a global scale. The past 15 years have seen the advent of global satellite coverage, computer models, free-drifting floats, and new international collaborative research programs to specifically understand the oceans variability. These have given oceanographers a significantly larger body of data to work with, and have greatly extended the understanding of ocean properties and circulation.

The ocean is one of the key components in understanding climate change for two main reasons. Firstly it acts to *regulate* global climate by transporting heat and freshwater fluxes between low and high latitudes through the global ocean circulation. Often referred to as the 'global conveyor belt' (shown in Figure 1.1 centred around the Southern Ocean), it is driven by both density differences and surface winds. Small changes in this transport have large implications on regional climates.

Secondly the ocean provides the main means of *storing* heat and freshwater over decadal and century times scales. The capacity is much greater than the atmospheric and terrestrial storage, with 97% of the worlds available water contained in the ocean system. Given this large storage capacity, proportionally small changes

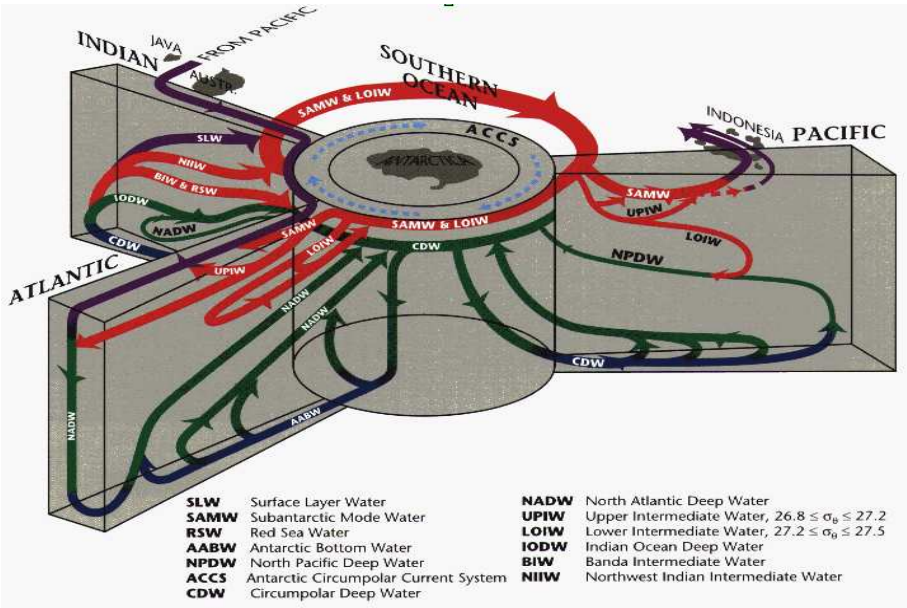

Figure 1.1: The overturning circulation of key Southern Hemisphere water masses copied from Schmitz (1996).

in the oceans heat budget will be the result of significant ongoing changes in the atmosphere.

In addition to being essential to the climate system, the oceans also reveal changes in this system by acting as an *historical record* of past atmospheric changes. As temperature and freshwater fluxes enter the interior of the ocean they tend to be propagated along surfaces of constant density (Ledwell et al., 1993), preserving anomalies imparted at the surface. As such, the changes in the ocean interior can be traced back and used to infer changes at the surface. Given the large proportion of the earth's surface that the ocean occupies, and the lack of direct historical temperature and rainfall surface observations over them, this provides a useful tool in understanding past climate change and a means of corroborating both ocean and atmospheric model outputs.

1.1 Twentieth century pattern of climate change

1.1.1 Ocean heat content change

The oceans are the main sink for solar radiation, contributing more than 90% to the estimated *increases* in the total earth's heat content since the 1960s (Bindoff

et al., 2007). This amounts to a net increase of $10.0 \pm 3.1 \times 10^{22}$ J since 1955, which is equivalent to an average temperature increase of 0.10°C over the upper 700 m of the water column (Bindoff et al., 2007).

Figure 1.2 shows the time-series of globally averaged heat content change. Up until 1970 there is relatively little change, followed by a warming during the 1970s and a sharp cooling in the early 1980s. Recently there have been suggestions that the 'bump' during the 1970s may in fact be an artifact of biases associated with XBT data, and the curve shown in Figure 1.2 should have a smoother rate of increase (Gouretski and Koltermann, 2007; Wijffels et al., 2007). Since 1990 there has been a large increase in the rate of global ocean heat uptake from 0.14 ± 0.04 W m^{-2} (1955-2003) to 0.5 ± 0.18 W m^{-2} (1993-2003) (Bindoff et al., 2007). These estimates of a heat content increase are based on temperature in the upper 700 m (Figure 1.2). Below 700 m there are also heat content increases that contribute approximately a third to the increases in the total heat budget (Levitus et al., 2005a). The total heat content change in the upper 3000 m for the global ocean is estimated to be 14.2 ± 2.4 W m^{-2} since 1955 (Bindoff et al., 2007), but given the lack of deep-water data this estimate is based on five-year averages.

While this net warming occurs across all basins, approximately half of the heat content increase comes from the Atlantic Ocean (Levitus et al., 2005a). This is despite the Atlantic Ocean representing only 30% of the World Ocean. In the subtropical North Atlantic, the downward displacement of density surfaces was the primary mechanism for the warming up to the early 1980s (Bryden et al., 1996; Arbic and Owens, 2001), while elsewhere in the Atlantic Ocean the upper-ocean warming appears to have been the result of along-isopycnal water mass change (Read and Gould, 1992; Bryden et al., 1996; Arbic and Owens, 2001; Joyce et al., 1999; Leadbetter et al., 2007). The Southern Ocean has shown stronger than average warming of 0.17°C between 700-1100 m from the 1950s to the 1980s (Gille, 2002), and appears to be circumpolar in extent. This warming has been associated with both a southward shift of subtropical gyres in the Indian Ocean sector in models (Alory et al., 2007), and a poleward displacement of the ACC (Gille, 2007).

Accompanying this southward shift is the warming of Southern Ocean surface waters that supply key water masses in all three ocean sectors (Bindoff and Church, 1992; Aoki, 1997; Bindoff and McDougall, 2000; Aoki et al., 2005).

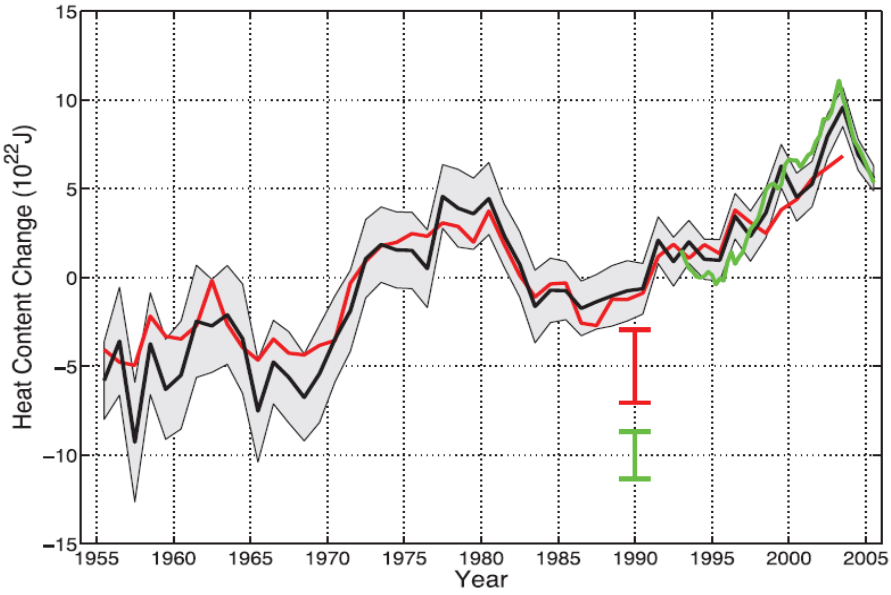

Figure 1.2: International Panel for Climate Change (IPCC) time-series of global heat content: from Bindoff et al. (2007): Figure 5.1. "time-series of global annual ocean heat content (10^{22} J) for the 0 to 700 m layer. The black curve is updated from Levitus et al. (2005a), with the shading representing the 90% confidence interval. The red and green curves are updates of the analyses by Ishii et al. (2006) and Willis et al. (2004, over 0 to 750 m) respectively, with the error bars denoting the 90% confidence interval. The black and red curves denote the deviation from the 1961 to 1990 average and the shorter green curve denotes the deviation from the average of the black curve for the period 1993 to 2003."

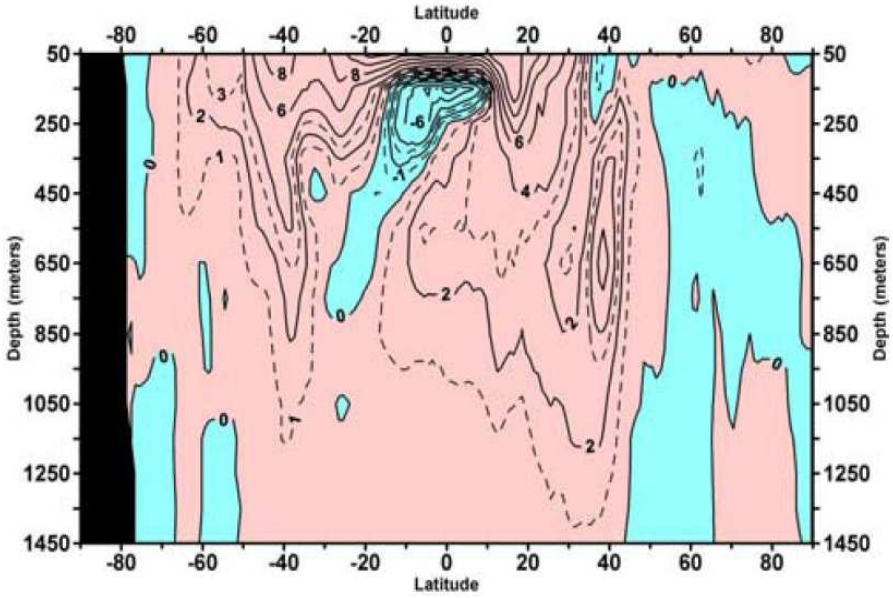

Figure 1.3: Copied from Levitus et al. (2005a) - "Linear trend (1955–2003) of the zonally integrated heat content of the world ocean by one-degree latitude belts for 100 m thick layers. Heat content values are plotted at the midpoint of each 100 m layer. Contour interval is 2×10^{18} J yr^{-1}."

The Pacific Ocean dominates the variability in the global time-series in Figure 1.2 (Bindoff et al., 2007) through the El Niño Southern Oscillation (ENSO) and the Pacific Decadal Oscillation (PDO), with significant decadal perturbations in climate having been observed in the upper 400 m (Deser et al., 1996). There has however been a net gain in heat in this ocean over the last 50 years (Wong et al., 2001), with strong surface warming at high-latitudes in the Southern Hemisphere (Johnson and Orsi, 1997; Holbrook and Bindoff, 1997).

Strong zonally averaged heat content increases over the last 50 years are evident in the upper 1000 m centred around 40° in both hemispheres (Figure 1.3 from Levitus et al. (2005a)). In the upper 300 m, there are strong heat content increases between 40°N and 40°S, except for a strong tongue of cooling which begins at the equator and extends to 800 m around 30°S. North of 50°N there are weak zonally averaged decreases in heat content which come primarily from the Atlantic Ocean (Levitus et al., 2005a).

In the South Indian Ocean an oscillation in water mass property change is evident in the observations and models, with SAMW switching sign from a cooling and freshening on density surfaces prior to 1987, to a warming and salinity increase in the following period (Bindoff and McDougall, 2000; Bryden et al., 2003). This oscillation can be explained by decadal variation in the upstream mode water formation area (Murray et al., 2007), and climate simulations show similar variability (Stark et al., 2006). A switch of sign around the early 1980s is also seen in both the North Atlantic upper waters (from cooling to warming) and the North Atlantic intermediate waters (from warming and salinity increases to a cooling and freshening). In the latter case the switch is caused by changes in the properties of the LSW source water (Read and Gould, 1992; Leadbetter et al., 2007).

1.1.2 Sea level change

There are strong similarities between the global heat content and the global mean sea level rise. For the 1961 to 2003 period, Bindoff et al. (2007) estimated an average rate of rise of 1.8 ± 0.5 mm yr^{-1}, with this increasing to 3.1 ± 0.7 mm yr^{-1} after 1993 (Cazenave and Nerem, 2004). A longer-term acceleration in sea-level rise over the last century is unclear from the sparse tide-gauge records alone (Gregory et al., 2001), although such an acceleration is evident in a reconstructed global time-series of sea level (Church and White, 2006).

The thermal expansion contribution to sea level rise coming from the upper 3000 m (1961-2003) is estimated to be approximately 0.42 ± 0.12 mm yr^{-1} (Bindoff et al., 2007), with the rate of the thermal expansion contribution being 3-4 times greater over the last 15 years (Willis et al., 2004; Antonov et al., 2005; Ishii et al., 2006; Lombard et al., 2006; Bindoff et al., 2007).

As well as the effects of global temperature change on sea level, there is also a contribution from salinity changes to the spatial patterns of sea-level rise (Antonov et al., 2002; Levitus et al., 2005b). The mass contribution to the overall sea level rise can in principle be indirectly estimated from salinity change (eg. Wadhams and Munk (2004)), but in practice the global salinity change is poorly known and the mass contribution cannot be resolved in this way (Bindoff et al., 2007). Instead sea-level rise is inferred from mass-balance contributions from glaciers and ice caps (0.50 ± 0.18 mm yr^{-1}: 1961-2003), the Antarctic ice sheet (0.14 ± 0.41 mm yr^{-1}), and the Greenland ice sheet (0.05 ± 0.12 mm yr^{-1}: Bindoff et al. (2007)). In ad-

dition there are direct links with volcanic eruptions cooling the ocean and leading to the depression and subsequent recovery of sea-levels. These sea level events after significant eruptions are partly responsible for a slight decrease in the underlying rate of global mean sea level rise over the last 40 years (Church et al., 2005).

The regional variations in sea level can be up to 5 times the global mean (Bindoff et al., 2007), and are associated with the El Niño Southern Oscillation. The effects of ENSO are primarily found in the equatorial Pacific Ocean, and are important given that the Pacific Ocean contributes approximately a third to the global mean sea-level rise over the last 50 years (Levitus et al., 2005b). The steady Atlantic Ocean sea level rise contributes most of the remainder (approximately 50% of the global mean sea-level rise), although the lack of observations in the Southern Ocean results in an underestimation of the thermosteric contribution to the global mean in this region (Antonov et al., 2005; Bindoff et al., 2007).

1.1.3 Changes in salinity and the hydrological cycle

As part of the global hydrological cycle, water formed in high precipitation-minus-evaporation (P-E) regions enters the oceans in the mid and high-latitudes, and water formed in low P-E regions enters in the low-latitudes. As a result of global warming over the last century, models suggest that there should have been both a small increase in the moisture holding capacity of the atmosphere (Trenberth et al., 2007), and an enhancement of the hydrological cycle (Allen and Ingram, 2002; Held and Soden, 2006; Zhang et al., 2007).

There are a few regional studies that begin to use the ocean as a rain gauge to infer such an increase in the global hydrological cycle. Over most of the Pacific Ocean a freshening originating from high-latitude surface waters has been observed, with salinity increases in the South Pacific subtropical regions since the 1970s (Johnson and Orsi, 1997; Wong et al., 1999, 2001; Boyer et al., 2005). These changes have been attributed to an enhancement of the hydrological cycle. In the North Pacific, the changing precipitation-minus-evaporation pattern appears to be one of the key components driving the observed variance in salinity in the mid-latitudes (Lukas, 2001).

Indian Ocean waters have become more saline in the upper 150 m, with freshening observed from 250-1000 m (Boyer et al., 2005). This freshening can largely be at-

tributable to low-salinity Antarctic Intermediate Water (AAIW), which is formed in the Southern Ocean and advected equatorward (Bindoff and McDougall, 2000; Wong et al., 2001). Upper-thermocline waters appeared to have freshened on pressure surfaces prior to the mid-1980s, and since then have increased in salinity (Bryden et al., 2003). South of the Polar Front in the Indian Ocean sector the surface waters have freshened since the 1950s, with the signal mixed into the ocean, and thus able to be observed in upwelling deep water (Aoki et al., 2005).

In the Atlantic Ocean, regional studies suggest that salinity increases in low-latitudes, and a freshening in most water masses formed in high-latitudes over the last 50 years has occurred (Bryden et al., 1996, 2003; Joyce et al., 1999; Curry et al., 2003; Boyer et al., 2007). However the intermediate-level waters found in the North Atlantic show a change of sign similar to that found in the South Indian Ocean, with these waters becoming increasingly saline up until the 1980s, and freshening since then. Salinity changes in the North Atlantic region generally appear to be indicative of increases in ice-melt in the Nordic and Labrador Seas, rather than due to any change in the hydrological cycle (Read and Gould, 1992; Curry and Mauritzen, 2005; Leadbetter et al., 2007).

Overall, a limited number of regional studies demonstrated salinity patterns that are consistent with a strengthening of the hydrological cycle, but none have quantified the link between ocean salinity and the atmosphere on ocean basin scales. In the last 15 years, this observational coverage has been significantly improved with the WOCE hydrographic (early 1990s) and the Argo float programs (since 2002).

1.1.4 Surface winds and stratification changes

Over the last 50 years, increasing atmospheric temperatures have been accompanied by a strengthening of the circumpolar westerly winds in the high-latitudes and decreasing westerlies in the mid-latitudes (Trenberth et al., 2007; Cai and Cowan, 2007). This is especially apparent in the Southern Hemisphere where increases in the high-latitude circumpolar westerly winds (Thompson and Solomon, 2002; Trenberth et al., 2007), increase the Ekman transport in the surface wind-driven layer around 60°S. This is coupled with a poleward shift of the Antarctic Circumpolar Current (ACC) (Fyfe and Saenko, 2006; Cai, 2006; Gille, 2007).

Changes in upper-ocean stratification are dependent on both changes in the sur-

face salinity and temperature, and on the vertical movement of density surfaces. A near-global pattern of surface warming has been well documented (Bindoff et al., 2007), and it seems likely that significant proportions of the World Ocean have become increasingly stratified. In the high latitudes where salinity has more of an influence on density, the observed freshening would also result in stratification increases.

1.1.5 Changes in ocean oxygen concentrations

Ocean General Circulation Models indicate decreases in oxygen across much of the globe (Keeling and Garcia, 2002). Approximately a quarter of this net loss in oxygen is due to the reduced oxygen capacity of warming surface waters, and the annual loss was equivalent to $0.3 \pm 0.4 \times 10^{14}$ mol throughout the 1990s (Keeling and Garcia, 2002). More importantly to the global ocean oxygen budget, these models show that the majority of the oxygen losses can be explained by increased stratification, reduced renewal rates, and hence more time for oxygen to be utilised by ocean biology (Bindoff et al., 2007).

As well as climate models, a number of regional studies have observed decreases in oxygen concentration over the last 50 years. The North Pacific Ocean has been studied in detail, with lower oxygen levels in upwelling water masses appearing to be primarily associated with increased upper-ocean stratification (Ono et al., 2001; Deutsch et al., 2005; Mecking et al., 2006; Nakanowatari et al., 2007). This stratification increase results from surface freshening (Emerson et al., 2004) that arises from changes in precipitation-minus-evaporation that are associated with the subarctic North Pacific Index (NPI) (Andreev and Watanabe, 2002). Similar decreases in oxygen are also seen in upwelling deep water in the Southern Ocean (Aoki et al., 2005), observations that are consistent with the results in climate change models that project increasing greenhouse gases in the atmosphere (Matear et al., 2000).

1.2 Quantifying uncertainty in global water mass changes

One of the major difficulties when working with ocean datasets is the uneven spatial and temporal distribution of observations. For the first half of the twentieth-century, ocean profiles tended to be obtained along major shipping routes, meaning that while there is comprehensive historical coverage in the North Atlantic, there is relatively little data in the Southern Ocean. The International Geophysical Year in 1957-58

saw the beginning of an increase in the number of scientific cruises, although it was not until the early 1990s that an international collaborative program was put in place to systematically map all ocean basins (the World Ocean Circulation Experiment - WOCE). The WOCE has since been followed by the Argo free-drifting float program (2002+) and CLIVAR repeat experiments, with the freely available data able to provide a comprehensive picture of the global ocean properties.

While these programs have given better global coverage over the last 15 years, sparsely distributed historical data has meant that studies of water property changes have tended to focus on regions where voyage tracks were specifically repeated for comparison. This has lead to a good understanding of some ocean basins, and left large regions of the World Ocean that have not been investigated as extensively. In addition the use of different time periods and methodologies have meant that it is difficult to quantitatively compare these different regions in order to build up a comprehensive understanding of the global changes.

There have been a handful of studies that have used large datasets to build up a global picture of ocean changes. These include Levitus et al. (2005a), Ishii et al. (2006) and Willis et al. (2004) for temperature and heat content, Boyer et al. (2005) for salinity change, and Keeling and Garcia (2002) for oxygen concentration changes. All of these studies have mapped and compared the data on constant pressure levels. Density surfaces are a more natural reference frame for considering water mass changes, and reflect circulation pathways by tracking individual water masses from the surface into the ocean interior. In addition the use of density surface allows the separation of dynamic changes on pressure surfaces (winds, eddies etc), from actual along-isopycnal water mass changes (propagated from the mixed layer). By following the path of a water mass through the ocean interior, a link can be made between the changes in the oceans and the atmospheric variability.

This thesis will address these gaps in the knowledge and distinguish itself from previous studies by investigating the global changes in temperature, salinity, oxygen and pressure on surfaces of a constant density. To improve the focus of the work, it is written with three key objectives in mind. These are;

- To identify changes in ocean water properties along density surfaces over the last 50 years, and identify globally coherent patterns of change.
- To understand how these changes relate to the formation, global circulation

and upwelling of water masses.

- To diagnose the physical mechanisms which have caused these water property changes, and where possible use the data to infer changes in atmosphere-ocean heat and freshwater fluxes.

To meet these objectives, this thesis is separated into six chapters, with a brief conclusion presented at the end. Each chapter contains an analysis of oceanographic data for change over three main periods, and a discussion about the possible causes and implications of these changes.

Chapter 2 begins by discussing the global datasets used in this thesis and the methods that have been adopted to compare data from different periods. Here the physical principles associated with the use of density surfaces are outlined, and the mathematical techniques used in the following four chapters are presented.

In Chapter 3, the WOCE dataset (with a mean year of 1992) is compared with historical data (mean year of 1970). The focus here is on the temperature changes, the salinity changes, and the vertical movement of density surfaces in the water column.

Chapter 4 extends this analysis in time by adding in the Argo dataset (mean year of 2005). The nature of these Argo floats means that the observations are limited to latitudes north of 60°S and the upper 1500 m of the water column.

In Chapter 5 an analysis of oxygen data is introduced, with changes between the WOCE-period and the historical data being explored on a global scale. Increased high-latitude winds and increased surface stratification are discussed as potential causes for the observed oxygen changes. Both of these scenarios occur in a globally warming world.

Chapter 6 examines the ambiguity in the interpretation of the observed changes on density surfaces, and partially resolves this through formal analysis.

The results from Chapters 3 to 6 will be tied together in a brief conclusion, with a conceptual model of the changes in the ocean being presented. Finally, avenues for further research are suggested.

Chapter 2 Dataset and methods

2.1 Datasets and approach

When looking at changes in water mass characteristics, a time-series approach is desirable in order to identify both interannual variability and longer-term regional oscillations (ENSO, NAO, PDO, SAM). However the distribution of historical observations in time and space in the Southern Hemisphere is inadequate for a full global time-series to be created. Instead a 'snapshot' approach is adopted where two time periods that are rich in data are compared.

This approach uses objective mapping to interpolate pre-1988 data to the location of well distributed, high quality, data from the 1988-2000 WOCE period. This type of technique has been used by a number of other studies in the past (Johnson and Orsi, 1997; Wong et al., 1999, 2001; Bindoff and McDougall, 2000; Curry et al., 2003; Bryden et al., 2003; Aoki et al., 2005). In Chapter 3, the pre-1988 data is weighted toward a mean year of 1970, while the more recent data had a mean year of 1992, allowing the differences to be estimated (over a 22-year period).

In Chapter 4, a third period is added for comparison by again using objective mapping to interpolate observations from the Argo dataset (2000-2007) to the same well-distributed 1988-2000 observations. Most analysis throughout this thesis is done along neutral density surfaces rather than the conventional isobaric (constant pressure) surfaces, thus identifying water mass changes and minimising the internal ocean noise associated with vertical displacement of isopycnals by eddies, Rossby waves and interannual variability.

HydroBase2 and the Southern Ocean database

Historical data came primarily from the HydroBase2 dataset (Curry, 2002), which consists of approximately 800,000 quality controlled CTD, bottle, mooring, and float profiles. This dataset included high quality and well distributed profiles from the World Ocean Circulation Experiment (WOCE) in the 1990s, and excluded XBT profiles which do not contain information on salinity and are known to contain

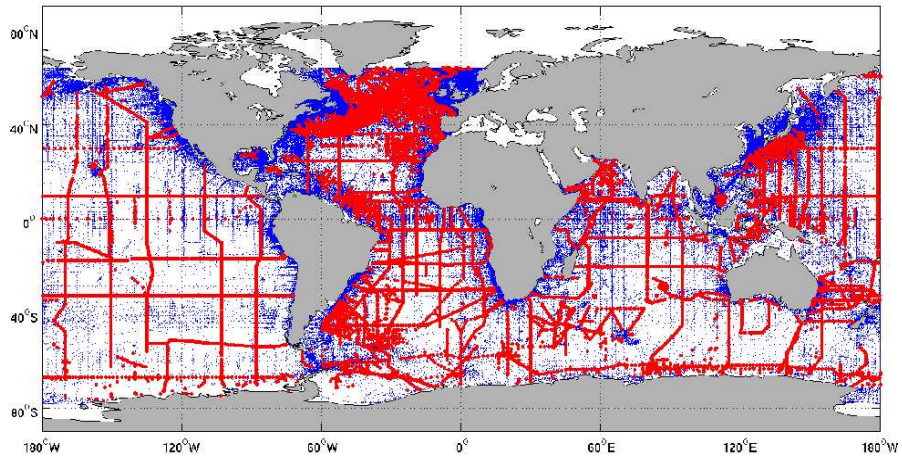

Figure 2.1: Distribution of temperature and salinity profiles used in this analysis. The blue points come from historical data (1940-1988: 816,193 profiles), while the red points largely come from the World Ocean Circulation Experiment (1988-2000: 38,463 profiles).

instrumental biases (Gouretski and Koltermann, 2007; Wijffels et al., 2007). To improve the spatial coverage in the Southern Ocean, Hydrobase2 was combined with the Southern Ocean Database (Orsi and Whitworth 2005), giving an additional 33,255 quality controlled profiles south of 30°S.

As with most *in situ* ocean datasets, historical coverage is weakest in the eastern-Pacific and the Southern Oceans, with coverage being greatest in the North Atlantic. In this thesis, only those profiles with ocean depths greater than 1000 m were retained, thus excluding the shallow coastal regions of the global ocean and minimising the effects of variability in boundary currents and near-shore eddy activity. This combined dataset was then separated into two time periods, 1940-1988 (759,713 'historical' profiles) and 1988-2000 (38,463 full-depth 'WOCE-period' profiles). Both periods had a good global distribution of observations (Figure 2.1), although there was a more systematic spatial distribution of profiles in the 1988 to 2000 period (red dots) than in the earlier 1940 to 1988 period (blue dots). The reason for this recent systematic distribution of ocean hydrographic sections is that the more recent data came largely from the World Ocean Circulation Experiment (of the World Climate Research Programme), a global collaborative experiment established with the aim of providing a near synoptic view of ocean circulation and properties. As such the cruise tracks are located in a systematic fashion across all the major ocean basins, therefore providing a good baseline to compare with the earlier and more evenly

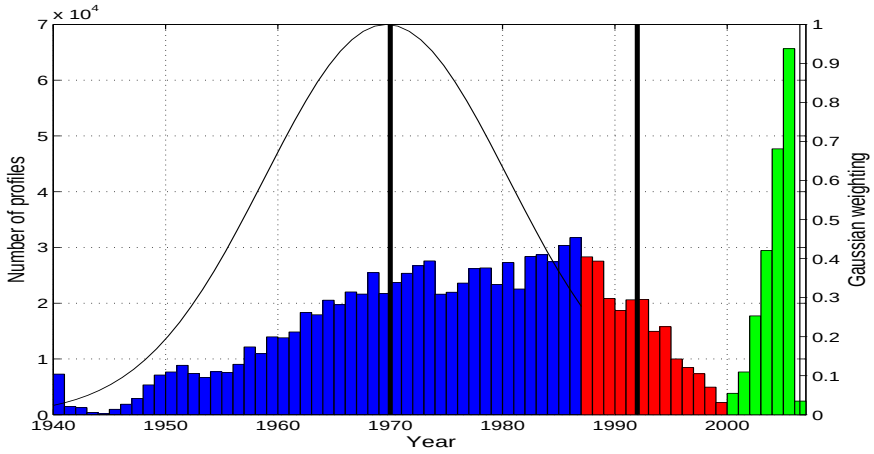

Figure 2.2: Temporal distribution of temperature and salinity profiles used from the combined datasets. Shown are the 'historical data' (blue), the 'WOCE-period' data (red), and the 'Argo' data (green). The historical data was weighted toward a mean date of 1970, the WOCE-period had a mean year of 1992, and the third Argo-period in the synoptic comparison was centred around 2005 (black lines). The Gaussian weighting for each year from Equation 2.8 is superimposed over the historical data and shown on the axis on the right side.

distributed data.

The majority of the HydroBase2 data was collected between 1960 and 1995, with approximately 25,000 profiles taken annually over this period (Figure 2.2). While more observations were taken during the 1980s than in the 1960s, the objective mapping process, allowed the interpolated data to be weighted toward 1970. This reduced the relative influence of observations close to the WOCE period, broadly creating a 22-year difference between the historical and the WOCE-period data (with a mean year of 1992).

Argo dataset

In Chapter 4, observations are used from free-drifting floats that have been deployed as part of the international collaborative Argo program. The same objective mapping technique was used to map 242,087 Argo profiles to the locations of the 38,463 WOCE-period locations (Figure 2.3). Given that the Argo dataset is continually growing, it was necessary to 'freeze' the dataset in February 2007, with no profiles being incorporated in the analysis after this time. These Argo profiles were well

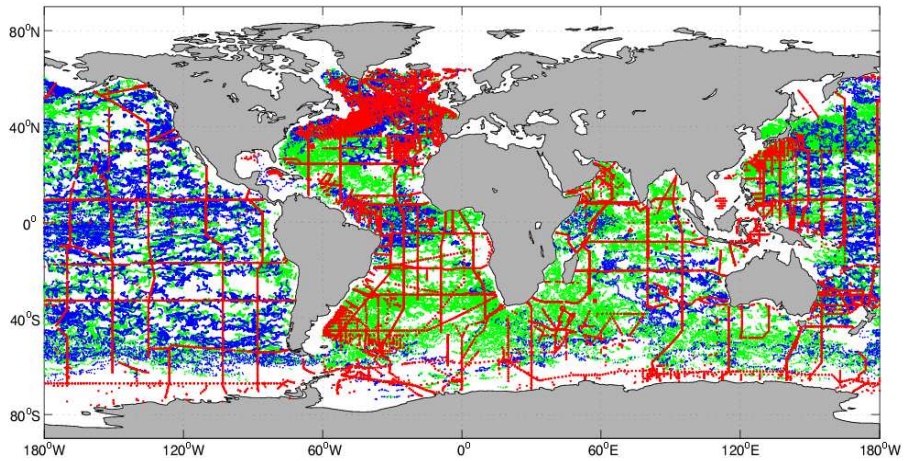

Figure 2.3: Distribution of the WOCE-period (red) and Argo profiles (2000-2007) used. The blue dots represent delayed mode Argo profiles (97,999), while the green dots represent real-time profiles (144,088).

distributed globally, although very few floats are deployed poleward of 60°S due to potential sea-ice damage to the instruments. While the more recent Argo floats profile to 2000 m, some of the earlier floats could not go this deep and approximately 30% of profiles are shallower than 1000 m. The Argo float data used here has a mean year of 2005 (Figure 2.2), allowing the differences between the 1992-2005 and the 1970-2005 periods to be compared with the 1970-1992 differences. More information on the Argo dataset can be found in Chapter 4. In this study a total of 172,918 profiles taken between 2000 and 2007 (with a mean year of 2005) were used from this dataset (Figure 2.2).

Oxygen data

In the combined HydroBase2-Southern Ocean Database dataset, all profiles contained temperature and salinity observations. However in these datasets comparatively few profiles have corresponding oxygen observations. This is especially evident in the historic period (1940-1988) where only 34% of profiles also contained oxygen (Table 2.1), although there is still a good spatial distribution (shown in Chapter 5, Figure 5.1). The addition of the Southern Ocean Database to HydroBase2 was especially important as it added an additional 29,894 unique quality-controlled oxygen profiles south of 30°S, a region central to the replenishment of oxygen and the renewal of water masses in the World Ocean circulation (Chapter 1, Figure 1.1). The WOCE program was a systematic global effort to quantify the world's oceans

Table 2.1: Statistical summary of datasets used in the synoptic comparisons.

	Historical	**WOCE period**	**Argo**
Period	1940-1987	1988-2000	2000-2007
Mean date	1972 weighted to 1970	1992	2005 weighted to 2005
Number of profiles	759,713	38,463	242,087 Delayed mode: 97,999 Real time: 144,088
Number of oxygen profiles	256,078	38,002	0

using modern ocean sampling methods and tracers, it is therefore not surprising that almost all profiles in this period include bottle or CTD oxygen measurements .

The pairing of oxygen with the associated temperature and salinity observations in Chapter 5 allows the oxygen change to be related directly to change in stratification, surface temperature change, and inferred air-sea fluxes. Unfortunately most Argo floats are not equipped with oxygen sensors meaning that the analysis of changes in the oxygen concentration is limited to only one period (1970-1992).

Treatment of other ocean variables, the surface layer, and seasons

While concentration levels of other ocean variables (nitrate, phosphate, silicate) were recorded along a number of WOCE transect lines, the number of *historical* observations of these variables is less than a quarter of the oxygen dataset. While the examination of Redfield ratios is possible in some regional studies, it was decided that the scarcity of nitrate, phosphate, and silicate observations did not warrant a global study and instead to focus on the better distributed, high quality oxygen observations.

In this study, observations above 100 m were removed from all calculations in order to reduce the potential seasonal variability in temperature, salinity, and oxygen observations. This depth level is assumed to approximate the average depth of the seasonal mixed layer globally, although it is below the observed mixed-layer in the low and mid-latitude regions (Kara et al., 2003). Previous studies of oxygen concentrations have also taken 100 m as being the approximate limit of the seasonal oxygen cycle (Garcia et al., 2005a,b).

In the Southern Ocean where the wintertime mixed layer depth can reach 300 m or

more, a check for a seasonal bias in the profiles was required. To do this, the timing of the average historical profile throughout the Southern Ocean (poleward of 30°S) was compared with the average post-1988 profile, producing a difference of only 9 days. The seasonal distribution of both sets of data were similar, with both centred in January, with approximately a 3 month spread (at one standard deviation). More importantly, the focus of this thesis is on the longer-term changes in water masses situated below the seasonal mixed layer.

Addition of the Hadley SST dataset

While the upper 100 dbar was removed when calculating changes along density surfaces, the large temperature changes in these surface waters can have a significant influence on dynamic height and heat content estimations. When these estimates are presented in Chapters 3 and 4, the upper 100 m is replaced with changes in the interpolated Hadley Sea Surface Temperature (SST) dataset (Rayner et al., 2003), taking a ten-year mean around 1970, 1992, and 2005. The assumption is made that the seasonal mixed layer had a homogeneous temperature that was equivalent to the sea-surface temperature, and that the *changes* in SST approximately reflect changes from the surface to 100 dbar. No equivalent dataset was available for sea surface salinity, and so in the steric sea-height calculations the salinity in the upper 100 dbar is assumed to be constant over time.

2.2 Interpreting changes in a neutral density coordinate system

One of the main advantages of estimating changes along constant density surfaces is that they tend to follow the flow paths of water masses, as no buoyancy forcing is required to move a parcel of water along these isopycnals (McDougall, 1987). In theory, this means that any salinity or temperature anomalies imparted by the atmosphere can be traced along a neutral density surface into the ocean interior. Diffusion along isopycnals is the primary mechanism for mixing over much of the ocean (Ledwell et al., 1993), with the exception being in regions of little circulation where diapycnal mixing is more prominent (Tomczak and Godfrey, 1994).

Using the more conventional pressure surfaces makes it more difficult to trace the surface changes into the ocean interior, and to estimate changes in an individual water mass. As well as a single isobar bisecting a number of different isopycnals

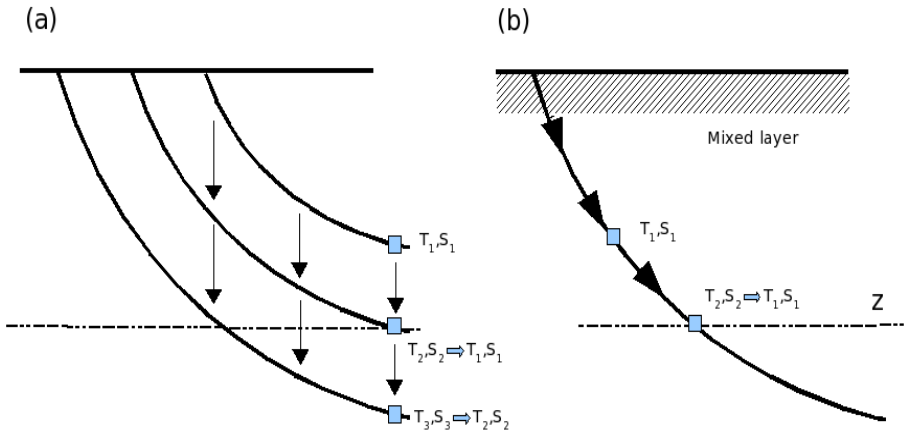

Figure 2.4: The two mechanisms that cause change on pressure surfaces. **(a)** shows a downward displacement of a density surface. This results in a constant pressure surface (dashed line) adopting the temperature and salinity properties of an overlying density layer. **(b)** shows a temperature and salinity change that originates from the mixed layer and is mixed into the ocean interior along surface of a constant density. The total temperature or salinity change is the sum of these two mechanisms.

(and hence water masses), ocean noise from mesoscale eddies, internal waves and interannual variability can cause significant short-term fluctuations in temperature and salinity by vertical displacement of density surfaces. An isopycnal surface moves with these internal processes by shoaling or deepening in the water column, while maintaining the same temperature and salinity properties. Throughout this thesis neutral density is the primary reference frame used, although for simplicity it is often referred to as a 'constant density surface" or simply as a 'density surface'.

Sometimes in this thesis, it is necessary to refer to changes on *pressure* surfaces, rather than along density surfaces. In such a pressure reference frame, there are two main mechanisms that lead to an observed change in temperature or salinity - *vertical displacement of isopycnals* and *along-isopycnal changes* (Figure 2.4). These two mechanisms are indicative of different atmospheric and oceanic forcing conditions and can only be separated by examining changes in water properties and pressure on surfaces of a constant density.

Mechanism 1: Vertical displacement of density surfaces

As illustrated in Figure 2.4 (a), a change in temperature or salinity on fixed pressure surfaces occurs when a neutral density surface is displaced vertically in the water column. Such a vertical movement results in the water properties at a fixed pressure surface changing to the water properties of the over or underlying water mass. Given the relatively constant gradient of temperature with depth, a shoaling without any change in along-isopycnal properties generally results in a cooling on pressure surfaces, while a deepening causes warming. For salinity, the sign of the change depends on the slope of the $\theta-$S curve that bisects the pressure surface.

This movement of density surfaces in the ocean can be caused by eddies, Rossby Waves, interannual variability, or by a change in the heat content or freshwater in the overlying water. In both hemispheres, a deepening of density surfaces also appears as a poleward shift in mid to high-latitudes.

Throughout Chapters 3 and 4, the vertical movement of isopycnals is identified and their effect on the temperature and salinity signal on pressure surfaces is discussed. In Chapter 5, the movement is also related to an oxygen change on pressure surfaces.

Mechanism 2: Changes along density surfaces

The second mechanism that can cause a change in temperature or salinity on a pressure surface is a change along an isopycnal with no vertical displacement of the density surface (Figure 2.4 (b)). As discussed earlier in this section, these changes originate in the mixed layer and propagate along density surfaces into the ocean interior.

On a surface of constant density, the above changes in temperature have a density-compensating salinity response (and vice versa). These are related by the equation;

$$\alpha\theta'|_n = \beta S'|_n \tag{2.1}$$

Neutral density has been used instead of the more conventional potential density, as it removes the uncertainty associated with a fixed reference pressure. Note that while the values for neutral density and potential density are identical at 23 kg m^{-3}, there are noticeable differences in denser waters.

When interpreting such along-isopycnal changes between two different epochs, a change in the θ-S curve might appear as a change of the opposite sign when examined at constant density (eg. through much of the main thermocline a warming on pressure surfaces appears as a cooling on a constant density surface) (Bindoff and Church, 1992; Bindoff and McDougall, 1994). To complete the transformation between reference frames, the stability ratio (R_ρ: essentially the slope of the $\theta-$S curve) is examined at the position of the isopycnal in temperature-salinity space;

$$R_\rho = \frac{\alpha\theta_z}{\beta S_z}, \tag{2.2}$$

where α is the thermal expansion coefficient and β is the haline contraction coefficient. θ_z and S_z are the vertical gradients of potential temperature and salinity in the water column respectively.

At this point it is worth noting that the following three paragraphs (and shown in Figure 2.5) deal with converting *along-isopycnal* temperature and salinity changes, to a change on pressure surfaces. The changes on pressure surfaces from this mechanism are to be *considered independently and in addition to any vertical displacement of isopycnals.*

Figure 2.5 (a) shows an observed cooling and freshening along an isopycnal (dashed line) in a positively sloped region of the temperature-salinity curve ($R_\rho > 1$), typical of the 27.0 kg m^{-3} density surface. That is, the positively sloped temperature-salinity line has shifted from T1 to T2, but has kept the same slope. Given no vertical displacement of the density surface, the observed change along the isopycnal (overlying thick arrow) appears as a warming and/or freshening on pressure surfaces (lighter vertical and horizontal arrows). For similar reasons, Figure 2.5 (b) shows an observed warming and salinity increase on an isopycnal, that appears as a cooling and/or a salinity increase on pressure surfaces (ie. T1 to T2).

In the region of the temperature-salinity diagram with a negative stability ratio (Figure 2.5 (c-d)) the sign of the observed changes on the isopycnal are the same as those on pressure surfaces. However if the density surface is found in the region $0 < R_\rho < 1$ (Figure 2.5 (e-f)), the sign of the temperature change remains the same, but the sign of the salinity change on the isopycnal appears reversed when explaining the observed along-isopycnal changes in an isobaric coordinate system.

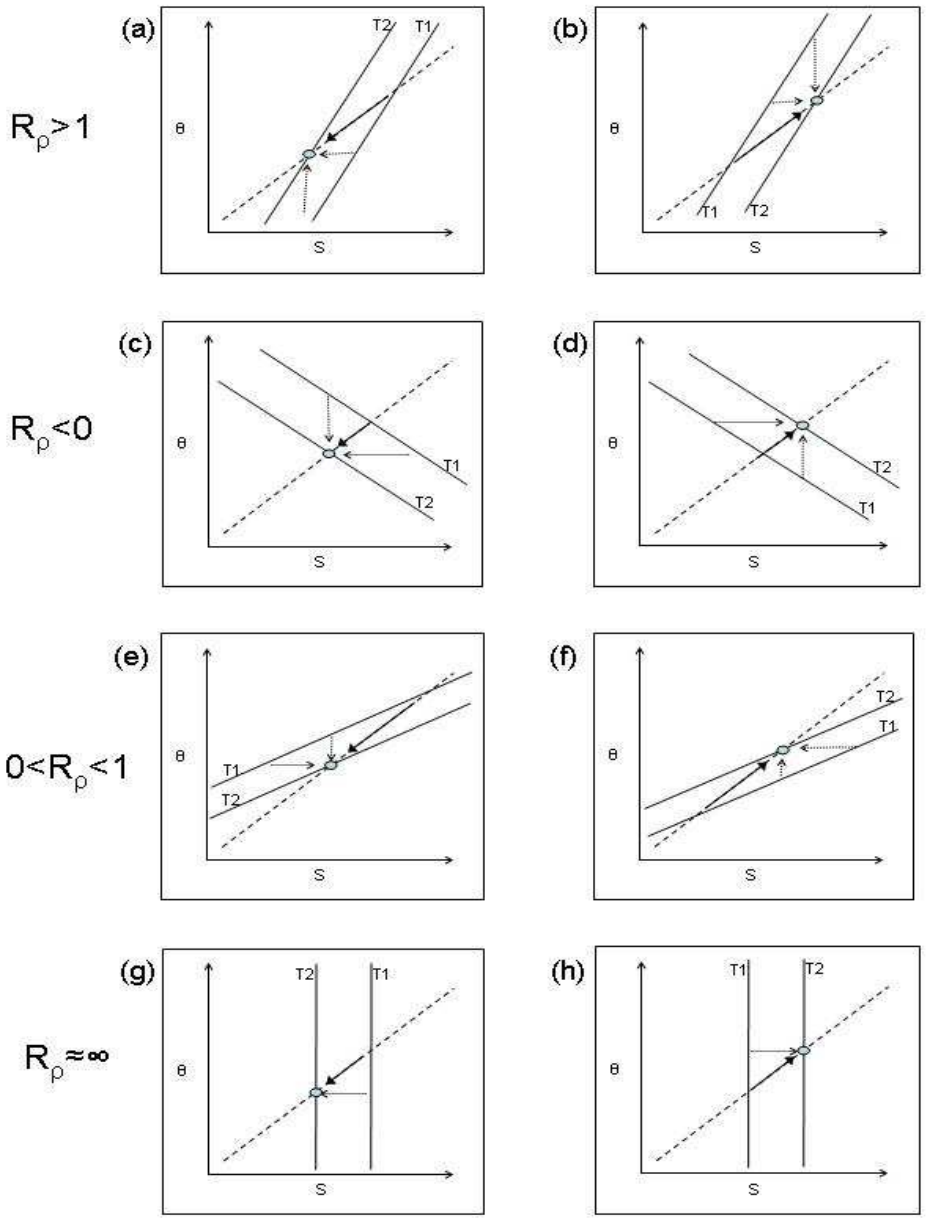

Figure 2.5: Interpreting observed changes along isopycnals under different stability ratios (R_ρ). **(a)** shows an observed cooling and freshening (solid diagonal arrow) along an isopycnal (dashed line) in a negatively sloped region of the θ-S curve ($R_\rho < 0$). This change can be interpreted as a warming and/or a freshening from an old (T1) to a new (T2) thermocline as is shown by the direction of the lighter horizontal and vertical arrows. **(b)** shows an observed warming and salinity increase in the same region of the water column. **(c-h)** show how changes along isopycnals can be interpreted in different regions of the water column. These are discussed in Section 2.2.

Table 2.2: Using the stability ratio (R_ρ) to convert between the signs of water mass property changes on density surfaces, and the sign of changes on pressure surfaces (assuming no vertical movement of the isopycnal).

Observation on isopycnal	Change on pressure surfaces		
	$R_\rho < 0$	$0 < R_\rho < 1$	$R_\rho > 1$
Warming & salinity increases	Warming &/or salinity increases	Warming &/or freshening	Cooling &/or salinity increases
Cooling & freshening	Cooling &/or freshening	Cooling &/or salinity increases	Warming &/or freshening

A unique situation that has particular relevance in this paper is when a density surface sits directly on the salinity maximum or minimum ($R_\rho \approx \infty$). This special case is shown in Figure 2.5 (g) where any cooling and freshening observed on the salinity minimum isopycnal appears as a freshening on pressure surfaces (ie. T1 to T2, with the cooling being a density-compensating response to the freshening). Likewise a warming and salinity increase on the density surface at the salinity maximum appears as a salinity increase on pressure surfaces (Figure 2.5 (h)). However on these pressure surfaces near the salinity maximum and minimum, a warming or cooling may still have occurred that is not detectable when only looking along isopycnals. The different scenarios of warming and salinity increases shown in Figure 2.5 are summarised in Table 2.2.

2.3 Conversion from pressure to neutral density coordinates

To convert temperature and salinity observations from pressure to neutral density surfaces, the Jackett and McDougall (1997) MATLAB routines were used. These programs reference the profile location to a global climatology in order to calculate the corresponding neutral density values. Using linear interpolation the temperature, salinity, and pressure values on regularly spaced density surfaces are then calculated, although these routines do not yet cover north of 64°N and the Mediterranean Sea. In this thesis, the oxygen concentrations on neutral density surfaces are estimated, by using temperature and pressure observations on neutral surfaces and isobars to linearly interpolate the oxygen from pressure to density surfaces.

Historical and Argo profiles were mapped to WOCE-period profiles on 40 neutral density layers (γ_n =23.0 to 26.0 kg m^{-3} in increments of 0.2 kg m^{-3} , and γ_n =26.1

to 28.4 kg m^{-3} in increments of 0.1 kg m^{-3}). This covers from the mixed layer in equatorial waters to the dense AABW in the Southern Ocean.

2.4 Objective mapping

To enable comparison between these time periods, the spatially scattered historical and Argo profiles were interpolated to each of the 38,463 profiles from the WOCE period using objective mapping (an optimal interpolation technique). This was done separately for each of the 40 neutral density surfaces, with an historical estimate (or Argo) for each WOCE-period position (d_g) being given by;

$$d_g = \overline{d} + \mathbf{C_{dg}}\mathbf{C_{dd}^{-1}}(\mathbf{d} - \overline{d}) \tag{2.3}$$

Using similar notation to Wong et al. (2001), $\mathbf{d}$ refers to all surrounding historical data, $\overline{d}$ is the mean of these observations, and d_g is the estimated temperature, salinity, oxygen, or pressure value at the WOCE-period profile location.

To limit the size of the initial matrix inversion, the spatially closest 500 historical points with an observation on the density surface were chosen. The two covariance functions which map the historical on to the single modern location ($\mathbf{C_{dg}}$) and the historical onto itself ($\mathbf{C_{dd}}$) are calculated by;

$$\mathbf{C_{dg}} = \mathbf{cov_{dg}}\sigma_d^2 \tag{2.4}$$

$$\mathbf{C_{dd}} = \mathbf{cov_{dd}}\sigma_d^2 + \sigma_n^2\mathrm{I} \tag{2.5}$$

The *a priori* noise (σ_n^2) accounts for natural variability in temperature and salinity, although it should be much smaller along neutral density surfaces than on pressure surfaces for the reasons discussed earlier. The *a priori* noise and the signal variance (σ_d^2) in the historical data are estimated by;

$$\sigma_n^2 = \frac{1}{2n}\sum_{i=1}^{n}(d_i - d_j)^2, \tag{2.6}$$

$$\sigma_d^2 = \frac{1}{n-1}\sum_{i=1}^{n}(d_i - \overline{d})^2, \tag{2.7}$$

where d_i and d_j are close neighbouring data points and n is the number of surrounding historical data points on a particular neutral density surface. This number of neighbouring profiles in each iteration varies depending on both the homogeneity of the surrounding ocean and the sparsity of the surrounding data. The noise variance (σ_n^2) provides an important role in that it quantifies background noise (eddies, internal waves, boundary currents), and indicates the significance of the observed signal. It is assumed that the *a priori* noise variance in temperature and salinity at any modern profile position is the same as this estimated historical variance.

The covariance matrices $\mathbf{cov_{dg}}$ and $\mathbf{cov_{dd}}$, elements required for Equations 2.4 ($\mathbf{C_{dg}}$) and 2.5 ($\mathbf{C_{dg}}$), are calculated using;

$$\mathbf{cov_{dg}} = \mathbf{cov_{dd}} = e^{-\left[(\frac{x_i - x_j}{lonscale})^2 + (\frac{y_i - y_j}{latscale})^2 + (\frac{t_i - t_j}{yearscale})^2\right]} \tag{2.8}$$

where x_j, (or y_j, t_j) is the longitudinal (latitude, time) position of each of the historical points. If $\mathbf{cov_{dd}}$ was being calculated in Equation 2.5 to map the historical data onto itself to check the fit, x_i, y_i, and t_i are the historical data position and date. For $\mathbf{cov_{dg}}$ they are the WOCE-period profile position and date.

A target year (t_i) of 1970 and a decay time ($yearscale$) of 15 years were chosen for mapping the historical data onto the WOCE-period locations (Figure 2.2). This choice was a balance between being able to use sufficient measurements in ocean basins with few measurements, and potentially having temperature and salinity signals from other decades creep into the historical estimate. The exponential relationship in Equation 2.8 means that a profile taken in 1940 has a weighting of 2% of the equivalent profile taken in 1970 (Figure 2.2: black curve). Similarly, a profile taken in 1988 at the upper end of the historical dataset has a 24% weighting.

Conventionally in objective mapping, the latitudinal ($latscale$) and longitudinal ($lonscale$) scales have been fixed, and the variance in the short scale residuals has been calculated to determine the appropriateness of the fit using;

$$r_g = d_g - (\overline{d} + \mathbf{C_{dd}}\mathbf{C_{dd}^{-1}}(\mathbf{d} - \overline{d})) = d_g - \hat{d}_g \tag{2.9}$$

This works well for a single section; however for the global dataset used in this study, an adaptive technique was needed to account for spatial variation in the distribution of profiles and noise in historical data. Using an adaptive iterative approach, the latitude and longitude scales in Equation 2.8 were adjusted until the residual variance ($\sigma^2_{r_g-d}$) and the *a priori* noise were;

$$0.75 < \frac{\sigma^2_{r_g-d}}{\sigma^2_n} < 1.25 \tag{2.10}$$

The longitudinal scale (*lonscale*) was parameterised to be twice that of the latitudinal scale (*latscale*) and was smallest in regions of little variation (generally away from the water mass formation regions) and in areas with good data coverage. These scales varied from less than 1° latitude and 2° longitude in the data-rich North Atlantic Ocean, to 5° latitude and 10° longitude in parts of the Pacific and Southern Oceans. When the condition set out in Equation 2.10 was met, typically with 2-4 iterations, the objectively mapped historical estimate (d_g) was accepted.

Exactly the same methodology was used for the Argo data, although the dataset (which spanned from 2000 to 2007) was weighted toward a mean year of 2005 (*yearscale*). Given the Argo coverage south of 60°S is not as spatially complete as the historical dataset this objective mapping method naturally has a bias toward warmer values in this region. To avoid this, a modern estimate at the WOCE-period location was only made when the 500 Argo observations were relatively evenly distributed north and south of the WOCE-period profile, with no fewer than 20% of the observations being found poleward of it.

Gridding of objectively mapped data

After using objective mapping to produce historical and Argo temperature, salinity, pressure, and oxygen estimates at each of the WOCE-period profiles, the data was averaged in grid cells for each of the 40 chosen neutral density surfaces. This reduces spatial bias in the distribution of observations, and helps smooth out any noise that may exist between adjacent profiles on the same isopycnal.

The choice of a 5° latitude by 10° longitude cell size was a balance between having too many empty cells and increasing the noise inside each cell by averaging over too large an area. Any empty cells were removed in the calculation of ocean

basin and global averages, a different approach to that of Levitus et al. (2005a) who treated empty cells as having had no change in properties. Despite being one of the most widely referenced sources on recent global ocean temperature variability, the approach that Levitus et al. (2005a) use potentially results in a conservative zonally-averaged value in regions with a coherent sign of change.

2.5 Minimising bias and estimating errors

Mean of residuals

One of the criticisms of the objective mapping process is that it can bias the objectively mapped estimate towards the *a priori* mean of the historical data. A check of the extent of this bias is the mean of the residuals (from Equation 2.9) calculated at the locations of each of the 38,463 post-1988 profiles. Across a number of density surfaces, this check showed negligible values that were typically 3 to 5 orders of magnitude smaller than the signal at the same point. In most grid boxes these values tended to be distributed around zero with no discernible spatial pattern, suggesting that in this respect the adaptive objective mapping process used in this thesis does not introduce systematic biases into the historical or Argo grid-point estimates of change.

T-tests

To check if there was sufficient data when comparing WOCE and historical averages in boxes and regions, standard two-tailed t-tests were conducted. In 73% of $5^\circ \times 10^\circ$ boxes there were sufficient observations to be 95% confident that the observed change on the 27.0 kg m^{-3} isopycnal is not a result of insufficient sampling. Other isopycnals showed similar results, suggesting that using grid box averages was generally a statistically robust approach.

Interannual variability

The magnitude of the interannual variability was estimated by repeating the objective mapping technique annually from 1960-1988 (varying t_i and setting the $yearscale$ to 5 years). On the 27.0 kg m^{-3} isopycnal this interannual variability was largest closest to ventilation regions and lowest in the equatorial regions. Typically in regions with large salinity changes, the salinity signal tends to be 2-3 times greater than one standard deviation of the interannual variability. Elsewhere the signal is 1-2 times larger, except in the low latitudes, where the weak signals of salinity

change are less that one standard deviation of the interannual salinity observations. Other density surfaces show similar ratios, with both the largest interannual variability and the largest signals being found near ventilated regions.

Signal to noise ratio

Inside each grid box or cell the initial noise (σ_n^2) was calculated in the same manner as before (Equation 2.6). Temperature and salinity noise was greatest in boxes over boundary currents, regions of few measurements, and in areas where different water masses mixed (ie. near the Mediterranean Sea outflow). This noise was used in the calculation of the signal-to-noise ratio;

$$\frac{S_f - S_i}{\sigma_n^2} \tag{2.11}$$

where S_f is the more recent, and S_i is the older, salinity (temperature, or oxygen) observation from the objectively mapped field. This signal-to-noise ratio provides an indication as to the strength of the signal when compared with background ocean variability.

Calculating standard errors

A second method of putting the observed changes on density surfaces in the context of ocean variability, was to calculate the *a posterior* noise for each historical estimate during the objective mapping process. This objective variance was then used inside each 5°×10° grid box to derive a standard cell error (σ_{cell}) by;

$$\sigma_{cell} = \sqrt{\frac{\sum \sigma^2_{posterior}}{n}} \tag{2.12}$$

where n is the number of WOCE observations within each 5°×10° grid box, and hence the number of objectively mapped historical and Argo observations. To estimate an approximate 95% confidence level, the standard errors for each cell are given to two standard deviations. Such standard errors are displayed in Figures 5.5-5.8. All observations in each cell were considered independent.

Calculating error bars

There are a number of different potential sources of error associated with every step of the analysis. These include observational errors in the original data, as well as errors arising from the conversion to neutral density surfaces, the objective mapping

process, and any final grid box or zonal averaging. To propagate the formal errors through the entire analysis process is complex. As well as it being difficult to quantify all of the potential error sources, there is also significant redundancy due to the interdependence between the derived values at each stage. To avoid these difficulties a simpler approach was adopted, where the error bars displayed on graphs throughout this thesis were calculated based on the noise variance estimated from the final values. This noise variance is calculated using Equation 2.6, and neighbouring values are assumed to be independent. Unless otherwise stated the bars are shown to one standard error.

Examples of this appear when changes in a zonally averaged property are integrated vertically (ie. Figure 3.11) or along density surfaces (ie. Figure 6.8). Given that the error bars are based on the variance in the final inferred surface changes, the standard error is calculated using n=80 observations for the zonal back-projections (40 density surfaces outcropping in each hemisphere), and n=90 for the vertical integrals (at a 2° latitude spacing).

2.6 Calculating changes in surface fluxes from ocean interior changes

In Chapters 3 to 6 the zonally averaged changes in water properties are integrated along the mean position of density surfaces during the observation period and projected back to the intersection of the outcropping density layers and the mixed layer (nominally taken as 100 m). The benefit of such an approach is that it allows an estimation of the surface fluxes, based on a physically more natural approximation of ocean circulation. One of the problems with the more conventional technique of integrating changes vertically in the water column, is that the interior anomalies originate from a wide range of different source regions of the ocean and are therefore difficult to interpret. The 'zonal back-projection' technique has been used primarily in the calculation of precipitation-minus-evaporation' changes by Wong et al. (2001); however it can also be used to estimate surface heat fluxes, oxygen fluxes, or to back-project vertical displacement and other interior processes on density surfaces. The method is essentially the same for all variables and the integrated surface change (C_S) for each density surface is;

$$C_S = \frac{\sum_{lat_C=0^o}^{lat_O} \mathrm{Vol}_C C_C}{S_O} \tag{2.13}$$

As illustrated in Figure 2.6, the changes are integrated from the equator ($lat_C = 0°$) to the outcropping region (at lat_O), C_C represents the along-isopycnal change in the particular tracer in each cell (ie. salinity, temperature, oxygen), and Vol_C is the volume in each cell calculated by;

$$\mathrm{Vol}_c = width \times thickness \times 1^{\mathrm{o}}[\cos(lat_C) \times R_{lat_C}] \tag{2.14}$$

The *thickness* is assumed to be fixed in time and is evaluated using the mean thickness over the two time periods, while the *width* was the meridional distance of the cell (Figure 2.6). Such as approach is supported in Chapter 3 (Figure 3.13 (c)) where relatively little volume change is observed for the density layers. R_{lat_C} is the estimated ocean:land ratio around the latitude band that each cell sits on. When multiplied by $\cos(lat_C)$ and 1° ($\approx 111 \times 10^3$ m), both the spherical nature of the globe and the influence of the continents are accounted for. As such, the changes in a cell found in the equatorial regions are given a greater weighting than an identical change in the higher latitudes in the Northern Hemisphere (where there is a higher proportion of land).

The sum of all cells along the isopycnal is divided by the surface outcropping area (S_O) available for fluxes to propagate into the ocean interior;

$$S_O = d \times 1^{\mathrm{o}}[\cos(lat_O) \times R_{lat_O}] \tag{2.15}$$

where d is half the distance between neighbouring outcropping density surfaces (Figure 2.6).

For the zonally back-projected heat and salinity changes, only the changes along density surfaces ($\theta'|_n$ and $S'|_n$) are included, with the vertical displacement terms ($N'\theta_z$ and $N'S_z$) being omitted. This integration of $\theta'|_n$ and $S'|_n$ avoids some artifacts associated with the vertical displacement of density surfaces (eg. the Pure Heave process: see Section 2.7), and therefore reflects the contributions of changes in surface properties alone. It does mean however that the estimated heat and freshwater fluxes are not independent of each other, since they include a density-compensating response through the neutral surface algorithms. Consequently, the heat and fresh-

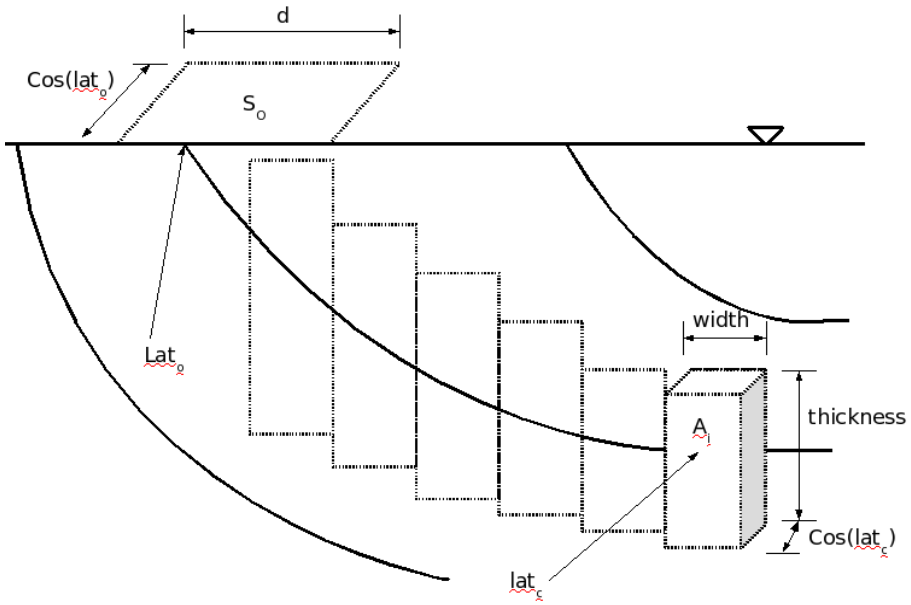

Figure 2.6: Schematic diagram showing the variables used in the zonal back-projected estimates. Each rectangle represents a cell on the isopycnal and all terms are identified in Section 2.6.

water estimates presented throughout this thesis are thus termed 'apparent' fluxes. In Chapter 6, a more through analysis of all six back-projected observable terms ($\alpha\theta'|_z$,$\beta S'|_z$,$\alpha\theta'|_n$,$\beta S'|_n$,$N'\alpha\theta_z$,$N'\beta S_z$: see Section 2.7) reflects the overall distribution of the apparent heat and freshwater fluxes produced in Chapters 3 and 4.

The changes on individual density surfaces are assumed to be representative of the entire density layer, and a constant rate of diapycnal mixing between the density layers is assumed. In addition this kinematic model is based on the premise that the primary mixing mechanism is *along* rather than *across* isopycnals, an assumption that is supported by the mixing experiment (Ledwell et al., 1993).

Since advection times are not taken into account, it is likely that inferred surface changes in apparent heat and freshwater fluxes are underestimated for the shallower density layers found in equatorial regions. This is because the ventilation time of these waters is shorter than the 'snapshot' period being investigated (approximately 22, 13, or 35 years: 1970-1992, 1992-2005, and 1970-2005 respectively), and hence some of the atmospheric signal impressed on the ocean would have been advected through the ocean interior and already released at the surface. Likewise the denser

waters with longer ventilation times would contain some signals imparted by the atmosphere before the beginning of the study.

Converting zonal back-projections into apparent freshwater fluxes

The calculation of apparent surface freshwater fluxes essentially follows the same methodology as Wong et al. (2001), where the freshwater changes (ΔFW) are related to the mean salinity ($\overline{S} = (S_f + S_i)/2$) and the change in salinity ($S'|_n = S_f - S_i$) by;

$$\Delta FW = -\frac{S'|_n}{\overline{S}} \tag{2.16}$$

Once multiplied by a volume and integrated along the density surface, the total freshwater input is then divided by the period length in order to express the change as an annual value (in millimetres). The change of sign is required to account for the fact that a freshening (salinity increase) is the result of a positive (negative) freshwater contribution.

Converting zonal back-projections into apparent heat fluxes

When estimating apparent surface heat fluxes from zonal back-projections, the change in heat content for each layer expressed in Joules was calculated using;

$$\Delta J = \mathrm{Vol}\rho C_p \theta'|_n \tag{2.17}$$

where the heat capacity (C_p) was assumed to be a constant 3.99×10^3 J K^{-1} kg^{-1} and density (ρ) was assumed to be a constant 1028 kg m^{-3} (as in Wong et al. (2001)). The zonally averaged stability ratio was calculated and wherever $R_\rho > 1$, the sign of the temperature change ($\theta'|_n$) was interpreted such that a cooling on density surfaces in the positively sloped thermocline represents a warming on pressure surfaces (and vice versa as discussed in Section 2.2). The heat content along an isopycnal layer was converted into an apparent surface heat flux SF in W m^{-2} using;

$$\Delta SF = \frac{J}{s * S_O} \tag{2.18}$$

where s is the number of seconds in the time period (693.8×10^6 for 1970-1992). When heat content is zonally averaged and then integrated vertically in the water column (as in Chapter 3, Figure 3.13), the surface width (S_O) in this case is simply

the width of the latitude band.

Converting zonal back-projections into oxygen fluxes

The integrated oxygen changes were estimated for each density layer from Equation 2.13, with the surface oxygen flux being expressed in mol/m^2/yr. For oxygen zonal back-projections a correction is made to account for the effects of temperature change on the oxygen saturation level of water in the mixed-layer. This correction applies to water advected into the ocean interior, and is derived in Chapter 5.2. In the case of zonal back-projections, the temperature correction was applied to all layers and hence both subducting and upwelling water masses.

Zonal back-projected contribution to sea level rise

In Chapter 6 the six observable terms outlined in Section 2.7 are estimated. These terms are dimensionless expansion coefficients and can be multiplied by the volume to calculate a steric sea-level contribution for each density layer. Note however that the changes *along* density surfaces ($\alpha\theta'|_n$ and $\beta S'|_n$) are compensating, and therefore have no contribution to steric sea-level change.

The pattern of sea level change presented using zonal back-projections does not reflect the actual observed surface patterns of sea level change, as a parcel of water that expands or contracts in the ocean interior will alter the surface dynamic height directly above it in the water column. However these back-projections along density surfaces do provide a good indication as to which latitude bands contribute the most to sea level change.

As outlined in Bindoff and McDougall (1994) there are some changes of sign required to convert $\alpha\theta'|_z$,$\beta S'|_z$,$N'\alpha\theta_z$, and $N'\beta S_z$ from density expansion terms into a contribution to sea level rise. As an example, a decrease in density equates to an expansion of the water, and a rise in sea surface height. These conversions will be discussed further in Chapter 6.

2.7 Pure subduction processes

While neutral density surfaces provide a more natural reference for studying anomalies imparted by the atmosphere to the ocean, they cannot give a complete understanding of the apparent air-sea fluxes. While changes observed along a density

surface are likely to be largely the result of changes in atmospheric forcing at the surface, it is not known whether this signal is caused by changes in atmospheric heat or freshwater fluxes, or some combination of both. In addition a change along an isopycnal gives no indication as to the change in the vertical position of the density surface caused by eddies or other ocean variability, which would be reflected as warming or cooling on a fixed pressure surface (ie. the first mechanism discussed in Section 2.2). By comparing observations on isopycnals with the equivalent observations on isobars, the processes that are driving the observed changes can begin to be understood.

Bindoff and McDougall (1994) identified three such ventilation process - pure warming (cooling), pure freshening (salinity increases), and pure heave, and combinations of these three subduction mechanisms can explain what is occurring in the ocean interior. Quantitatively these three processes, are based on both the stability ratio discussed earlier (R_ρ) and the linear relationships;

$$\alpha\theta|'_z = \alpha\theta|'_n - N'\alpha\theta_z; \tag{2.19}$$

$$\beta S|'_z = \beta S|'_n - N'\beta S_z; \tag{2.20}$$

where $|_n$ refers to the changes in potential temperature (θ) or salinity (S) on a neutral surface, $|_z$ refers to changes at a fixed pressure, and N' is the vertical movement of the isopycnal in the water column. Positive values refer to an increase in temperature or salinity, and a shoaling (upward movement) of the density surface. The gradients of temperature and salinity in the water column are labelled θ_z and S_z respectively, meaning that $N'\alpha\theta_z$ and $N'\beta S_z$ are the contribution to density change from temperature and salinity respectively at a fixed position on a density surface due to vertical isopycnal displacement. Note that all terms are expressed in terms of density using the thermal expansion (α) and haline contraction coefficients (β) where;

$$\alpha = -\frac{1}{\rho}\frac{\partial\rho}{\partial\theta}\Big|_{S,p} \tag{2.21}$$

$$\beta = -\frac{1}{\rho}\frac{\partial\rho}{\partial S}\Big|_{\theta,p} \tag{2.22}$$

Calculating the six observable quantities

In Equations 2.19 and 2.20 the relationship between changes on pressure and density surfaces are detailed using six 'observable' quantities namely $\alpha\theta'|_n$,$\beta S'|_n$,$\alpha\theta'|_z$,$\beta S'|_z$,$N'\alpha\theta_z$ and $N'\beta S_z$. These are evaluated by;

$$\alpha\theta'|_n = \alpha(\theta_m, S_m, p_m)[\theta^f|_n - \theta^i|_n], \tag{2.23}$$

$$\alpha\theta'|_z = \alpha(\theta_m, S_m, p_m)[\theta^f(p_m) - \theta^i(p_m)], \tag{2.24}$$

where the mean potential temperature (θ_m), salinity (S_m), and pressure (p_m) are calculated from the initial (superscript i) and final (superscript f) observations on the isopycnal by;

$$\begin{aligned} S_m &= \frac{S^f|_n + S^i|_n}{2}, \\ \theta_m &= \frac{\theta^f|_n + \theta^i|_n}{2}, \\ p_m &= \frac{p^f|_n + p^i|_n}{2} \end{aligned} \tag{2.25}$$

Changes in salinity on isopycnal and isobaric surfaces can be calculated in the same way as Equations 2.23 and 2.24 respectively, by replacing the thermal expansion coefficient (α) with the haline contraction coefficient (β), and replacing the changes in potential temperature (θ) with changes in salinity (S).

Estimating the temperature and salinity changes due to isopycnal displacement ($N'\alpha\theta_z$ and $N'\beta S_z$) can be done in two ways. The simplest is to rearrange and solve Equation 2.19, given that the other two terms are now known. The second method is to test for closure by calculating the two terms independently using;

$$N'\alpha\theta|_z = \frac{1}{2}[N'\alpha(\theta_m, S_m, p_m)[\theta^f_z(p_m) + \theta^i_z(p_m)]], \tag{2.26}$$

$$N'\beta S|_z = \frac{1}{2}[N'\beta(\theta_m, S_m, p_m)[S^f_z(p_m) + S^i_z(p_m)]], \tag{2.27}$$

where $\theta^i_z(p_m)$ and $\theta^f_z(p_m)$ are the gradients of potential temperature at the aver-

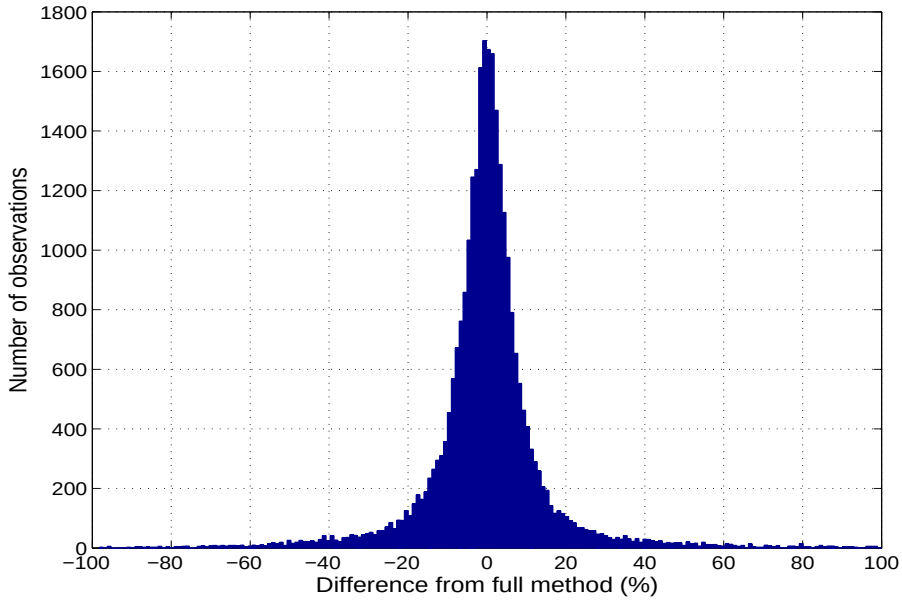

Figure 2.7: Differences between the 'full' and the 'difference' methods of calculating $N'\alpha\theta_z$. Differences are shown for all profiles on the 27.0 kg m^{-3} density surface using the 1970-1992 period.

age pressure (p_m) in the initial and final profiles respectively. Likewise $S_z^i(p_m)$ and $S_z^f(p_m)$ are the gradients of salinity. There was generally less than a 20% difference in the output of the two methods when applied pointwise to our global dataset between 1970 and 1992. The proportional differences are illustrated in Figure 2.7 for changes on the 27.0 kg m^{-3} density surface.

Pure warming (cooling) scenario

A Pure Warming scenario is one where the potential temperature at a constant depth increases, with no equivalent change in salinity ($\alpha\theta'|_z>0$, $\beta S'|_z=0$). Such a situation results from a warming of surface waters with no change in salinity surface properties. The way in which this subduction mechanism appears on an isopycnals is dependent on the stability ratio (Equation 2.2), with pure warming in a region where $R_\rho > 1$ appearing as both a cooling and a freshening on the density surface (Figure 2.5 (a)). In physical space, this is non-density compensating with pure warming representing subduction of water along a lighter surface and hence a downward displacement (deepening) of surrounding isopycnals. Pure cooling ($\alpha\theta'|_z<0$, $\beta S'|_z=0$) has the opposite effect in the same region of the water column, with subduction occurring along a denser surface and an associated upward

movement of surrounding isopycnals. Following Bindoff and McDougall (1994) pure warming or cooling equates to :

$$\alpha\theta'|_n = \frac{\alpha\theta'|_z}{1 - R_\rho} = N'\beta S_z = \beta S'|_n, \tag{2.28}$$

along a neutral surface. Equation 2.28 shows that the temperature or salinity change on the neutral surface is a function of both the temperature-salinity gradient in the thermocline (through R_ρ), and the magnitude of the temperature changes at fixed depth level ($\alpha\theta'|_z$).

Pure freshening (saltification)

The process behind the pure freshening (saltification) subduction mechanism is similar to that of pure warming, except in this scenario a surface freshening (salinity increases) with no change in temperature occurs. This results in the water subducting along a lighter surface and the potential temperature at a fixed depth remaining constant while freshening occurs ($\alpha\theta'|_z$=0, $\beta S'|_z$<0). However unlike pure warming, a body of water subject to pure freshening will have the same freshening sign of change on an isopycnal (if $R_\rho > 1$), and in the region $0 < R_\rho < 1$ (Figure 2.5 (a-b,e-f)) where a change of sign is required to convert salinity changes from isopycnal to isobaric surfaces (Figure 2.5 and Table 2.2). Along a neutral surface, Pure Freshening equates to:

$$\beta S'|_n = -\frac{\beta S'|_z}{(1 - R_\rho)^{-1}} = N'\alpha\theta_z = \alpha\theta'|_n \tag{2.29}$$

Throughout this thesis, Pure Warming and Pure Freshening are capitalised when referred to as a *process*, but are lower-case if indicating a *sign of change* (ie. pure warming or pure cooling).

Pure heave

Pure heave is unlike the Pure Warming and Pure Freshening processes, in that no change in surface properties occurs, and hence there is no change in properties on an isopycnal in the ocean interior ($\alpha\theta'|_n$=$\beta S'|_n$=0). All changes on pressure surfaces can be attributed to the vertical displacement of density surfaces and the underlying temperature and salinity gradients in the water column. As discussed previously, the primary long-term mechanism for these changes are a spatial shift, or a change in the magnitude, of surface winds. Broadly, such wind changes affect the wind stress

curl and hence the volume of water (and thickness of density layers) subducted into the ocean interior. This process often has the associated effect of changing interior water properties as a consequence of a change in advection and/or mixing rates. On shorter time scales mesoscale eddies, Rossby waves, and other interior ocean variability can also shift the vertical position of density surfaces. For the pure heave explanation of water property change, the changes on pressure surfaces are;

$$\begin{aligned} \alpha\theta'|_z &= -\alpha N'\theta_z, \\ \beta S'|_z &= -\beta N' S_z \end{aligned} \tag{2.30}$$

where θ_z and S_z are the underlying mean temperature and salinity gradients.

Resolving into the three subduction coefficients

Using the six observed components from Equations 2.19 and 2.20 (the temperature, salinity, and the vertical displacement terms on isobaric and isopycnal surfaces), we can determine the relative contributions of the three 'pure' processes of Pure Warming, Pure Freshening and Pure Heave. Using the method first proposed by Bindoff and McDougall (1994) the six observable quantities are related to the subduction coefficients by;

$$\frac{\rho^{-1}\rho'|_z}{(R_\rho - 1)} \begin{bmatrix} -(R_\rho - 1) & 0 & -R_\rho \\ 1 & R_\rho & 0 \\ R_\rho & R_\rho & R_\rho \\ 0 & (R_\rho - 1) & -1 \\ 1 & R_\rho & 0 \\ 1 & 1 & 1 \end{bmatrix} \begin{bmatrix} A^w \\ A^f \\ A^h \end{bmatrix} = \begin{bmatrix} \alpha\theta'|_z \\ \alpha\theta'|_n \\ N'\alpha\theta_z \\ \beta S'|_z \\ \beta S'|_n \\ N'\beta S_z \end{bmatrix}, \tag{2.31}$$

where A^w, A^f and A^h are dimensionless and represent the strength of the warming, freshening, and heave processes respectively. As it stands, Equation 2.31 is rank deficient with only two non-zero eigenvalues and cannot be solved directly. However one way to resolve this rank deficiency is to view it as an overdetermined problem, by first setting A^h=A^f=0 and solving for A^w. This process is then repeated, solving for A^f (A^w=A^h=0) and A^h (A^w=A^f=0). Given that any ocean observation contains a signal from all three subduction processes, using such an overdetermined solution allows each process to be distinguished and treated independently. In doing so the subduction process that best fits the observations in each region and water mass

can be determined.

The proportion of variance (R^2) explained by each of the three subduction coefficients is then calculated by;

$$R^2 = \frac{\boldsymbol{d_{est}^T d_{est}}}{\boldsymbol{d^T d}}, \tag{2.32}$$

where $\boldsymbol{d}$ are the six observable terms on the right hand side of Equation 2.31, and $\boldsymbol{d_{est}}$ is the overdetermined solution to this equation. To avoid problems associated with averaging a pointwise least-squares solution, the proportion of variance and the three subduction coefficients were calculated from cell or zonally averaged temperature, salinity and pressure data.

Chapter 6 uses these methods to interpret the ocean temperature and salinity changes that are outlined and discussed in Chapters 3 and 4. In doing so we can better understand the relative importance of difference atmospheric processes in driving the observed ocean changes over the last 40 years.

Chapter 3 Temperature and salinity changes: 1970-1992

3.1 Introduction

While there have been a number of regional studies, there has previously been no global analysis of temperature and salinity changes along density surfaces. This chapter presents such an analysis, building on a number of regional studies, which show a spatially coherent pattern of temperature and salinity changes on density surfaces. As discussed in Chapter 2, the focus here is on the 1970-1992 period, using the combined HydroBase2 and Southern Ocean Database to ensure a near global analysis throughout the water column.

In the Atlantic Ocean, previous studies suggest that a net warming has occurred in the second half of the 20th century, with vertically integrated changes in the northern and Southern Hemispheres being of a similar magnitude (Levitus et al., 2005a). The mechanisms that cause these changes vary, with the warming on North Atlantic Deep Water (NADW) pressure surfaces being largely explained by deepening isopycnals, while by contrast the warming in overlying layers appears instead to be caused by along-isopycnal changes (Arbic and Owens, 2001; Bryden et al., 1996). Such along-isopycnal changes in water properties are propagated into the ocean interior from the mixed-layer, and are the explanation for both the freshening of mode and intermediate waters in the mid-latitudes, as well as the increase in salinity in the upper ocean subtropical gyres (20°S-40°N) between the 1950s and the 1990s (Curry et al., 2003). There has been significant freshening observed north of 40°N in the NADW formation region (Curry and Mauritzen, 2005).

The Pacific Ocean has cooled and freshened on isopycnals in the low salinity intermediate waters across the entire southern basin (Johnson and Orsi, 1997; Wong et al., 1999, 2001), with warming and salinity increases in mode waters in the upper thermocline. Little change is observed in the weakly circulating North Pacific Deep Water (Johnson and Orsi, 1997), a water mass far from its ventilated origin in the North Atlantic and Southern Oceans. In the Northern Hemisphere upper 400 m, Deser et al. (1996) observed warming on pressure surfaces in the east and cooling

in the west from 1970-1991, while the North Pacific Intermediate Water (NPIW) appears to have warmed on density surfaces (Nakanowatari et al., 2007). El Niño is the dominant mode in upper ocean variability in the western tropical and subtropical Pacific Ocean (Holbrook and Bindoff, 1997).

The literature suggests that the Indian Ocean has exhibited an oscillation in temperature and salinity in the south of the gyre, with both Antarctic Intermediate Water (AAIW) and Subantarctic Mode Water (SAMW) isopycnals cooling, freshening, and deepening between the mid-1960s and the mid-1980s (Bindoff and McDougall, 2000; Aoki et al., 2005). On pressure surfaces this is a warming and freshening. The sign of mode water changes appears to have reversed since 1987 and become saltier (Bryden et al., 2003; Murray et al., 2007). Depth integrated heat content changes (0-3000 m) in the north of the Indian Ocean gyre are an order of magnitude smaller than in the southern part of this gyre (Levitus et al., 2005a).

The Southern Ocean is the major physical link between the Atlantic, Indian and Pacific Oceans, the formation region for Antarctic Bottom Water (AABW), and the site of water mass upwelling and subduction, meaning that it has an unique role in the global circulation (Chapter 1, Figure 1.1). It appears to exhibit the same warming trend as the other oceans, with an approximate 0.17°C average increase from 700 to 1100 dbar between the 1950s and the 1990s (Gille, 2002). South of the Polar Front in the Indian Ocean sector, upwelling CDW has warmed, increased in salinity, and deepened (Aoki et al., 2005).

All these previous studies have focused on changes in individual ocean basins or along specific hydrographic sections. Here this earlier work is added to by using the same neutral density reference frame, but for the first time incorporating a high-quality *global* dataset, allowing investigation of the magnitude and spatial coherence of global patterns of change. In addition, there is sufficient data coverage to integrate temperature and salinity changes along neutral density surfaces, for the first time allowing global changes in *apparent* heat and freshwater fluxes at the surface to be inferred.

In this chapter, the changes in temperature, salinity, and pressure between a mean date of 1970 and 1992 were looked at along 40 neutral density surfaces through the water column. Initially, the temperature, salinity, and pressure changes are inves-

tigated in four representative water masses, before changes are zonally averaged on density surfaces throughout the water column. These zonal patterns are then back-projected along isopycnals to give changes in isopycnal volume, apparent heat fluxes, and apparent freshwater fluxes, and vertically integrated to give changes in sea surface height. In Section 3.5 the relationship between the different forcing mechanisms are discussed, the findings are compared with model results, and a plausible physical explanation is presented.

3.2 Changes in representative water masses along density surfaces

To gain an understanding of the global spatial coherence of any temperature, salinity, and pressure signals, the initial focus was on changes along 4 of 40 density surfaces: the salinity-maximum, the 27.0 kg m^{-3} isopycnal, the salinity minimum, and along the 27.8 kg m^{-3} isopycnal. These surfaces represent upper thermocline, mode, intermediate, and deep water respectively.

Salinity increases at the shallow salinity-maximum

In the upper thermocline waters at the shallow salinity-maximum, a globally averaged salinity increase on density surfaces of 0.043 psu (with a corresponding temperature increase of 0.12°C) from 1970 to 1992 was observed. Despite being affected by regional oscillations (ENSO, North Atlantic Oscillation, South Pacific Oscillation), this pattern is spatially widespread with approximately 67% of ocean grid cells showing an increase in salinity (Figure 3.1 (a)). This spatial coherence is strongest in the Indian Ocean (81% of cells increasing in salinity at an average of 0.067 psu and a warming of 0.20°C: Figure 3.2 (f-j)), with the largest changes occurring in the main Southern Hemisphere gyre (Figure 3.2 (i)). In the Atlantic Ocean a similar pattern emerges with a mean salinity increase of 0.064 psu (0.17°C), with the largest changes occurring around 20°S (Figure 3.2 (b)).

Compared with the other two oceans, the majority of the Pacific Ocean shows less change on large spatial scales, with comparatively small signal/noise ratios (Figure 3.1 (d)). However there is a region of weak salinity increases on isopycnals in the north-west (Figure 3.3 (b)), and a strong salinity increase in the south-east (Figure 3.1 (a)). Directly on the equator, we see salinity decreases across a narrow latitude band. This shows up in both Figure 3.1 (a) and Figure 3.3 (c,h), where the salinity

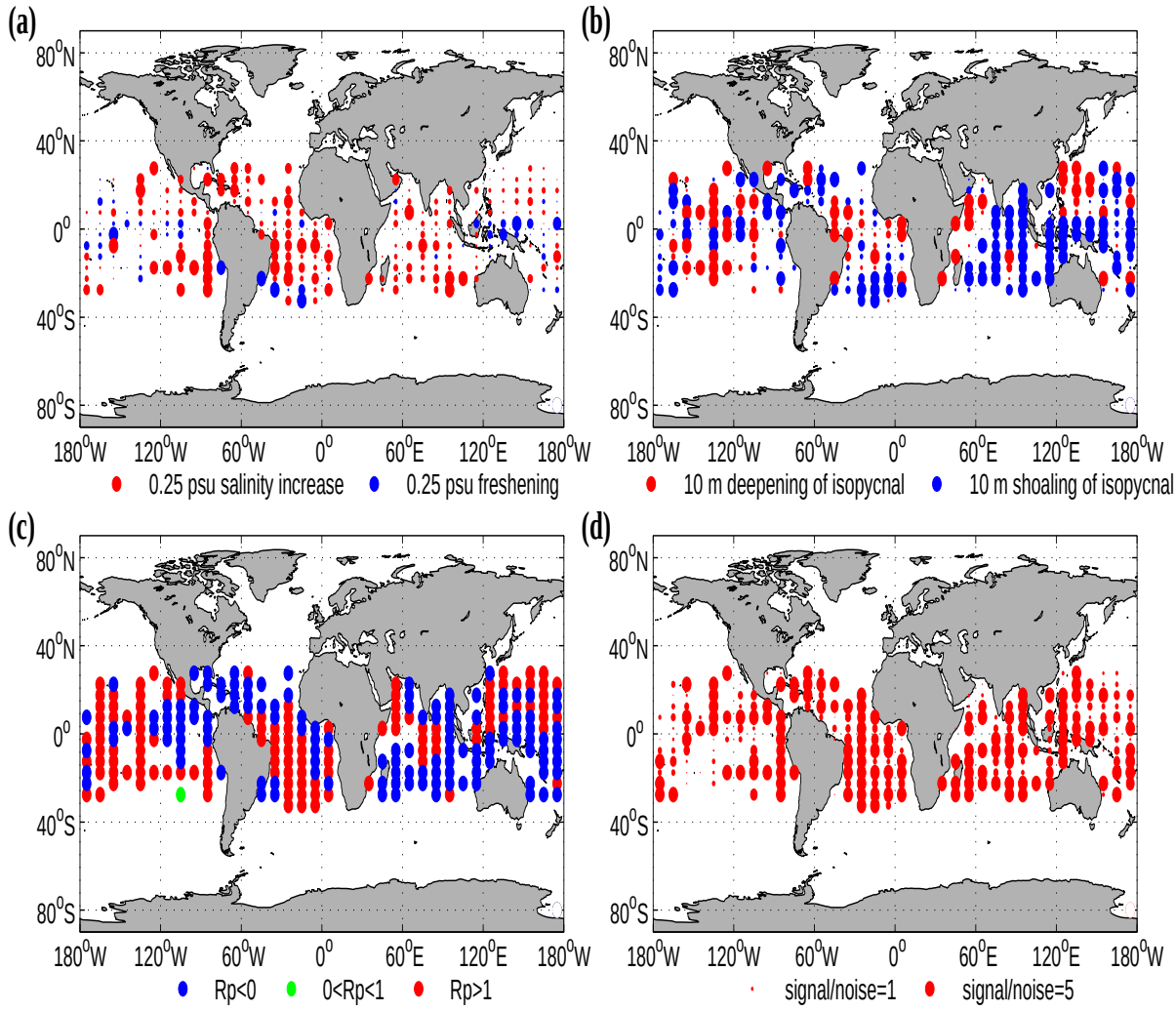

Figure 3.1: Changes at the shallow salinity-maximum (∼1970-1992). **(a)** Changes in salinity on the most representative salinity-maximum isopycnal. **(b)** Changes in the depth of this surface. **(c)** The stability ratio R_ρ. **(d)** The signal/noise ratio was obtained using Equation 2.11.

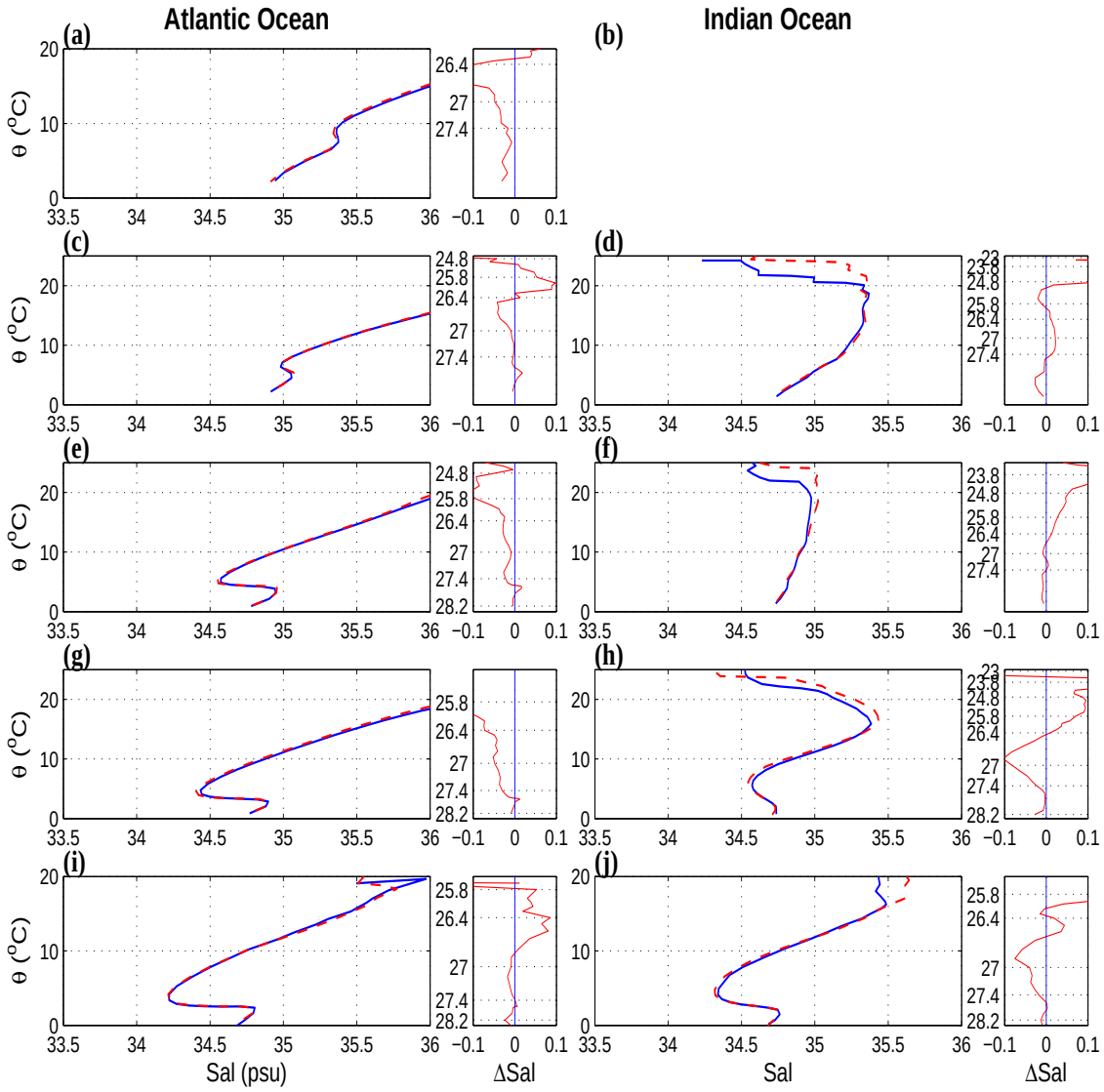

Figure 3.2: Temperature-salinity curves for the Atlantic and Indian Oceans in five regions between **(a-b)** 50°N-30°N, **(c-d)** 30°N-10°N, **(e-f)** 10°N-10°S, **(g-h)** 10°S-30°S, **(i-j)** 30°S-50°S. The blue curves represents the average historical profile (1970) while red curve represents the average WOCE-period profile (1992). Beside each regional θ-S plot is the associated change in salinity (psu) on isopycnals, with negative values indicating a freshening. Key density surfaces are labelled on the y-axis adjacent to their associated position on the θ-S plot.

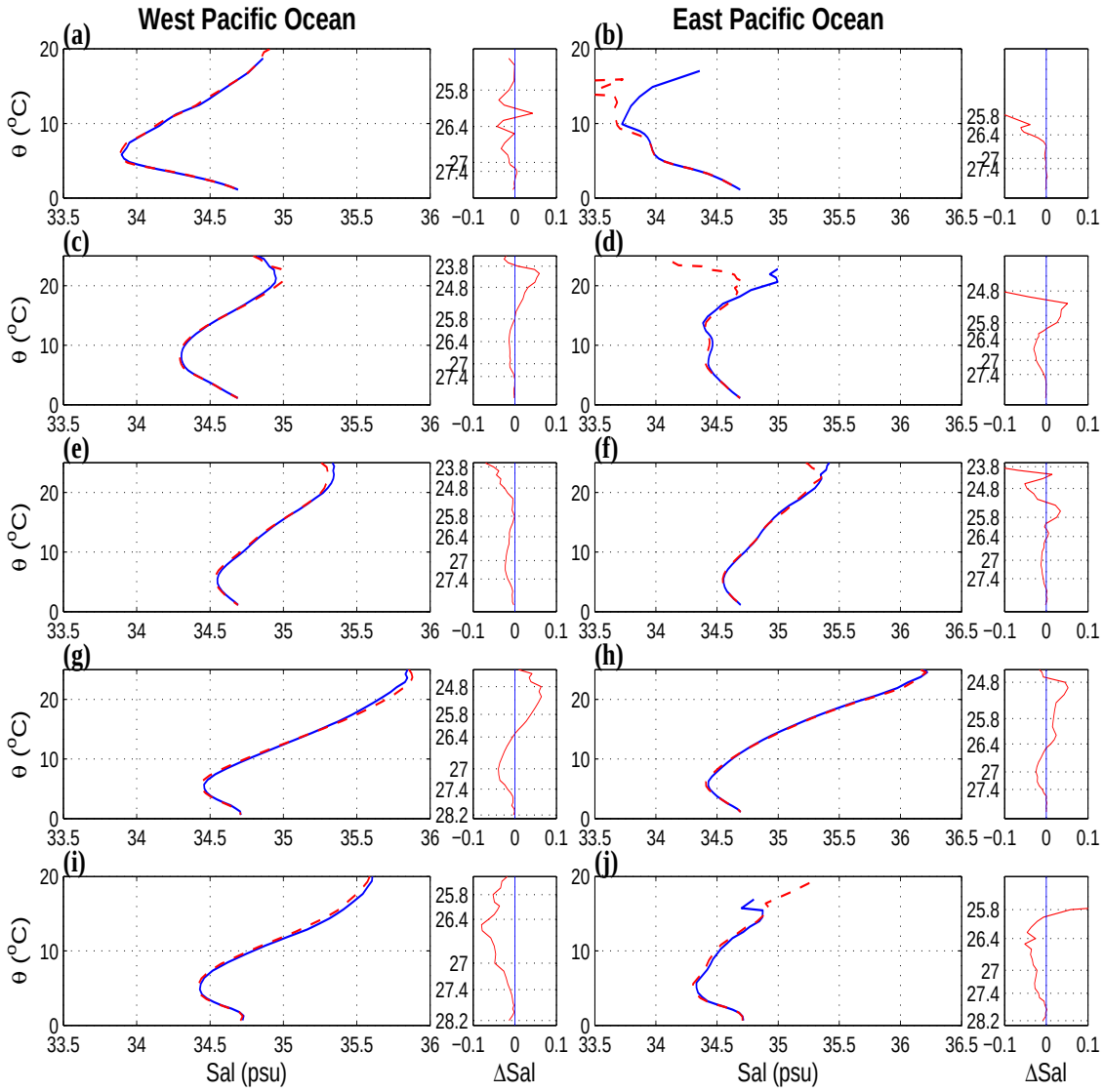

Figure 3.3: Temperature-salinity curves for the Pacific Ocean in five regions between **(a-b)** 50°N-30°N, **(c-d)** 30°N-10°N, **(e-f)** 10°N-10°S, **(g-h)** 10°S-30°S, **(i-j)** 30°S-50°S. The blue curves represents the average historical profile (1970) while red curve represents the average WOCE-period profile (1992). Beside each regional θ-S plot is the associated change in salinity (psu) on isopycnals, with negative values indicating a freshening. Key density surfaces are labelled on the y-axis adjacent to their associated position on the θ-S plot.

minimum is found near the comparatively light 23.8 kg m^{-3} isopycnal.

The increase in salinity and temperature on isopycnals around the shallow salinity-maximum was accompanied by shoaling in both the West-Pacific and Indian Oceans (averaging 6 dbar), two regions linked in the global circulation of upper-ocean waters (Figure 3.1 (b)). There was a deepening in the East-Pacific and throughout the low-latitude Atlantic Ocean.

Changes along the 27.0 kg m^{-3} density surface

The 27.0 kg m^{-3} surface, representative of mode water over much of the globe, shows spatially coherent signals of change. The largest changes on this surface are close to Subantarctic Mode Water (SAMW: 26.5-27.0 kg m^{-3} (Wong, 2005)) formation regions in the mid-latitude South Atlantic and South Indian Oceans (Figures 3.2 (d,i), 3.4 (a)). There is a global coherence in the sign of changes on this surface with 71% of cells showing a cooling and freshening on isopycnals at an average of 0.10°C (0.022 psu). These changes are larger than the changes on the overlying and underlying layers (not shown).

The repeatedly sampled 32°S section in the Indian Ocean shows a 0.26°C cooling and freshening (0.06 psu) along the 27.0 kg m^{-3} isopycnal (1970-1992). This sign of the change is comparable to Bryden et al. (2003) who found a continuous freshening on this density surface since the 1930s, although the changes they observed were weaker in magnitude (approximately 0.03 psu freshening from 1932-1987). In the South Pacific Ocean the signal on the 27.0 kg m^{-3} density surface is a weaker cooling of 0.14°C and a freshening of 0.030 psu.

In the North-West Pacific, the 27.0 kg m^{-3} density surface lies below the salinity minimum (Figure 3.3 (a-b)) and is therefore closer to NPIW (centred on the 26.8 kg m^{-3} density surface (Talley, 1993)) than mode water. Here there is an observed coherent cooling and freshening pattern on the 27.0 kg m^{-3} surface, with the implications of the different stability ratios in this region (Figure 3.4 (c)) being discussed in Section 3.3. The magnitude of this change, -0.11°C and -0.020 psu in the NPIW region (20°N-45°N:120°E-130°W (Talley, 1993)) is smaller than the changes in the Atlantic Ocean, but is significant when compared with the background noise (Figure 3.4 (d)).

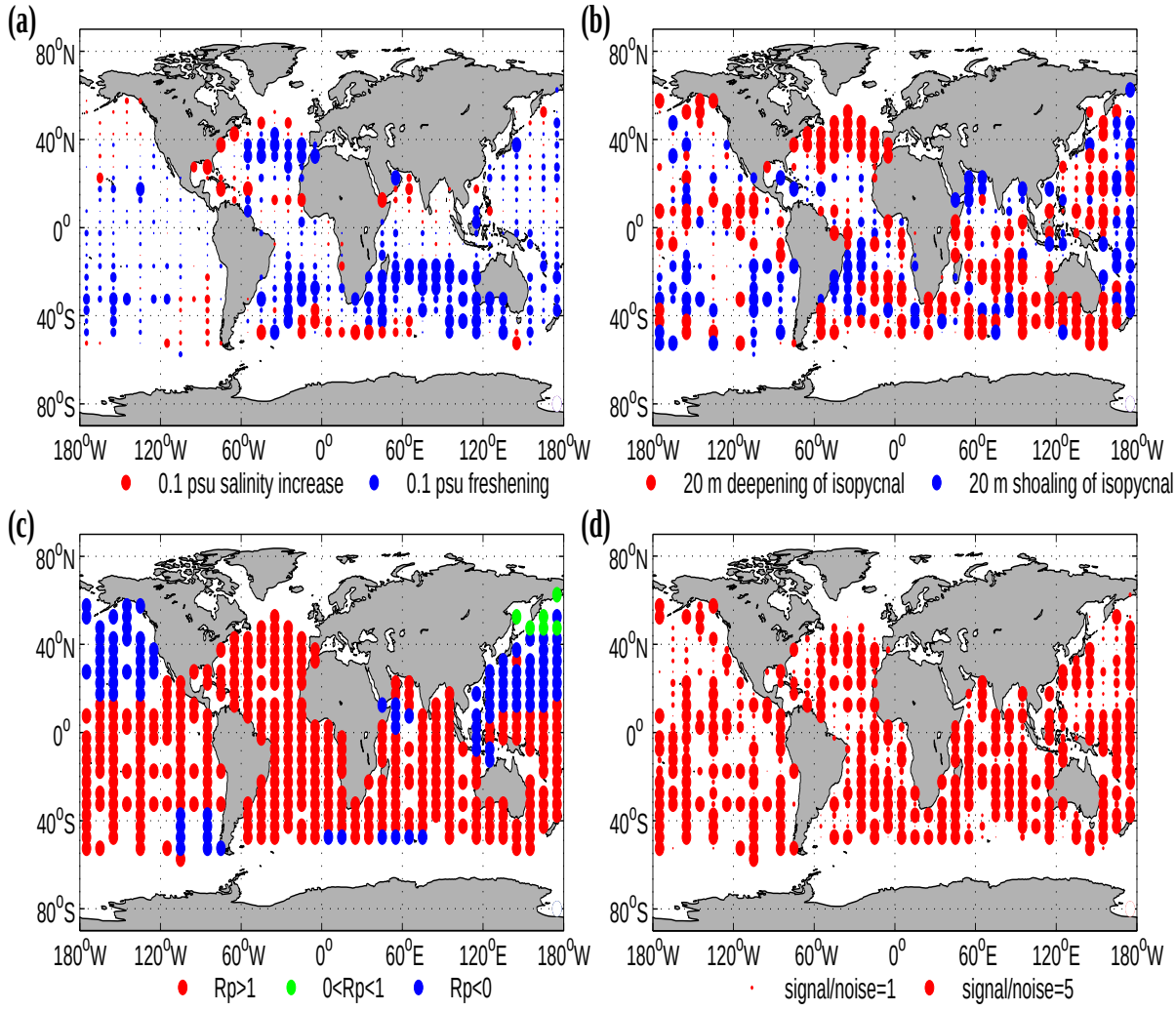

Figure 3.4: Changes along the 27.0 kg m^{-3} density surface (∼1970-1992). **(a)** Changes in salinity along the density surface. **(b)** Changes in the depth of this 27.0 kg m^{-3} isopycnal. **(c)** The stability ratio R_ρ. **(d)** The signal/noise ratio was obtained using Equation 2.11.

In the North Atlantic, the 27.0 kg m^{-3} surface has cooled (by an average 0.18°C) and freshened (0.052 psu). The same cooling signal is also apparent in the low-latitude Atlantic Ocean (Figure 3.2 (c)), and is smaller than at latitudes near the ventilated source region consistent with large scale circulation of this region.

Pressure changes on the 27.0 kg m^{-3} density surface do not have the same globally coherent pattern as temperature and salinity changes, although they do show large scale structures on basin scales. The isopycnal in the North Atlantic Ocean (north of 30°N), the Indian Ocean, and to a lesser extent the North Pacific Ocean, all deepened while it appeared to shoal in the South Pacific. Density surfaces in the South Atlantic Ocean shoaled in the west and deepened in the east.

Freshening at the salinity-minimum

As on the overlying 27.0 kg m^{-3} surface, the salinity minimum shows coherence on large spatial scales, with an average 0.014 psu freshening and 0.07°C cooling globally.

Comparatively small changes in salinity are observed in the equatorial zone (10°S-10°S) far from intermediate water source regions (Figures 3.2 (e-f)-3.3 (e-f)). While the observed small changes are all of the same freshening sign in the equatorial Pacific Ocean, the Indian Ocean shows less coherence (38% of cells showing a salinity increase between 10°S and 10°N).

Although not having a well defined salinity minimum in the northern Atlantic Ocean (Figure 3.2), the slightly fresher waters around 27.4 kg m^{-3} show a widespread pattern of freshening and cooling between 25°N-40°N.

Formed in the Sea of Okhotsk North-West Pacific Ocean, North Pacific Intermediate Water (NPIW) shows reasonably strong freshening and cooling at the salinity minimum (approximately 26.8 kg m^{-3} (Talley, 1993)). While this freshening of NPIW was weaker in magnitude (averaging 0.036 psu: 20°N-50°N:120°E-180°E) than the freshening observed in the Southern Atlantic and South Indian Oceans, it has a good coherence on larger spatial scales, with 81% of cells freshening in this region.

Antarctic Intermediate Water (AAIW) formed in the South-East Pacific Ocean and transported eastward in the Antarctic Circumpolar Current (Hanawa and Talley,

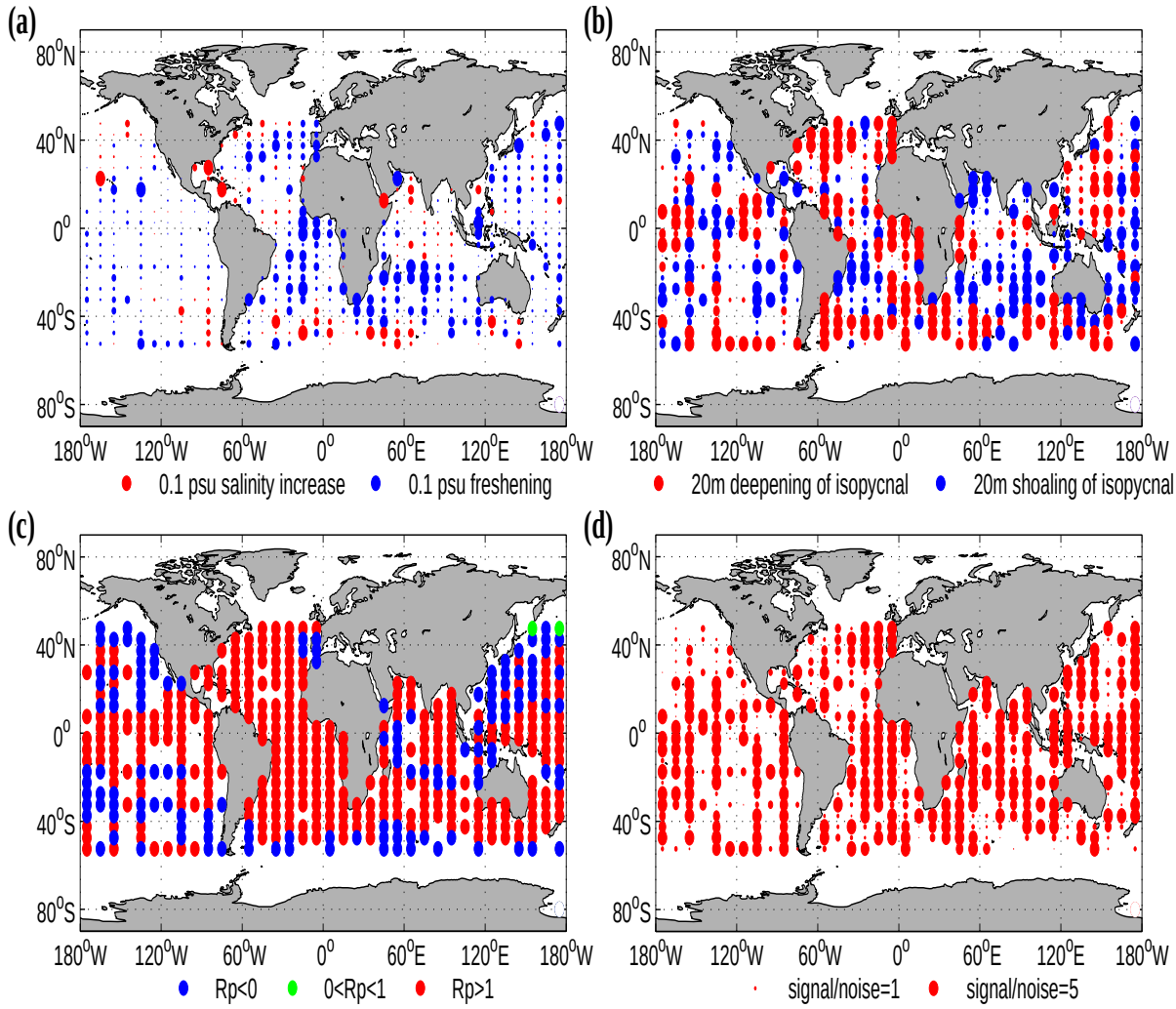

Figure 3.5: Changes at the salinity-minimum (∼1970-1992). **(a)** Changes in salinity on the most representative salinity-minimum isopycnal. **(b)** Changes in the depth of this surface. **(c)** The stability ratio R_ρ. **(d)** The signal/noise ratio was obtained using Equation 2.11.

2001), shows the largest freshening between 1970 and 1992 (Figure 3.5 (a)). South of the equator in the Atlantic Ocean (40°S-0°), 81% of cells show a coherent freshening (averaging 0.025 psu) and cooling (0.12°C). This strong freshening signal in AAIW propagates through to the South Indian Ocean basin. The west of the subtropic gyre (40°S-25°S: 30°E-80°E) freshened by 0.051 psu, while further from the Pacific Ocean source region in the east, a weaker 0.033 psu freshening was observed.

In the South-West Pacific Ocean and North-Indian Ocean there is a shoaling of the salinity minimum isopycnal in the water column (Figure 3.5 (b)). Elsewhere the pattern is one of deepening, with changes between 10 dbar and 100 dbar in the high-latitude Atlantic Ocean and throughout the Southern Ocean. In the North and West-Pacific Ocean the vertical movement of the salinity minimum isopycnal (Figure 3.5 (b)) is not as coherent on large spatial scales as the water mass changes (Figure 3.5 (a)).

Changes along the 27.8 kg m^{-3} density surface

The 27.8 kg m^{-3} density surface is found below the salinity minimum and close to the deep salinity-maximum (1200-1700 dbar). There is significant spatial variation in the magnitude of temperature and salinity changes on density surfaces in different basins. The Pacific and Indian Oceans, both oceans with weak deep water circulation and distant from formation regions, show a small signal of salinity change which is not significant (generally less than 0.01 psu).

The pattern of change on the 27.8 kg m^{-3} density surface is strongly tied to the global circulation of deep water. The salinity and temperature signals in the North Atlantic and Southern Oceans are generally an order of magnitude larger than elsewhere in the globe. In these Indian and Pacific Oceans the flow of these denser layers is much weaker and the age of the water mass since atmospheric ventilation is older. Salinity changes on the 27.8 kg m^{-3} surface in the Atlantic and Southern Oceans are significantly less than in the overlying layers, and as such the scales used in Figure 3.6 (a) are smaller than in Figures 3.1, and 3.4-3.5.

There are four main regions of significant change on the 27.8 kg m^{-3} isopycnal. The first of these is in the North Atlantic Ocean near the NADW formation area (60°N-45°N), where a broad regional cooling (averaging 0.24°C) and freshening (0.041 psu) along this isopycnal is seen.

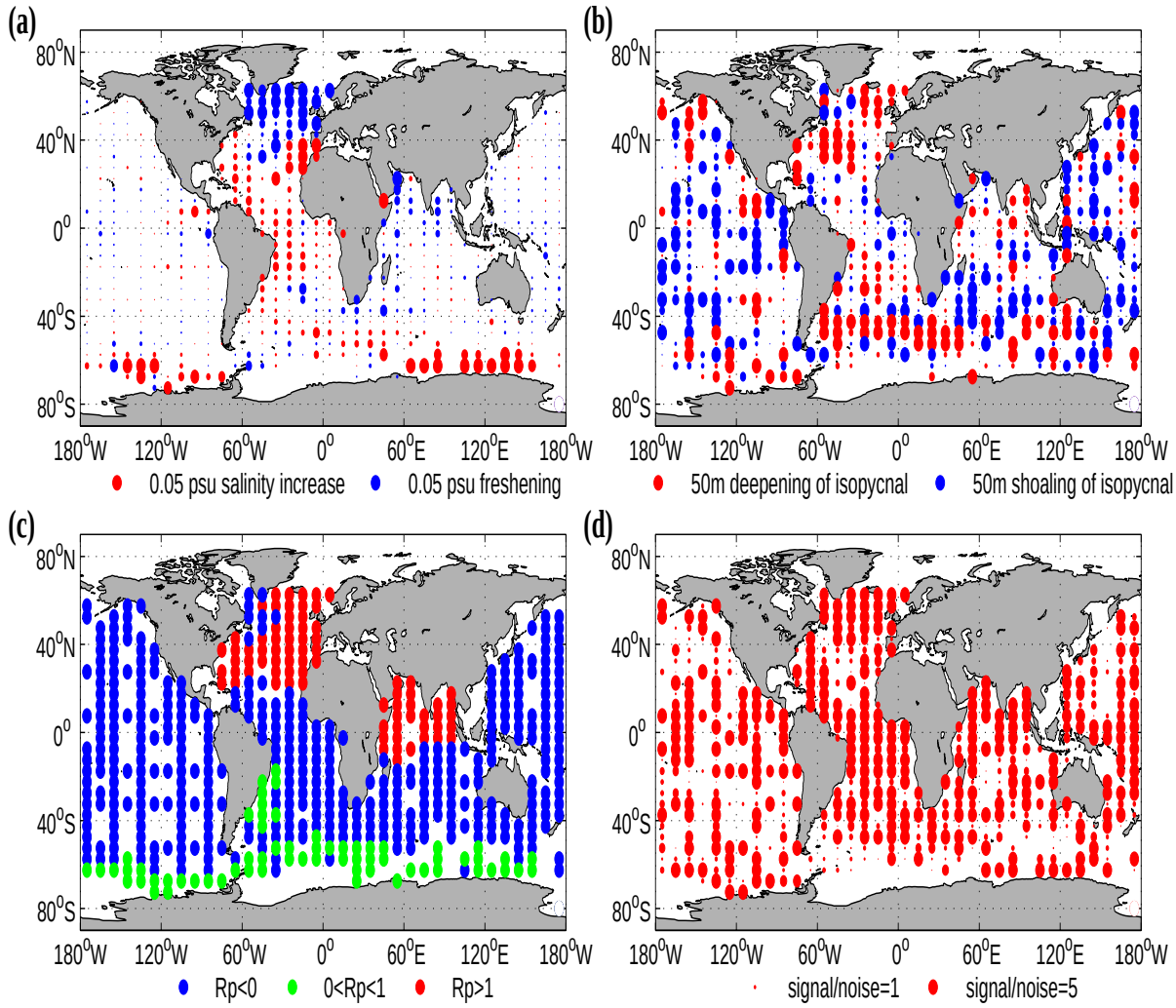

Figure 3.6: Changes along the 27.8 kg m^{-3} density surface (∼1970-1992). **(a)** Changes in salinity along the density surface. **(b)** Changes in the depth of this 27.8 kg m^{-3} isopycnal. **(c)** The stability ratio R_ρ. **(d)** The signal/noise ratio was obtained using Equation 2.11.

Table 3.1: Changes in in situ temperature, salinity, and pressure along isopycnals of representative water masses (∼1970-1992). Note that a negative value represents a cooling, freshening, or shoaling. Figure 3.7 shows the regions over which the average changes were calculated.

	Surface:	**Represents:**	**Ocean:**	**ΔT** (°C)	**ΔS** (psu)	**Δp** (dbar)
A	Smax		Global	0.08	0.030	0
B	Smin	Int. waters	Global	-0.09	-0.018	8
C	Smin	NPIW	N. Pacific	-0.21	-0.033	0
D	Smin	AAIW	S. Atlantic	-0.14	-0.027	8
E	Smin	AAIW	S. Indian	-0.18	-0.034	-3
F	26.8-27.6	300 m+	N. Atlantic	-0.11	-0.034	37
G	27.8	CDW	Southern Ocean	0.05	0.005	5
H	27.8	NADW	N. Atlantic	-0.09	-0.015	34
I	27.4-28.0	300 m+	Subpolar N. Atlantic	-0.19	-0.035	24

South of this (45°N-20°S) in the Atlantic Ocean there is a weaker warming and salinity increase (0.012 psu) that occurs across the whole ocean basin, with the pattern and magnitude of the signal being stronger in the east near the Mediterranean Sea. Some of these salinity increases in the east may be caused by the well documented salinity increases in Mediterranean Outflow Water (Curry et al., 2003; Arbic and Owens, 2001). The results presented here are broadly consistent with Bryden et al. (1996) who found salinity and temperature increases in deep water density surfaces above 2000 dbar, and with Curry et al. (2003) who observed salinity increases of 0.05 psu (30°N-40°N) and 0.02-0.04 psu (30°N-25°S) on the 27.8 kg m^{-3} density surface.

Further south in the Atlantic Ocean between 20°S and 30°S, there are continued salinity increases and warming of the density surface; however these are of a smaller magnitude than in the more recently formed NADW water.

In the Southern Ocean south of the Polar Front there is a distinct circumpolar warming and salinity increase on the 27.8 kg m^{-3} density surface. This signal is circumpolar in extent around Antarctica and averages 0.30°C (0.023 psu) south of 60°S.

In the Southern Ocean (Atlantic and Pacific Ocean sectors), the isopycnal is observed to deepen significantly (up to 80 dbar: Figure 3.6 (b)) between the Subtrop-

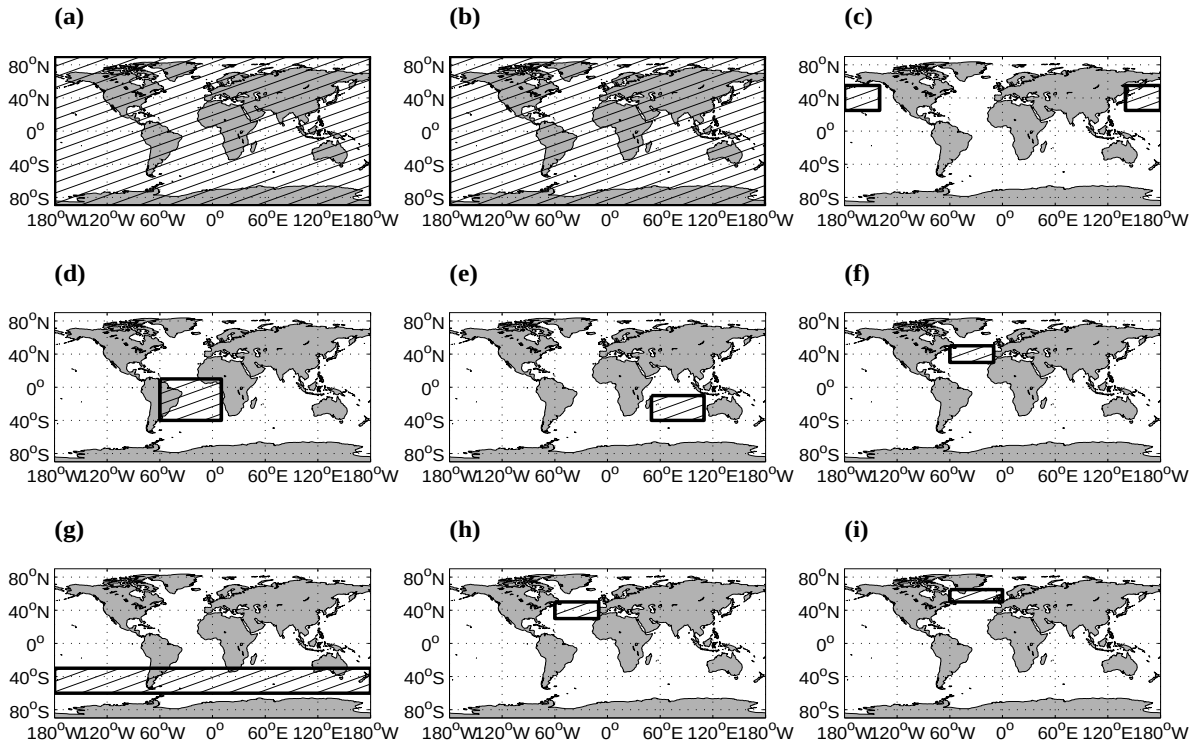

Figure 3.7: Regions used for temperature and salinity changes reported in Table 3.1.

ical Front and the Polar Front. In contrast there is comparatively little change in pressure on this density surface in the mid and low-latitude Atlantic Ocean, with any vertical movement being of a mixed sign. In the South Pacific Ocean the 27.8 kg m^{-3} density surface has shoaled on large spatial scales, averaging 30 dbar (140°E-80°W:40°S-0°) between 1970 and 1992. This is in a region where the corresponding water property changes are mixed and relatively small in magnitude.

3.3 Interpreting changes on density surfaces in a pressure reference frame

As discussed in Chapter 2.2, there are two mechanisms that cause a change in ocean temperature and salinity on pressure surfaces. The first is simply a *vertical displacement of density surfaces* in the water column without any water mass change. The second are temperature and salinity anomalies from air-sea or sea-ice interactions that are advected into the ocean interior *along density surfaces*.

So far in this chapter the movement of isopycnals has been illustrated in Figures 3.1 (b) and 3.4-3.6 (b), and the spatial coherence of this signal has been discussed. The contribution of this displacement to the temperature and salinity signal on pressure surfaces has not been quantified.

Interpreting along-isopycnal changes in a pressure reference frame

The remainder of this section deals with the use of the stability ratio (R_ρ) to interpret along-isopycnal temperature and salinity changes as a change on a pressure surface. It should be stressed that the following section relates *only* to the observed along-isopycnal water property changes, and that there is also an additional displacement component to the changes on pressure surfaces that is not discussed here (see Chapter 6 for this discussion).

As explained in Chapter 2.2 and illustrated in Figure 2.5 (h), the widespread salinity increases observed at the shallow salinity-maximum will appear as salinity increases on pressure surfaces. While there is obviously a density-compensating warming on the density surface, it is not clear from Figures 3.1-3.6 (a) whether there is also a warming component that occurs independently of these salinity increases on pressure surfaces. This separation of the temperature and salinity signals is discussed further in Chapter 6.

With the exception of the North Pacific, the 27.0 kg m^{-3} density surface is found below the shallow salinity-maximum and above the salinity minimum in the water column across all ocean basins (Figures 3.2-3.3), and is therefore in a region with a positive stability ratio (Figure 3.4 (c): Red dots). Following the reasoning in Chapter 2.2 (Figure 2.5 (a) and summarised in Table 2.2), most of the observed cooling and freshening on the density surface seen in Figure 3.4 (a), should be interpreted as a contribution to a warming and freshening on pressure surfaces (in the absence of any vertical isopycnal displacement).

In the North Pacific, the 27.0 kg m^{-3} density surface is situated below the salinity minimum in a region with a negative $\theta-$S slope (Figure 3.4 (c)). As such, the cooling and freshening on isopycnals appears as a cooling and freshening on pressure surfaces.

Following on from this, the spatial coherence of the temperature and salinity changes on pressure surfaces was examined (resulting from along-isopycnal changes only). This was done by reversing the sign of the signal in Figure 3.4 (a) in each grid box if R_ρ (Figure 3.4 (c)) was greater than 1 for temperature and $0 < R_\rho \leq 1$ for salinity (Figure not shown). Globally this revealed good spatial coherence on pressure surfaces, with 68% of grid cells warming, and 71% freshening. Note again that this change on pressure surfaces is independent of the vertical displacement of the 27.0 kg m^{-3} isopycnal, which would also have a contribution to the temperature and salinity change on pressure surfaces.

On the 27.0 kg m^{-3} density surface the relationship between the stability ratio and the sign of the water property changes is clearly demonstrated in the East Pacific Ocean. Off the west coast of Chile in the AAIW formation region, Figure 3.4 (a) clearly shows a region of increasing salinity. While this may initially appear different from the rest of the southern basin, examination of Figure 3.4 (c) shows that this occurs in a region where the 27.0 kg m^{-3} isopycnal sits below the salinity minimum ($R_\rho < 0$), with these along-isopycnal changes being equivalent to a warming on pressure surfaces ($\sim$200 dbar). Therefore, it is in agreement with the rest of the surrounding basin which shows a cooling on isopycnals where $R_\rho > 1$ (also a warming on pressure surfaces if considered independently of isopycnal movement). The same phenomenon is evident in the North-East Pacific Ocean, giving a coherent pattern of change across the whole Pacific Ocean.

In the analysis used in the thesis, the isopycnal that *best represents* the salinity-minimum can be situated slightly above or below the *actual* salinity-minimum in the water column. This can explain the lack of coherence in the sign of R_ρ over regions of the globe with a well defined salinity-minimum (Figure 3.5 (c)). However given that the large number of density surfaces used in this analysis, the salinity-minimum is reasonably approximated on a regional scale. As such the observed freshening along density surfaces at the salinity-minimum can only be explained by a freshening on pressure surfaces (Chapter 2.2, Figure 2.5 (g)). Like the signal on the shallow salinity-maximum, it is uncertain whether there is also an accompanying warming on pressure surfaces caused by the along-isopycnal cooling and freshening. There will also be an additional temperature and salinity signal on pressure surfaces due to the vertical displacement of density surfaces in the water column.

On the 27.8 kg m^{-3} surface, the stability ratio (R_ρ) is negative throughout the Pacific, mid-latitude Atlantic, and the South Indian Oceans (Figure 3.6 (c)). This means that if there were no vertical displacement of the surface, the observed warming and salinity increases on the isopycnal would result in warming and salinity increases on pressure surfaces (Chapter 2.2, Figure 2.5 (d)). In the NADW formation region in the North Atlantic Ocean, the positive slope of the θ-S curve (Figure 3.6 (c)) is such that the observed cooling and freshening has a warming and freshening contribution to the change on pressure surfaces (Chapter 2.2, Figure 2.5 (a)). South of the Polar Front in the Southern Ocean the stability ratio is between 0 and 1, meaning the strong circumpolar warming and salinity increases found in CDW reflects a warming and freshening on pressure surfaces (Figure 2.5 (a)) if considered independently from the isopycnal displacement mechanism.

3.4 Integrated temperature and salinity changes

Examining temperature and salinity changes along a single density surface is a useful way of determining the changes in a particular water mass. However by taking the changes on all 40 neutral density layers used in this thesis, we can gain a more complete analysis of changes throughout the water column and can more accurately estimate steric sea-level change.

Zonally averaged temperature and salinity changes

Figure 3.8 (a) shows the salinity (and consequently the temperature) changes on isopycnals when zonally integrated, and then interpolated to depth surfaces. The cooling and freshening observed in northward-spreading AAIW from 40°S-5°N is the dominant coherent spatial feature, and is evident in all basins (Figure 3.9), with the magnitude of change being largest closer to the source regions in the Atlantic and Indian Oceans. These clear changes along isopycnals in subducting intermediate water illustrate well how water mass changes propagate through the ocean on density surfaces rather than pressure surfaces.

The second cooling and freshening pattern can be found along intermediate level and deep water isopycnals north of 40°N (Figure 3.8 (a)). This cooling and freshening predominately comes from strong freshening of the North Atlantic Ocean between 1970 and 1992 (Figure 3.9 (a)). In this same latitude band, the Pacific Ocean (Figure 3.9 (c-d)) also shows a freshening and cooling on isopycnals; however the relatively

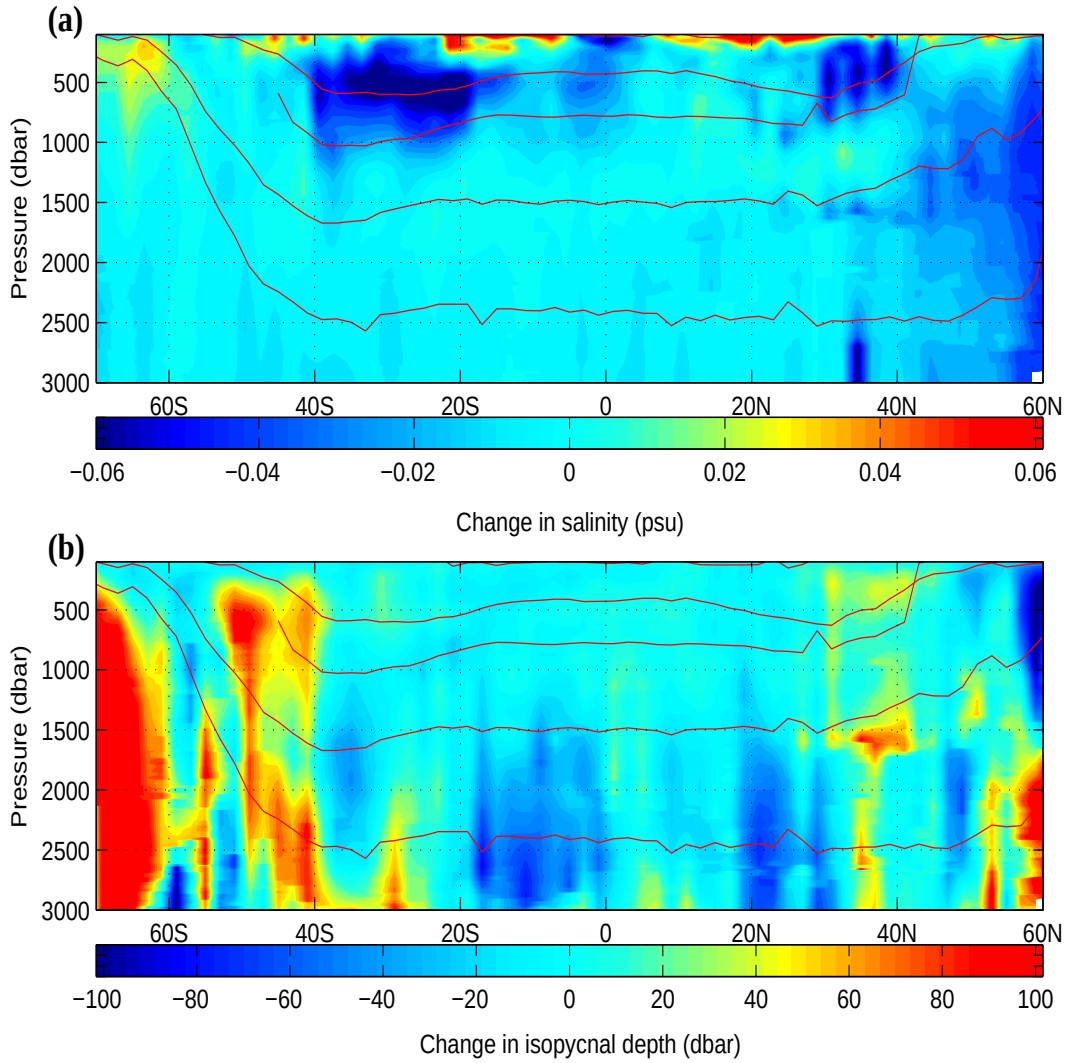

Figure 3.8: Zonally averaged changes (∼1970-1992) in **(a)** salinity (psu) along isopycnals mapped to pressure surfaces, where blue is freshening (top). **(b)** shows changes in isopycnal pressure (dbar) where red is a zonally averaged deepening of isopycnals. The shallow salinity-maximum (very top), the 27.0 kg m^{-3}, the salinity-minimum, the 27.8 kg m^{-3}, and the 28.0 kg m^{-3} neutral density surfaces are shown in both panels, with the blue line representing the zonally averaged pressure in 1970 and the red being 1992. Note that the top 100 m has been removed to minimise seasonal bias in observations.

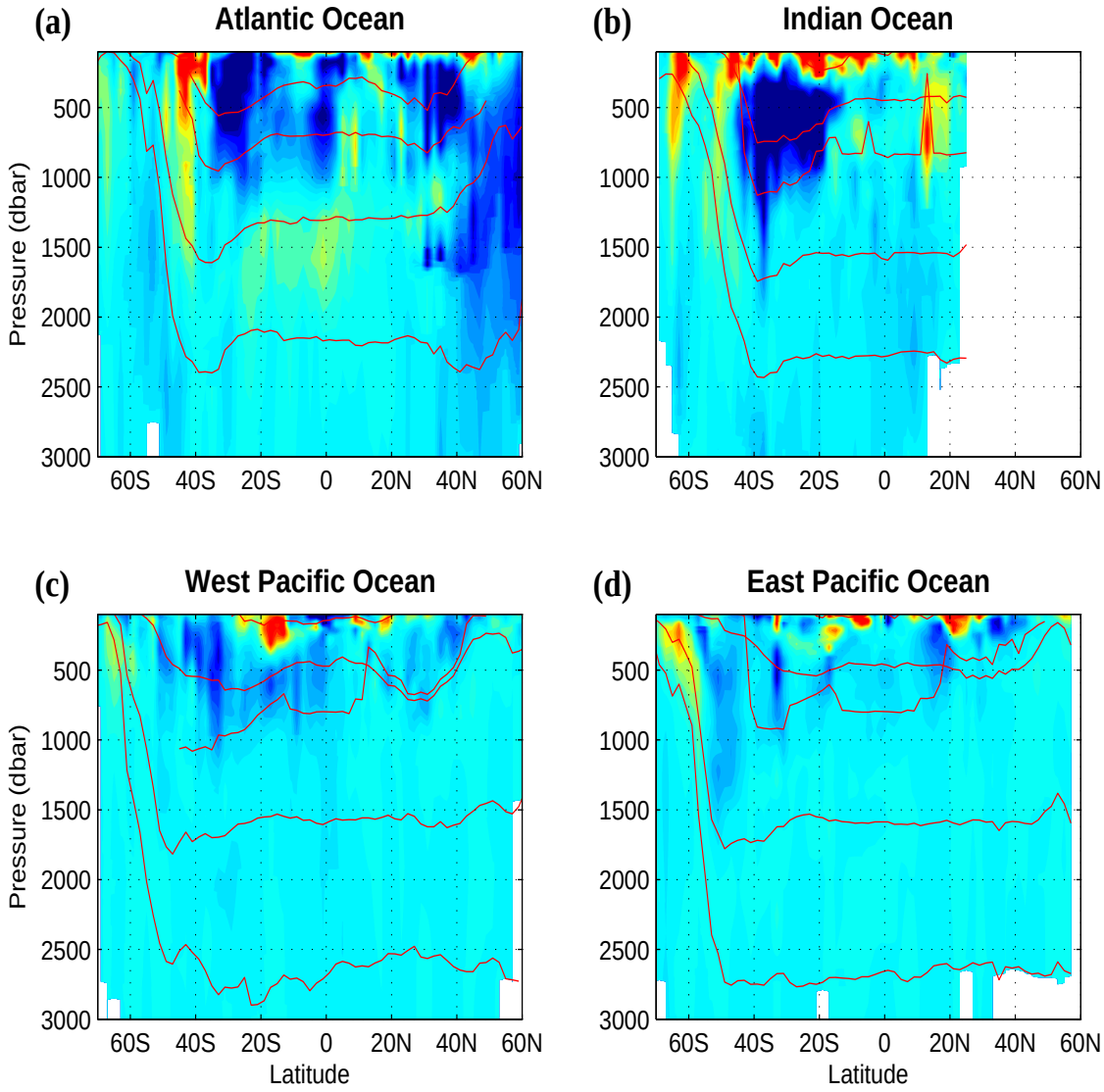

Figure 3.9: Zonally integrated salinity change on density surfaces (mapped to pressure surfaces) by ocean basin (∼1970-1992). Red represents increasing salinity along isopycnals (and an associated temperature increase) while dark blue is a freshening (cooling). The average depths of the shallow salinity-maximum, the 27.0 kg m^{-3}, the salinity-minimum, the 27.8 kg m^{-3}, and the 28.0 kg m^{-3} surfaces are superimposed. Note that the salinity-minimum is found above the 27.0 kg m^{-3} surface in the North Pacific. Salinity changes that make up the zonal average tend to have a range of 0.7 psu at the salinity maximum, 0.3 psu on the 27.0 kg m^{-3} surface, and 0.1 psu in deeper waters.

weak circulation of deep waters mean that the magnitude of the deep water changes deeper than 1500 dbar are significantly smaller than those of the dominant North Atlantic Ocean signal.

In the mid and low-latitudes of all ocean basins, it is clear that the largest changes in water mass properties on isopycnals occur in the upper 1500 dbar of the water column (Figure 3.8 (a)). This is not surprising given the deeper water masses have remained isolated from the atmosphere for longer periods of time.

Zonally averaged pressure changes on isopycnals

While atmospheric temperature and salinity anomalies subducted into the ocean interior tend to be preserved along surfaces of constant density, the surfaces themselves are free to fluctuate vertically in the water column with mesoscale eddies, internal waves, and general internal ocean variability and change. Figures 3.8 (b) and 3.10 show deepening of isopycnal surfaces between 40°S and 50 °S, and further deepening poleward of 60°S.

In the mid-latitude Northern Hemisphere, isopycnals in the 27.2-27.8 kg m^{-3} range deepen by an average 10-20 dbar (Figure 3.8 (b)). As with the salinity change in the same region, the majority of this signal comes from the North Atlantic (Figure 3.10 (a)) rather than from the Pacific Ocean (Figure 3.10 (c-d)). The zonally averaged mid-latitude deepening of isopycnals is not as large or coherent in the Northern Hemisphere as it is in the Southern Hemisphere.

In the subtropical gyres (10°-30°) of both the northern and Southern Hemispheres, there is a zonally-averaged shoaling pattern in the isopycnals found below 1500 dbar (Figure 3.8 (b)). This shoaling comes mainly from the Pacific and East Indian Oceans (Figures 3.6 (a), 3.10 (b-d)), with the large surface areas of these basins meaning that they tend to dominate any global zonally averaged signal.

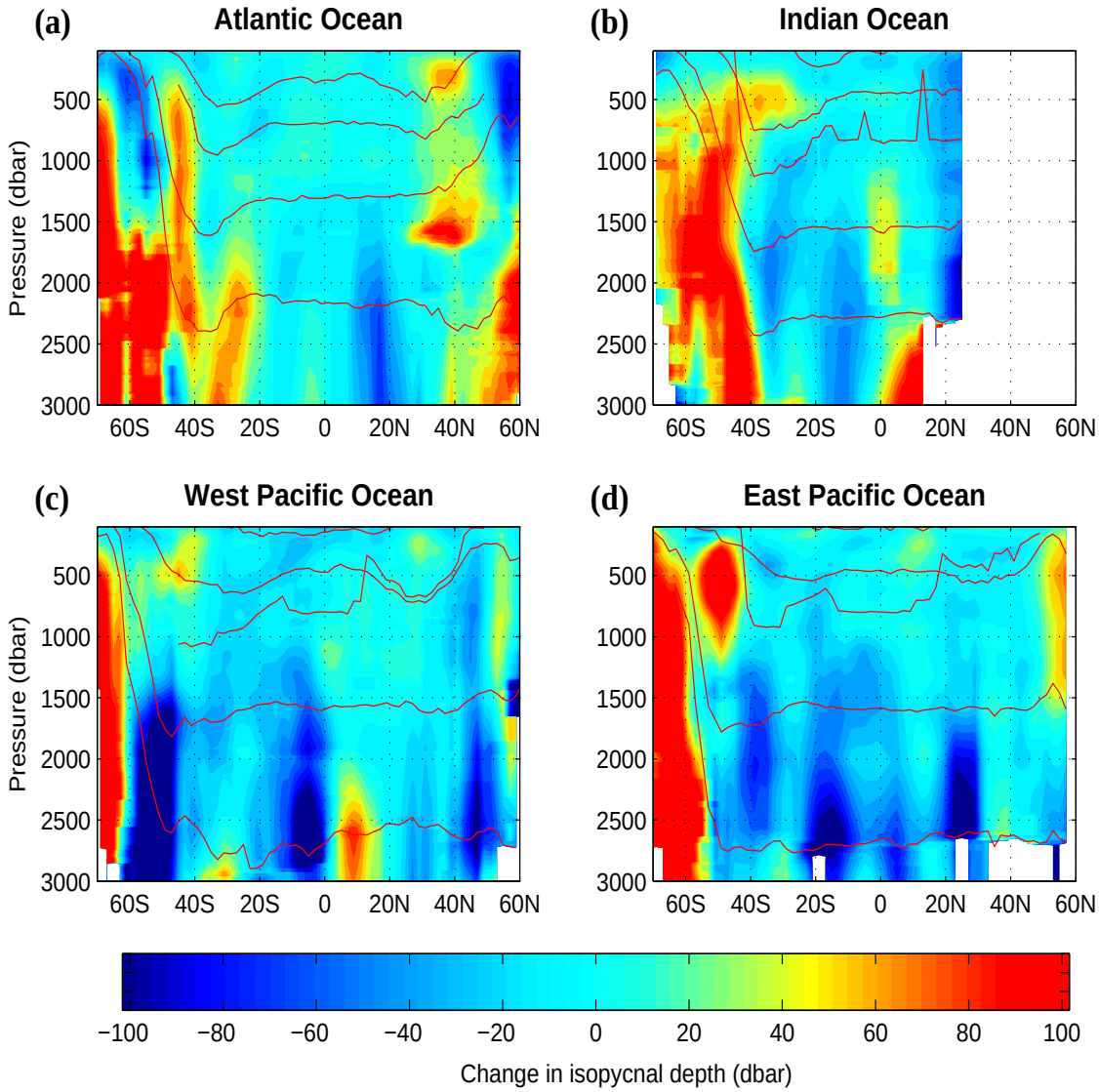

Figure 3.10: Regional zonally averaged change in isopycnal depth by ocean basin (∼1970-1992). Red represents a zonally averaged deepening of isopycnals, while blue is shoaling. The average depths of the shallow salinity-maximum, the 27.0 kg m^{-3}, the salinity-minimum, the 27.8 kg m^{-3}, and the 28.0 kg m^{-3} surfaces are superimposed. Note that the salinity-minimum is found above the 27.0 kg m^{-3} surface in the North Pacific.

Changes in steric height integrated to 1000 dbar

As a consequence of the warming of the upper water column and the deepening of isopycnals, there have been widespread increases in steric sea surface height from 1970 to 1992. Figure 3.11 shows the zonally averaged 0-1000m and 0-3000m steric height changes across all three oceans, while Figure 3.12 shows the two dimensional spatial distribution of these changes (0-1000 dbar). As discussed in Chapter 2, the changes in steric height in the upper 100 dbar are estimated from the Hadley SST time-series (Rayner et al., 2003).

Zonally averaged increases in steric height of 20-40 mm (0-1000 dbar) are evident in all ocean basins south of 30°S (Figure 3.11 (a,c,e,g)). This increase tends to be weakest near 60°S and in most ocean basins is greatest between 40°S and 50°S. There are equivalent globally averaged steric sea-level rises in the Northern Hemisphere between 20°N and 40°N, although this signal is dominated by the contribution from the Atlantic Ocean (Figure 3.11 (c)). The zonally integrated changes in equatorial regions are small when compared with the mid-latitude increases. This small equatorial increase is a result of a Pacific Ocean fall in steric sea surface height offsetting small Atlantic Ocean rises in equatorial regions (Figure 3.11 (c,e)).

Globally averaged large steric rises of 0-30 mm are evident between 40°S and 60°S in the Southern Hemisphere (Figure 3.11 (a), 3.12: 1970-1992). A symmetrical pattern around the equator exists, with equivalent changes of 0-40 mm seen in the Northern Hemisphere mid-latitudes (20°N-45°N: Figure 3.11).

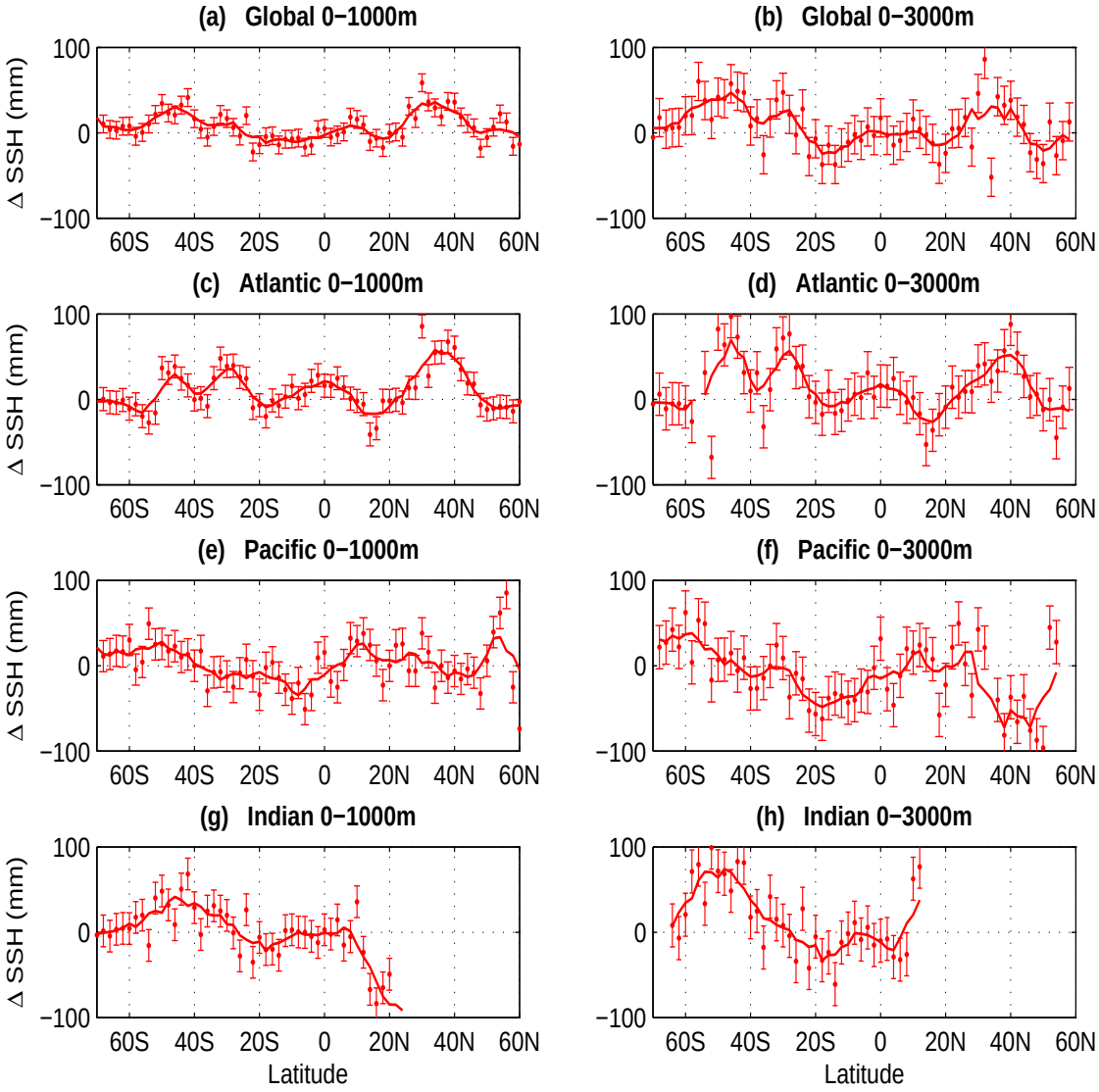

Figure 3.11: Zonally averaged surface steric height change from 1970 to 1992 (mm). **(a-b)** Globally. **(c-d)** In the Atlantic Ocean. **(e-f)** In the Pacific Ocean. **(g-h)** In the Indian Ocean. The plots on the left side show steric sea-level change referenced to 1000m, while on the right they are referenced to 3000m. Positive values on the y-axis indicate a rise in sea surface height, while the x-axis shows latitude. The Hadley SST time-series (Rayner et al., 2003) estimates of steric height have been added to the top 100 dbar. Error bars are shown to one standard deviation and are calculated used methods described in Chapter 2.5.

It should be remembered that the global zonal averages in Figure 3.11 (a-b) have a large contribution from the Pacific Ocean, particularly in the equatorial region. In both Pacific and the Indian Oceans, deep water isopycnals are observed to have shoaled, which has led to a cooling over much of the upper-1000 dbar, and a net drop in steric sea-level in the low and equatorial latitudes (Figure 3.12).

In the Atlantic Ocean there was an average increase of approximately 25 mm (0-1000 dbar). There was a clear zonal pattern to these changes, with increases in steric sea surface height of up to 50 mm in the mid latitudes, with comparatively little change in low latitudes (Figure 3.12). The steric height increases in the upper 1000 dbar of the Atlantic Ocean were greater in the Northern Hemisphere (peaking at 35°N-40°N) than in the Southern Hemisphere (20°S-50°S).

In both the low-latitude Pacific Ocean (35°S-20°N) and Indian Ocean (30°S-10°N), there is evidence of a decrease in steric height (Figures 3.11 (e-h), 3.12). This decrease of up to 50 mm is strongest in the West Pacific Ocean, through the Indonesian Throughflow, and into the Indian Ocean. The majority of the steric sea-level decrease in the low and mid-latitude Pacific Ocean is as a result of cooling in the upper 1000 dbar (figure not shown), reflecting the small temperature and salinity variability in the deep water in these two oceans. Poleward of 20°N in the Pacific Ocean the sign of change is less coherent, with an increase in steric height off Japan driven by warming and freshening on pressure surfaces in the NPIW formation region, and a steric sea-level decrease elsewhere. A steric sea-level rise is observed in the East Pacific Ocean centred on 10°N, 120°W.

The zonally averaged changes in the Indian Ocean follow a similar pattern to the Pacific, with a 20 mm decrease in steric height centred around 20°S and comparatively little change directly on the equator. Poleward of 30°S there are significant increases in steric height, peaking at around 40 mm at 45°S (0-1000 dbar: Figure 3.11 (g)). The average change in the east of the Indian Ocean (0°-30°S) is approximately 60% larger that in the west (Figure 3.12).

Poleward of the Subtropical Front, the Southern Ocean shows a near circumpolar increase in steric height of a similar magnitude to the largest changes found elsewhere (Figure 3.12). The one exception is in the Atlantic Ocean sector, which shows slight decreases (10-20 mm) between 50°S and 60°S (Figures 3.12, 3.11 (c-d)).

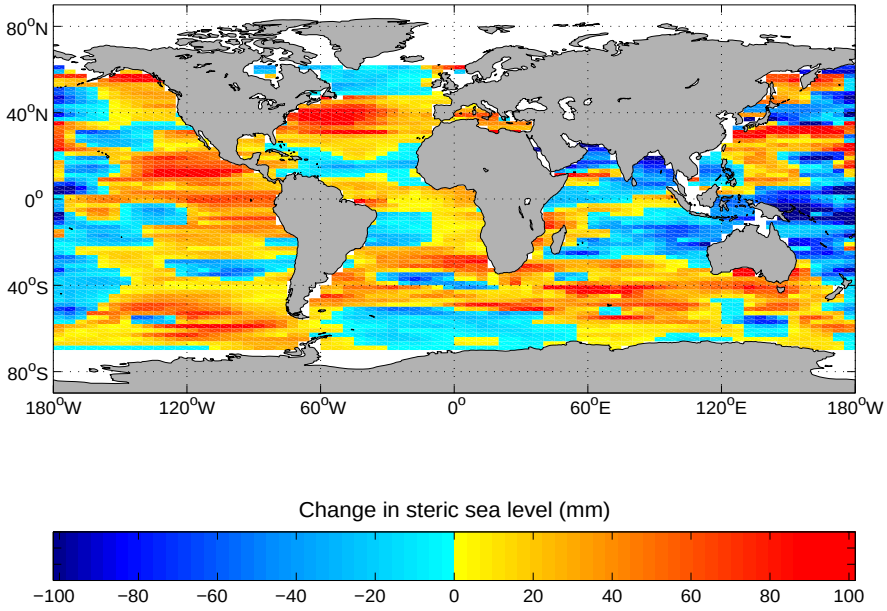

Figure 3.12: Surface steric height change from 1970 to 1992 relative to 1000 dbar (mm). Grid boxes with no observations have been filled with an interpolated value (east-west linear interpolation), and the Hadley SST dataset has been used for the upper 100 dbar. Positive (red) values indicate a rise in sea surface height.

Changes in steric height integrated to 3000 dbar

Extending the changes in steric height from the surface to 3000 dbar encompasses the deep water layers (Figure 3.11 (b)). In all oceans the general zonally averaged pattern remains the same as the 0-1000 dbar integral; however the magnitude of change increases. In Figure 3.11 (b) the globally averaged mid-latitude steric rises are more pronounced at approximately 40 mm in both hemispheres. Likewise the low-latitude zonally averaged drops in steric height (10°-20° in both hemispheres) encompasses more of the Pacific and Indian Ocean deep water shoaling (and hence a cooling on pressure surfaces), and the global signal is magnified to approximately 20 mm (Figure 3.11 (b)). Little change in zonally averaged steric sea-level is evident directly on the equator (Figure 3.11 (b)).

When changes in sea-surface height in the Atlantic Ocean were integrated from 3000 dbar to the surface, the rise south of 30°S is larger, and the magnitude of the steric sea-level changes between the two hemispheres becomes similar (Figure 3.11 (d)). In the Southern Hemisphere, this 1000-3000 dbar layer encompasses the salinity minimum intermediate water (Figure 3.8 (a)) and more importantly the observed deepening of isopycnals in the Atlantic Ocean (Figure 3.10 (b)). In the equatorial region the difference in steric height between 0-1000 dbar and 0-3000 dbar is minimal, and is consistent with the comparatively weak temperature, salinity, and pressure changes observed in this depth range (Figures 3.9 (a), 3.10 (a)). Including the 1000-3000 dbar layer in the Indian Ocean adds a further 30-40 mm increase in the mid-latitudes (Figure 3.11 (h)).

Zonally back-projected heat content, volume, and P-E changes

The freshwater inputs required to produce the observed salinity changes can be seen in Figure 3.13 (a). The method used to estimate these apparent freshwater fluxes at the surface are described in Chapter 2.6. In the density layers that outcrop between 30°S and 30°N (near the salinity-maximum) there are small decreases in precipitation-minus-evaporation. While these decreases in the apparent precipitation-minus-evaporation appear small when compared with the changes poleward of 45° north and south and with the confidence intervals, the volume of these layers (both vertically and when integrated to the equator) are much smaller than the density layers that outcrop at higher latitudes. However between 30°S and 30°N the pattern of decreases in apparent precipitation-minus-evaporation is coher-

ent across all density layers that outcrop in this latitude band and suggests that the decreases are important.

Statistically significant increases in precipitation-minus-evaporation or summer sea-ice melt of 20-90 mm yr^{-1} are inferred to occur between 40°N and 60°N (1970-1992) (Figure 3.13 (a)). In the Southern Hemisphere from 45°S to 60°S these increases are between 20 and 110 mm yr^{-1} from 1970 to 1992. This is in a region where the zonally averaged annual P-E in models is approximately 600 mm yr^{-1} (CSIRO Mk3.0: Gordon et al. (2002)), and therefore represents approximately an 20% increase. In the Northern Hemisphere there is a symmetrical increase for the 1970-1992 period, although the changes are slightly weaker than in the south.

It should be noted that as discussed in Chapter 2.6, we can only be certain of these freshwater flux changes at the outcropping region of the shallow salinity-maximum (∼20°S and ∼20°N) and the salinity minimum (∼55°S and ∼45°N). Elsewhere the estimates may include some density compensating response to heat flux changes, and hence have been termed 'apparent' P-E.

Across most latitudes of the globe there are increases in apparent heat fluxes (Figure 3.13 (b)). Again there is strong symmetry about the equator between the two hemispheres, with the strongest increases in the mid and high-latitudes. As in Figure 3.13 (a) at these high latitudes the large apparent surface flux increases can be partially attributed to integrating across the large volumes of the density layers that outcrop at high-latitudes.

Calculating heat content change vertically in the water column (Figure 3.13 (e)) results in a different pattern to the along-isopycnal changes. Using this more conventional method, there are heat content increases poleward of 35°S in the Southern Hemisphere, with decreases occurring between 35°S and 5°N. This suggests that the deeper isopycnals in the mid-to-low latitudes have shoaled, an idea that is supported in Figure 3.8 (b) and is equivalent to a change in steric sea level (Figure 3.13 (d)).

Despite both being a measure of heat content, Figures 3.13 (b) and (e) show distinctly different patterns. Figure 3.13 (e) is the more conventional method, where the observed ocean temperature changes are integrated vertically in the water column. This indicates where additional heat is *stored* in the ocean, and gives a more

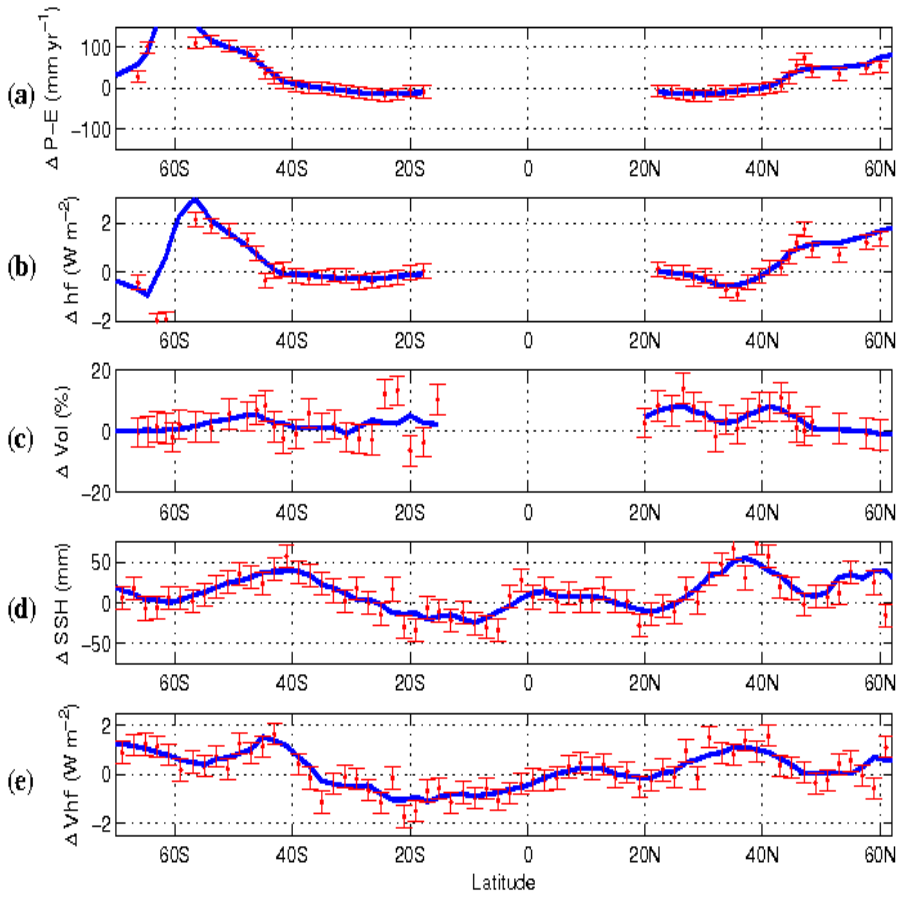

Figure 3.13: Zonally back-projected changes from 1970 to 1992 in **(a)** apparent P-E fluxes, **(b)** apparent heat fluxes, and **(c)** volume. Each red dot represents the change on a density layer integrated from the outcropping region to the equator. **(d)** Steric height and **(e)** heat content changes on pressure surfaces are zonally averaged and then integrated vertically (0-1000 m) in the water column. The Hadley SST dataset has been used in the upper 100 dbar to supplement calculation of heat content and steric sea height. On all plots the blue line represents a running mean, and latitude is shown on the x-axis.

geographic distribution of the zonally averaged heat content. Figure 3.13 (b) takes a different approach and projects the observed temperature changes along isopycnals back to the latitude where the anomalies originated. This back-projection method more accurately reflects the general transport of water masses and suggests where changes in air-sea fluxes have *entered the ocean interior*. As such, looking at changes along density surfaces could be considered a more relevant method for examining global climate change signals. Essentially the differences between Figures 3.13 (b) and 3.13 (e) emphasise the large contribution of the high-latitude regions to the global uptake of heat from the atmosphere, with the water masses formed in these latitudes showing significantly larger overall heat content changes than water masses formed in the low-latitudes. Despite conceptual differences, there is an internal consistency between the two methods of viewing temperature changes in the oceans. In Chapter 6 the two approaches are combined in order to further understand the mechanisms of ocean water property change.

Figure 3.13 (c) shows the change in the volume of each density layer as a fraction of the layer volume ($\Delta \mathrm{Vol}/\overline{\mathrm{Vol}}$) between the historical and the WOCE-period ($\sim$1970-1992). Over most latitudes of the global ocean there is little significant change evident ($<5\%$) in the volume of density layers (Figure 3.13 (c)), supporting the use of a fixed volume in the zonal back-projection estimates. In the lighter layers found between 30°S and 40°N the 10-20% changes in volume do not show any structure and are often balanced by changes of the opposite sign in the overlying or underlying density layers.

The absence of any significant changes in the volume of density layers is important. It shows that while there have been large and statistically significant changes in water mass temperature and salinity on global scales, the overall distribution of layers and their volume has remained largely unchanged. This lack of volume change suggests that isopycnal layers have tended to deepen or have moved poleward uniformly, with no single density class being preferred. Given that the change in volume is given in a zonally averaged sense and integrated along the length of a density layer, the lack of overall volume changes does not preclude volume or stratification changes in key water mass formation regions.

A lack of change in the thickness of density layers does not preclude a net warming of the water column and hence a change in steric sea level. As an example, a warming

of the surface waters with no salinity change would introduce new lighter density surfaces into the mixed layer. Consequently there would be a downward displacement of density surfaces throughout the water column, without a requirement for any thickness change. Any such thickness change that does occur would be driven by a change in a water mass that is formed at more poleward latitudes.

3.5 Summary and discussion

In this chapter the global temperature, salinity, and pressure changes on neutral density surfaces are investigated between 1970 and 1992. While the approach of using isopycnals rather than the conventional isobaric surfaces has been used before in diagnosing changes in ocean temperature and salinity, past studies have generally compared observations along a single cruise section to interpolated historical data. The work in this chapter builds on these approaches, by undertaking a global analysis made up of many cruise tracks, in order to help understand the spatial variability in the sign and magnitude of changes in water mass properties.

On the shallow salinity-maximum isopycnal, the global pattern of warming and salinity increases on density surfaces unambiguously indicates that an increase in salinity has occurred (Chapter 2.2); however changes on surrounding density surfaces suggest that this water mass has also warmed. The shallow depth of the salinity-maximum layer (100-150 dbar) means that short term atmospheric forcing (eg. ENSO) can alias the 1970-1992 signal when analysing the upper ocean for changes (Godfrey et al., 2001). However the global consistency of the spatial pattern on this surface throughout the Atlantic, Indian, and to a lesser extent the Pacific Ocean suggest that these differences between the 1970s and the early 1990s are part of long term variation consistent with increased evaporation over precipitation. Over land this is reflected in a spatial pattern of increased drying between the extra-tropics and mid-latitudes (Trenberth et al., 2007; Zhang et al., 2007).

The cooling and freshening on density surfaces in mode water (approximately 27.0 kg m^{-3}) also occurs on large spatial scales over much of the globe. This pattern of change is consistent with mode water formation areas being found closer to the underlying intermediate waters (which are freshening and cooling), than to the overlying shallow salinity-maximum waters (which are increasing in salinity and warming) over much of the global ocean.

The relationship between the mean circulation and the signal of change comes through clearly in salinity-minimum and North Atlantic Intermediate Water. In the Southern Hemisphere, the largest changes occur in the South Atlantic Ocean close to the South-East Pacific Ocean AAIW formation region (McCartney, 1977), and are transported eastward by the ACC into the West Indian Ocean subtropical gyre. The freshening of AAIW is weakest in the West Pacific and East Indian Oceans, both regions containing older AAIW. The same relationship between the large scale circulation and salinity changes occurs in the North Pacific, with the strongest freshening found in the west of the gyre near the NPIW source region in Sea of Okhotsk. In contrast to the rest of the globe, the North Indian Ocean shows increases in salinity at the salinity-minimum. When related to the global Ocean circulation this is less surprising, as little cooler and fresher AAIW is advected northward across the equator into this region. Instead changes in local atmospheric conditions tend to be the primary source of inner-ocean anomalies.

While the signal at the salinity minimum is very coherent on large spatial scales, the vertical movement of the salinity minimum in the water column is less globally coherent. This suggests that the changes at this isopycnal depth are largely determined by dynamic forcing (eg. winds, Rossby waves, and mesoscale eddies), that are often only indirectly related to changes in the temperature and salinity properties of water masses. However there are still some coherent spatial changes in depth of surfaces (Figure 3.5 (b)), for example a deepening of isopycnals on the southern side of the SAF and a shoaling in the northern side of the SAF, suggesting a decrease in the North-South tilt of isopycnals and implying a weakening of the vertical shear in the ACC on this surface.

As with intermediate water, the changes in NADW and CDW (represented by 27.8 kg m^{-3}) are strongly tied to the global circulation of this water mass. In the regions with older CDW (ie. the Pacific and Indian Oceans), the water mass changes are very small and not statistically significant. The absence of large water mass changes is consistent with these regions being far from their ventilation regions in the North Atlantic and Southern Oceans. However near the North Atlantic where the lower-limb salinity-maximum water is formed, the cooling and freshening signal on the isopycnal is strongest, with a clear decrease in magnitude of the signal apparent downstream of this source region. In the Southern Ocean where the 27.8 kg m^{-3}

surface outcrops as Upper Circumpolar Deep Water, a strong signal is again evident (Figure 3.6 (a)).

When deep water warming and salinity increases on density surfaces are interpreted as a change on pressure surfaces (and considered independently from vertical isopycnal movement), a coherent pattern of warming and/or freshening on pressure surfaces becomes apparent throughout the Atlantic and Southern Oceans. Elsewhere these changes in deep water appear to have a zonal pattern, with cooling and freshening on density surfaces in the more recently ventilated high latitudes, and warming and salinity increases in mid and low-latitude regions. The strong freshening in the high-latitude North Atlantic has been well documented, and is likely to have been caused by an increased supply of Arctic freshwater, increased precipitation and the North Atlantic Oscillation (Read and Gould, 1992; Curry et al., 2003; Curry and Mauritzen, 2005). In the mid-latitude Atlantic Ocean the observed salinity increases on density surfaces is comparable with the findings of Bryden et al. (1996) and Curry et al. (2003).

In the Southern Ocean, the strong deepening of the 27.8 kg m^{-3} isopycnal helps with the interpretation of results reported by Gille (2002), who observed a warming of pressure surfaces between 700 m and 1100 m (1950s-1990s). This deepening of isopycnals south of the Subantarctic Front appears as a warming on pressure surfaces. The water mass changes in this depth range are small, and consequently the large warming at depth in the Southern Ocean by Gille (2002) of a water mass far from its source region can be reconciled as a dynamical adjustment of this region. This is possibly a poleward shift of isopycnals in response to the increasing westerly winds (Thompson and Solomon, 2002; Trenberth et al., 2007), rather than a response to direct ventilation from the surface water.

In most ocean basins, the signals on the four representative isopycnals examined appear robust when compared to the *a priori* noise estimate (using a signal to noise ratio: Figures 3.1, 3.4-3.6 (d)), and are a large enough sample to be confident that the differences are statistically significant (Figure 3.13). The one exception is on the 27.8 kg m^{-3} density surface found in the mid and low-latitudes of the Pacific Ocean where the small signals have a comparatively large noise associated with them.

When projecting salinity and temperature changes in density layers to the surface,

the observed changes in the ocean are used to infer atmospheric changes in apparent heat flux (W m^{-2}) and apparent precipitation-minus-evaporation (mm yr^{-1}). The assumption is made that all temperature and salinity anomalies are largely mixed *along* rather than *across* isopycnals, and that climatic anomalies of water masses subducted into the ocean interior are preserved.

Since the advection time has not been explicitly taken into account, it is likely that inferred surface changes in apparent heat and freshwater fluxes are underestimated for the 1970 to 1992 period in the lighter density layers formed in the low and mid-latitudes. The reason for this is that given the short renewal rates of these water masses, an atmospheric anomaly imparted to the ocean in 1970 may have been advected through the ocean and "lost" to the atmosphere by 1992. In the deeper density layers the slower renewal rates may mean that some temperature and salinity signals in the ocean interior may have been imparted prior to 1970. However the magnitude of the salinity and temperature changes along isopycnals tend to be weakest furthest from the source region (Figures 3.8-3.9), reducing the influence of older data in these global estimates.

The salinity increases in the low latitudes and the warming and freshening originating from the mid-latitudes are coherent across a number of density layers and are statistically significant (Figure 3.13 (a-b)). This suggests changes in atmospheric conditions (precipitation-minus-evaporation, air-sea fluxes) or high-latitude changes in surface processes such as increase in sea-ice formation (Santoso and England, 2004) has occurred. While variability in Ekman transport caused by changing winds can affect water mass properties in mode water (Rintoul and England, 2002; Banks and Bindoff, 2003), these tend to occur over short time scales (interannual). In the longer term, the zonally averaged inferred heat and salinity changes of the surface waters (Figure 3.13) suggests that heating and freshening of the surface ocean is largely driven by increased heat and freshwater exchange from the atmosphere, rather than by increased local winds driving local transport of heat and freshwater. Such warming of surface waters north and south of the SAF is observed during the period 1970 to 1990 (Rayner et al., 2003) and therefore the ocean changes are consistent with surface warming by the atmosphere in the SAMW formation region.

The selected density surfaces illustrate well the observed salinity increases in low-latitude regions, the freshening originating from mid-latitudes, and the overall warm-

ing of the upper water column. The global scale of these signals suggests that a combination of increasing surface heat fluxes and changes in rainfall patterns is the explanation. A strengthening of the hydrological cycle with increasing rainfall over the mid-latitudes, and decreasing precipitation-evaporation in the equatorial regions would produce the observed oceanographic changes. Previous observational studies have also inferred that such a strengthening of the hydrological cycle could have occurred (Wong et al., 2001; Curry et al., 2003). In addition, the pattern of apparent freshwater flux change inferred from the inventory of salinity along density layers for the 1970s to the 1990s shows a striking similarity to the zonal rainfall change pattern in IPCC class models for the 20th century (Meehl et al., 2007), and to the observed patterns of precipitation and evaporation from rain gauge data over land (Trenberth et al., 2007).

Prior to high quality satellite coverage in the 1990s, the direct measurements of precipitation and evaporation data over the open oceans are sparse, meaning that it is necessary to use ocean observations to infer atmospheric changes. Ideally observational datasets should have sufficient temporal and spatial coverage to allow the creation of a time-series on small spatial scales, while minimising the associated errors that arise from mapping irregularly spaced data. Since 2003 the Argo dataset has provided this sort of spatial coverage, although the five years that the Argo float program has been operating is not long enough to provide a continuously evolving signal. This modern dataset is the basis for the next chapter, which extends the analysis from 1992 to 2005.

Chapter 4 Temperature and salinity changes: 1970-2005

4.1 Introduction

In Chapter 3 the changes in water properties on density surfaces between the 1970s and the early-1990s were examined, with these results being used to infer changes in apparent surface salinity and heat fluxes. This chapter makes use of the recent Argo dataset to extend this analysis into the early 21st century.

While there is some overlap with Chapter 3 from 1970 to 1992, the depths that Argo floats profile to has limited the range of this analysis to the upper 1500 m. As such the focus here is on changes in the shallow salinity-maximum and the salinity-minimum water masses, complementing the results in Chapter 3 by providing a longer coverage period and potentially reducing the effect of inter-decadal variability and shorter-term regional oscillations. However in some ways the Argo dataset is less comprehensive than the shipboard profiles taken between 1940 and 1988. For example, the Argo float dataset does not contain oxygen observations, does not extend as far south, or measure as deep in the ocean. Argo data is continually being collected, but only in the last year have sufficient profiles existed to provide good global coverage.

This chapter follows on from Chapter 2 with a more detailed description of the Argo dataset, before discussing the temperature and salinity differences on density surfaces between the Argo-period and the historical-period (approximately 1970 to 2005). Next the temperature and salinity data for these two periods are analysed on individual ocean basins to determine which basins have consistent changes. The regions with similar trends to the earlier period (ie. the Southern Ocean and the North Pacific) and with changed trends (ie. the North Atlantic and the South Indian Oceans) are discussed and compared with the existing literature. While there is some necessary repetition with Chapter 3 in the 1970-1992 period, the analysis here focused more on the signals emerging from the longer time period ($\sim$1970-2005).

Argo dataset

The Argo program began in 2000 as an international collaborative effort, designed to document both the current state and the variability of temperature and salinity in the global upper-ocean (www.argo.ucsd.edu) and to build on projects commenced during WOCE. The program involved deploying approximately 3000 free-drifting (Lagrangian) floats distributed across the globe. These floats drift at a maximum depth of 2000 m and every 10 days rise to the surface, measuring both temperature and salinity at regular pressure intervals. At the surface, the float transmits the profile data to a satellite, and with a short delay this information is freely available to download and analyse ('real time' data). Additional 'delayed mode' quality control of these profiles by designated data-centres can take a further 6 months. With approximately 3000 floats currently in the ocean, the Argo dataset is rapidly obtaining dense near-global sampling of the oceans.

In this study, a total of 172,918 profiles taken between 2000 and 2007 (with a mean year of 2005) were used (Chapter 2, Figure 2.2). These were well distributed globally (Chapter 2, Figure 2.3), although very few floats are deployed south of 60°S due to potential damage from sea-ice to the instruments. While the more recent Argo floats can profile to 2000 m, some of the earlier models could not go this deep and approximately 30% of the available profiles are shallower than 1000 m.

Of the profiles downloaded from the CSIRO data repository in February 2007, 55,946 (32%) had been subject to delayed-mode quality-control. At this stage there had been delays from some data processing centres, meaning that there were large regions (ie. the South Atlantic Ocean) with few quality controlled observations. Although not ideal, it was necessary to combine these delayed-mode profiles with 116,972 real-time profiles in order to ensure good global coverage. The real-time profiles have some simple quality control checks prior to release, and are assigned a flag indicating the degree of confidence in the results. These flags for temperature, salinity, pressure, and location were examined, and only those profiles with no initial indication of any errors were retained.

Recently there have been problems associated with the pressure sensors in some types of Argo buoys that has lead to the appearance of an erroneous cooling signal in the upper 750 m (Willis et al., 2007; Schiermeier, 2007). Profiles originating from these types of buoys had been identified and removed from this analysis and in

principle the cooling signal from these pressure sensors should have been removed.

4.2 Water property changes: Historical to Argo (∼1970-2005)

The optimal interpolation technique used to map Argo profiles to the WOCE-period locations is almost the same as is outlined in Chapter 2 and used in Chapter 3. In this Chapter the correlation function for the optimal interpolation used a mean year of 2005 (t_i) with a time-scale of 10 years ($yearscale$). Given the short time scale in which the Argo profiles were taken, this effectively removed the time component from the Gaussian function (Chapter 2, Equation 2.8). The addition of the Argo data to the profile database allows three time periods to be compared globally: 1992-2005, 1970-1992, and 1970-2005. While a time-series of water mass change would be desirable, the sparsity of full depth profiles in the Southern Hemisphere limits the usefulness such an approach.

The analysis from 1970 to 2005 shows temperature and salinity increases in the upper-300 dbar virtually throughout the world ocean (Figures 4.1 (a), 4.2 (b)). On density surfaces, an increase in salinity above the shallow salinity-maximum isopycnal may potentially be just the compensating result of surface warming. However at the upper ocean maximum in salinity (γ_n value of about 24.8 kg m^{-3}), the globally averaged 0.103 psu increase in salinity is unambiguous in its interpretation and can only occur through an increase in salinity on the isopycnal rather than by a change in temperature. This indicates (at least to first order) a decrease in precipitation-minus-evaporation in the low-latitude formation regions of these water masses (Bindoff and McDougall, 1994).

In the Atlantic and Indian Oceans there are average salinity increases of 0.154 psu and 0.086 psu at the shallow salinity-maximum (Figure 4.1 (a)). In the Pacific Ocean, approximately 80% of grid cells show a salinity increase at an average of 0.088 psu. Note that the optimal interpolation method used smooths out interannual signals, thus reducing the effects of an aliasing from the El Niño Southern Oscillation in the Pacific Ocean.

The waters of the main thermocline (below 26.4 kg m^{-3}, 200-300 dbar) to the salinity-minimum intermediate waters ($\approx$ 1000 dbar) have freshened and cooled on

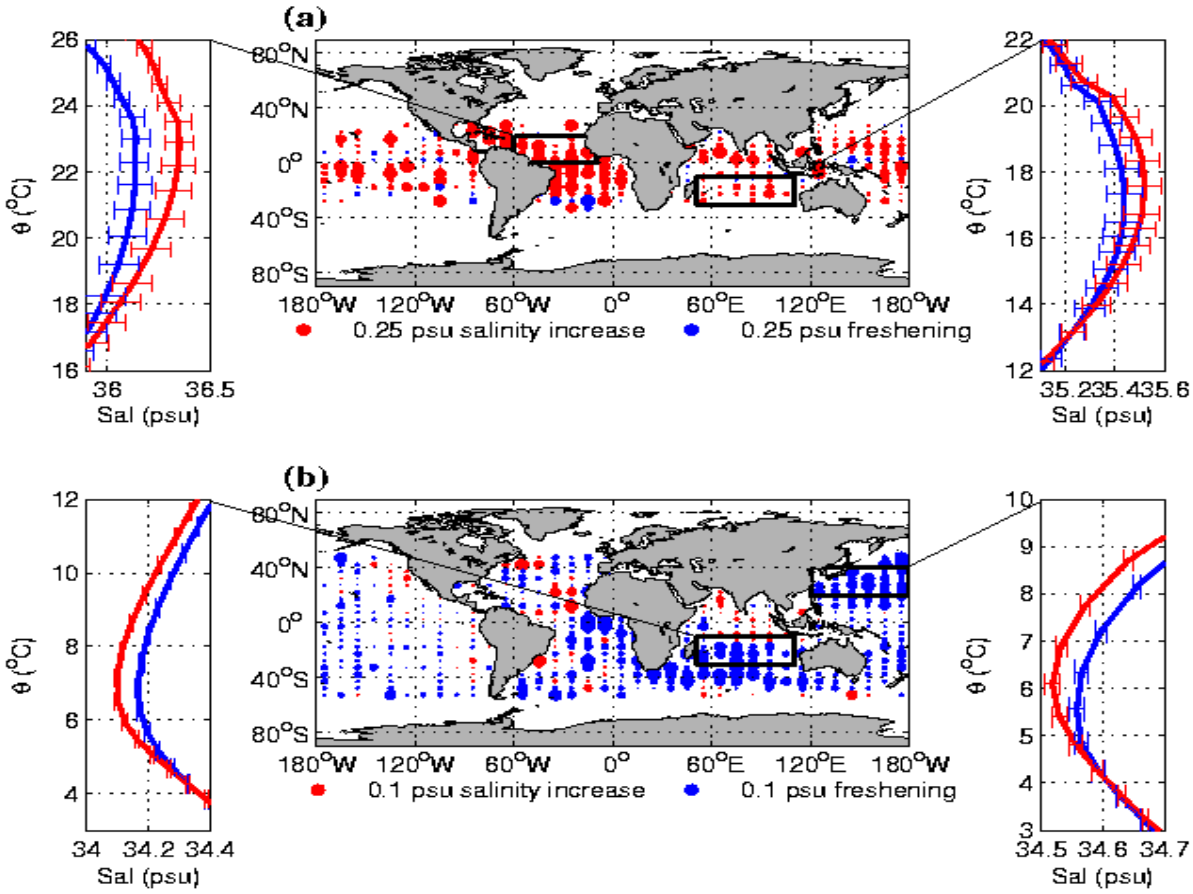

Figure 4.1: Salinity changes (psu) on **(a)** the shallow salinity-maximum, and **(b)** the salinity-minimum. Each dot represents the average change inside the 5°×10° grid cell. The top left and right panels show a temperature-salinity plot for the corresponding boxed region and is centred at the shallow salinity-maximum (∼ 100 dbar). The red line is formed using data from the Argo period and the blue line uses 1970 data. The bottom left and right panels are for the salinity-minimum (600-1000 dbar). The horizontal error bars on the temperature-salinity curves represent a 90% confidence interval of the salinity observations and are calculated using methods described in Chapter 2.5.

density surfaces across most of the globe (Figures 4.1 (b), 4.2 (b)). For intermediate waters in the density range 26.8-27.2 kg m^{-3} (300-1000 dbar), this freshening at the salinity-minimum is almost certainly in response to decreased salinity in the surface source regions (Figure 4.1 (b)). The largest freshening is in the South Indian and North Pacific subtropical gyres (latitudes 20° to 40° N and S), and in the eastern tropical Atlantic Ocean. Although the North Atlantic does not have a well defined salinity-minimum, recently ventilated intermediate-depth waters in this ocean show the same coherent freshening and cooling on density surfaces as the rest of the global ocean. There are smaller changes in the North Indian Ocean, where land and the equatorial region act to isolate this gyre from the rest of the global circulation and the main source regions of AAIW.

Antarctic Intermediate Water (AAIW), distributed throughout all of the Southern Hemisphere subtropical gyres at about 1000 dbar and characterised by a salinity-minimum, has freshened and cooled on isopycnals between 1970 and 2005 (Figure 4.1 (b)). In the zonally averaged vertical section (Figure 4.2 (b)), the freshening in the Southern Hemisphere subtropical gyres is clearly visible and there is a secondary maximum on the 27.2 kg m^{-3} density surface (∼ 800 dbar) near the equator. This AAIW with modified properties reaches the equatorial region via low-latitude western boundary currents, particularly in the South-West Pacific where the large changes observed are consistent with this circulation pathway (Figure 4.1 (b)). Changes in Subantarctic Mode Water in the Southern Ocean also show a global-scale pattern of cooling and freshening on density surfaces (similar to Figures 4.1 (b) and 4.2 (b), 20°S-40°S), extending the earlier regional results (Wong et al., 1999, 2001; Curry et al., 2003) to a global scale.

In the Atlantic Ocean between 30°S and 10°N, the freshening in AAIW centred on the 27.2 kg m^{-3} neutral density surface (600 dbar) averaged 0.031 psu between 1970 and 2005, with the majority of this change occurring between 1970 and 1992 (0.027 psu). North Pacific Intermediate Water (approximately 26.8 kg m^{-3} and 600 dbar) shows a broad pattern of freshening between 20°N and 35°N, averaging 0.065 psu between 1970 and 2005.

In North-West Atlantic intermediate-depth waters, there has been a change in the sign of water property changes between 1970 and 2005. In the density range 26.8 to 27.2 kg m^{-3} (300-700 dbar) the initial 0.033 psu freshening and cooling (1970-

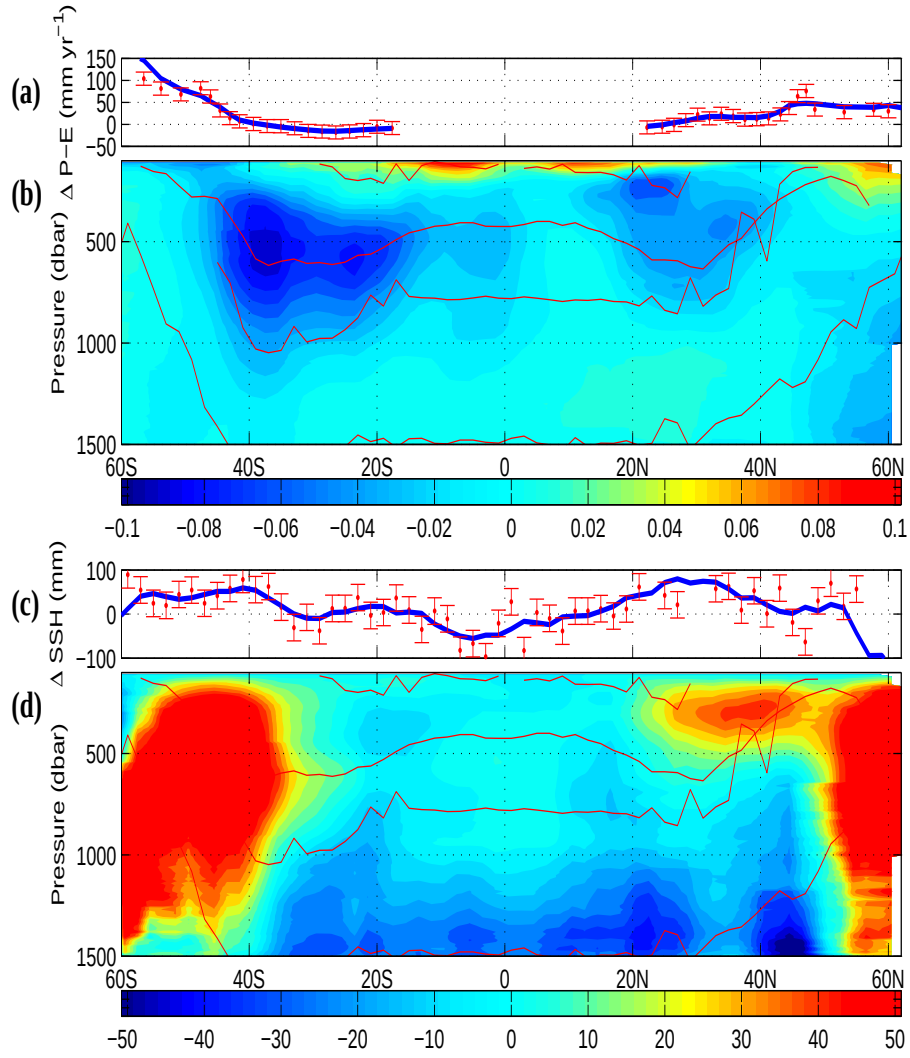

Figure 4.2: Zonally averaged changes along density surfaces (1970-2005). **(a)** Inferred change in apparent surface freshwater fluxes (mm yr^{-1}) at the subduction region of each isopycnal. The blue line is a running mean, while the error bars represent a 90% confidence interval. **(b)** Salinity difference (psu) where blue is freshening. **(c)** Changes in the vertically integrated steric sea-level (0-1000 dbar). **(d)** Changes in isopycnal pressure (dbar) where red is a zonally averaged deepening of isopycnals. For both (b) and (d), the shallow salinity-maximum (very top), the 27.0 kg m^{-3}, the salinity-minimum, the 27.8 kg m^{-3}, and the 28.0 kg m^{-3} surfaces are shown in both panels.

1992) reversed to a 0.032 psu salinity increase and warming on density surfaces (1992-2005). The net result between 1970 and 2005 is no water property change on isopycnals originating from the Labrador Sea.

From 1970 to 2005 the Southern Ocean region south of the Subantarctic Front (between 40°S and 60°S) has warmed on pressure surfaces from about 200 dbar to 1400 dbars, and this warming is circumpolar in extent (extending the earlier results from the Indian Ocean sector of the Southern Ocean (Aoki et al., 2005)). Most of this circumpolar warming appears to have been expressed through deepening of isopycnals (Figure 4.2 (d)), with relatively little salinity and temperature change on density surfaces themselves (Figure 4.2 (b)). These small water mass changes are consistent with the large distances from the deep water ventilation region, except for south of the Polar Front where upwelling deep water is mixed with surface waters (Chapter 3, Figure 3.6). The circumpolar deepening of density surfaces instead explains the warming trend from 700 to 1100 m in the Antarctic Circumpolar Current region (Gille, 2002) as a dynamic response rather than the direct ventilation of the ocean at this depth. This is probably due to a poleward shift of the Southern Hemisphere gyre boundaries, potentially driven in part by increasing westerly winds (Thompson and Solomon, 2002; Trenberth et al., 2007).

As in Chapter 3, the apparent changes in freshwater required to explain the observed interior changes are estimated by integrating the salinity changes along density layers between the equator and where they intersect with the ocean surface (in more polar latitudes) (1970 to 2005). Below 1500 dbar there is insufficient Argo data on isopycnals and these denser (deeper) water masses are excluded from the zonal integrals. The zonally averaged surface freshwater budget (Figure 4.2 (a)) shows a pattern of strong apparent freshwater addition south of 45°S (up to 30 mm yr^{-1}) with significant but smaller decreases in the mid-latitudes in both hemispheres. The zonally averaged decrease in freshwater in high northern latitudes comes mainly from the Atlantic Ocean and results from the observed increase in salinity in the Labrador Sea (Bindoff et al., 2007).

The apparent freshwater flux change in the Southern Ocean represents about a 5% increase in the mean freshwater input, and in the Southern Hemisphere mid-latitudes a decrease of about 1%. The overall pattern of a decrease in the apparent freshwater fluxes in the mid-latitudes and an increase in the Southern Ocean sup-

ports the model patterns of climate change (1980-1999: Wentz et al. (2007)), and is consistent in pattern and amplitude with the future "commitment" projections where the atmospheric CO_2 is held at 2000 levels (Meehl et al., 2007).

Changes in the vertical distribution of ocean temperature and salinity have consequences for sea level through thermal expansion and haline contraction. There is a clear zonal pattern of steric sea-level rise between 1970 and 2005 (Figure 4.2 (c)), with a rise in sea-surface height poleward of both 30°S and 20°N. As in Chapter 3, the estimates include a contribution to thermal expansion from the top 100 dbar, estimated from the Hadley Sea Surface Temperature dataset (Rayner et al., 2003). South of 40°S the steric sea-level increases coincides largely with the deepening of density surfaces (Figure 4.2 (d)). The warming in the upper 100 dbar contributes approximately 20% of the steric sea-level change in this region. Comparatively, there was little zonal change in steric sea-level in the equatorial regions (Figure 4.2 (c)), where salinity increases (Figure 4.2 (b)) and a cooling in the West Pacific and Indian Ocean during the 1980s has been observed.

The strength of the global observed changes suggests that while regional variability may occur (ENSO, NAO etc), there are large trends in the global hydrological cycle and a net deepening of density surfaces. The clarity, magnitude, and spatial coherence of the water mass signal over a long time period is consistent with observed trends over land of decreasing precipitation-minus-evaporation in low latitudes and increasing precipitation-minus-evaporation poleward of 40°. These trends are found in climate change predictions and suggest an acceleration of the hydrological cycle.

4.3 Comparison of changes in both time periods

4.3.1 The shallow salinity-maximum

In both the 1970-1992 (0.030 psu) and the 1992-2005 (0.055 psu) periods, globally coherent salinity increases (and warming) at the shallow salinity-maximum were observed. These globally averaged increases in temperature and salinity for the upper thermocline are illustrated in Figure 4.3 and summarised in Table 4.1 (a), and imply that at the shallow salinity-maximum the rate of salinity increase has risen from 0.001 psu yr^{-1} to 0.004 psu yr^{-1}.

In the Atlantic Ocean these salinity increases occur at a relatively constant rate

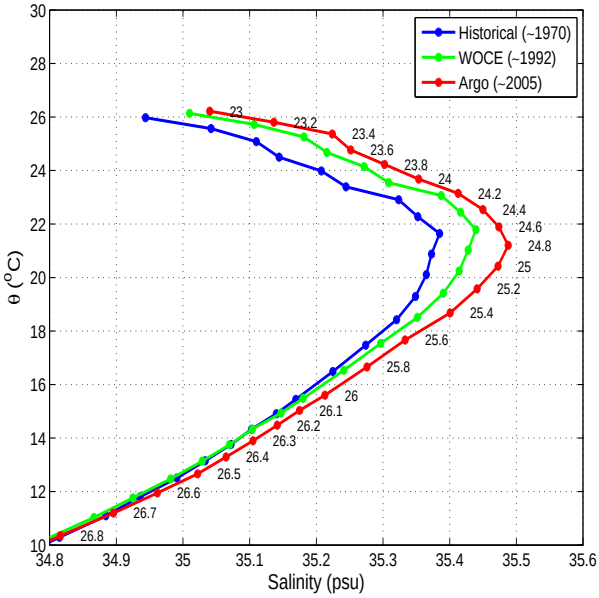

Figure 4.3: Global temperature-salinity plot for historical (∼1970), WOCE (∼1992), and Argo (∼2005) periods centred around the shallow salinity-maximum. Neutral density levels (kg m^{-3}) are shown for the Argo period.

between the 1970-1992 (0.005 psu yr^{-1}) and the 1992-2005 (0.004 psu yr^{-1}) periods. (Figure 4.4 (a-b)).

Since 1992 a localised freshening (and cooling) on the shallow salinity-maximum isopycnal is apparent in both the South Indian Ocean and in the East Pacific Ocean (Figure 4.4 (b)). Both of these regions show relatively large increases in salinity and warming in the preceding period, with weak decreases after 1992 likely to be indicative of an El Niño oscillation. While a freshening directly on the equator in the Pacific Ocean was noted from 1970 to 1992 in Chapter 3 (and in Figure 4.4 (a)), this feature is not apparent from 1992 to 2005 (Figure 4.4 (b)).

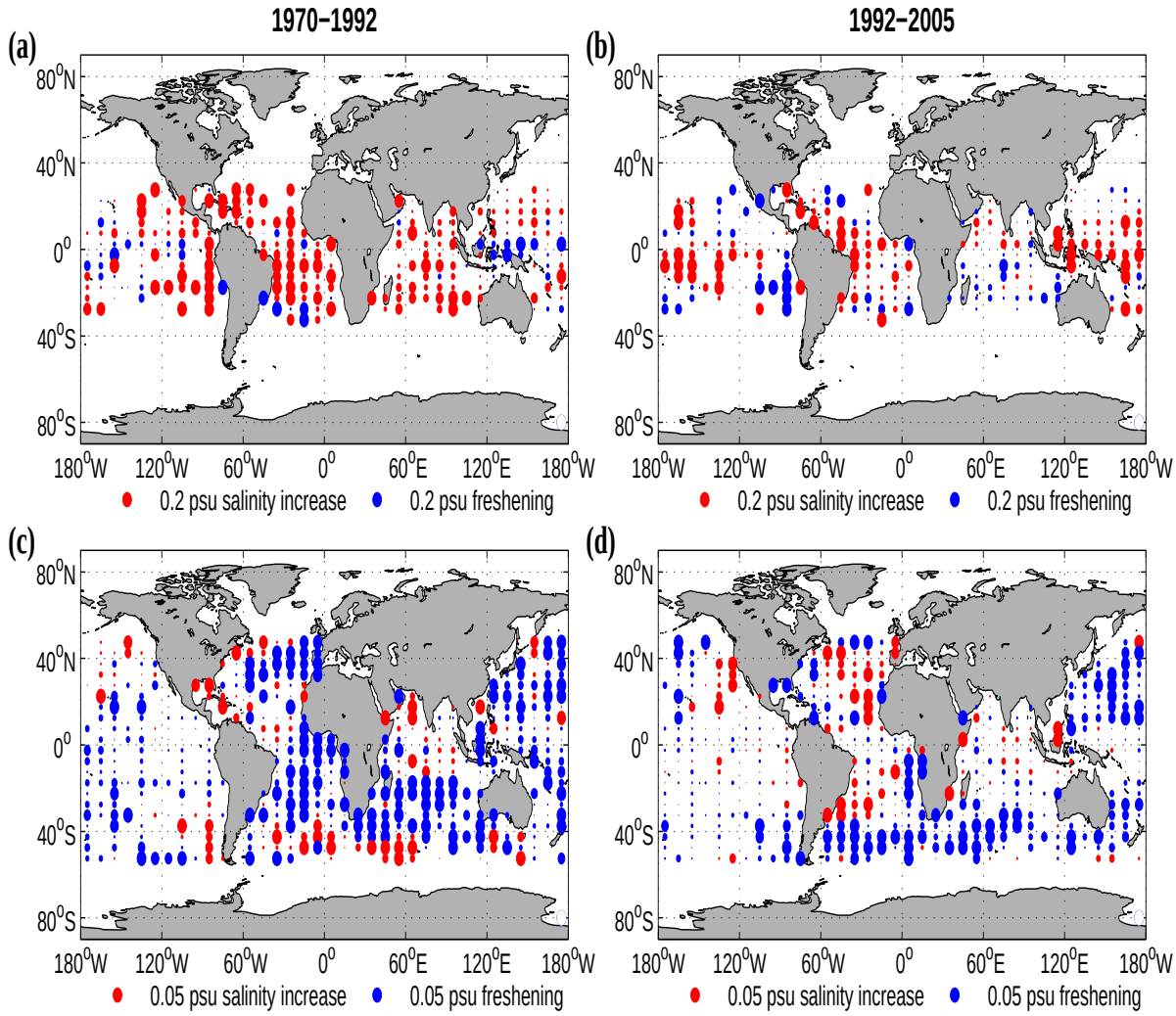

Figure 4.4: Salinity changes along density surfaces on the **(a-b)** Shallow salinity-maximum and **(c-d)** salinity-minimum intermediate-level waters. The left panels (a,c) represent the 1970-1992 period, while the right panels show the 1992-2005 period.

4.3.2 The salinity-minimum

Both 1970-1992 and 1992-2005 periods have a freshening (and hence cooling) on the density surface best representing the salinity-minimum. While there is clear coherence inside individual ocean basins between 1992 and 2005, the freshening is not as pronounced on a *global* scale in the earlier time period (1970-1992), reflecting the contribution of decadal variability in individual ocean basin to a longer term trend. This result is reflected in the global averages (Table 4.1 (b)), with the salinity changes from 1992 to 2005 being approximately half that in the 1970 to 1992 period.

In Figure 4.4 (c-d) there are coherent patterns of change inside individual ocean basins. Freshening and cooling of intermediate waters is observed across both time periods in the Southern Ocean south of 30°S (Figure 4.5 (i-l): ∼27.0-27.2 kg m^{-3}), in the South Pacific Ocean north of 30°S (Figure 4.5 (e,h)), and in NPIW in the North-West Pacific Ocean (Figure 4.5 (d): ∼26.8 kg m^{-3}). In the equatorial and low-latitude Indian Ocean (30°S-30°N) there is freshening and cooling from 1970 to 1992, with negligible changes in the 1992 to 2005 period (Figure 4.5 (g): ∼27.2 kg m^{-3}).

The zonal averages are dominated by consistent freshening and cooling at the salinity-minimum in the spatially large Pacific and Indian Oceans. Figure 4.6 (b,e) illustrates this freshening signal, with the largest freshening and cooling in both periods occurring between the 26.8 and the 27.2 kg m^{-3} density surfaces (300-1000 dbar) from 20° to 40° in both the northern and Southern Hemispheres.

All salinity-minimum intermediate waters found close to source regions (Table 4.1 (c-e)), have freshened and cooled on density surfaces over both periods. This cooling and freshening has occurred at a reasonably constant rate in the North Pacific and South Indian Oceans (∼0.002 psu yr^{-1} for both periods), but the rate of freshening in the South Atlantic Ocean has decreased from ∼0.001 psu yr^{-1} to be negligible (Table 4.1 (d)).

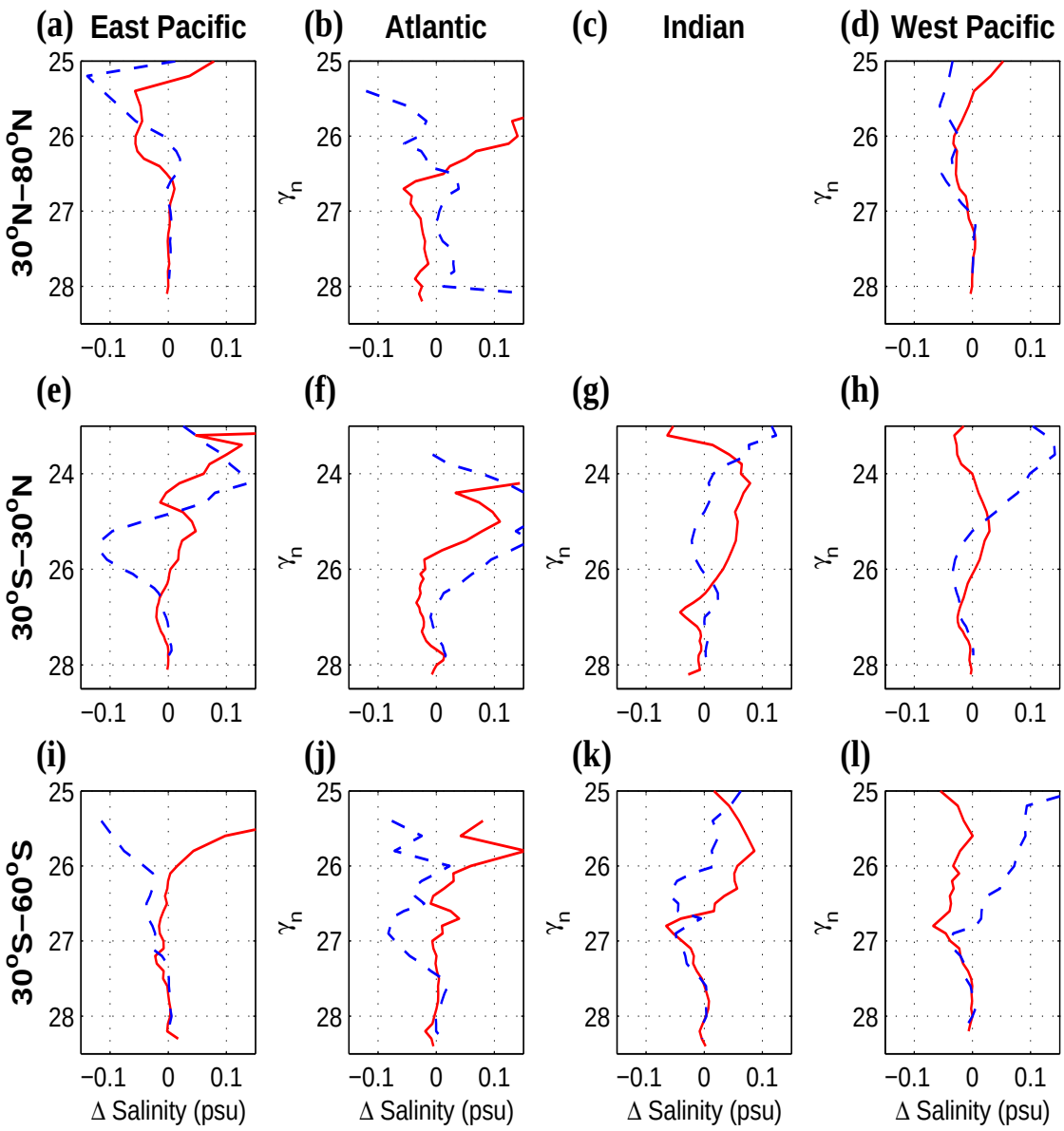

Figure 4.5: Changes in salinity (x-axis: psu) along neutral density surfaces (y-axis). The red solid line represents changes between the historical and the WOCE periods (∼1970-1992), while the blue dashed line shows changes between the WOCE and the Argo periods (∼1992-2005). Note that the changes in the lighter density layers (<25 kg m^{-3} for equatorial regions and <26 kg m^{-3} for latitudes poleward of 30°) represent only a small proportion of the water column. While typical error bars are around 0.05 psu for these upper layers, there is much less variability for surfaces below 27 kg m^{-3} (averaging approximately 0.01 psu).

Table 4.1: Changes in in situ temperature and salinity along isopycnals of key water masses between the two time periods. Note that a negative value represents a cooling or freshening. Figure 3.7 (Chapter 3) shows the regions over which the average changes were calculated.

	Surface:	**Represents:**	**Ocean:**	**ΔT (°C)**		**ΔS (psu)**	
				'70-'92	**'92-'05**	**'70-'92**	**'92-'05**
A	Smax		Global	0.08	0.14	0.030	0.055
B	Smin	Int. waters	Global	-0.09	-0.06	-0.018	-0.009
C	Smin	NPIW	N. Pacific	-0.21	-0.10	-0.033	-0.021
D	Smin	AAIW	S. Atlantic	-0.14	-0.01	-0.027	-0.001
E	Smin	AAIW	S. Indian	-0.18	-0.11	-0.034	-0.02
F	26.8-27.6	300 m+	N. Atlantic	-0.11	0.05	-0.034	0.017
G	27.8	CDW	Southern Ocean	0.05	0.04	0.005	0.005
H	27.8	NADW	N. Atlantic	-0.09	0.13	-0.015	0.026
I	27.4-28.0	300 m+	Subpolar N Atlantic	-0.19	0.23	-0.035	0.044

4.3.3 Changes throughout the water column

In both the 1970-1992 and the 1992-2005 periods there are strong similarities in the zonally averaged patterns of salinity change. Both periods show a mid-latitude freshening that penetrates into the ocean interior, and surface salinity increases in the vicinity of the shallow salinity-maximum (Figure 4.6 (b,e)).

Despite salinity increases between 1992 and 2005, density surfaces poleward of 45°N have deepened in the water column (200-1000 dbar: Figure 4.6 (f)). In the earlier period the Northern Hemisphere deepening occurs between 30°N-40°N, with strong shoaling poleward of 55°N (Figure 4.6 (c)). The magnitude of the changes since 1992 dominates the pattern seen in Figure 4.2 (d) (1970-2005), despite occurring over a shorter time period. Deepening of density surfaces in the Northern Hemisphere subtropical gyres around 26.4-27.0 kg m^{-3} is evident in both the 1970-1992 and the 1992-2005 time-periods.

When these salinity changes are integrated along density surfaces to the outcropping zone, the same patterns of high-latitude Southern Hemisphere increases in mixed-layer freshwater content are observed in both periods. However there has been a shift in the magnitude of the surface freshwater addition with a near doubling in the Southern Hemisphere rate of freshwater increases during the 1990s (from 20 to 40 mm yr^{-1}). These results point toward an increase in the rate of freshwater addition through an accelerating global hydrological cycle or increased rates of production

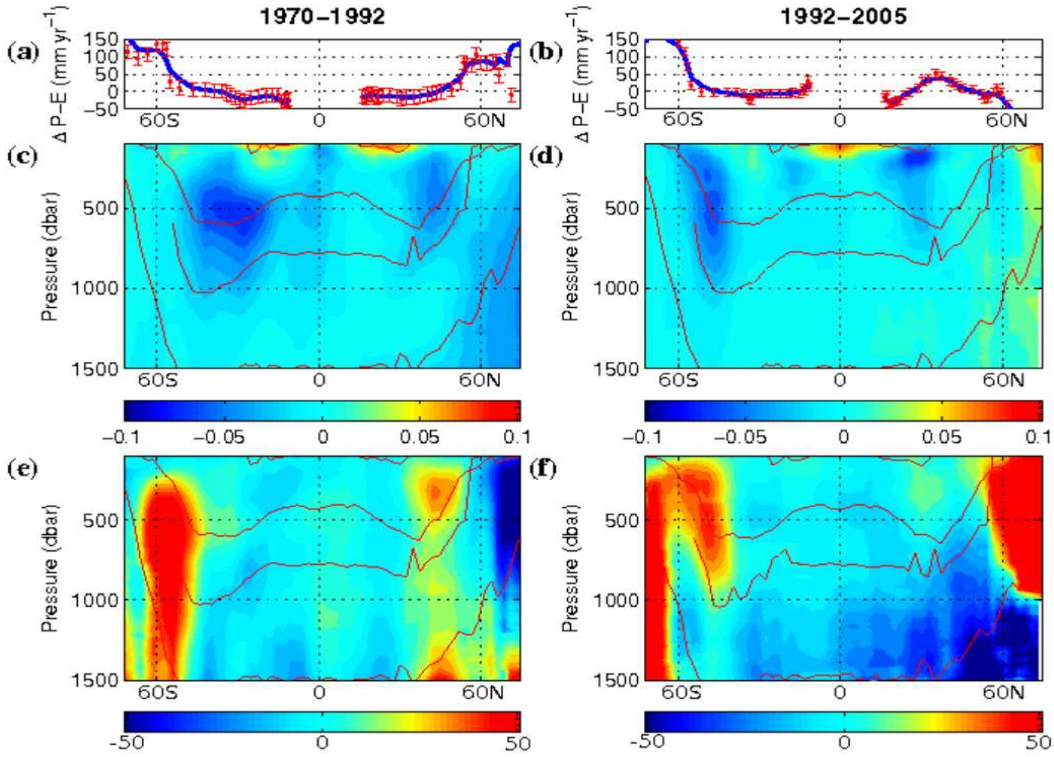

Figure 4.6: Zonally averaged changes along density surfaces in the two periods, where the panels on the left (a,c,e) show 1970-1992 and the panels on the right (b,d,f) show 1992-2005. **(a-b)** Inferred change in apparent surface freshwater fluxes (mm yr^{-1}) at the subduction region of each isopycnal. The blue line is a running mean, while the error bars represent a 90% confidence interval. **(c-d)** Salinity difference (psu) where blue is freshening. **(e-f)** Changes in isopycnal pressure (dbar) where red is a zonally averaged deepening of isopycnals. The average depths of the shallow salinity-maximum (very top), the 27.0 kg m^{-3}, the salinity-minimum, the 27.8 kg m^{-3} neutral density surfaces are shown in panels c-f.

and melt of sea-ice formed during winter.

In the low-latitudes, both the WOCE-historical and the WOCE-Argo period also show apparent P-E decreases, and like the changes in the high latitudes, these have a higher rate of change over the latter period. The WOCE-Argo period shows apparent P-E increases occurring between 20°N and 40°N (Figure 4.6 (d)), a feature that is not evident in the earlier time period (Figure 4.6 (a)). However there are large error bars, associated with the relatively short lengths of the density surfaces that outcrop in this region.

Over much of the globe there is very good agreement between the two time periods in the zonally averaged patterns of density surface movement, suggesting a relatively constant increase in apparent freshwater fluxes to the surface ocean.

With the exception of the North Atlantic Ocean (and near the limits of data coverage in the high-latitude Southern Ocean), there is little evidence of change in water mass properties below 1500 dbar (Figure not shown) between 1970 and the WOCE period, consistent with these deep regions being far from their source regions (Chapter 3, Figure 3.6 (a)). This general absence of change in the deep waters is largely in agreement with CFC concentrations in the global ocean (Talley, 2007).

4.3.4 Southern Ocean consistent changes

The Southern Ocean exhibits similar patterns of water property changes in the upper 1000 dbar from 1970 to 1992 as it does between 1992 and 2005. In both periods there is coherent freshening and cooling of subducting intermediate waters around 40°S. In the denser waters below 300 dbar that upwell south of 40°S there is comparatively little change in temperature and salinity on density surfaces. This result is consistent with the long time period since ventilation of this upwelling limb of the overturning circulation.

However below 300 dbar, these density surfaces have shown consistent deepening in the water column since the 1970s. The downward motion of density surfaces with minimal water mass changes is consistent with a dynamic response and helps explain the large circumpolar warming (700-1100 m) observed by Gille (2002) from the 1960s to the 1990s. This downward motion of isopycnals is discussed in Chapter 3.2; however the longer time period used in this chapter suggests that the warming

Table 4.2: Changes in salinity in the North Atlantic and subpolar North Atlantic documented in previous studies where: NA=North Atlantic, SNA=Subpolar North Atlantic, and UW=upper waters.

	Region:	**Change:**	**Period:**
Boyer et al. (2007)	NA (0-400 m)	Salinity increases	1986-2006
	NA (1300 m +)	Freshening	mid-1990s-2005
Curry et al. (2003)	NA (40°N+)	Freshening	1950s-1990s
Arbic and Owens (2001)	NA (48°N)	Cooling	1950s-1980s
Leadbetter et al. (2007)	NA (36°N: UW)	Cooling	1959-1981
		Warming	1981-2005
Read and Gould (1992)	SNA (55°)	Cooling & Freshening	1962-1991
Curry and Mauritzen (2005)	SNA	Freshening	Since 1960s
Hatun et al. (2005)	SNA	Salinity increases	mid-1990s-2005
Boyer et al. (2007)	SNA	Freshening	1960s-1990s
	SNA	Salinity increases	1990s-2006
Ivchenko et al. (2006)	SNA	Warming	1999-2005

on pressure surfaces in the upper 1000 dbar has continued since the 1990s, is driven not by water mass change, but instead by an internal ocean response to changes in surface wind forcing.

4.3.5 Switch of sign in the North Atlantic Ocean

In the North Atlantic (30°N-50°N) there are clear signs of a cooling and freshening on density surfaces between 1970 and 1992 (Figure 4.7 (a): red line), with a switch to warming and salinity increases in the latter 1992-2005 period (Figure 4.7 (a): blue line). These changes occur below the mixed layer on all density surfaces below 26.4 kg m^{-3} ($\sim$ 200 m). During the 1970s and 1980s the freshening was greatest around 26.8 kg m^{-3} ($\sim$ 300 m), and has been documented in a number of previous studies (see Table 4.2: Curry et al. (2003); Leadbetter et al. (2007)), while upper-ocean salinity increases have been observed in the upper 400 m over the last two decades (Boyer et al., 2007). The similarity in the sign of salinity changes between the North Atlantic and the Subpolar North Atlantic is consistent with circulation patterns in this region. Here the salinity anomalies that are mixed into the water column in the subpolar high-latitudes are advected along density surfaces and into the North Atlantic basin (Johnson and Gruber, 2007)

The Subpolar North Atlantic (poleward of 50°N) had similar changes to the North Atlantic, with freshening on all density surfaces denser than 27.3 kg m^{-3} ($\sim$ 300

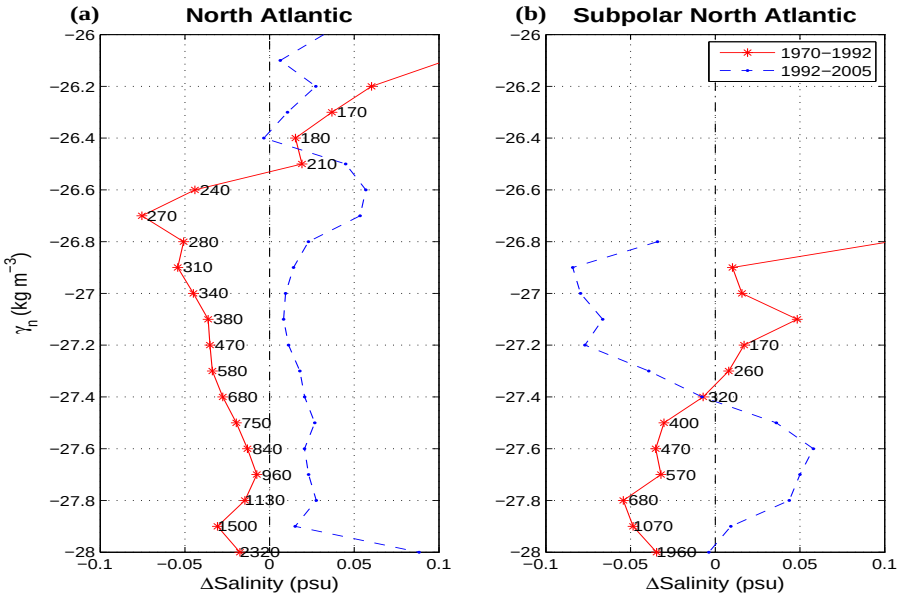

Figure 4.7: Changes in salinity along density surfaces in the **(a)** North Atlantic (30°N-50°N), and **(b)** the subpolar North Atlantic (defined as poleward of 50°N-65°N: Curry and Mauritzen (2005); Boyer et al. (2007)). The solid red line represents changes between the historical and the WOCE periods (∼1970-1992), while the blue dashed line shows changes between the WOCE and the Argo periods (∼1992-2005). The average pressure (dbar) on each density layer is shown for the Argo period.

dbar) from 1970 to 1992 (Figure 4.7 (b): red line). In the second period (1992-2005: Figure 4.7 (b): blue line) a change of sign occurred, with salinity increasing on density surfaces below 27.3 kg m^{-3}. This change after 1992 is evident in the zonal averages shown in Figure 4.6 (b), noting that in these Northern Hemisphere high-latitudes the zonal average is dominated by the Atlantic Ocean.

Previous studies reflect these observations (summarised in Table 4.2) with a documented subpolar freshening between the 1960s and the early 1990s (Read and Gould, 1992; Curry and Mauritzen, 2005), and the change to salinity increases occurring since then (Hatun et al., 2005; Boyer et al., 2007). In addition this subpolar North Atlantic region has been observed to warm since at least 1999 (Ivchenko et al., 2006), reversing a cooling trend between the 1960s and 1980s (Arbic and Owens, 2001).

Using time-series and models, links have been found between the properties of Subpolar Mode Water (SPMW) and the North Atlantic Oscillation (NAO), where nega-

tive values of the NAO are generally associated with warming and salinity increases in this water mass (Johnson and Gruber, 2007). This subpolar North Atlantic region is a key formation region in the Atlantic overturning circulation, with the temperature and salinity anomalies formed here being advected southward, and acting as one of the key mechanisms of water property changes below 1000 m in the North Atlantic (Hatun et al., 2005; Boyer et al., 2007). Given that the NAO has gone through a few cycles over the 1970-2005 period (Johnson and Gruber, 2007), the synoptic method of analysis that was adopted here may smooth over or alias some of this variance.

One documented feature is the "Great Salinity Anomaly", which entered the subarctic seas in the late-1960s and was characterised by a decade of freshening surface waters (Curry and Mauritzen, 2005). These propagated anomalies may be partly responsible for the observed dense water freshening observed between 1970 and 1992 further south in the Atlantic Ocean.

In both the North Atlantic and the subpolar North Atlantic, the *net* freshening in the 1970-1992 period is greater than the more recent salinity increases (Figure 4.4 (c-d) and Table 4.1), resulting in a less coherent, but an overall freshening pattern emerging in Figure 4.1 (b) (1970-2005). However the *rate* of salinity change has actually been greater since 1992, with the overall freshening being primarily due to the difference in the lengths of the two time periods (22 and 13 years). Prior to the 1980s, Leadbetter et al. (2007) found that these intermediate waters warmed and increased in salinity along density surfaces, although this cannot be confirmed with the analysis used here, where freshening was the observed dominant trend between 1970 and 1992.

The inferred changes in surface freshwater inputs (Figure 4.6 (a)) qualitatively agree with this switch in salinity, with the surface freshwater increases north of 45°N (averaging 10-20 mm) not apparent in the post-1992 integrals, although recent strong decreases in freshwater around 55°N were obvious.

Further south in the low to mid-latitude Atlantic Ocean, pre-1990 changes on pressure surfaces have been attributed to the downward displacement of density surfaces, rather than surface-driven water property changes (Arbic and Owens, 2001).

4.3.6 Switch in sign in the South Indian Ocean

Another region with a well documented switch in the sign of water property changes is the South Indian Ocean. Here a transect from Australia to South Africa has been repeated 4 times since 1936. Bryden et al. (2003) pointed out that the freshening and cooling of upper thermocline waters prior to 1987 had reversed sign to become saltier and colder on density surfaces since. These observations have since been reflected in model results (Murray et al., 2007), caused by propagating anomalies in SAMW that is formed to the south and east of this section (Stark et al., 2006).

Although not shown, the methods employed in this chapter reveal a similar switch in this region (35°E-80°E:32°S-35°S), with the 26.7 kg m^{-3} density surface freshening and cooling by 0.044 psu from 1970-1992, before increasing in salinity by 0.010 psu from 1992-2005. Below these mode waters, AAIW continued freshening from 1970 to the present and is qualitatively in agreement with the results from Bryden et al. (2003). These similarities between the two studies gives confidence that the methods adopted here are robust enough to identify regional decadal oscillations in other ocean basins that have not been as well documented in the exiting literature.

4.4 Summary and discussion

This chapter builds on the results presented in Chapter 3 by using the Argo dataset to extend the analysis of water property changes over a longer time period (1970-2005). The extended time-series generally reveals a continuation of the patterns of change that were seen between the 1970s and the early 1990s. Separating the analysis into two time periods confirms this similarity, with both the 1970-1992 and the 1992-2005 time periods showing relatively consistent changes on a global scale. Both periods showed a coherent spatial pattern of salinity change, and similar patterns of upper-ocean warming and the associated steric sea-level changes. The consistency in the global patterns was most apparent near the shallow salinity-maximum with salinity increases, and near the salinity-minimum with freshening observed. As discussed in Chapter 2, the changes on these two surfaces are unambiguously the result of salinity change rather than a density-compensating response to temperature change. As such they can be used to reflect surface freshwater changes in both hemispheres. In the Southern Ocean, there was little difference in the changes between the two periods, with both showing deepening of density surfaces, and the salinity signal inferring a large surface freshening.

Both the North Atlantic and the South Indian Ocean had a switch in the sign of salinity and temperature changes on density surfaces between 1970-1992 and 1992-2005. In previous studies such changes in the sign of water property changes have been linked with regional ocean and atmospheric oscillations (ie. NAO, ENSO).

An approach that separates decadal-scale oscillations from the long-term trends, requires a different methodology to the one used in this study. This is likely to include the use of models and/or a time-series analysis in regions with sufficient observations. Unfortunately in this study the lack of observations in the Southern Hemisphere meant that a synoptic approach was the only way to ensure complete global coverage. While this approach may not *identify* short-term (interannual) and longer-term (multi-decadal) oscillations, the time weighting functions in Equation 2.8 (Chapter 2) tends to naturally *smooth* out some of these. This means the differences are more likely to be the result of longer-term variability or trends than the aliasing of a short-term oscillation. With the exception of possibly ENSO, the use of global averages tends to minimise the effect of any single regional oscillation, revealing a clear, consistent, and coherent pattern of salinity and temperature change on density surfaces over the last 50 years.

Chapter 5 Oxygen changes: 1970-1992

5.1 Introduction and review of oxygen literature

After temperature and salinity, one of the most important observations for studying ocean circulation is oxygen concentration, which can be used to infer both the age of the water since ventilation and the circulation pathways of the water masses. By combining changes in oxygen with changes in temperature and salinity the variability in the global circulation and renewal rates can be better understood, and ultimately oxygen observations can be used to test coupled ocean-atmosphere models.

Models reveal global oxygen decreases in the upper 1000 m that average between 1-5 μmol kg^{-1} year^{-1} since the 1980s. These appear to be largely caused by changes in renewal rates and not changes in biological activity (Keeling and Garcia, 2002; Bindoff et al., 2007). In the future some of the largest changes are expected to occur in the Southern Ocean due to reduced Antarctic Bottom Water (AABW) formation (Matear et al., 2000). The continued warming of surface waters will firstly reduce oxygen capacity in thermocline waters through reduced ventilation (Matear and Hirst, 2003), and secondly will increase the upper-ocean stratification. This increased stratification will reduce the capacity of deep water to mix into surface layers, and therefore increase the time available for biological oxygen utilisation to occur (Matear and Hirst, 2003).

Observations over the last 50 years suggest that this predicted pattern of change has been occurring already, with Keeling and Garcia (2002) estimating a global net oxygen loss from the ocean of approximately 0.29$\pm$0.4 mol yr^{-1} (1990-2002). Strong oxygen decreases have been observed and associated with reduced ocean ventilation, and are apparent in the Southern Ocean (Matear et al. (2000); Keeling and Garcia (2002); Aoki et al. (2005): south of the Polar Front on γ_n =27.9 kg m^{-3}).

There have been a number of studies along repeat sections in the North Pacific, where large oxygen decreases in lower thermocline waters since the 1960s have largely

been explained by circulation changes, increased stratification, and reduced vertical exchange in the subarctic outcropping regions (Ono et al., 2001; Andreev and Watanabe, 2002; Emerson et al., 2004; Deutsch et al., 2005). These stratification increases and inferred weakening vertical circulation are largely due to freshening of the surface waters, and appear to also explain oxygen decreases on underlying density surfaces (down to 27.4 kg m^{-3}: Nakanowatari et al. (2007)).

This physical explanation for oxygen decreases is supported by Mecking et al. (2006) in one of the few studies to separate the biological and physical processes. Here they used chlorofluorocarbon-12 to derive ventilation age of the waters, finding relatively constant oxygen utilisation rates over much of the Pacific Ocean. The one exception was off the coast of California, where slight decreases in the utilisation rates suggest a biological explanation for oxygen increases in this region.

Outside of the North Pacific there are preliminary signs of a change in biological activity in some regions, with global decreases in primary production of up to 6% being inferred by Gregg et al. (2003) using satellite records of chlorophyll since the 1980s. These decreases occurred mainly in high-latitude regions and have significant implications for oxygen levels. Less primary production implies less organic detritus through the surface waters, decreasing biological activity within the deeper layers, and thus decreasing the amount of oxygen being utilised. This is contrary to the observed oxygen decreases in the ocean.

Although there have been a few model-based and regional observational studies that have investigated changes in oxygen concentration in relation to physical ocean properties, there are no *global* studies that include changes occurring before the 1990s. In this chapter the first such study is presented, and quantitative estimates of oxygen change along constant density surfaces are estimated. Changes in temperature, salinity, and the vertical movement of these surfaces are used to qualitatively support the argument that it is upper-ocean stratification changes that are largely driving the widespread oxygen decreases. The low number, poor quality, and sparse distribution of phosphates and nitrate profiles, limit our ability to understand the full effects of biological production changes, and are not addressed in this study.

Section 5.2 begins by discussing the dataset used and the method of analysis. Section 5.3 analyses global oxygen concentration changes on four representative surfaces (the

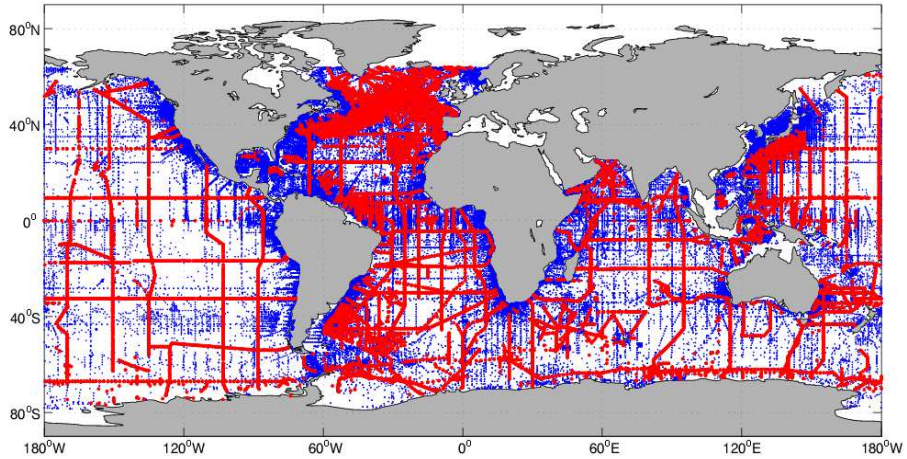

Figure 5.1: Distribution of historical (blue) and WOCE-period (red) profiles containing oxygen observations. The historical profiles were taken between 1950 and 1988, with the WOCE-period covered from 1988 to 2000.

shallow salinity-maximum, the 27.0 kg m^{-3} density surface, the salinity-minimum, and the 27.8 kg m^{-3} density surface), before the zonal, global, and along-isopycnal integrals are investigated in Section 5.4. In Section 5.5 the effects of temperature and salinity changes on the observed stratification are then analysed. Finally the results are discussed, and a physical model is proposed to explain the changes in the observed oxygen, temperature and salinity.

5.2 Data and methods

The methods used to determine oxygen change are identical to the analyses in Chapters 3 and 4 and as described in Chapter 2. This analysis involves mapping 201,174 globally distributed profiles to the locations of 38,002 profiles from the WOCE-period (Figure 5.1). This mapping was done along neutral density surfaces and has been detailed in Chapter 2.4. Although the number of historical oxygen profiles was much less than the historical temperature and salinity profiles used in Chapters 3 and 4, there was still an even temporal distribution of oxygen observations (Figure 5.2). Only those profiles with an associated set of oxygen observations are retained in the temperature and salinity analysis in this chapter, and the lack of oxygen sensors on most Argo floats has meant that only a single synoptic comparison could be made (1970-1992).

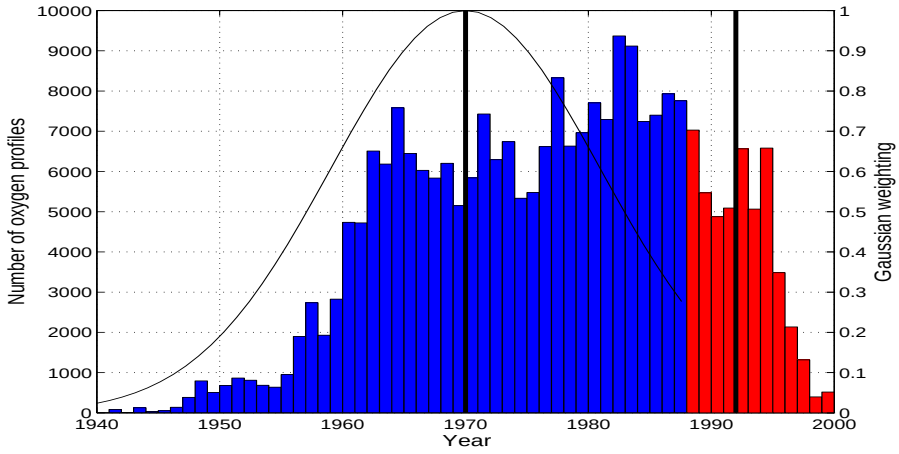

Figure 5.2: Temporal distribution of oxygen profiles. Blue indicates historical data, while red is the data that falls into the WOCE-period (with a mean year of 1992). The black vertical bar at 1970 is the year the historical data was interpolated to, and 1992 is the mean year of the data from 1988 to 2000.

While less common ocean tracers (nitrate, phosphate, silicate) were measured along a number of WOCE cruises, the number of historical profiles of these tracers is less than a quarter of the profiles in the oxygen dataset. While the examination of Redfield ratios and the relationship between the different tracers such as phosphate and nitrate would be possible in smaller regional studies, with this global approach and it was decided to only focus on the better distributed (in space and time) and high quality oxygen observations and relating the changes to physical mechanisms (stratification, surface temperature change).

Effect of warming on saturated oxygen concentrations

Saturated oxygen levels in the mixed layer are directly dependent on the surface water temperature, with warmer waters having a lower oxygen saturation level. Figure 5.3 illustrates this relationship, and it should be noted that salinity plays an almost negligible role in the saturation levels of oxygen. Oxygen concentration is approximately twice as sensitive to temperature changes in the high-latitude colder waters, than it is to an identical temperature change in the warm surface waters in equatorial regions.

In any analysis of oxygen change, there is a need to separate the oxygen signal due to biological or circulation changes, from an oxygen signal that is due to changes in

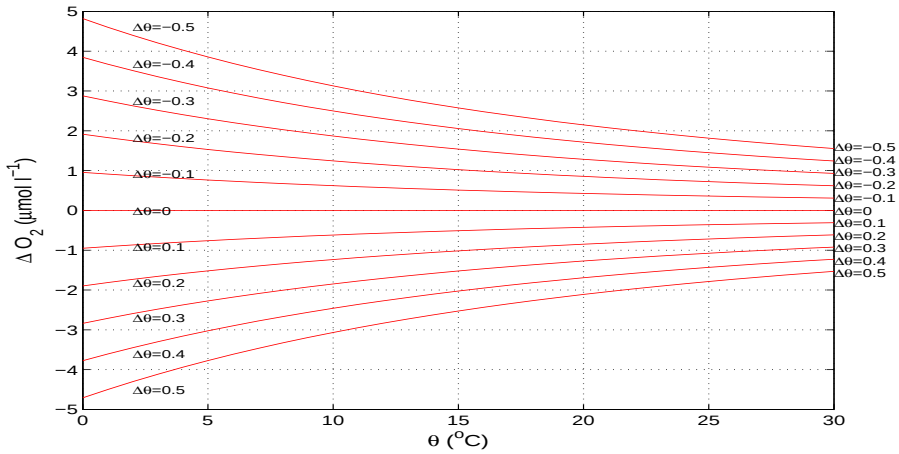

Figure 5.3: Sensitivity of the saturated oxygen concentrations to changes in temperature. A number of temperature change scenarios are shown ($\Delta\theta$), with the effect on saturated oxygen being shown (y-axis). Climatological temperatures are shown on the x-axis, and the salinity is fixed at 35 psu. Negative values indicate a cooling and a decrease in the saturated oxygen concentration.

the oxygen capacity of the water. Given that the initial oxygen concentration for a parcel of water is set in the mixed layer where the water is saturated in oxygen, any changes in the mixed layer temperature will appear as a change in the oxygen concentration levels as the parcel is advected into the ocean interior. In this chapter the change in temperature is calculated in situ in the ocean interior, and is assumed to be equal to the temperature differences at the surface at the time when the water was ventilated. Therefore the temperature-driven changes in the saturated oxygen capacity (ΔO_{sat}) are estimated by;

$$\Delta O_{sat} = O^2_{sat} - O^1_{sat}, \tag{5.1}$$

where O^1_{sat} and O^2_{sat} are the oxygen capacity of the water in the 'historical' ($\sim$1970) and WOCE ($\sim$1992) periods respectively. These estimates of the saturated oxygen change were calculated using CSIRO computation routines that were based on equations from Weiss (1970). As in previous chapters, the upper-100 dbar was assumed to represent the seasonal mixed layer, and hence was excluded from the estimates of oxygen concentration change.

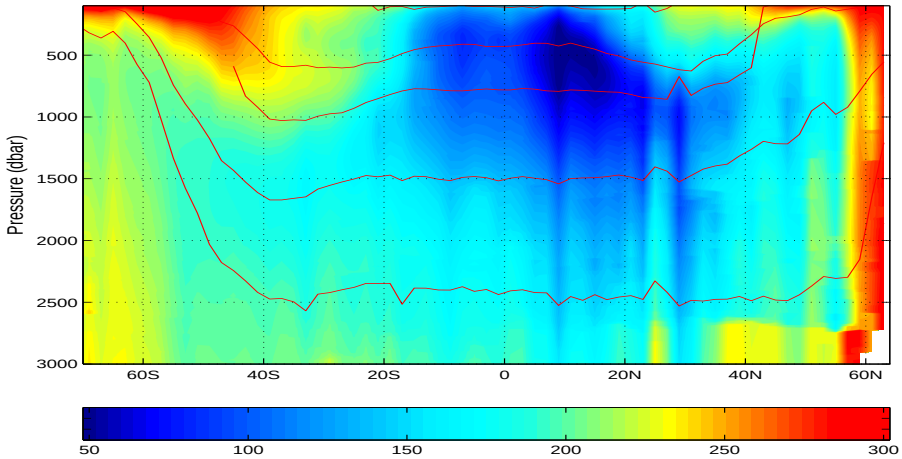

Figure 5.4: Zonally averaged oxygen values (μ mol l^{-1}) from the historical data. The average depth of the 27.0 kg m^{-3} isopycnal, the salinity-minimum surface, and the 27.8 kg m^{-3} and 28.0 kg m^{-3} density surfaces are shown.

5.3 Oxygen concentration changes in key water masses

Four density surfaces were identified as representing the key water masses in the upper 3000 dbar - the shallow salinity-maximum, 27.0 kg m^{-3}, the salinity-minimum, and the 27.8 kg m^{-3} surfaces. These density surfaces tend to follow the upwelling of low oxygen waters, and the subducting saturated oxygen waters (Figure 5.4). The lateral gradients of oxygen on these surfaces indicate where ventilated water masses subduct into the ocean interior, and the regions where oxygen is consumed by ocean biology over time (eg. Sarmiento and Gruber (2006)).

Using oxygen utilisation rates in conjunction with observed oxygen changes can allow changes in the age of water masses to be estimated. While knowing the time since ventilation is valuable in understanding ocean changes, this number has not been explicitly calculated in this thesis due to the lack of data on oxygen utilisation rates across much of the globe.

5.3.1 Oxygen change in shallow salinity-maximum waters

The first of the water masses is the shallow salinity-maximum surface, which is found just beneath the mixed layer in equatorial and tropical zones. Because of the relatively short flushing time of this shallow layer, the oxygen concentration of this water mass is generally near saturation, and the shallow depths mean that this surface could potentially be aliased by regional oscillations (ie. ENSO).

Table 5.1: Oxygen and salinity changes in key water masses: ∼1970-1992

Surface:	**Water mass:**	**Region:**	Δ $\mathbf{O_2}$ μmol l^{-1}	$\Delta\theta$ psu
Salinity max.	Upper thermocline	Global	-2.6	0.10
27.0 kg m^{-3}	SAMW	Southern hemisphere	-4.4	-0.13
	18° water	North Atlantic	-7.9	-0.03
Salinity min.	AAIW	Southern hemisphere	-3.0	-0.10
	Intermediate depths	North Atlantic	-0.4	-0.11
	NPIW	North Pacific	-0.7	-0.13
27.8 kg m^{-3}	NADW	Atlantic Ocean	-0.6	-0.02
	CDW	Southern Ocean	-10.0	0.06
	CDW	Indian Ocean	-1.2	-0.04
	CDW	Pacific Ocean	-1.9	-0.01

At the shallow salinity-maximum there has been a globally averaged decrease in oxygen (2.6±0.7 μmol l^{-1}: see Table 5.1) between 1970 and 1992. However there is little inter-basin coherence (Figure 5.5 (a)) and the magnitude of this decrease is comparatively small when compared with the oxygen decreases observed along intermediate and deep water density surfaces. Across almost all ocean basins the change in the oxygen concentration signal is statistically significant in individual grid cells (Figure 5.5 (d)).

On the shallow salinity-maximum surface in the Atlantic Ocean there are oxygen increases in the poleward extremes and decreases in the equatorial regions. However overall, 65% of grid cells in this ocean show oxygen increases in this ocean (Figure 5.5 (a)). The Indian Ocean shows similar oxygen increases in the Southern Hemisphere gyre (averaging 1.6 μmol l^{-1}), while the changes north of the equator are of the opposite sign (-4.4 μmol l^{-1}), and are largest in cells bordering land. A similar hemispheric difference occurs in the West-Pacific Ocean, and although coherent on large spatial scales, is of the opposite sign to the Indian Ocean, with oxygen increases in the north and oxygen decreases in the south. The East Pacific shows a similar signal on the shallow salinity-maximum to the Atlantic Ocean, with weak oxygen increases in the poleward extremes and decreases of up to 50 μmol l^{-1} on the equator (representing up to a 10% decrease in oxygen: Figure 5.5 (b)).

A deepening of the shallow salinity-maximum will contribute to an increase in oxy-

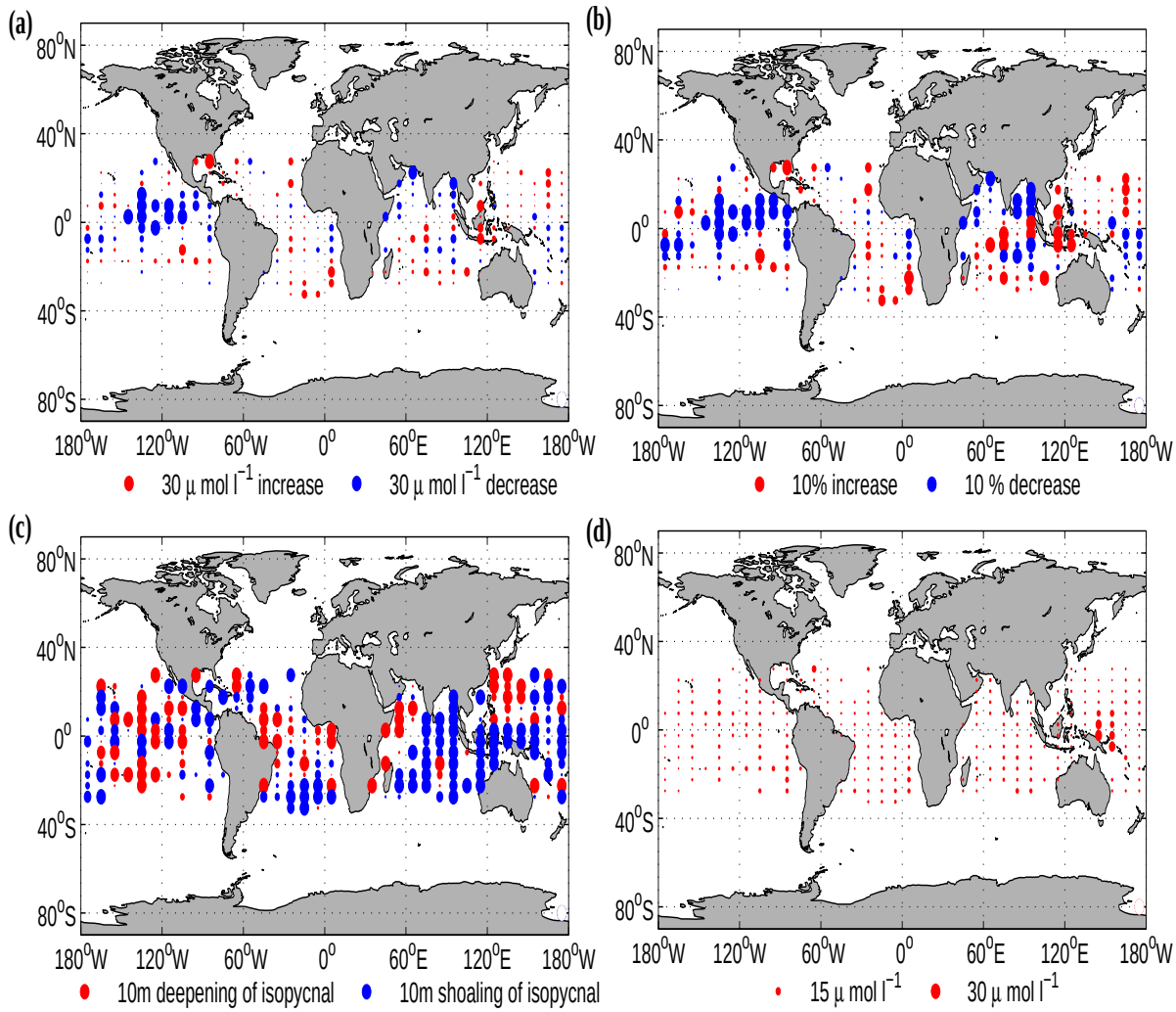

Figure 5.5: Changes at the shallow salinity-maximum. **(a)** Oxygen change in μmol l^{-1}. **(b)** Proportional change in relation to the climatological oxygen values. **(c)** Vertical movement of the density surface in the water column. **(d)** An approximate 95% confidence interval of the oxygen change inside each cell.

gen on pressure surfaces, as in general the lighter density layers have higher oxygen concentrations than the denser surfaces (Figure 5.4). The West-Pacific Ocean shows a mixed pattern, with deepening of the shallow salinity-maximum accompanying the oxygen increases along density surfaces north of the equator, and shoaling accompanying the decreases south of the equator (Figure 5.5 (c)). In the Atlantic Ocean there is shoaling at the poleward extremes and deepening in the equatorial region. The East Pacific Oceans shows little coherence in the movement of the density surface, but clear evidence of shoaling throughout most of the southern and eastern Indian Ocean (averaging 10 dbar).

5.3.2 Oxygen change in mode waters

The 27.0 kg m^{-3} density surface is typically found between 300 and 600 dbar and is representative of mode water in the Southern Ocean. Together with underlying intermediate water, this water mass provides one of the main pathways for oxygen rich water to subduct into the ocean interior. This is shown in Figure 5.4, where the high-oxygen tongue begins in the mixed layer at approximately 50°S and subducts northward into the ocean interior with the oxygen being depleted by biological utilisation as the water spreads away from its ventilated source region. A similar pattern is found in shallower waters in the Northern Hemisphere.

Globally this 27.0 kg m^{-3} surface (Figure 5.6 (a)) shows some of the largest oxygen decreases in the water column, averaging 4.1 μmol l^{-1} (a change of about 3%). The signal on this surface is strongest in the Atlantic Ocean, with an average decrease of 7.5 μmol l^{-1}. Here we also observe a spatially coherent signal, with 84% of cells showing a decrease in oxygen. The strongest decreases in the Atlantic Ocean occur in the north where the isopycnal properties are formed through mixing with recently ventilated Labrador Sea Water, and in the Southern Hemisphere tropics between the equator and 30°S.

Unlike the shallow salinity-maximum surface, the Pacific Ocean shows comparatively weak oxygen decreases in the east, and little coherence in the middle of this ocean basin. The North-West Pacific Ocean shows slight increases on the 27.0 kg m^{-3} surface, but the switch of sign in the oxygen changes at the equator that was observed at the shallow salinity-maximum, is no longer apparent. Except for a small region in the middle of the Southern Hemisphere Indian Ocean subtropical gyre, the Indian Ocean has decreased in oxygen, with the strongest decreases observed in the

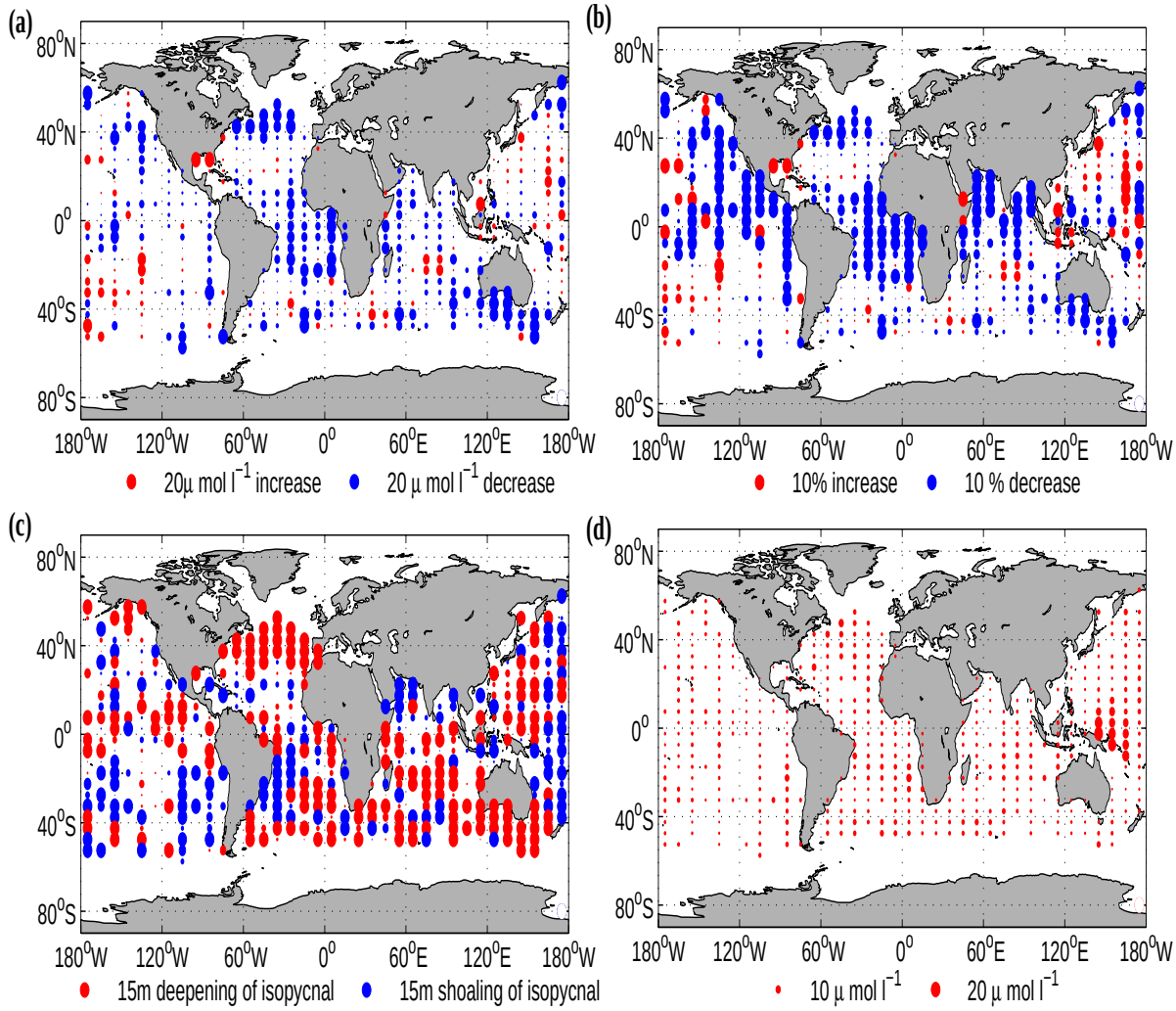

Figure 5.6: Oxygen changes on the 27.0 kg m^{-3} density surface. **(a)** Oxygen change in μmol l^{-1}. **(b)** Proportional change in relation to the climatological oxygen values. **(c)** Vertical movement of the density surface in the water column. **(d)** An approximate 95% confidence interval of the oxygen change inside each cell.

Northern Hemisphere gyre and south of Australia in the southern margins of the 27.0 kg m^{-3} density surface.

The 27.0 kg m^{-3} density surface shows a coherent pattern of deepening across all but the South Pacific Ocean (Figure 5.6 (c)), with the changes being largest near ventilation regions in the North Atlantic and in the margins near the surface in the Southern Ocean. In general the 27.0 kg m^{-3} surface represents an oxygen maximum near the source regions in the Southern Hemisphere, and therefore this deepening results in an oxygen decrease on pressure surfaces.

5.3.3 Oxygen change in intermediate waters

On the salinity-minimum there has been an average global decrease in oxygen of 1.9 μmol l^{-1}, although the changes are not as coherent on large spatial scales as they are on the 27.0 kg m^{-3} density surface (Figure 5.7 (a)). The salinity-minimum isopycnal (in the Southern and North Pacific Oceans) represents intermediate water that originates from the high precipitation regions ($\sim$50° north and south). The subducting tongue of recently ventilated water (and therefore high in oxygen) can be seen clearly in the Southern Hemisphere (Figure 5.4). In the North Pacific this salinity-minimum is less dense than in the Southern Hemisphere (approximately 26.8 kg m^{-3}), while in the North Atlantic the intermediate waters are not characterised by a salinity-minimum in the water column, and are instead formed from sources in the Labrador Sea.

In the North Pacific between 0° and 30°N we see coherent oxygen increases in the west and middle of the basin (NPIW), with oxygen decreases in the east of up to 10%. Further north in the Pacific Ocean (30°N-50°N), close to the Sea of Okhotsk NPIW source region, decreases of up to 5% are observed on the salinity-minimum surface (Figure 5.7 (b)). Similar decreases are observed in the equatorial Pacific Ocean (15°S-15°N) where there are basin wide decreases averaging 3.0 μmol l^{-1}.

The Atlantic Ocean shows coherent patterns of change on basin scales. In the far north the recently mixed water shows comparatively weak increases in oxygen, while weak but coherent decreases are observed throughout the rest of the ocean, with the exception of the middle of the South Atlantic Ocean gyre (20°S-40°S) where the oxygen level increases.

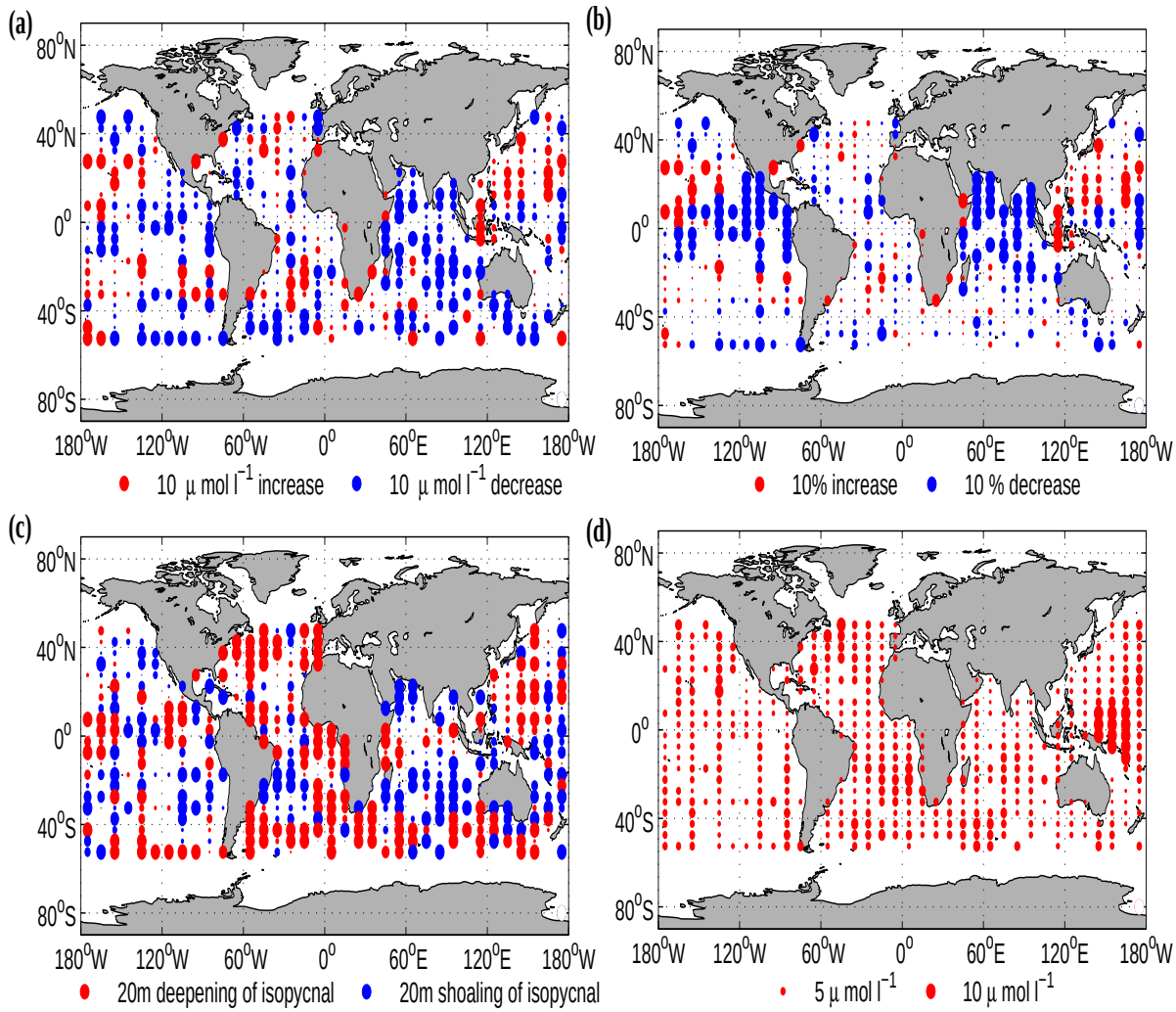

Figure 5.7: Oxygen changes at the salinity-minimum. **(a)** Oxygen change in μmol l^{-1}. **(b)** Proportional change in relation to the climatological oxygen values. **(c)** Vertical movement of the density surface in the water column. **(d)** An approximate 95% confidence interval of the oxygen change inside each cell.

The Indian Ocean shows the most coherent pattern of change of any of the oceans, with 73% of cells decreasing in oxygen by an average 3.7 μmol l^{-1}. This was accompanied by an average shoaling of 13 dbar in the subtropical gyre (10°S-35°N: Figure 5.7 (c)). Elsewhere there tended to be shoaling of the salinity-minimum isopycnals between 10°S and 30°S (except in the East Atlantic Ocean), and deepening of the surface across the rest of the globe.

5.3.4 Oxygen change in deep waters

The 27.8 kg m^{-3} density surface is characteristic of North Atlantic Deep Water in the Atlantic, and Circumpolar Deep Water in the Southern Indian and Pacific Oceans. NADW is ventilated in the North Atlantic, flows between 1000 and 2500 dbar before upwelling in the Southern Ocean. Note that in the Southern Ocean the 27.8 kg m^{-3} density surface more closely represents the oxygen minimum (UCDW: Figure 5.4: red line), than it does with the lower-limb salinity-maximum (LCDW: $\sim$28.0 kg m^{-3}).

The changes in oxygen on the 27.8 kg m^{-3} density surface show good coherence on large spatial scales, although the sign of change varies by ocean basin (Figure 5.8 (a)). In the Atlantic Ocean from 40°N-25°S there is an average increase of 1.6 μmol l^{-1} in NADW, with 63% of cells showing this sign of change. South of 30°S in the Southern Ocean, there is a strong circumpolar decrease in oxygen (averaging 10.0 μmol l^{-1}), associated with CDW.

This water mass spreads northward and coherent decreases can be found up to the equator in the Indian and Pacific Oceans. In the low-latitude Pacific Ocean the oxygen changes are of a smaller magnitude and are a mixture of increases and decreases in concentration. However north of 30°N in the Pacific Ocean there is a large and basin-wide decrease in the observed oxygen levels.

As with the oxygen changes on density surfaces there were widespread differences between ocean basins in the vertical movement of the 27.8 kg m^{-3} density surface. In both the NADW formation region and south of the Subtropical Front this surface deepened, while in the low and mid-latitude Pacific Ocean the density surface has shoaled. Both the Indian and Atlantic Ocean mid-latitudes only had small changes, with little coherence in the direction of isopycnal movement.

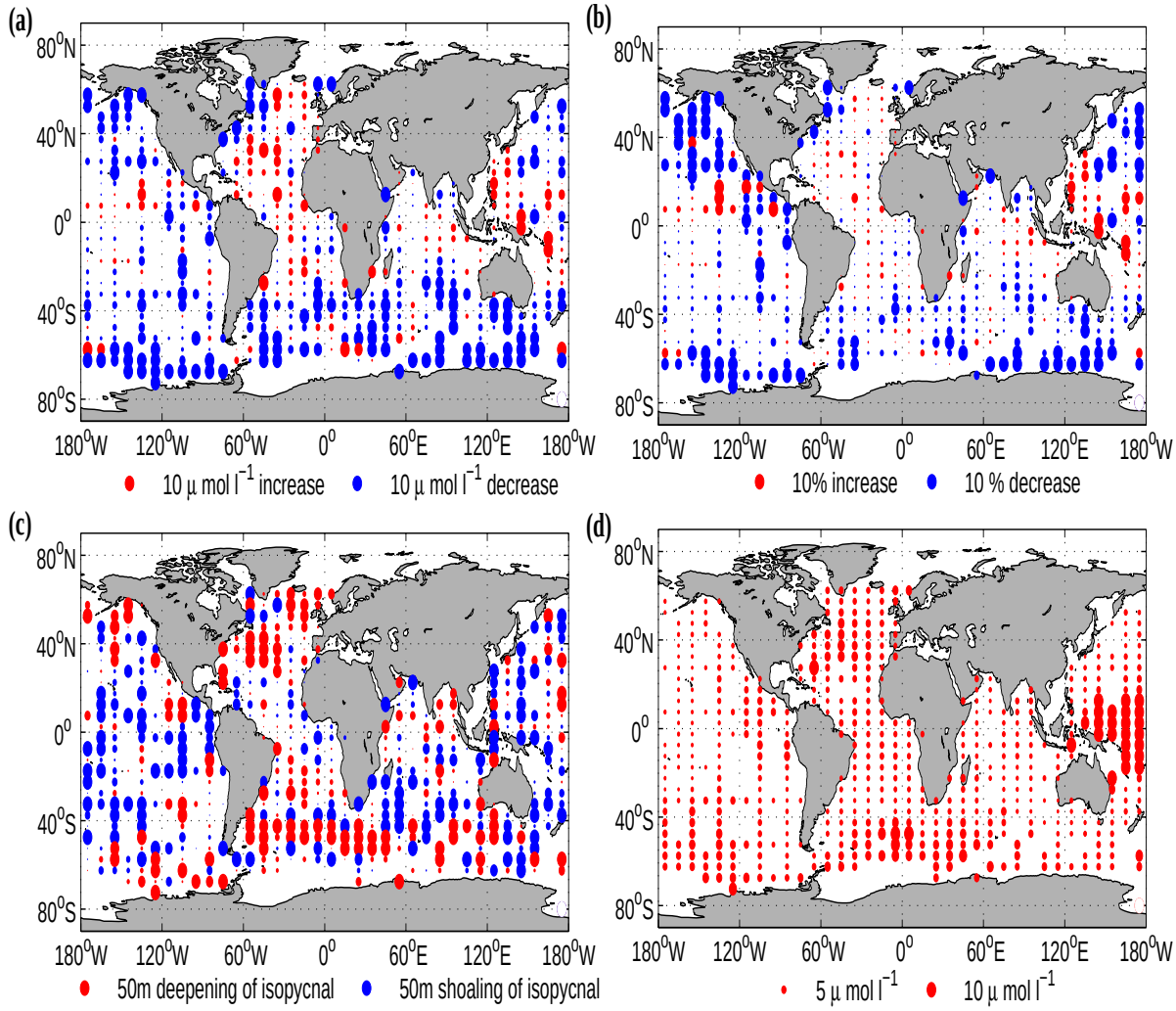

Figure 5.8: Oxygen changes on the 27.8 kg m^{-3} density surface. **(a)** Oxygen change in μmol l^{-1}. **(b)** Proportional change in relation to the climatological oxygen values. **(c)** Vertical movement of the density surface in the water column. **(d)** An approximate 95% confidence interval of the oxygen change inside each cell.

5.4 Integrated oxygen changes

5.4.1 Zonally integrated changes

While looking at oxygen changes on a single surface is useful for revealing the broad-scale patterns and regional variability in an individual water mass, zonal averages of all the density surfaces allows more coherent patterns to emerge, and makes it possible to assess changes in the inventories of oxygen throughout the global oceans.

Oxygen changes can occur along density surfaces due to changes in the exchange between the ocean interior and the mixed layer, and in Figure 5.9 (a) these zonally averaged changes on density surfaces are shown as a function of pressure. The zonal averages of oxygen on density surfaces show global patterns, with decreases in oxygen concentration across almost all the upper 1500 dbar. Poleward of 30°S and 40°N these deep and penetrating decreases extend to at least 3000 dbar in the water column and included the CDW, AAIW, SAMW, and NADW water masses. Interestingly, while temperature and salinity changes show a significant reduction in magnitude with depth, the difference between the surface and the deep oxygen concentration changes is not as marked. On deep isopycnals between 30°S and 25°N (below 1500 dbar) there is evidence of oxygen increases ($\sim$2 μmol l^{-1}) on large spatial scales. These oxygen increases come largely from the Atlantic and Indian Oceans (Figure 5.8 (a)).

The largest zonally averaged oxygen decreases are found in the high-latitude regions of both hemispheres, with comparatively small decreases in the equatorial regions (Figure 5.9 (a)). Poleward of 45°S (100-500 dbar) decreases of between 15 and 40 μmol l^{-1} are seen across the upwelling CDW ventilation and the AAIW subduction regions, while decreases in oxygen concentration of a similar magnitude are also found north of 40°N in the upper 300 dbar. In the high Northern Hemisphere latitudes the strong surface oxygen decreases extend throughout the water column in a narrow band, with the decreases between 50°N and 60°N being twice the magnitude of the surrounding oxygen decreases. This zonally averaged oxygen decrease is largely the result of NADW changes in the North Atlantic (Figure 5.8 (a)). In the subtropical gyres relatively weak zonally averaged oxygen increases are seen (200-600 dbar: 20°-30° north and south).

Changes in oxygen concentration on pressure surfaces can occur independently of

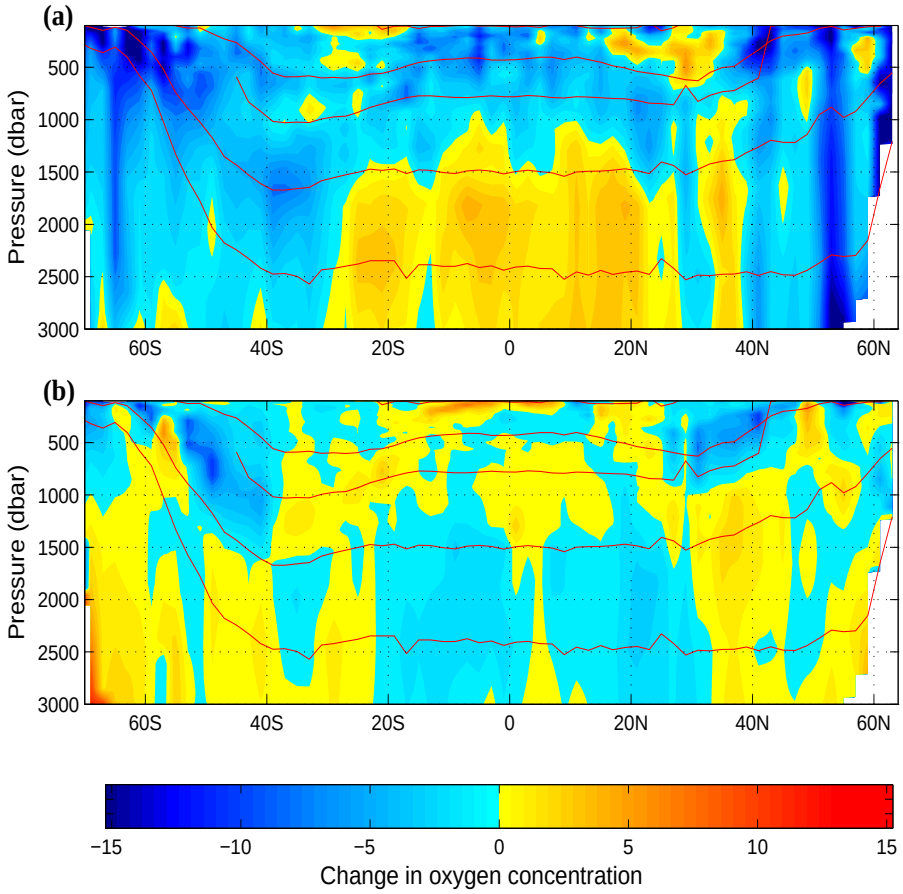

Figure 5.9: Zonally averaged oxygen changes on density surfaces as a function of pressure in μmol l^{-1}. **(a)** Oxygen changes on density surfaces between 1970 and 1992. **(b)** The oxygen change due to heave of isopycnals alone ($N' \frac{\partial O_2}{\partial z}$). The average depth of the shallow salinity-maximum, the 27.0 kg m^{-3}, the salinity-minimum, the 27.8 kg m^{-3} and the 28.0 kg m^{-3} surfaces are shown.

any changes along an isopycnal as a result of the vertical movement of density surfaces in the water column (N'). This movement has the effect of shifting a density surface with higher or lower oxygen concentration vertically in the water column, thus appearing as an oxygen change on a pressure surface. In Figure 5.9 (b) the product of density surface movement (N') and the vertical oxygen gradient ($\frac{\partial O_2}{\partial p}$) was estimated and shown as a function of pressure. The oxygen changes due to displacement of the density surface revealed a zonally averaged pattern with a less coherent structure and lower magnitudes of oxygen concentration change than in Figure 5.9 (a).

North of 40°N in Figure 5.9 (b), isopycnal movement tended to produce an increase in oxygen concentration on pressure surfaces between 700 and 1500 dbar. South of 40°S, deepening of density surfaces in the upper 1500 dbar appears as a decrease in oxygen concentration on pressure surfaces, although below 1500 dbar this deepening results in oxygen increases on pressure surfaces. At latitudes between 40°S and 40°N the movement of isopycnals produced a less coherent pattern of oxygen change on isobars .

The magnitude of oxygen concentration change due to isopycnal motion (Figure 5.9 (b)) is generally less that half that of Figure 5.9 (a), meaning that the sum of oxygen change (ie. the total change on isobars - not shown) tends to be dominated by changes along density surfaces, rather than by the vertical movement of isopycnals. As such, the globally coherent pattern of total oxygen concentration change seen in Figure 5.9 (a) is largely retained when considering the total change on pressure surfaces (ie. $\Delta O_2|_n + N' \frac{\partial O_2}{\partial z}$).

5.4.2 Back-projected changes along density surfaces

While changes in temperature and salinity along density surfaces can be traced back and attributed to changes in the properties of the mixed layer, changes in oxygen require a different interpretation. In the mixed layer oxygen is at saturation, meaning that the changes on density surfaces can only be driven by a change in the exchange of water between the mixed layer and the ocean interior, a change in the saturation level, or a change in the oxygen utilisation rates. In this analysis, we have corrected for temperature-driven changes in oxygen saturation in the upper 100 dbar (see Section 5.2), and based on the literature (Mecking et al., 2006) the oxygen utilisation rates are assumed to be relatively constant over the last 50 years.

Clear oxygen decreases were revealed in the deeper density surfaces (26.5-27.9 kg m^{-3}: Figure 5.10 (a)). These density surfaces intersect (effectively 'outcrop') with the mixed layer poleward of 40° in both hemispheres. This pattern of decreases is relatively symmetrical between the hemispheres, with the largest changes occurring in the layers that outcrop poleward of 60°S and around 55°N and are greater than the estimate of uncertainty. Comparatively little oxygen change was observed in the density layers that outcrop between 30°S and 40°N.

With the exception of 60°S-65°S and 45°N-55°N (dominated by NADW cooling), Figure 5.10 (b) shows a widespread increase in the zonally integrated heat content when back-projected along density surfaces to the outcropping region (as discussed in Chapter 3.4). This effect is amplified by the temperature changes in the upper 100 dbar, which show a global increase in heat content between 1970 and 1992 (Figure 5.10 (c)), as estimated from the Hadley SST time-series (Rayner et al., 2003). The changes in precipitation-minus-evaporation (Figure 5.10 (d)) show a similar zonal pattern of change, with the largest increases occurring poleward of 40°S, and slight decreases occurring in subtropical regions. Both this freshening and the heat content increases (Figure 5.10 (b-c)) of the surface layer are likely to increase the stratification of the ocean (Figures 5.12-5.13), and therefore decrease the volume of subducting water in formation zones, and reduce the volume of water upwelled into the mixed layer. This would thus allow more time for biological oxygen consumption in the ocean interior.

Figure 5.10 (e), from Chapter 3.4, shows little change in volume in isopycnals that outcrop in the mid and high-latitudes in both hemispheres, possibly suggesting a poleward displacement of isopycnals with no overall stratification change. While there has been little *total* volume change in density layers in a *zonally averaged* sense, this does not preclude *regional* stratification changes around the key water mass ventilation areas that control the overall renewal rates of water masses.

5.4.3 Globally integrated changes

Taking a global area-weighted average for each density surface reveals oxygen concentration decreases throughout the water column. In the lighter density layers found around the shallow salinity-maximum (24.0-26.0 kg m^{-3}), globally averaged decreases of up to 2 μmol l^{-1} can be seen, which represents a decrease of approxi-

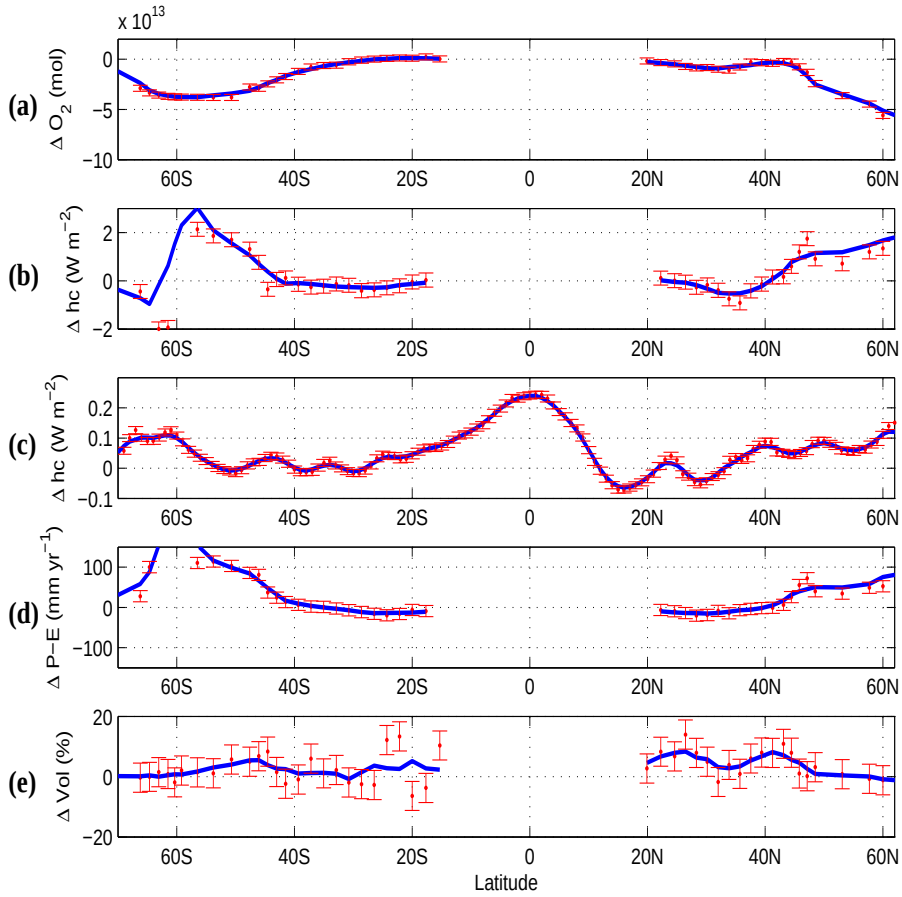

Figure 5.10: Zonally integrated changes from 1970 to 1992 along density layers from the outcropping zone to the equator. **(a)** Changes is surface oxygen exchange (mol). **(b)** Apparent surface heat content input (W m^{-2}). **(c)** Heat content input from 0-100 m (W m^{-2}: from the Hadley SST dataset). This was integrated vertically in the water column rather than along density surfaces. **(d)** Apparent precipitation-minus-evaporation changes (mm yr^{-1}) based on salinity observations. **(e)** Density-layer volume changes (%). On all panels the error bars are shown are at one standard error.

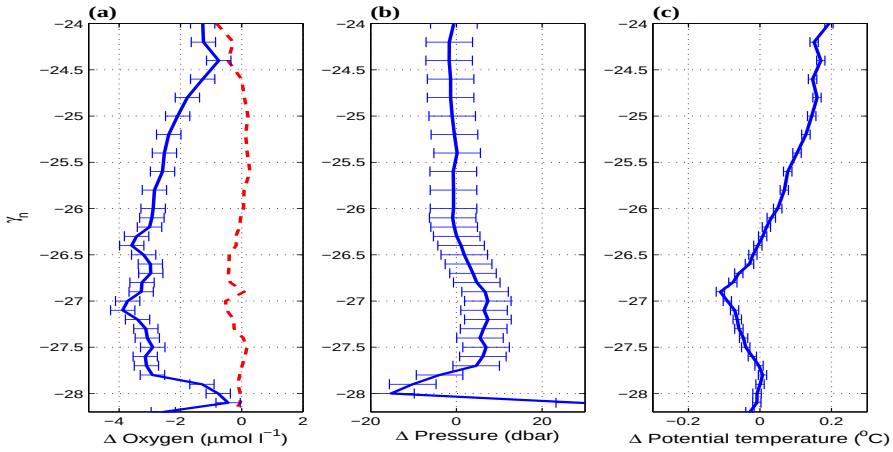

Figure 5.11: Globally averaged changes from 1970 to 1992 by density layer. **(a)** Oxygen change in μmol l^{-1} on isopycnal layers below 100 dbar (blue). The red line shows the globally averaged oxygen change on each density layer that can be apportioned to temperature change. **(b)** Change in isopycnal depth where positive values indicate a deepening of the density surface in the water column. **(c)** Temperature change on density surfaces. On all panels, the error bars indicate the 95% confidence level.

mately 1% in the average oxygen concentration. Larger oxygen decreases occur in density surfaces covering the lower thermocline and the deep layers (Figure 5.11 (a): 26.0-27.8 kg m^{-3}).

In Figure 5.11 (a) (red line) the sensitivity to mixed layer temperature change is apparent, with approximately half the oxygen decreases near the shallow salinity-maximum being attributable to warming of surface waters. This influence reduces strongly with depth, with more than 85% of the global oxygen signal in lower thermocline and mode waters ($\sim$26.5-27.0 kg m^{-3}) caused by mechanisms other than surface temperature changes. In the underlying intermediate and deep waters, the effect of surface temperature change on oxygen is negligible, largely due to the relatively small size of the surface mixed layer when compared with the overall volume of these water masses.

The widespread decreases in oxygen concentration correspond with a globally-averaged deepening in the density surfaces between 26.0 and 27.8 kg m^{-3}, with a shoaling in denser densities (Figure 5.11 (b)). This overall shoaling below 27.8 kg m^{-3} mainly occurs in the low-latitude Pacific Ocean (Chapter 3, Figure 3.9

(c-d)). There is a globally averaged warming on density surfaces above the upper-thermocline (26.4 kg m^{-3}), while there is cooling on isopycnals below this (Figure 5.11 (c)).

When the oxygen changes are weighted by the thickness of the isopycnal layer, a global decrease in oxygen of 1.82±0.92 μmol l^{-1} (80°S-64°N) throughout the entire water column is observed between 1970 and 1992. The weighted average gives a globally averaged oxygen value of approximately 180 μmol l^{-1}, this oxygen change amounts to a decrease of 1% of the global oxygen content. This decrease in global oxygen content is equivalent to a net flux of oxygen to the atmosphere of $0.58 \pm 0.3 \times 10^{14}$ mol yr^{-1}, and compares with ocean models that suggest recent losses in oxygen of $0.2 - 0.7 \times 10^{14}$ mol yr^{-1} (Keeling and Garcia, 2002).

5.5 Stratification changes

One possible explanation is that the widespread oxygen decreases could be due to changes in the ocean stratification ($\partial\rho/\partial z$). Increased stratification reduces the subduction between the mixed layer and the ocean interior, while reduced stratification has the opposite effect. For upwelling waters, increased stratification allows more time for oxygen depletion to occur, while in subducting regions, increased stratification directly reduces ventilation rates and thus the renewal of oxygen saturated waters.

While on a global scale there is no one clear global pattern of stratification changes (Figure 5.12), there is general coherence within ocean basins, and strong correlations between water mass ventilation regions and patterns of stratification change. On the southern flank of the Subtropical Front (shown in black in Figure 5.12), the majority of SAMW is formed in both the Atlantic and Indian Ocean sector of the Southern Ocean (Talley, 1999; Hanawa and Talley, 2001; Sallée et al., 2006). These regions have undergone significant stratification increases from 200-1000 dbar, with a strong coherent signal evident. Poleward of this in the ACC there appears to be weak stratification decreases that are especially coherent in the Atlantic Ocean.

The South-East Pacific Ocean off the coast of Chile is the main formation regions for AAIW (Rintoul et al., 2001). Here the stratification changes appear to be weak, and of a mixed sign (Figure 5.12: circled).

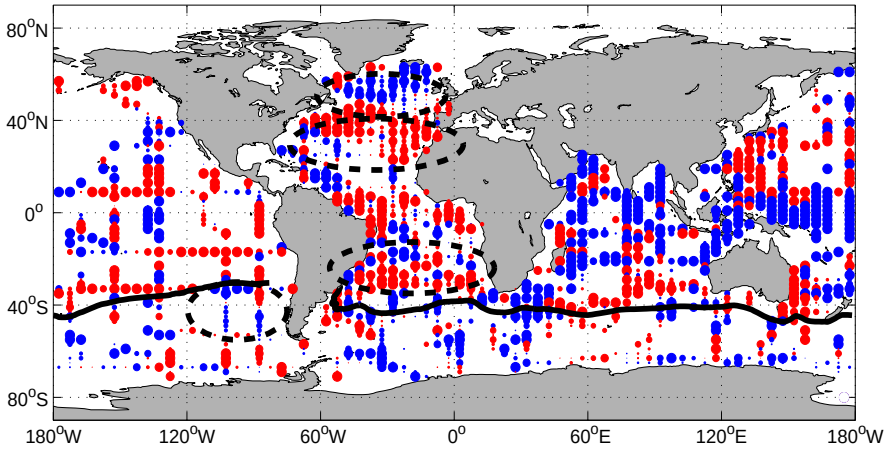

Figure 5.12: Stratification changes (1992-1970) from 200 to 1000 dbar ($\frac{\partial(\rho_2-\rho_1)}{800}$). Red values indicate increasing stratification, while blue indicates decreasing stratification. The black line shows the position of the Subtropical Front, and the circled regions are referred to in the text.

The mid-latitudes in the Atlantic Ocean have strong stratification increases (Figure 5.12: circled). These are regions of significant upper-ocean mixing, with newly formed upper-thermocline and mode waters being advected into the ocean interior and replaced by the deeper intermediate waters upwelling and entering the mixed layer. In the Pacific Ocean there is an additional east-west pattern to the changes. A strong, coherent equatorial region of stratification decreases is present in the west, while there are general stratification increases in the east.

This sort of equatorial east-west pattern in the Pacific Ocean is indicative of an El Niño-type signal, where the loss of heat from the upper-waters in the west causes shoaling of density surfaces below 200 dbar, and thus a decrease in stratification. Likewise the eastward transfer of surface ocean heat along the equator results in lighter water in the water column, and therefore causes deepening of density surfaces in the east.

While the mid-latitude North Atlantic Ocean shows clear evidence of stratification increases, there is a coherent stratification decrease poleward of 50°N (Figure 5.12: circled). This in the NADW formation region where cooling along density surfaces has been observed from 1970 to 1992 (Chapter 4).

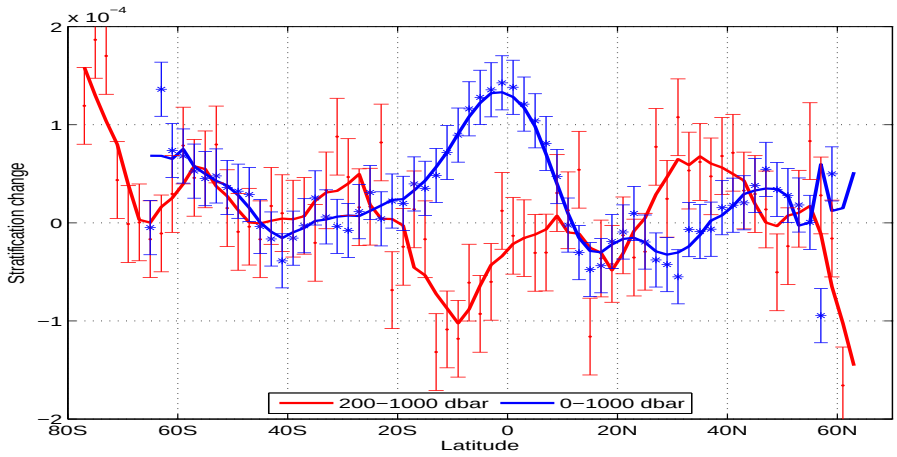

Figure 5.13: Zonally averaged stratification changes (1992-1970) from $(\frac{\partial(\rho_2-\rho_1)}{\partial z})$. The red line is a running mean for stratification changes between 200 and 1000 dbar. The blue line is a running mean of stratification changes between the surface and 1000 dbar, where the density changes in the top 100 dbar are based on a changing temperature (from the Hadley SST dataset: Rayner et al. (2003)) and a fixed salinity (from the Levitus annual salinity climatology: Levitus (1999)). Error bars are calculated used methods described in Chapter 2.5.

The zonally averaged stratification changes (Figure 5.13: red line) between 200 and 1000 dbar generally show increased global stratification in the mid and high-latitudes, and decreased stratification in the subtropical and equatorial regions (driven by large regions of cooling in the Pacific and Indian Oceans). Such a zonally averaged pattern of change reflects the changes in apparent heat and freshwater fluxes that are identified both here (Figure 5.10 (b,e) and Chapter 3), and in previous global studies (Bindoff et al., 2007; Levitus et al., 2005a).

The estimated change in surface density from the SST climatology and the apparent freshwater fluxes from this thesis reveals that the strong equatorial heat content changes in the upper 100 dbar (Figure 5.10 (c)) create new lighter density surfaces, and are sufficient to change the sign of the stratification changes in the equatorial latitudes (Figure 5.13: blue line). Potentially this signal is associated with aliasing of the El Niño phenomenon over the dataset. In the mid-latitude Northern Hemisphere there is a slight decrease in the zonally averaged stratification change that occurs when the top 200 dbar is included, due to the gradient of density change in the surface layers being weaker than in the underlying 800 dbar (ie. $\frac{\partial(\rho_2-\rho_1)}{1000-200} > \frac{\partial(\rho_2-\rho_1)}{1000-0}$).

Poleward of 45°S and from 35°S-55°N, there are clear increases in stratification (0-1000 dbar) that are associated with increasing heat content (Figure 5.10 (c)) and greater freshwater in the mixed layer (Figure 5.10 (b)). Both processes generate lighter surface density layers.

In Figure 5.13 (blue line) there is evidence of reduced stratification from 10°N-35°N and weak stratification increases from 30°S-45°S. This stratification decrease may appear counter-intuitive given that when both regions have clearly increased in heat content. However, the deepening of density surfaces in these two regions (Figures 5.6-5.8 and inferred from Figure 5.9 (b)) has the effect of moving lighter isopycnals downward across the 1000 dbar level, thus reducing the density at that depth. Given that this density decrease at 1000 dbar is larger than the density change at the surface, a reduced stratification is evident.

The instantaneous subduction rate (S) of fluid from the mixed layer into the ocean interior can be calculated by;

$$S = -\frac{\mathbf{B}_{net}}{gh\frac{\partial \rho}{\partial z}|_{z=-h}}, \tag{5.2}$$

where h is the mixed layer depth and g is the gravitational force (Nurser and Marshall, 1991; Marshall et al., 1993; O'Dwyer and Williams, 1997; Downes et al., 2008). The surface buoyancy term $\mathbf{B}_{net}$ comprises of freshwater and heat fluxes, both into the ocean and from drift in the Ekman layer (a function of wind stress curl and horizontal temperature and salinity gradients).

This relation shows that if there was no change in the depth of the mixed layer or surface buoyancy, an increase in stratification will result in a decrease in subduction rates. Likewise a change in wind stress alters the buoyancy term, which can also change the rate of subduction (independent of any stratification changes). Any change in subduction has implications for oxygen concentration, with an increase in subduction leading to oxygen concentration increases, and decreasing subduction rates appearing as an oxygen decrease.

5.6 Summary and discussion

This chapter extends the results of previous regional studies, by investigating global changes in oxygen on density surfaces between the 1970s and the 1990s. Widespread oxygen decreases were observed on both pressure and density surfaces which can not be explained by either simple vertical shifts in the depth of density surfaces, or by surface warming (see Section 5.4). These statistically significant decreases were globally coherent in the intermediate and deep waters regions, and represented a reduction of up to 10% in the climatological oxygen concentrations. Temperature and salinity changes show a similar pattern to the zonally averaged oxygen decreases, with the largest increases in both heat content and freshwater also occurring in the high-latitude water mass formation regions. This has lead to lighter density surfaces being formed in the mixed layer and increased upper-ocean stratification.

Relationship with previous studies

The global oxygen changes reported in this chapter are consistent with previous regional studies, giving confidence in our analysis and the global implications of these results.

In the Pacific Ocean, repeat sections north of 30°N show similar decreases in oxygen concentration to those found in the literature (Ono et al., 2001; Andreev and Watanabe, 2002; Emerson et al., 2004; Deutsch et al., 2005; Mecking et al., 2006; Nakanowatari et al., 2007). Likewise the high-latitude surface freshening and upper ocean stratification increases in these studies have also been inferred from the zonally-averaged integrals along isopycnals seen in Figures 5.10 (b) and 5.13 respectively. The slight oxygen increase on isopycnals in the shallow subtropical gyres (Figure 5.9 (a)) also appears in model simulations in the North Pacific Ocean model runs between the 1980s and 1990s (Deutsch et al., 2005).

In the Southern Hemisphere, Bindoff and McDougall (2000) observed oxygen decreases in the South Indian Ocean (0-1000 dbar), which were attributed to a slowing of the gyre circulation. Our results show similar decreases at the salinity-minimum (Figure 5.7 (a)), although in mode water we did observe weak oxygen increases in the middle of the gyre (Figure 5.6 (a)). These Indian Ocean increases are consistent with later studies in the upper thermocline (McDonagh et al., 2005).

Further south in the Indian and Western Pacific sectors of the Southern Ocean,

Aoki et al. (2005) reported oxygen decreases and deepening of isopycnals south of the Polar Front on the 27.9 kg m^{-3} density surface. Although we reported on a slightly lighter density surface, our results extend their work and suggest that such decreases are circumpolar in extent (Figure 5.8 (a)). In addition, we found that the large temperature changes on pressure surfaces at depth (∼500-1000 dbar) are largely the result of downward isopycnal movement. However, in spite of significant isopycnal movement the oxygen changes are larger on density surfaces, and thus are likely to be a consequence of a change in exchange with the mixed layer.

Challenges presented by these global results

With no information on the changes in key biological tracers (ie. phosphates, nitrate), it is a challenge to separate the changes in oxygen consumption that are driven by ocean productivity, and those that are driven by changes in circulation and renewal rates. Supported by the findings of Mecking et al. (2006), we assume that biological activity and the oxygen utilisation rate are relatively constant, and therefore the observed oxygen changes can largely be accounted for by reduced renewal rates of ocean water masses.

Fundamental to the discussion of any water property change (oxygen, salinity, and temperature) is the circulation pattern of the world's oceans. This circulation is best understood in terms of representative water masses (Section 5.3), and can be related to the ventilation with the atmosphere, the subduction and transport of a water parcel along a constant density surface, and an upwelling and re-entrainment of oxygen.

Mode waters around the world's oceans are represented by the 27.0 kg m^{-3} surface. In the Southern Hemisphere this water is known as SAMW, and forms between the Subantarctic Front and the Subtropical Front. This water mass can be seen on the zonally averaged Figure 5.4 as a high-oxygen tongue subducting into the ocean interior at around 50°S. In the Atlantic Ocean the 27.0 kg m^{-3} density surface encompasses 18° water, while in the North Pacific it is found below the salinity-minimum. Comparing observations with climatological values, the largest changes in oxygen on the 27.0 kg m^{-3} surface occur in the Southern Hemisphere mid-latitudes (Figure 5.6 (b)), where the water masses are less than a decade old and close to their formation regions (Suga et al., 1989).

The salinity-minimum surface follows a similar circulation path to the overlying

27.0 kg m^{-3} density surface. Representing AAIW in the Southern Hemisphere, this water mass is largely formed in the South-East Pacific Ocean and spreads eastward with the ACC, and into the Atlantic and Indian Ocean subtropical gyres. Once here, it propagates northward, and along with mode waters, helps form the high-oxygen tongue discussed previously (Chapter 5.3.3). As this water mass moves toward the equator the entrained oxygen is progressively consumed and the oxygen-rich tongue becomes less distinct (Figure 5.4). It is this tongue that has some of the largest zonally-averaged decreases in both oxygen concentration (Figure 5.9 (a): approximately 15 μmol l^{-1}) and salinity (Chapter 3, Figure 3.8).

The salinity-minimum in the North-West Pacific Ocean is found at lighter densities (26.8 kg m^{-3}), but has the same pattern of equatorward decreasing oxygen as AAIW in the Southern Hemisphere. In both the northern and Southern Hemispheres the largest decreases in oxygen on the salinity-minimum surface occur in the Atlantic and Indian Ocean formation regions where the water masses are relatively new, with slight oxygen increases in the subtropical gyres (Figure 5.6 (a)).

The deep 27.8 kg m^{-3} density surface represents a number of different water masses. NADW, formed from LSW in the North Atlantic, spreads southward between 1000-3000 dbar (below the oxygen minimum layer). In the Southern Ocean, the water properties of NADW are progressively modified through mixing with overlying layers where it spreads into the Indian and Pacific Oceans as CDW. South of 30°S near-circumpolar decreases in oxygen concentrations on this 27.8 kg m^{-3} surface are observed (Figure 5.8 (a)). This is in the same region where isopycnals deepen throughout the water column, upper-ocean waters freshen, and the associated stratification increases (Figures 5.8 (c), 5.10 (d), 5.13).

In both the Indian and Pacific Oceans CDW has comparatively weak circulation, is far from the source regions and consequently has weak temperature and salinity changes along associated density surfaces ($\sim$27.8-28.1 kg m^{-3}) (Chapter 3, Figure 3.6). These small changes are in contrast to oxygen observations in Figure 5.8 (a) which show statistically significant (Figure 5.8 (d)) decreases of up to 10% across much of the North Pacific where the 27.8 kg m^{-3} density surface shoals and mixes with the overlying layers. Similar to the Southern Hemisphere high-latitudes, this region shows increasing stratification between 30°N and 50°N (Figure 5.12).

Table 5.2: Expected changes in water properties along density surfaces ($\Delta\gamma_n$) that would result from either a change in the exchange, or a change in the mixed layer properties. These changes are detailed for both the subduction and the upwelling limbs of the circulation, under scenarios of increasing winds and increasing stratification. Note that with the changes in the mixed layer $\Delta\gamma_n$ is dependent on the slop of the θ-S curve and can vary across both subduction and upwelling regions. W=warming, C=cooling, S=more saline, F=freshening, and a downward arrow indicates a decrease in oxygen.

	Winds		**Stratification**	
	Subduction	**Upwelling**	**Subduction**	**Upwelling**
Δ Mixed layer	None	None	W,F, $\downarrow O_2$ (from W)	W,F, $\downarrow O_2$ (from W)
$\Rightarrow \boldsymbol{\Delta\gamma_n}$	None	None	W,S,$\downarrow O_2$ or C,F,$\downarrow O_2$	C,F,$\downarrow O_2$ or W,S,$\downarrow O_2$
Δ Exchange $\Rightarrow \boldsymbol{\Delta\gamma_n}$	Increased C,F,$\uparrow O_2$	Increased C,F,$\uparrow O_2$	Decreased W,S,$\downarrow O_2$	Decreased W,S,$\downarrow O_2$

Two scenarios to explain the oxygen decreases

Here two plausible scenarios that potentially explain the observed oxygen and water property changes are examined. For each scenario the implications on the temperature, salinity and oxygen signals in both the mid-latitude subducting and high-latitude upwelling limbs of the ocean circulation are discussed and summarised in Figure 5.14 and in Table 5.2. It is assumed that the oceans response to globally changing surface conditions is symmetrical about the equator, and for this reason both the northern and Southern Hemispheres can be viewed in the same way. Finally the ocean changes that are expected under the two scenarios are compared with the actual temperature, salinity, and oxygen observations from this thesis.

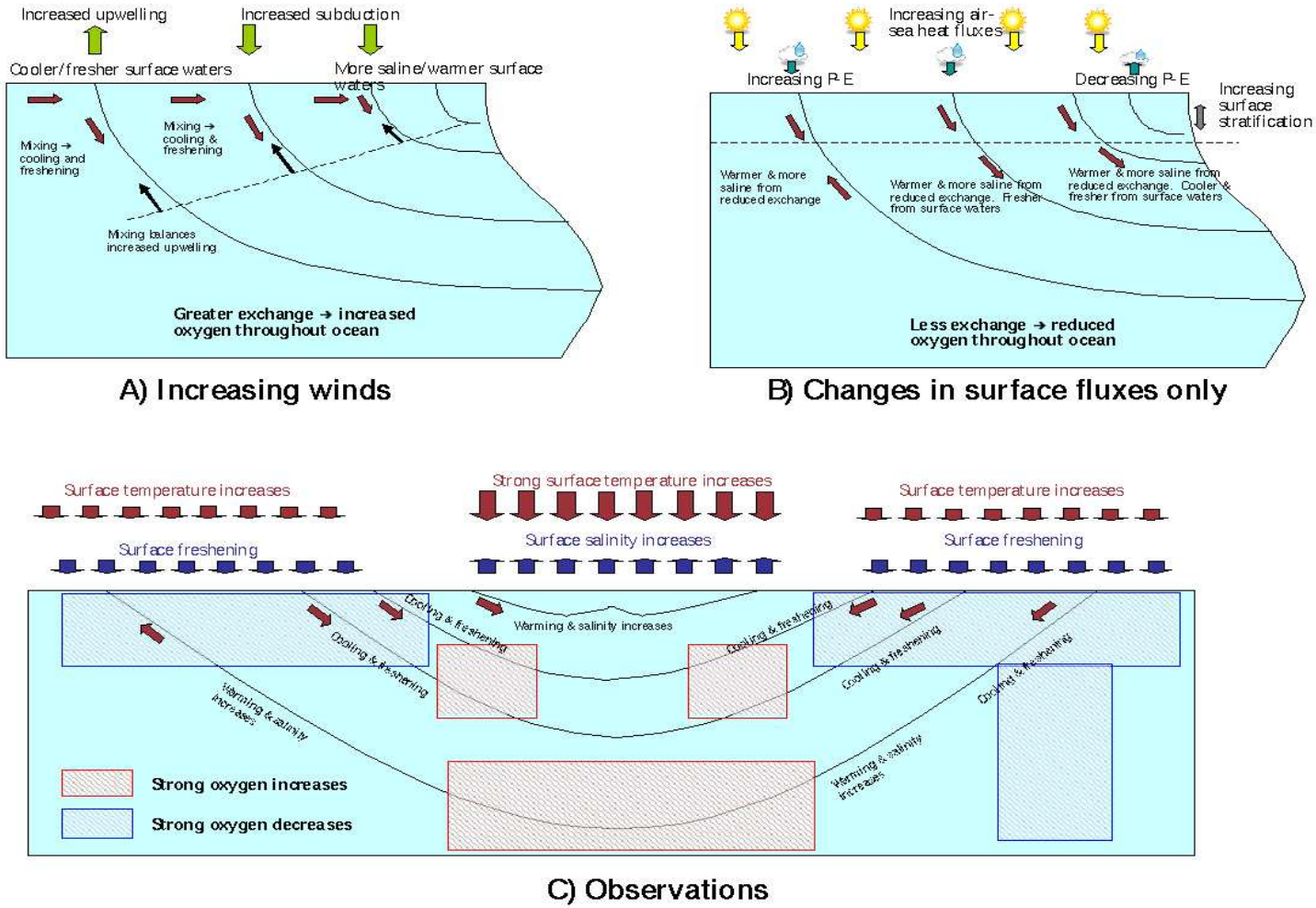

Figure 5.14: Expected zonally averaged changes on density surfaces under **(a)** a scenario of increasing winds but no change in atmospheric fluxes, and **(b)** changing atmospheric fluxes but no change in winds. **(c)** illustrates the observed changes in both hemispheres. In all panels, surfaces characteristic of salinity-maximum water, mode water, intermediate water, and deep water are shown. Panels (a) and (b) show from the high Southern Hemisphere latitudes to the equator (left to right); however the changes are assumed to be symmetrical about the equator in the Northern Hemisphere.

The first scenario assumes high-latitude circumpolar winds have increased, with no change in the upper-ocean stratification due to changes in air-sea or ice-sea fluxes and hence no vertical movement of isopycnals. Clearly this is an idealised scenario of change; however such increases in wind do appear in most coupled ocean-atmosphere models (Randall et al., 2007), in the NCEP reanalysis products (Kalnay et al., 1996), and have been inferred from land observations over the last 50 years (Thompson and Solomon, 2002). Essentially strengthening winds increase the subduction and upwelling between the surface mixed layer and the ocean interior; however here we are also assuming that the volume of the mean density layers have not changed significantly (as supported by ocean observations: Figure 5.10 (e)).

In the subducting limb (ie. mode and intermediate waters), the mixed layer temperature, salinity, and oxygen are assumed to remain constant. As a consequence the only change along density surfaces is due to strengthened winds pumping more surface water downwards in the water column, which is then advected northward (in the Southern Hemisphere). Given that the water in the mixed layer is cooler and fresher than any point found more equatorward along the density layer, increasing the rate at which water is pumped along density layer should result in increased spreading of these waters, and hence a cooler and fresher signal on isopycnals (Figure 5.14). Likewise given the gradient of oxygen along a constant density surface (ie. the highest concentrations are found near the mixed layer), increasing the rate of subduction should result in oxygen increases at a fixed point in the interior.

In the upwelling region between the strong easterly and strong westerly winds (ie. the Antarctic Divergence to the Subantarctic Front), the observed strengthening westerly winds increase upward Ekman pumping. Assuming that mixing from the surface mixed layer balances the increased upwelling, the saltier and warmer waters that originated from upwelling CDW will entrain the cooler and fresher surface water and become cooler and fresher on density surfaces. This increased mixing will stir more water saturated in oxygen from the surface into the interior, hence increasing oxygen on the isopycnal. Such a situation would apply from the base of the mixed layer to the lower-limb salinity-maximum (ie. CDW). Again it is assumed that there is no change in the mixed layer properties.

The second scenario that may explain the observed oxygen decreases, is one where there is no change in the wind-driven Ekman pumping, but an increase in stratifica-

tion due to surface warming and/or surface freshening. Such surface warming and freshening conditions were inferred from our global results in Chapters 3 and 4, and have been identified as occurring in a number of regional studies (ie. Bindoff and McDougall (2000); Wong et al. (2001); Curry et al. (2003)). In terms of exchange, increased stratification has the opposite effect to strengthening winds, reducing the rate of water exchanged between the mixed layer and the ocean interior (ie. a slower renewal of water masses). In this case of reduced exchange, there is increased time for oxygen utilisation to occur, and hence a lower oxygen concentration signal at a fixed point.

This is demonstrated most clearly in the subduction of mode and intermediate water, where an increased density gradient means less water is able to advect equatorward (along density surfaces). Such a relationship is demonstrated in Equation 5.2, where an increased stratification term in the inner ocean results in reduced subduction. Less mixing along density layers will cause a shift toward the older equatorward water properties at a fixed point (ie. warmer, more saline, and lower in oxygen).

As well as a reduction in exchange, the warming and/or freshening of the mixed layer waters that causes the increased stratification is also likely to advect into the ocean interior and affect water mass properties on density layers. Following the reasoning set out in Chapter 2.2, this will appear as a cooling and freshening on density surfaces (Figure 2.5: given $R_\rho > 1$ in the subduction region). Without an analysis of model results, it is difficult to determine the relative significance of the seemingly contradictory effects of reduced exchange and changing mixed layer properties, on the signal along density surfaces.

In the upwelling limb, increased stratification means that upwelling water encounters greater resistance to mixing, and less surface water (which is fresher, colder, and with greater oxygen than upwelling water) is exchanged with the ocean interior. As in the subducting limb, this results in isopycnals in the upper 500 dbar tending toward the properties of the older upwelling water (ie. warmer, more saline, and lower in oxygen), and is broadly the opposite response to the increasing winds scenario. With oxygen, this decrease in renewal rate also means there is more time for the oxygen in the upwelling deep water to be utilised by ocean biology (and hence a lower concentration would be observed).

Despite the reduced exchange, some of the warmer and fresher mixed layer waters that cause the stratification would be mixed with the upwelling deep water. On density surfaces, this warmer and fresher water will either appear as a warming and salinity increase if the temperature term dominates (as $R_\rho < 0$) (Chapter 2, Figure 2.5 (d)), or as a cooling and freshening closer to the lower-limb salinity-maximum (Figure 2.5 (e)). In either case, the warmer surface waters will have a lower oxygen capacity which will appear as a decrease on density surfaces, in addition to the oxygen decreases due to reduced exchange.

Comparison with observations

Of the two models for ocean change (ie. winds or stratification), it is the increasing stratification that agrees best with the observations of temperature, salinity, and oxygen change, and qualitatively appears to be the most plausible mechanism for the observed oxygen decreases.

In mode waters (represented by the 27.0 kg m^{-3} surface), we observed oxygen decreases and a cooling and freshening on density surfaces, which is a similar response to that expected under increasing stratification. In the increased-wind scenario, both the temperature and salinity signals on density surfaces would qualitatively agree with the observations; however the oxygen change is of the opposite sign.

In salinity-minimum and North Atlantic intermediate-level waters, the observed cooling and freshening observed on subducting density surfaces, qualitatively supports both hypotheses. However the increasing winds would also imply increases in Ekman pumping, and therefore increased exchange between the mixed layer and the density surface at depth. This should result in higher oxygen levels. The observations outlined in Section 5.3 suggest that this has not been occurring, and instead supports the oxygen decreases implied by a reduced renewal (ie. an increasing-stratification scenario).

In the Southern Ocean, increased winds should result in both oxygen concentration increases, and in freshening and/or cooling along the upwelling 27.8 kg m^{-3} density surface. Our observations show the opposite, with near circumpolar decreases in oxygen concentration and warming and salinity increases on the density surface. This therefore suggests that the effect of increasing surface stratification

has a larger effect than that of increasing winds in this region.

Conclusion

One of the main motivations for investigating ocean oxygen concentration levels, is that they can be used as an indicator of the age of the water. As such *changes* in oxygen concentration suggest changes in renewal rates of water masses, with a decrease in oxygen indicating an increased flushing time under a constant rate of biological utilisation. Based on evidence from previous studies, this chapter has assumed that variability in oxygen concentration levels can largely be attributed to changing physical mechanisms rather than biological change. Instead it is the scenario of increasing stratification that qualitatively provides the most plausible explanation for the observed changes in oxygen, temperature, and salinity.

Chapter 6 Interpretation and synthesis of ocean changes: 1970-1992

6.1 Introduction

In Chapters 3 and 4, clear changes in water mass properties were identified along neutral density surfaces over the last 40 years. These changes imply a strengthening of the global hydrological cycle and an overall warming of the upper ocean. This chapter builds on these results by focusing more on the cause of the changes and addressing some of the subtleties associated with using a density coordinate system. To separate out the warming, freshening, and heave contributions to density change, a least-squares analysis developed by Bindoff and McDougall (1994) is used to attribute different subduction mechanisms to the observed ocean changes.

Despite having advantages over an isobaric reference frame, there are two main areas of uncertainty when trying to understand changes in the ocean using constant density surfaces. The first is that there is ambiguity as to which component (temperature or salinity) is the primary *cause* of the observed changes on density surfaces. This ambiguity occurs when converting between density and pressure surfaces and arises independently of any vertical movement of the isopycnal. Here the actual sign of the water property change is dependent on the slope of the temperature-salinity relationship (the stability ratio: R_ρ). The concept is discussed at length in Chapter 2, and changes on density surfaces are only unambiguous directly at the salinity minimum or maximum (where $R_\rho \approx \infty$: Chapter 2, Figure 2.5 (g-h)).

The second subtlety is that neutral density surfaces are not fixed in space and can be displaced vertically in the water column, as a response to either overlying water mass change, or as a dynamic response to a change in surface winds (Ekman pumping), Rossby waves, mesoscale eddies, or other internal-ocean variability. As discussed in earlier chapters, this second mechanism can lead to a temperature or salinity change on a fixed pressure surface without any actual change in atmospheric heat and freshwater fluxes and water mass properties.

In this chapter, three different techniques are used to try and quantitatively remove

some of this interpretational ambiguity. The first third of this chapter essentially involves separating the signal into six individual components - the temperature (or salinity) change on a neutral surface, the temperature (or salinity) change on a fixed pressure surface as the result of isopycnal movement, and the total temperature (or salinity) change on a fixed pressure surface. By estimating these components, the importance of the temperature and salinity changes on neutral surfaces can be compared with the changes due to the vertical movement of isopycnals, by looking at the relative contributions to density change.

In Chapter 2.7 the methodology used to estimate the six observed variables ($\alpha\theta'|_n$,$\beta S'|_n$,$\alpha\theta'|_z$,$\beta S'|_z$,$N'\alpha\theta_z$,$N'\beta S_z$) was outlined, and for a more comprehensive mathematical derivation of these expressions and their relationship to the three 'pure process' discussed in Section 6.3 of this chapter, the reader is referred to Bindoff and McDougall (1994).

Here the six observable quantities are first illustrated for a single density surface (27.0 kg m^{-3}), and are interpreted in relation to circulation pathways, the age of the water, and the water mass formation regions. The four representative surfaces that have been examined in Chapters 3 to 5 are then investigated on a global scale, before taking the zonal averages of all 40 neutral density surfaces.

The second third of this chapter uses a least-squares approach to understand which subduction processes are most important. The analysis method was developed by Bindoff and McDougall (1994) and has subsequently been adopted by other studies that have investigated water property changes along surfaces of a constant density (Wong, 1999; Bindoff and McDougall, 2000).

This analysis is done on individual neutral density layers, and it is assumed that mixing occurs primarily along these surfaces. Note that all estimates of each subduction process in this chapter are calculated from zonally averaged temperature, salinity and pressure values (ie. Figures 6.2-6.3, 6.6-6.11). This zonal averaging avoids errors associated with non-linear averaging of the point least-squares solutions of the three pure processes (Chapter 2.7, Equation 2.31).

The final third of this chapter builds on this analysis of subduction mechanisms, by using what have been termed 'zonal back-projections' as a method of estimating

the surface buoyancy and density transformation between the surface mixed layer and the ocean interior. A similar method was used in Chapters 3 to 5 to estimate changes in heat content, freshwater and oxygen fluxes between the mixed layer and the ocean interior; however here each of the six zonally averaged terms are integrated to the surface to estimate buoyancy change along density surfaces from the three different processes.

The zonal back-projection technique has been used in the previous chapter to infer apparent surface changes in heat and freshwater fluxes based on observations in the ocean interior. Here it is used to integrate the density changes in temperature and salinity arising from vertical displacement of isopycnals ($N'\alpha\theta_z$ and $N'\beta S_z$ respectively). While the source of the movement (winds, Rossby waves) usually occurs vertically throughout the water column, rather than along a density surface, these zonal back-projections offer a mechanism for comparing the *magnitude* of the $N'\alpha\theta_z$ and $N'\beta S_z$ changes and for identifying which isopycnals have the most coherent movements, and thus the greatest contribution to steric sea-level change.

Calculating density and steric sea-level change

The inclusion of the thermal expansion and haline contraction coefficients allows the changes along neutral density surfaces ($\alpha\theta'|_n$, $\beta S'|_n$), the changes due to vertical isopycnal displacement ($N'\alpha\theta_z$,$N'\beta S_z$), and the total change on pressure surfaces ($\alpha\theta'|_z$, $\beta S'|_z$) to be expressed in terms of relative density perturbations (ie. $\Delta\rho/\rho$).

In Chapter 2.7 the total temperature and salinity change was discussed on pressure surfaces as a sum of both the vertical movement of isopycnals, and the along-isopycnal changes. To reiterate, these are related by;

$$\alpha\theta|'_z = \alpha\theta|'_n - \alpha N'\theta_z; \tag{6.1}$$

$$\beta S|'_z = \beta S|'_n - \beta N' S_z; \tag{6.2}$$

As discussed in Chapter 2.7 a sign convention has been adopted here, so that shoaling of an isopycnal (ie. $N' > 0$) into a warmer region of the water column (ie. a positive $\frac{\partial\theta}{\partial p}$ gradient) will result in a positive $N'\alpha\theta_z$ value. From Equation 6.1, this contributes a decrease in temperature on a fixed pressure surface ($\alpha\theta'|_z$). Given that Equations 6.1-6.2 are presented as a change in density, when interpreting these changes on

pressure surfaces as a contribution to steric sea height it is necessary to use the relation;

$$\Delta h = -\int \frac{\Delta\rho}{\rho} dz = -\int (\beta S'|z - \alpha\theta'|z) dz \tag{6.3}$$

Here both a warming ($\alpha\theta'|_z > 0$) or a freshening ($\beta S'|_z < 0$) will increase steric sea-level.

Changes along a neutral density surface are in the 'null space' of steric-sea level, since by definition $\alpha\theta'|_n$ and $\beta S'|_n$ are density-compensating and therefore have no net contribution to sea level change. It is only the vertical displacement of isopycnals that contributes to steric sea-level change (Bindoff and McDougall, 1994). This can be thought of in two equivalent ways. Firstly it can be seen in physical space by viewing a density surface being forced deeper in the water column by the addition of new lighter waters (and raising the sea level) and vice versa. Secondly the relationship between density change on a pressure surface and the vertical displacement of density surfaces can be derived from the equation of state using;

$$\begin{aligned} \rho^{-1}\rho'|_z = \beta S'|z - \alpha\theta'|z &= (R_\rho - 1) N' \beta S_z, \\ &= (\frac{\alpha\theta_z}{\beta S_z} - 1) N' \beta S_z, \\ &= N'(\alpha\theta_z - \beta S_z) \end{aligned} \tag{6.4}$$

The sign of the temperature and salinity changes are consistent with the sign convention for vertical gradients and the movement of isopycnals defined in Chapter 2.2. Note that throughout this chapter the two terms representing the contribution to density change due to vertical movement of isopycnals ($N'\alpha\theta_z$ and $N'\beta S_z$), are displayed in the figures as -$N'\alpha\theta_z$ and -$N'\beta S_z$. This makes it visually easier to compare the along-isopycnal ($\alpha\theta'|_n$) and isopycnal-displacement temperature observations, as in both cases a negative value will represent a cooling on pressure surfaces. Likewise negative salinity values displayed on a figure will represent a freshening on pressure surfaces ($\beta S'|_z$).

In this chapter only data from the 1970-1992 period was used as it can be found further south and covers a greater depth range in the ocean than profiles taken dur-

ing the Argo period. However Chapter 4 has shown strong consistency between the 1970-1992 and the 1992-2005 periods, suggesting that over much of the global ocean there is little to indicate a significant change in the patterns that emerge from this chapter.

6.2 Observed changes in density-weighted space

6.2.1 Observable changes on the 27.0 kg m^{-3} density surface

In the Southern Hemisphere the 27.0 kg m^{-3} density surface is generally representative of SAMW, and is found between the shallow salinity-maximum and the salinity minimum. This water mass is formed throughout the Southern Ocean south of the Subtropical Front and north of the Subantarctic Front. From here is advected northward, by the anticyclonic circulation of the Southern Hemisphere subtropical gyres, reaching a typical maximum depth of approximately 600 dbar. In the North Atlantic Ocean the 27.0 kg m^{-3} density surface outcrops near 45°N, while in the North Pacific it is found below the North Pacific salinity-minimum.

Figure 6.1 illustrates the global patterns in the density-weighted temperature and salinity terms along the 27.0 kg m^{-3} density surface. The *actual water* mass change on the isopycnal surface is expressed as a change in density ($\alpha\theta'|_n$ and $\beta S'|_n$: Figure 6.1 (c-d)). Note that the along-isopycnal term ($\alpha\theta'|_n$) can change; however by definition, a neutral density surface requires a compensating salinity ($\beta S'|_n$) change of equal magnitude and hence Figure 6.1 (c) and Figure 6.1 (d) are identical. Similar figures but expressed as a change in salinity have been shown previously in Chapter 3 (Figure 3.4 (a)). As discussed previously, the largest density anomalies are found closest to the SAMW source regions, where density perturbations from temperature or salinity anomalies have had relatively little time to mix and decrease in amplitude.

While the changes of $\alpha\theta'|_n$ and $\beta S'|_n$ (Figure 6.1 (c-d)) are relatively smooth and spatially coherent, the changes in $N'\alpha\theta_z$ and $N'\beta S_z$ due to the *vertical displacement* of the 27.0 kg m^{-3} density surface are less so, both globally and within individual ocean basins (Figure 6.1 (e-f)). Part of this difference in the character of the changes between these two variables is not surprising since the vertical motion of density surfaces is more prone to ocean noise such as internal eddies, upper-ocean decadal variability and other short-term changes driven by the atmospheric winds.

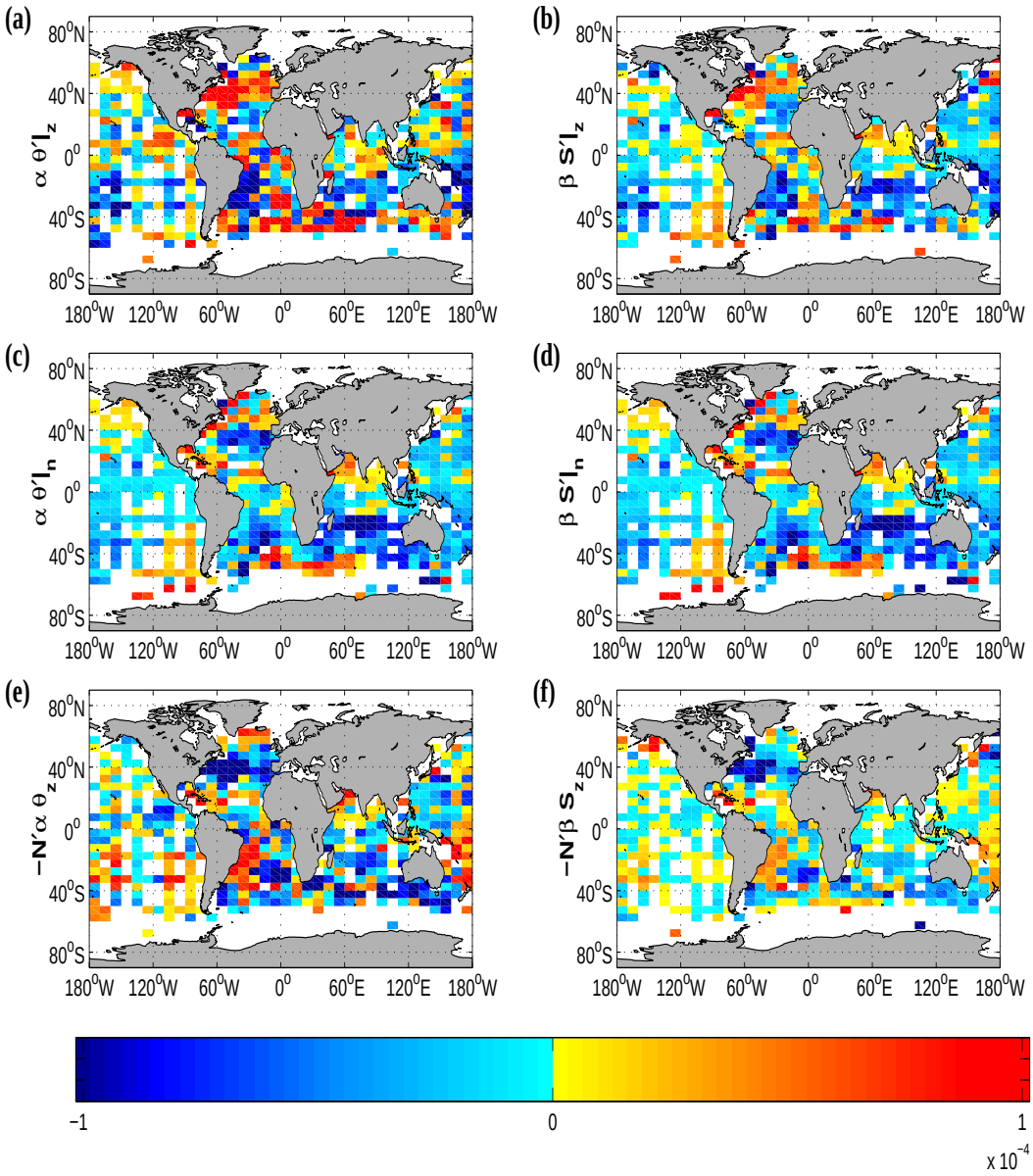

Figure 6.1: Changes in the six 'observable' quantities on the 27.0 kg m^{-3} isopycnal expressed as a dimensionless relative density perturbation ($\Delta\rho/\rho$) **(a-b)** On pressure surfaces ($\alpha\theta'|_z$,$\beta S'|_z$ where $\alpha\theta'|_z$=$\alpha\theta'|_n$-$N'\alpha\theta_z$ and $\beta S'|_z$=$\beta S'|_n$-$N'\beta S_z$). **(c-d)** On density surfaces ($\alpha\theta'|_n$, $\beta S'|_n$). **(e-f)** From isopycnal displacement (displayed as -$N'\alpha\theta_z$,-$N'\beta S_z$). Blue represents a density change from a cooling or freshening, while red comes from a warming or salinity increase.

The general lack of spatial structure in $N'\alpha\theta_z$ and $N'\beta S_z$ but generally coherent cooling and freshening in $\alpha\theta'|_n$ and $\beta S'|_n$ respectively, tends to suggest that the main cause of variability in the 27.0 kg m^{-3} density surface is not simply a displacement of isopycnals, but also due to mixed layer anomalies of temperature and salinity propagating into the ocean interior along density surfaces. The influence of $\alpha\theta'|_n$ and $\beta S'|_n$ (Figure 6.1 (c-d)) is especially apparent in the mid-latitude water mass formation regions, with $N'\alpha\theta_z$ and $N'\beta S_z$ being more dominant in regions where the water mass is older (Figure 6.1 (e-f): equatorial Pacific Ocean, North Indian Ocean).

In spite of the sources of noise in the $N'\alpha\theta_z$ and $N'\beta S_z$ variables, there are a few broad coherent regions of note. The North Atlantic has deepened north of 30°N (Chapter 3, Figure 3.4 (b)), resulting in strong temperature and salinity changes due to displacement in Figure 6.1 (e-f). In the North Atlantic the largest cooling signal on density surfaces on the 27.0 kg m^{-3} density surface occurs around 40°N (Figure 6.1 (c)), although this is approximately three times smaller than the vertical displacement component ($N'\alpha\theta_z$). Combining these two terms (Chapter 2, Equation 2.19), shows a net warming on fixed pressure surfaces (Figure 6.1 (a): $\alpha\theta'|_z$). The North Atlantic variations in temperature and salinity are largely dominated by the vertical movement of density surfaces rather than by the transformation of water masses. This result suggests that the main changes in the North Atlantic can be characterised as a dynamic response (possibly to the NAO).

In the South Indian Ocean the opposite occurs. Here the downward displacement of the 27.0 kg m^{-3} density surface (Figure 6.1 (e): $N'\alpha\theta_z$) causes warming on fixed pressure levels. The warming due to downward isopycnal movement is approximately half the magnitude of the cooling along the density surface itself (Figure 6.1 (c): $\alpha\theta'|_n$). This increase in $N'\alpha\theta_z$ is largest in the middle of the South Indian Ocean subtropical gyre (Figure 6.1 (c): $\sim$20°S). The pattern of salinity change is even more obvious, with freshening on the density surface (Figure 6.1 (d)) being up to three times greater than the contribution to salinity change from the downward motion of isopycnals (Figure 6.1 (f)). This pattern of density change for the period of the observations suggests that in the South Indian Ocean it is water mass change rather than dynamic forcing that is the dominant process for controlling either temperature or salinity change on pressure surfaces (Figure 6.1 (a-b)). This is a similar conclusion to Bindoff and McDougall (2000); Wong et al. (2001); Aoki et al. (2005) and Murray et al. (2007). North of the equator, the 27.0 kg m^{-3} isopycnal is isolated

from much of the global circulation and as such represents a much older water mass. In this region, vertical motion of the isopycnals has a larger influence on $\alpha\theta'|_z$ than the along-isopycnal changes.

6.2.2 Observable changes on representative surfaces

In Figure 6.2 the analysis is shown for the zonally-averaged components of temperature change on the four representative surfaces discussed in Chapters 3 to 5. The magnitude of water property changes are much larger on surfaces found in shallower depths, with the density contribution from temperature changes on pressure surfaces ($\alpha\theta'|_z$) being an order of magnitude larger on the shallow salinity-maximum surface than on the deeper 27.8 kg m^{-3} density surface. This is due to a combination of both the larger vertical gradients of temperature and salinity, and the shorter ventilation time of the shallower water masses in relation to the deeper surfaces. To allow for this, a different scale (y-axis) has been used in Figure 6.2 for each representative surface.

The shallow salinity-maximum surface (Figure 6.2 (a)) is found just below the mixed layer in low-latitude regions, and as such this surface is more strongly affected by internal variability (eddies, internal waves) and regional atmospheric anomalies (El Niño) than the deeper surfaces. The movement of density surface through a mean vertical gradient of temperature is the main mechanism for explaining the temperature component of density variability on this surface (green line).

The 27.0 kg m^{-3} density surface has already been discussed at length; however the zonal averages in the Southern Hemisphere (Figure 6.2 (b)) again illustrate the cooling (ie. negative $\alpha\theta'|_n$) along the density surface. This cooling occurs in the poleward side of subtropical gyres containing recently formed SAMW (40°S-10°S). The regions where the cooling occurs, coincides with isopycnal deepening in the Southern Hemisphere, and with a deepening of mode waters in the North Atlantic and North Pacific. This deepening has lead to a warming on pressure surfaces (Figure 6.2 (b: green line): $N'\alpha\theta_z$).

Likewise in the Northern Hemisphere mid-latitudes, the total change on pressure surfaces ($\alpha\theta'|_z$: Figure 6.2 (b: red line)) is of a similar magnitude, but show a warming rather than the cooling that is found in the Southern Hemisphere. In the Northern Hemisphere case the $N'\alpha\theta_z$ cooling is larger than the along-isopycnal

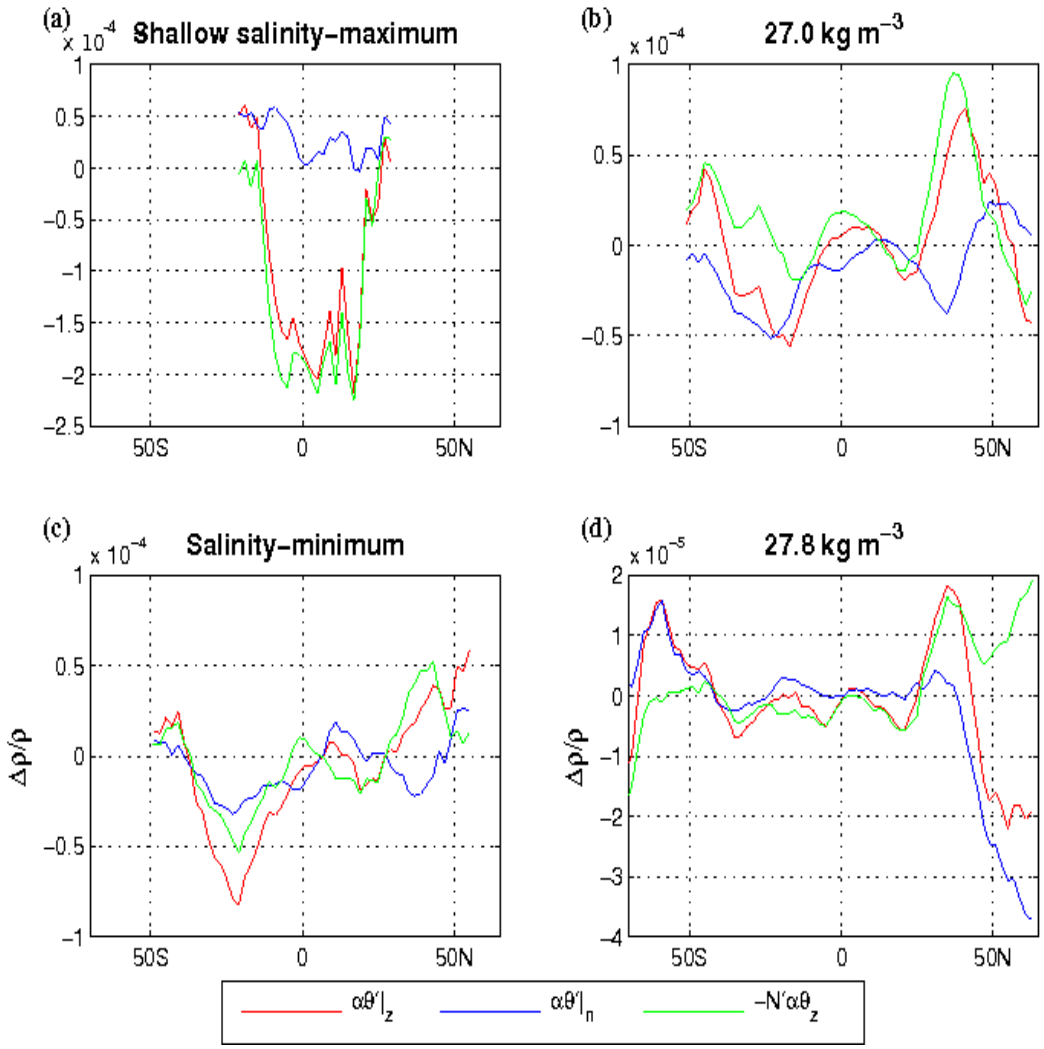

Figure 6.2: Zonally averaged relative density perturbations ($\Delta\rho/\rho$) from temperature changes on the four representative surfaces. The three terms shown are $\alpha\theta'|_z$ (red), $\alpha\theta'|_n$ (blue), and -$N'\alpha\theta_z$ (green), with the four surfaces being; **(a)** the shallow salinity-maximum, **(b)** the 27.0 kg m^{-3} isopycnal, **(c)** the salinity-minimum, **(d)** and the 27.8 kg m^{-3} isopycnal. Negative terms represent a density change from cooling and positive is from warming. Note the different scale on the vertical axes.

change ($\alpha\theta'|_n$: Figure 6.2 (b: blue line)). In the equatorial regions on the 27.0 kg m^{-3} density surface where the water mass is at its oldest, there is the least zonally averaged change.

Around the salinity-minimum south of the equator, both isopycnal displacement (Figure 6.2 (c: green line)) and water mass change (Figure 6.2 (c: blue line)) have similar contributions to a net cooling on pressure surfaces (Figure 6.2 (c: red line)). In the Northern Hemisphere, the zonally averaged pattern of change is similar to that on the 27.0 kg m^{-3} density surface, with a cooling on the salinity-minimum (primarily from NPIW changes), and a larger warming from downward displacement of isopycnals. Together these two mechanisms have the net effect of a Northern Hemisphere warming on pressure surfaces (Figure 6.2 (c: red line)). In both hemispheres, the largest changes are centred in the subtropical gyres close to water mass formation regions, with comparatively little zonally averaged change in the equatorial latitudes.

The deep water 27.8 kg m^{-3} density surface (Figure 6.2 (d)) shows comparatively little change between 40°S and 40°N, away from ventilation regions of this density surface. Poleward of 40°N where the surface represents recently formed NADW, a large cooling (positive contribution to density) on the isopycnal is observed (Figure 6.2 (d: blue line)). Here there is also a significant deepening which has the opposite sign of change equatorward of 40°S, meaning that displacement leads to a warming (Figure 6.2 (d: green line)) and a hence a decrease in density at a fixed depth ($N'\alpha\theta_z$).

In the Southern Ocean south of 50°S, comparatively large water mass changes ($\alpha\theta'|_n$) are observed along the 27.8 kg m^{-3} density surface, with little contribution from isopycnal movement. In this region CDW upwells into the surface layer. Poleward of 55°S, there is a vertical displacement of isopycnals that contributes to a cooling on pressure surfaces, and is of a similar magnitude although of the opposite sign, to the warming on pressure surfaces from displacement in the high-latitude Northern Hemisphere (Figure 6.2 (d: green line)). This Southern Ocean cooling is driven by a deepening 27.8 kg m^{-3} density surface from a warmer to a cooler region of the water column. Despite deepening of this 27.8 kg m^{-3} surface south of 50°S, $N'\alpha\theta_z$ in Figure 6.2 (d: green line) is significantly smaller than in the overlying density layers due to the small gradient of temperature at these depths. Such a result was also observed in the Indian Sector of the Southern Ocean (Aoki et al., 2005), but in

this case the observed changes are circumpolar in extent.

6.2.3 Observable changes throughout the water column

In Figure 6.3 the six observable terms have been calculated as a zonal average for all 40 neutral density surfaces, before being interpolated to pressure surfaces. The total temperature change on pressure surfaces (Figure 6.3 (a)) shows the same overall temperature change patterns as Levitus et al. (2005a) between 1955 and 2003. However, now the temperature change on pressure surfaces can be separated into two components - the water mass change *along* isopycnals (Figure 6.3 (c-d)), and the change due to the *vertical displacement* of isopycnals (Figure 6.3 (e-f)). Both are expressed in density-weighted terms in Figure 6.3.

The actual water mass changes (Figure 6.3 (c-d)) have already been shown and discussed in Chapter 3. To briefly summarise, one of the clearest signals to emerge is a coherent cooling and freshening signal on intermediate water density surfaces. In the Southern Hemisphere, this signal originates from latitudes around 40°S-50°S and is strongest around 30°S. Warming and salinity increases on density surfaces (Figure 6.3) were apparent near the surface in both the low and mid-latitudes, and throughout the water column south of 50°S.

The density changes due to vertical movement of isopycnals (Figure 6.3 (e-f)) has resulted in strong warming and salinity increases poleward of both 40°S and 25°N, and is especially strong in the upper 1000 dbar. In the upper 300 dbar from 20°S-20°N, a cooling occurs near the equator as the result of shoaling in the lighter density layers. Other than in this region, the vertical displacement of density surfaces has generally resulted in a pattern of increasing salinity.

The change on pressure surfaces (Figure 6.3 (a-b)) is a combination of the along-isopycnal and the isopycnal-displacement terms. Examining a few of the key features in Figure 6.3 (a) and heat content trends from Chapter 1 (Figure 1.3: Levitus et al. (2005a)), both appear to have a tongue of cooling beginning at the equator which extends to around 30°S at 1000 dbar. In the upper 300 metres of this tongue, the strong signal centred around the equator is due mainly to the vertical isopycnal movement shown Figure 6.3 (e), rather than any actual water mass property change. Below 500 dbar in the Southern Hemisphere subtropical gyres, the cause of temperature and salinity changes on pressure surfaces (Figure 6.3 (a-b)) is predominately

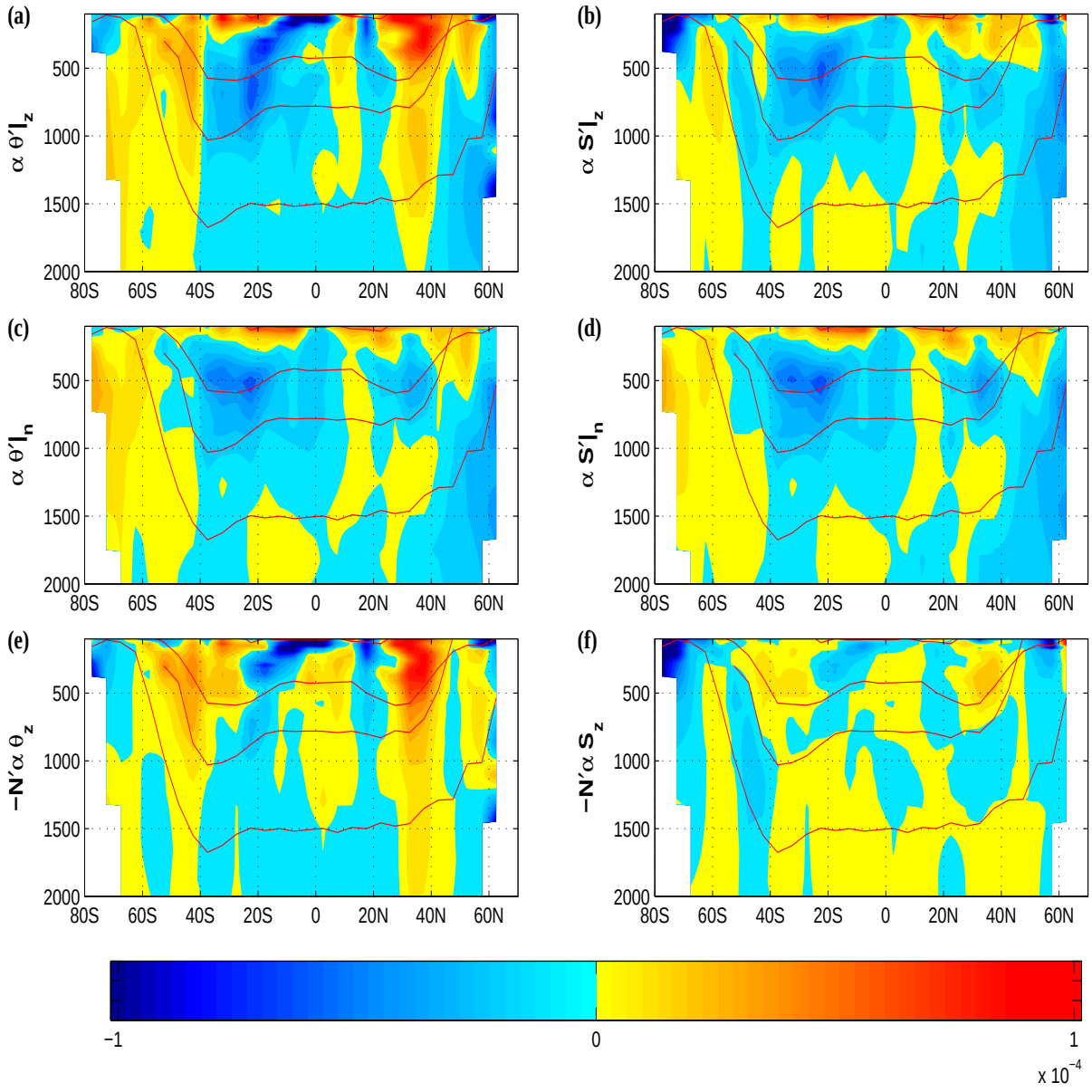

Figure 6.3: The six 'observable' quantities zonally averaged on neutral density surfaces and mapped to pressure surfaces. The six terms are; **(a.)**$\alpha\theta'|_z$ **(b.)**$\beta S'|_z$ **(c.)**$\alpha\theta'|_n$ **(d.)**$\beta S'|_n$ **(e.)**-$N'\alpha\theta_z$ **(f.)**-$N'\beta S_z$. Units are expressed as a relative density perturbation ($\Delta\rho/\rho$) where blue results from a cooling or freshening and red comes from a warming or salinity increases. Superimposed are the average depths of the shallow salinity-maximum, the 27.0 kg m^{-3}, the salinity-minimum, and the 27.8 kg m^{-3} surfaces.

a cooling and freshening on intermediate water density surfaces seen in Figure 6.3 (c-d).

Both Figure 1.3 (Chapter 1) and Figure 6.3 (a) show a deep penetrating warming down to at least 2000 dbar throughout the Southern Ocean. The strongest changes occur at 40°S and here it is again shown that this deep warming can largely be attributed to deepening of density surfaces (Figure 6.3 (e)). Poleward of 50°S in the Southern Hemisphere, the warming is mainly due to water mass change, with a smaller additive contribution from deepening isopycnals.

The final key feature of note is the strong warming on pressure surfaces between 25°N and 40°N (Chapter 1, Figure 1.3 and Figure 6.3 (a)). This feature is strongest in the upper 1000 dbar, and can be completely attributed to a displacement of density surfaces seen in Figure 6.3 (e). The cause of this is a coherent deepening of density layers in the mid-latitude Atlantic Ocean (Chapter 3, Figures 3.4-3.6 (b)), where despite its smaller surface area, the strong changes from this ocean basin still dominate the zonal averages. In contrast the Pacific Ocean zonal average has little coherence in isopycnal movement, with much smaller zonally averaged vertical displacements (Chapter 3, Figure 3.6 (b)).

By separating the changes on pressure surfaces into the two contributing components, the significance of isopycnal movement and water mass change on temperature and salinity observations on pressure surfaces is shown for the first time. When analysing changes on pressure surfaces without separating these components, there is no way to distinguish such dynamically driven changes from the thermodynamic changes likely to originate from the atmosphere. These raise questions about the interpretation of heat content and steric sea height changes and the attribution of these changes to changes in air-sea heat and freshwater fluxes on regional scales.

6.3 Least-squared analysis of observed changes

The six observable terms discussed so far in this chapter can help differentiate between vertical movement of isopycnals and water mass change contributions to the observed changes on pressure surfaces. However there is an unresolved contribution of subduction mechanisms from the ocean surface that drive these changes. The movement of isopycnals can be the result of the addition of lighter water into an

ocean layer (caused by surface warming or surface freshening), or simply vertical displacement of density surfaces without any actual water mass change (ie. winds, internal waves). To resolve this ambiguity the six observable terms and the stability ratio are used to calculate separately the skill of the 'Pure Warming' (A_w), 'Pure Freshening' (A_f), and 'Pure Heave' (A_h) subduction scenarios that can be used to explain the observations (Bindoff and McDougall, 1994). By skill we mean the percentage variance of the observations able to be explained by each of the three subduction processes.

The reason for examining the three processes separately is so that the underlying model is overdetermined in a least squares sense. Thus each map of the percentage variance can be interpreted in terms of the relative importance of the 'subduction mechanism' in particular regions. These maps of percentage variance can then be related to the mean circulation patterns of the water masses they represent. A brief discussion of the zonally averaged changes follows. While this simplest solution approach has value in interpreting the observations, it is likely that more than one process is operating in the different water mass formation regions.

6.3.1 Pure subduction terms on representative surfaces

Along the shallow salinity-maximum surface the observed warming and salinity increases (weighted by density anomalies) are better explained by Pure Warming (Figure 6.4 (a)) and Pure Heave (Figure 6.4 (e)), with only approximately 20% of the variance in the zonally averaged signals being able to be explained by a Pure Freshening scenario (Figure 6.4 (c)). Across the low-latitude regions of all three ocean basins, Pure Warming and Pure Heave are tightly correlated, and are the processes most capable of explaining the density variations. However the dominance in the low-latitudes is not as pronounced in the Atlantic Ocean, with a slightly greater freshening influence being evident.

On the underlying 27.0 kg m^{-3} density layer (Figure 6.4 (right panels)) there is greater inter-ocean variability than on the shallow salinity-maximum. In both the eastern equatorial, and to a lesser extent the low-latitude Pacific Ocean, the signals are able to be largely explained (ie. 70-90% of variance) by Pure Heave or Pure Warming (an ENSO-type forcing signal), with a Pure Freshening scenario only able to explain less than 30% of the variance in the observations (Figure 6.4 (d)). This pattern changes in the Southern Hemisphere mid-latitude regions (especially

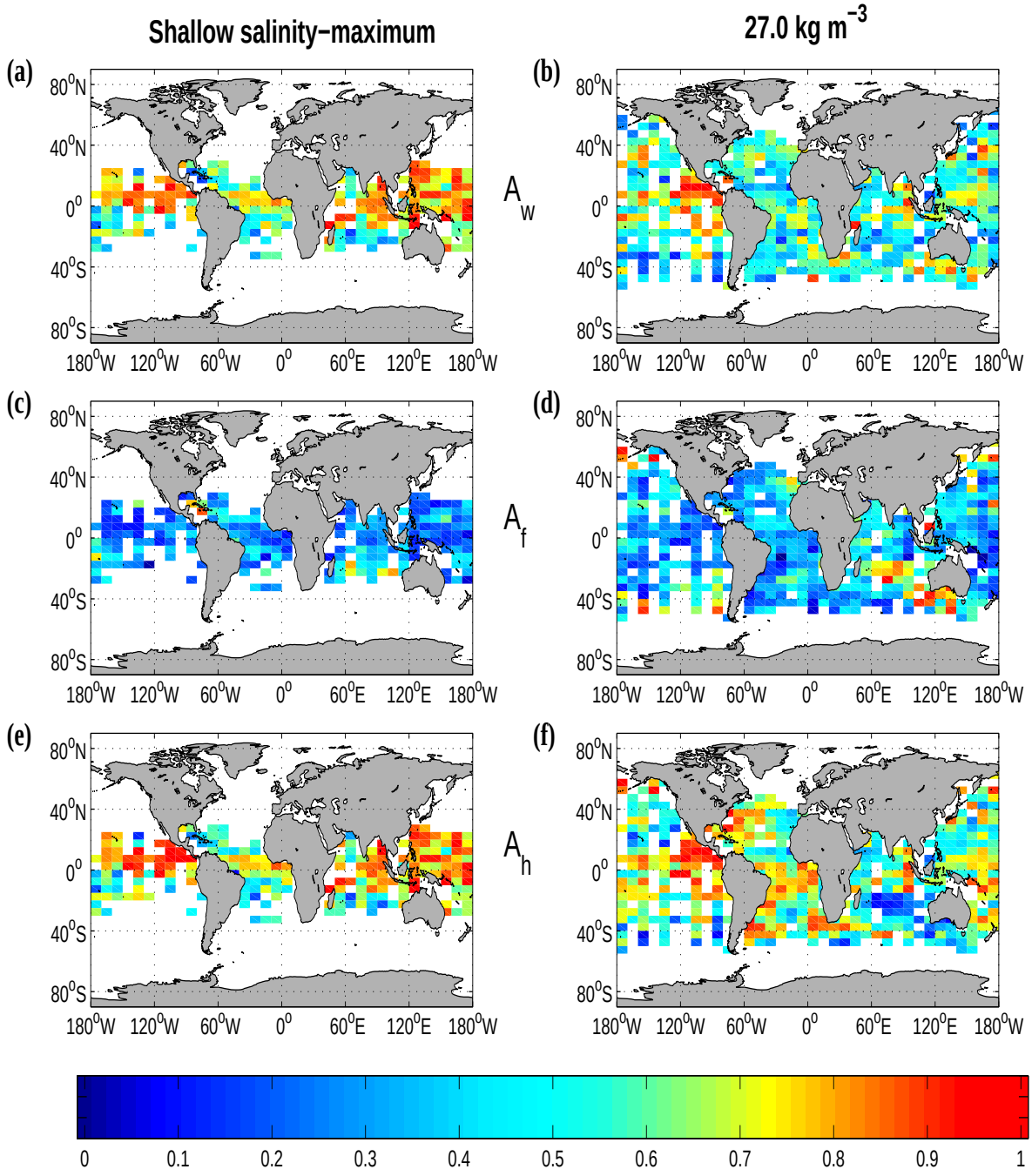

Figure 6.4: The pure subduction processes for the shallow salinity-maximum (left) and the 27.0 kg m^{-3} density surfaces (right). The proportion of variance (R^2) explained by each process is shown for **(a-b)** Pure Warming, **(c-d)** Pure Freshening, and **(e-f)** Pure Heave. Note that this does not show the sign or magnitude of the observed changes on the surfaces (refer to Chapter 3, Figures 3.1 and 3.4 for this information).

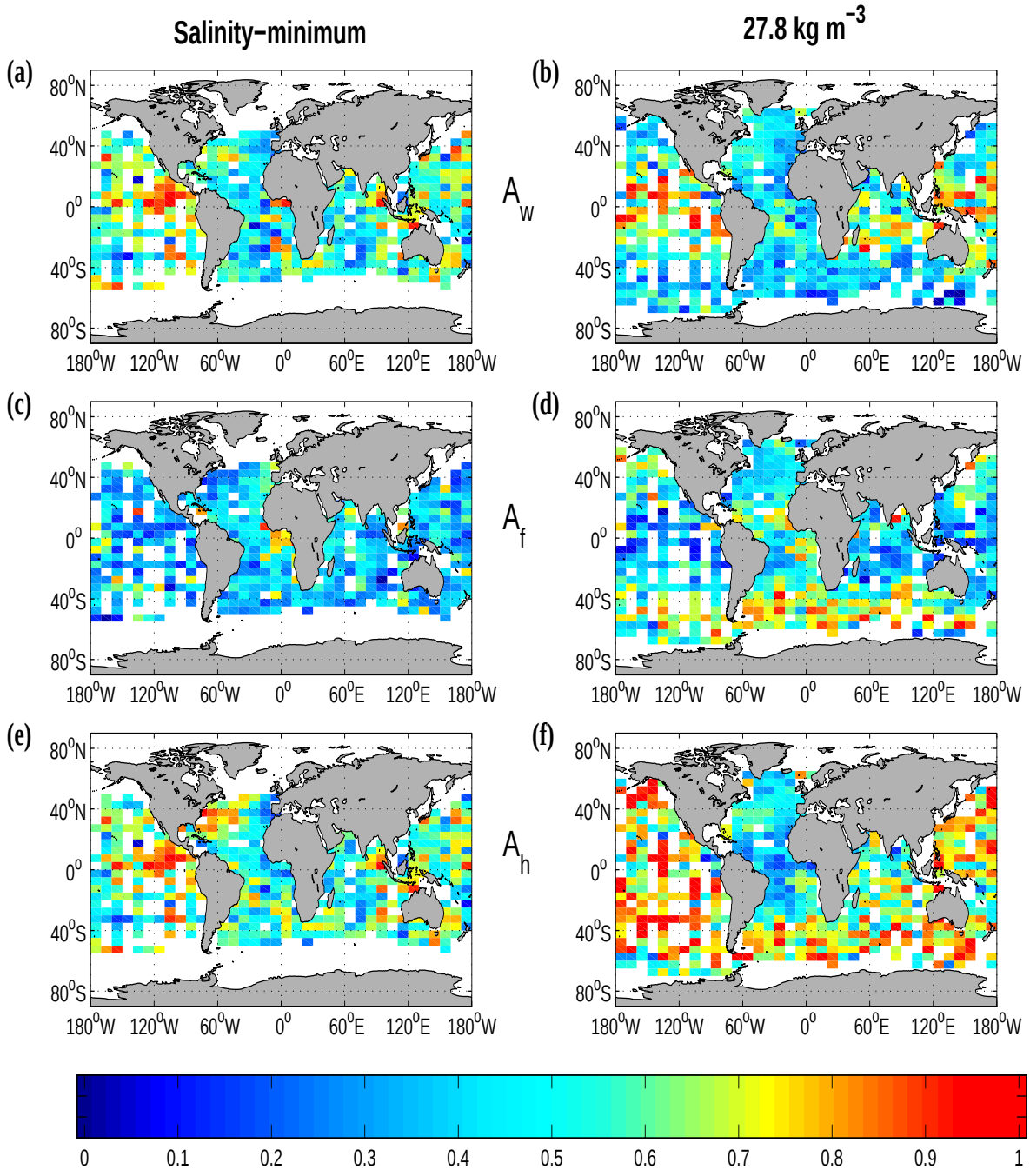

Figure 6.5: The pure subduction processes for the salinity-minimum (left) and the 27.8 kg m^{-3} density surfaces (right). The proportion of variance (R^2) explained by each process is shown for **(a-b)** Pure Warming, **(c-d)** Pure Freshening, and **(e-f)** Pure Heave. Note that this does not show the sign or magnitude of the observed changes on the surfaces (refer to Chapter 3, Figures 3.5 and 3.6 for this information).

in the Indian and Pacific Oceans), where a much larger proportion of variance in the recently formed SAMW can be explained by Pure Freshening. Such a pattern is reflected in the zonally averaged Figure 6.6 (b), which shows approximately 60% of the variance able to be explained by Pure Freshening between 20°S and 40°S.

The salinity-minimum and intermediate-level waters show similar patterns to the 27.0 kg m^{-3} density surface, with Pure Warming and Pure Heave explaining almost all of the signal variance in the East Pacific (Figure 6.5 (left panels)). The strong vertical displacement component ($N'\alpha\theta_z$) shown in Figure 6.3 (e) between 30°N and 40°N also appears in the Atlantic Ocean in Figure 6.5 (e), where approximately 80% of variance can be explained by Pure Heave in the west of the basin. In the Southern Hemisphere, there is a small discernible pattern in the zonally averaged subduction processes, with each of the individual subduction mechanisms only able to account for 20-40% of the variance in the signal (Figure 6.6 (c)). These results suggest that no single subduction process is appropriate in the mid-latitudes, and that at least a combination of two of the subduction processes is required.

As on the other three surfaces, the Pure Heave and Pure Warming scenarios were able to explain the observed changes with relatively equal skill. Interestingly the Southern Hemisphere freshening signal in AAIW that has appeared in Chapters 3-4 does not correspond with a strong Pure Freshening signal, suggesting that while freshening is a significant component of the interior ocean water mass changes, it is a relatively small contributor to the density changes and steric sea-level variability.

In the Northern Hemisphere it is a different story between 10°N and 40°N on the salinity-minimum (Figure 6.6 (c)). Here the freshening in NPIW dominates the zonal averages with the Pure Freshening scenario able to explain approximately 60% of variance, while the Pure Warming and Pure Heave scenarios can only account for approximately 40% of the variance.

The 27.8 kg m^{-3} density surface clearly reveals the striking relationship between the global circulation patterns and the amount of variance able to be explained by each of the pure subduction processes (Figure 6.5 (right panels)). In the low to mid-latitude Pacific and Indian Oceans the 27.8 kg m^{-3} density surface represents CDW, an old water mass with weak circulation and renewal rates. As such there is little variance in the signal able to be explained by freshening, with Pure Heave (and

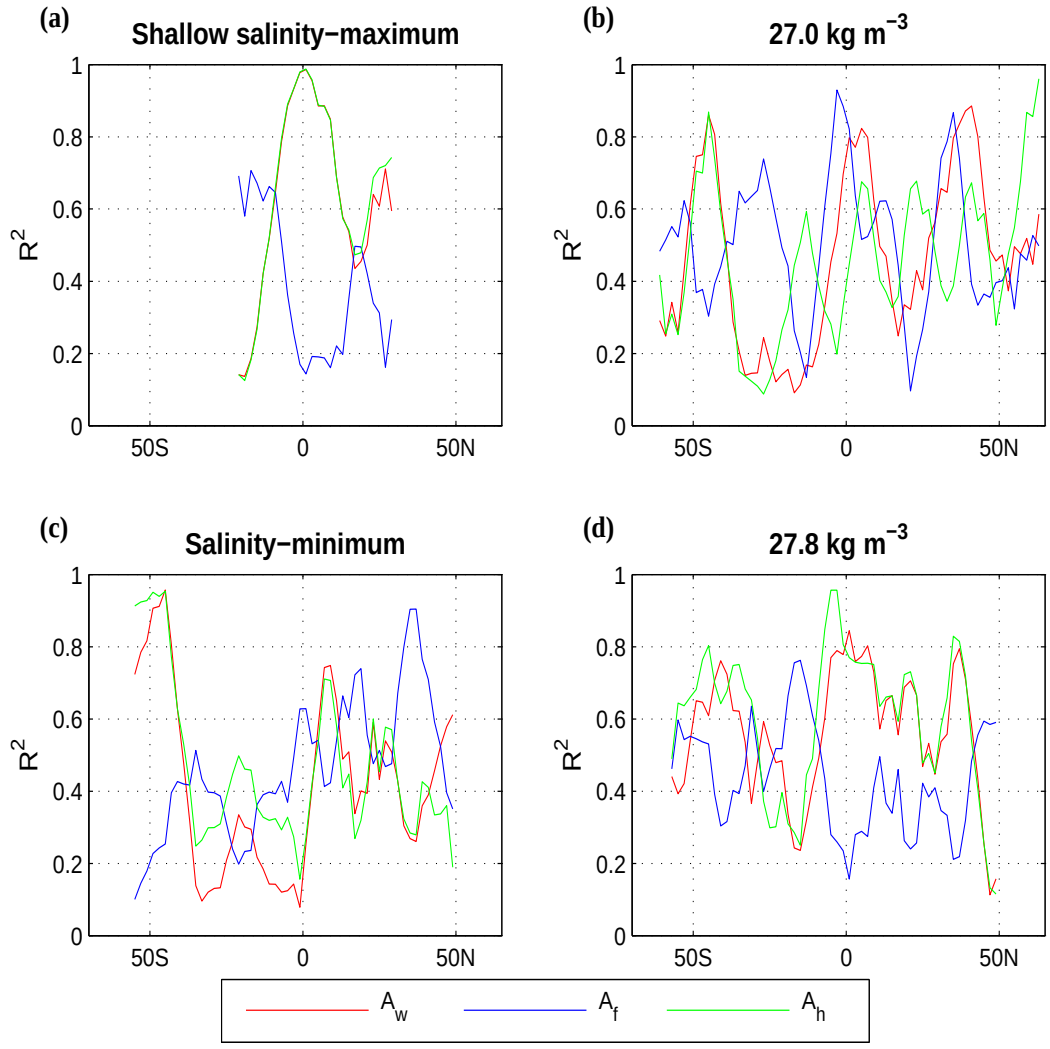

Figure 6.6: Zonally averaged pure subduction terms for the four representative surfaces by latitude. The proportion of variance (R^2) explained by each process is shown for Pure Warming (red), Pure Freshening (blue), and Pure Heave (green), with the surfaces being; **(a)** the shallow salinity-maximum, **(b)** the 27.0 kg m^{-3} isopycnal, **(c)** the salinity-minimum, **(d)** and the 27.8 kg m^{-3} isopycnal.

to a lesser extent Pure Warming in the low latitudes) being the primary mechanism responsible for the small temperature and salinity changes observed on this surface (∼90% of variance). While it may appear surprising that Pure Warming can explain any of the observed variance in latitudes far from ventilation regions, it should be remembered that the deep water along-isopycnal changes that are being explained are so small as to be statistically insignificant (Chapter 3, Figure 3.6 (d)).

North of the Subantarctic Front (∼40°S) in the Southern Hemisphere, Pure Warming, Pure Freshening, and Pure Heave all explain a similar proportion of variance (30-50%), except in the low latitudes where Pure Freshening is the dominant process.

In the Southern Ocean where the 27.8 kg m^{-3} density surface (UCDW) has been very recently ventilated and mixed with surface water, both Pure Freshening and Pure Heave are able to account for a significant proportion of the signal variance (over 70%). This pattern is circumpolar in extent (Figure 6.5 (d,f)). More importantly the strength of the Pure Freshening process adds further weight to the inferences in Chapters 3 and 4 of high-latitude surface freshening, and that the freshening is a significant contributor to the steric sea-level increases in this region.

The strength of the Pure Heave process qualitatively fits with a poleward shift (and hence appearing as a deepening) of the Southern Ocean density surfaces as part of the explanation for the strong warming on pressure surfaces in the upper 1500 dbar. It is likely that Pure Warming or freshening also has a strong influence given the similar skill in which it explains the observed changes in this region. The global zonal averages tend to somewhat hide the true signal in the low and mid-latitudes due to the markedly different patterns of change in the Pacific and Atlantic Oceans.

6.3.2 Pure subduction terms throughout the water column

Here the proportion of variance explained by the Pure Warming, Freshening, and Heave subduction scenarios are examined throughout the water column. This comprehensive approach builds on the previous analysis along representative density surfaces, reveals strong coherence in the density ranges that make up individual water masses, and shows markedly different explanations for the observed changes in the upwelling and subducting limbs of the overturning circulation in the Southern Ocean.

Figure 6.7 presents Pure Warming, Pure Freshening, and Pure Heave mapped from density to pressure surfaces. In estimating the strength of these processes smoothing of the zonally averaged stability ratio R_ρ was required to reduce the impact of noise. The first clear signal is the large Pure Warming and Pure Heave signals in the upper 500 dbar from 40°N-40°S, where the density surfaces are lighter than 26.6 kg m^{-3} (Figure 6.7 (a,c)). This pattern indicates temperature dominance in the equation of state (and the vertical displacement of density surfaces) in the upper thermocline, with the salinity changes not having a significant contribution to steric sea-level change. However at the shallow salinity-maximum (∼10°S-25°S) the observed salinity increases are best explained by a Pure Freshening subduction scenario, and this can just be seen in the contours under the top red density surface in Figure 6.7 (b) (at around 100 dbar).

In the lower thermocline between the 26.6 kg m^{-3} density surface and the salinity minimum, less variance is explained by a Pure Warming scenario and more by Pure Freshening (Figure 6.7 (b): circled). Closer to the source regions the changes in the same water masses (SAMW, AAIW) are equally well explained by temperature changes (ie. a thermal expansion), or by a vertical displacement of isopycnals without any water mass change (Pure Heave). The Pure Freshening model does not contribute as much to the observed changes near the source regions. Between 40°S and 50°S, the Pure Heave mechanism can explain a large proportion of the deeper zonally averaged changes down to 1500 dbar (Figure 6.7 (c): circled).

Between 40°S and 60°S a distinction can be made between these water masses which are being subducted into the ocean interior, and the upwelling and mixing with surface waters (Figure 6.7 (a): arrows and circled). The subducting waters are largely dominated by Pure Warming with little contribution from the Pure Freshening process, while in upwelling salinity maximum waters just above the 27.8 kg m^{-3} surface (ie. CDW) the reverse is true. Given the old age of these upwelling waters, any signal should be due to a change in exchange between the mixed layer and the interior, as is evident in the oxygen concentration decreases described in Chapter 5.

One final region of note is the higher proportion of variance explained by Pure Freshening (∼60%) throughout the water column near the formation zone of NADW (poleward of 40°N: Figure 6.7 (b): circled). This result fits well with the literature that suggests that the 1970s saw a significant freshening propagating into the ocean

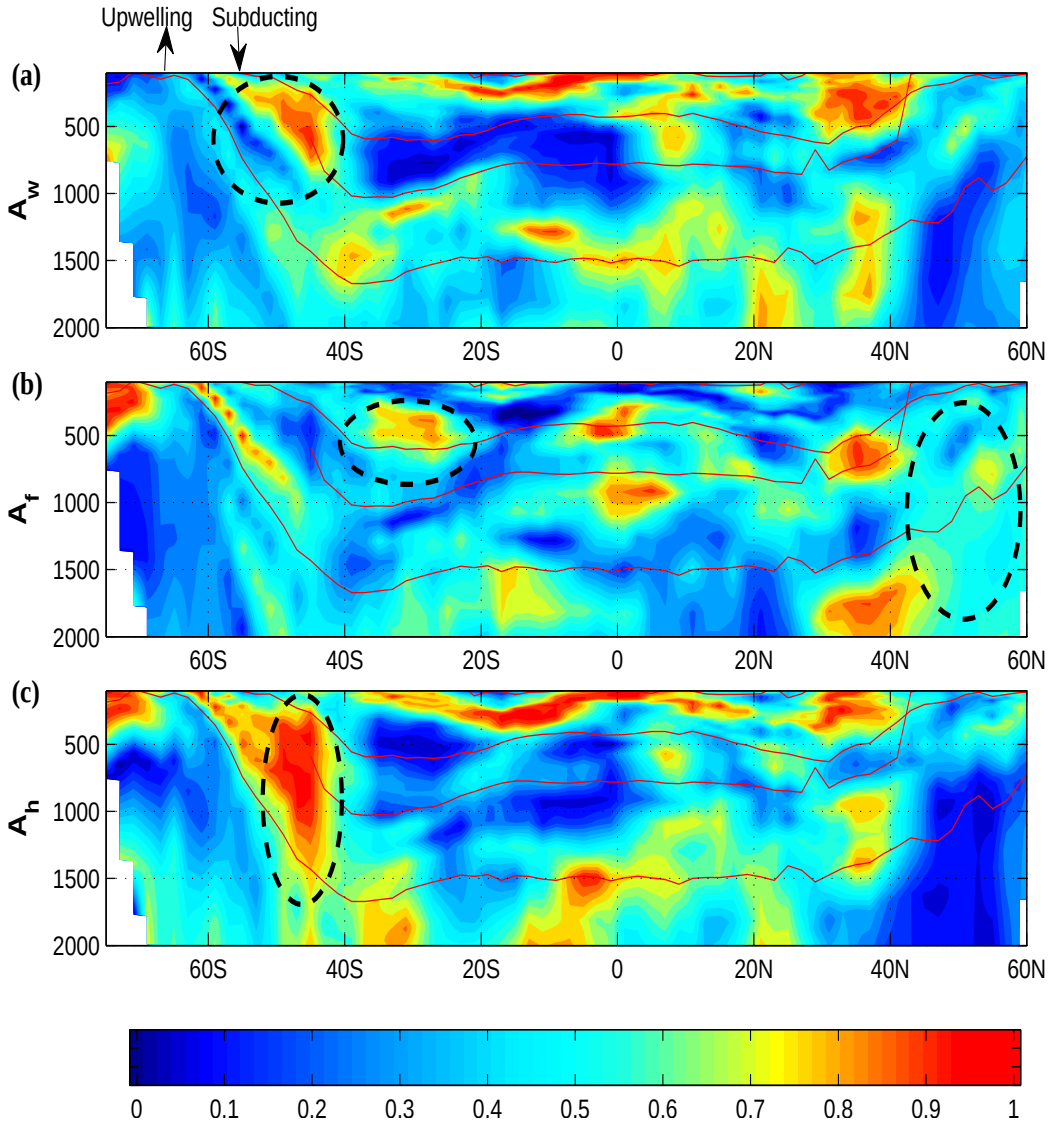

Figure 6.7: Zonally averaged pure subduction terms mapped to pressure surfaces. The proportion of variance (R^2) explained by **(a)** Pure Warming (A_w), **(b)** Pure Freshening (A_f), and **(c)** Pure Heave (A_h) is shown. Superimposed are the average depths of the shallow salinity-maximum, the 27.0 kg m^{-3}, the salinity-minimum, and the 27.8 kg m^{-3} surfaces. Circled regions are explicitly discussed in the text. The 27.0 kg m^{-3} density surface and the salinity-minimum cross in the Northern Hemisphere because the salinity minimum in the North Pacific is lighter than 27.0 kg m^{-3}.

interior through deep water masses in the North Atlantic (Curry and Mauritzen, 2005). In addition it suggests the observed corresponding cooling on the 27.8 kg m^{-3} density surface was more of a density-compensating response to the salinity changes, rather than an actual change in atmospheric heat flux forcing.

Conclusion: Least-squared analysis of observed changes

The most striking feature in Figures 6.4-6.7, is the similar skill in which the Pure Warming and Pure Heave explain the density perturbations on pressure surfaces (equivalent to sea-level change). This pattern of heave and Pure Warming that arises from the formal analysis is indicative of a poleward shift of the subtropical gyres and ACC. However the fact that both heave and warming show equal skill in explaining the observations, means the shift could either be a response to winds causing displacement with the Pure Heave scenario, or could be caused by surface warming and the addition of new lighter surface waters into the ocean displacing isopycnals downwards and more poleward.

In the least-squares analysis applied in this thesis, there has been no weighting applied to any of the observed quantities ($\alpha\theta'|_n$,$\beta S'|_n$,$N'\alpha\theta_z$,$N'\beta S_z$,$\alpha\theta'|_z$,$\beta S'|_z$), and thus it is assumed that each of these observed quantities has equal importance. However the larger error bars suggest greater variability or noise in the temperature and salinity displacement terms (Figure 6.8 (d)), than in the along-isopycnal water mass changes (Figure 6.8 (a)). Quantifying this larger variability in the inverse calculations would tend to downweight the importance of Pure Heave relative to Pure Warming and Pure Freshening in explaining the observed changes, and increase the amount of variance explained by these latter two processes.

It is clear that there are strong regional differences in the cause of property changes on density surfaces, and therefore different subduction processes operating. Chapters 3 to 5 of this thesis primarily examined changes on isopycnals, and therefore were able to link water mass property changes to surface variations using zonal back-projections. These water mass changes result in isopycnal displacement in the water column, and as such we have seen in this chapter that Pure Warming can explain the variance in the observations in some areas with good skill. However it has also become clear in this chapter that Pure Heave (ie. the movement of density surfaces with no water mass change: $\alpha\theta'|_n$=$\beta S'|_n$=0) appears to play an additional and significant role.

6.4 Zonally back-projected changes in density-weighted space

The remainder of this chapter shifts direction slightly. While all three pure process result in the vertical displacement of density surfaces, here we focus less on the cause, and instead use zonal back-projections to quantify the magnitude of this movement in terms of a density change. In this way we can go on to compare the contributions of individual density layers to global steric sea-level change.

6.4.1 Observable density changes

Figures 6.8 and 6.9 show the zonal back-projections of the six observable quantities presented in terms of latitude and neutral density respectively. These zonal back-projections represent a 'buoyancy flux' or water mass transformations in the mixed layer. Note that these density changes are actually the ratio of density change ($\Delta\rho/\rho$), and hence are dimensionless. Each point represents a single isopycnal and has been integrated from the equator to the surface outcrop, with each zonal average being weighted by the longitudinal width of the cell (as detailed in Chapter 2.6).

Figure 6.8 (a) shows similar patterns to the freshwater zonal back projections in Chapter 3 (Figure 3.13 (a)). The mid and high-latitudes in the Southern Hemisphere are the source for the increased density anomalies (ie. contraction) arising from cooling (although the reverse is true for the along-isopycnal salinity term: Figure 6.8 (b)). The low-latitudes see negative density changes (ie. expansion) in the region of warming. Although density-compensating (Figures 6.8-6.9 (c)), the largest along-isopycnal changes in temperature and salinity occur near the Southern Hemisphere 27.0 kg m^{-3} surface (SAMW) and in upper thermocline waters between the shallow salinity-maximum ($\sim$24.8 kg m^{-3}) and 26.4 kg m^{-3} (Figure 6.9 (a-b)). Compared to the Southern Hemisphere there is less along-isopycnal water mass change in surfaces found in the Northern Hemisphere (Figure 6.8 (a)).

The main feature of the vertical displacement temperature term is the large density increase (ie. contraction) centred near the shallow salinity maximum ($\sim$24.8 kg m^{-3}: Figure 6.9 (d)) which subducts around 20°S (Figure 6.8 (d)). This change due to vertical displacement represents a cooling (decrease in density) arising from a shoaling of density surfaces into a warmer region of the water column in the low-latitudes.

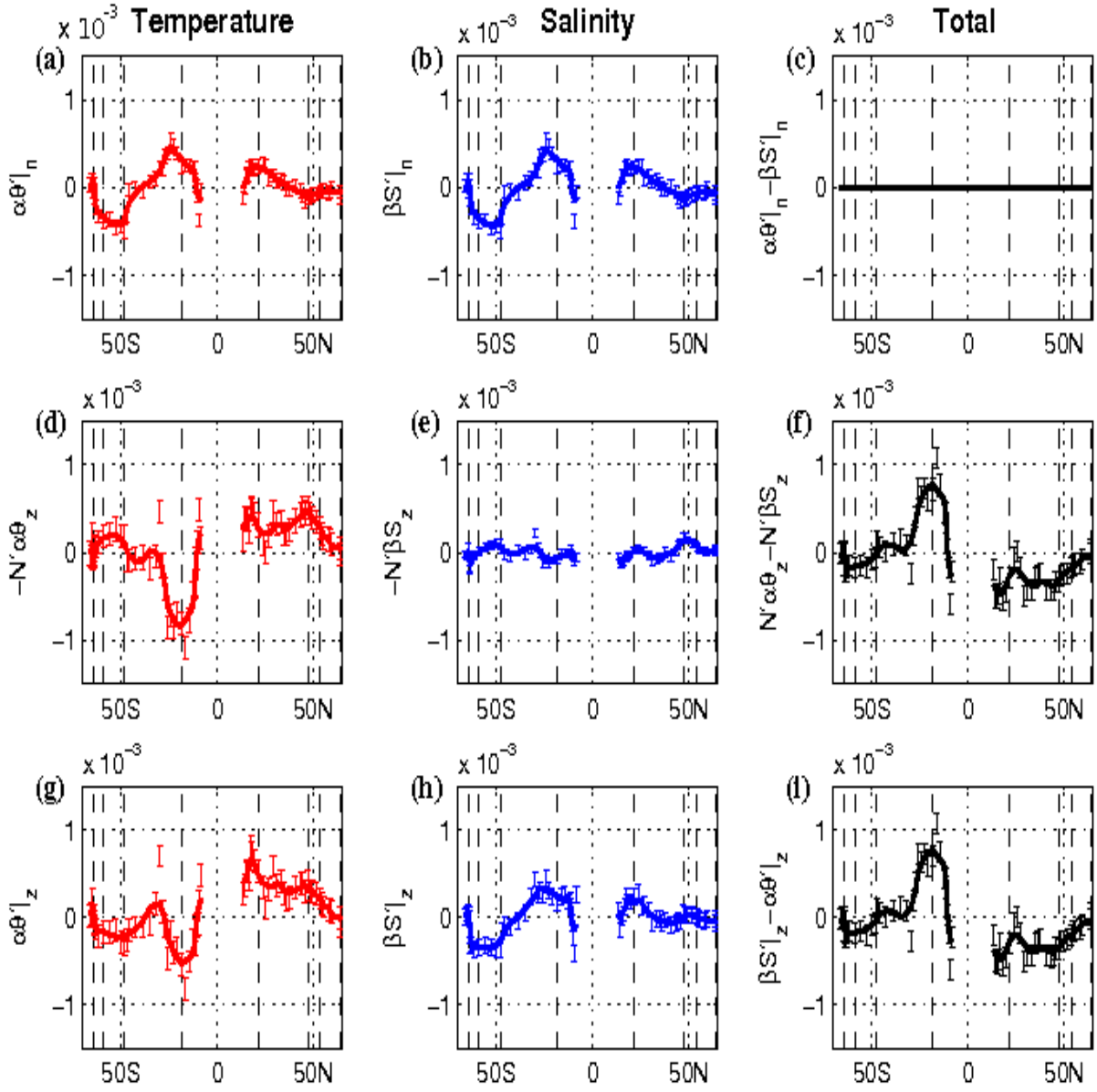

Figure 6.8: Zonal back-projections of the observable terms as a function of latitude. Black vertical dashed lines represent the outcropping regions of the 24.8, 26.8, 27.2, and 27.8 kg m^{-3} density surfaces in both hemispheres. Each point represents the integrated back-projected density perturbation ($\Delta\rho/\rho$: dimensionless). For the temperature (a,d,g) and combined (c,f,i) terms a negative term represents a density increase, while for salinity (b,e,h) a negative term represents a decrease in density. A running mean is plotted through the data, with error bars to one standard deviation. Error bars are calculated used methods described in Chapter 2.5.

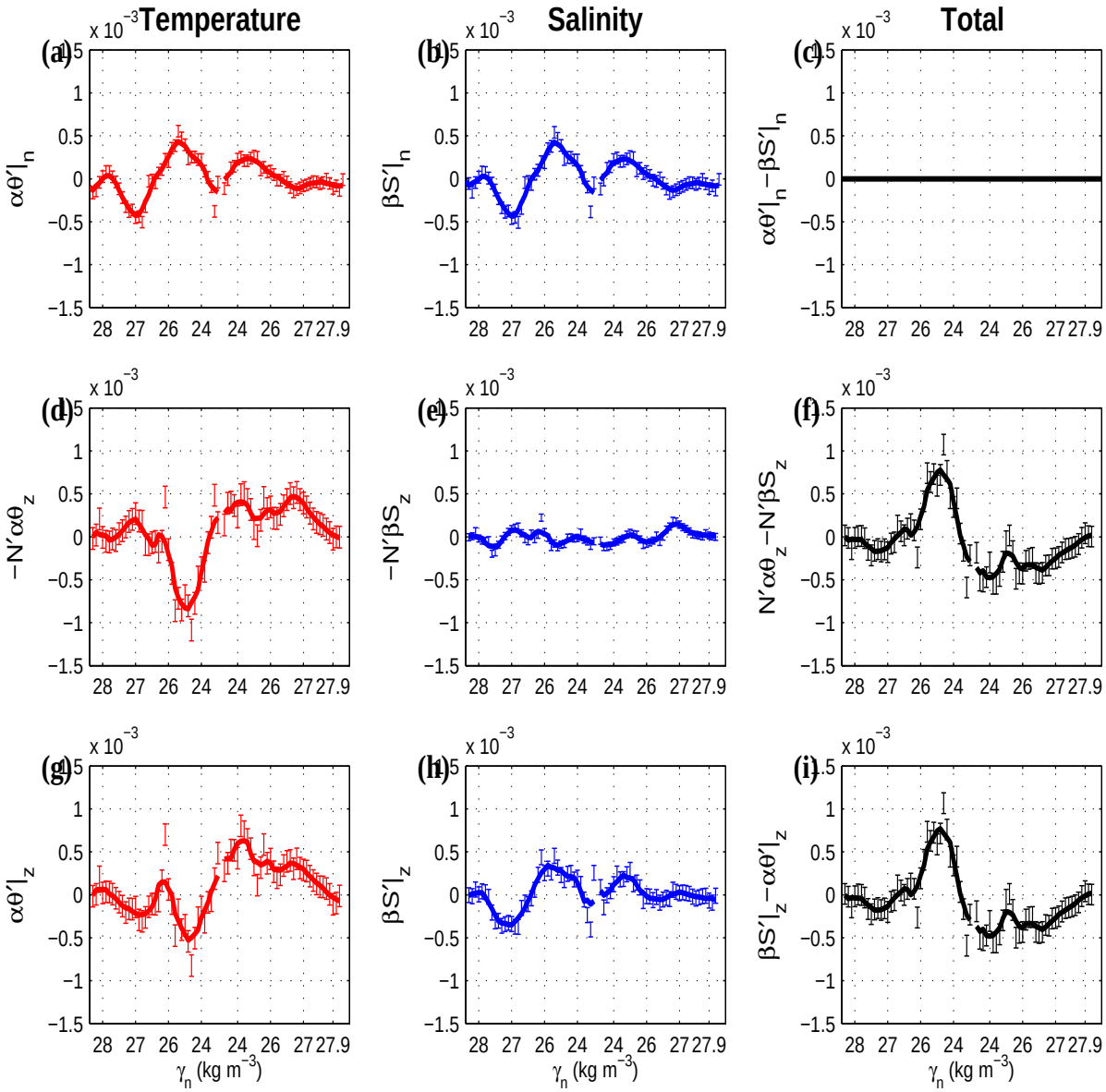

Figure 6.9: Zonal back-projections of the observable density perturbation terms (dimensionless). The same as Figure 6.8 but plots the back-projected change as a function of neutral density instead of latitude. Note that the horizontal axis splits in the centre and increases both to the right and left, reflecting the latitudinal density variations.

The vertical displacement leads to little density change on pressure surfaces from the salinity term ($N'\beta S_z$: Figures 6.8-6.9 (e)).

There is also a warming (density decreases) on pressure surfaces as the result of deepening of the density surfaces that outcrop in the mid and high-latitudes of both hemispheres (Figures 6.8-6.9 (d)). Although not as large in magnitude as the Southern Hemisphere low-latitude density increases ($N'\alpha\theta_z$), these deeper isopycnal surfaces occupy a much larger volume of the ocean and are therefore important to sea level change and heat and freshwater content changes. In the Southern Hemisphere, this decrease in density is centred on the SAMW density range ($\sim$27.0 kg m^{-3}), while in the north it occurs in slightly lighter densities in the NPIW range ($\sim$26.8 kg m^{-3}). As on the shallow salinity-maximum, a striking feature is the comparatively small contribution to density from salinity changes due to vertical isopycnal displacements (Figures 6.8-6.9 (e)). This result implies that it is the strong vertical gradient in temperature rather than the vertical gradient of salinity that will dominate the total steric sea-level change estimates.

The total density change on pressure surfaces (Figures 6.8-6.9 (g-h)) from each isopycnal is the sum of both the along-isopycnal and the vertical displacement terms (Equations 6.1-6.2). For the density changes associated with temperature, the two components partly negate each other, with the pattern similar to the displacement signal (Figures 6.8-6.9 (d)), but smaller in magnitude (Figures 6.8-6.9 (g)). For salinity, the weak contribution to density from vertical isopycnal displacement (Figures 6.8-6.9 (f)) means that the along-isopycnal changes (Figures 6.8-6.9 (b)) are the dominant salinity contribution to the change on pressure surfaces (Figures 6.8-6.9 (h)). For the combined temperature and salinity signals, the along-isopycnal changes by definition are density-compensating (Figures 6.8-6.9 (c)), and hence it is only the displacement terms (Figures 6.8-6.9 (f)) that contribute to the total density change on pressure surfaces (Figures 6.8-6.9 (i)).

6.4.2 Steric sea-level changes

To convert the dimensionless expansion contributions from temperature or salinity into an actual steric sea-level contribution, each term is multiplied by the volume of the zonally back-projected density layer in each latitude cell. Figure 6.10 shows the displacement-driven contribution to sea surface height change (left) and the total contribution to sea level arising from changes on pressure surfaces (right) from both

the salinity and temperature components.

Given the salinity and temperature changes along neutral density surfaces are density-compensating, the only contribution to steric sea-level change comes from the vertical displacement of isopycnals. As a consequence Figure 6.10 (e) (the total steric sea-level change from displacement) and Figure 6.10 (f) (the total steric sea-level change from changes on pressure surfaces), are almost identical. The small differences in the high-latitudes can be attributed to the fact that $\alpha\theta'|_z$ and $\beta S'|_z$ were calculated independently, and therefore did not ensure complete closure in Equations 6.1-6.2. This incomplete closure is discussed in Chapter 2.7 (Equation 2.24).

Multiplying by layer volume tends to reduce the magnitude of changes originating from the low-latitudes because of their low volume, and increases the high-latitude contribution because of their correspondingly larger water mass volumes.

The integrated change in density due to isopycnal displacement is largest in density layers that outcrop poleward of 26.5 kg m^{-3} (Figure 6.10 (e)), a consequence of the deepening of isopycnals that occurs from 40°S-50°S and 30°N-40°N (Figure 6.3 (e)). In the Northern Hemisphere the steric sea-level rises centred on 26.8 kg m^{-3} are larger than in the Southern Hemisphere, and from Chapter 3 it is clear that it is largely the result of deepening of density surfaces in the Atlantic Ocean. These results agree with other studies that have also shown the importance of the vertical displacement of isopycnals over actual along-isopycnal water mass change in this region (Bryden et al., 1996; Arbic and Owens, 2001). Over all latitudes, most of the change in the steric sea-level comes from the displacement of isopycnals through the temperature gradient, with the back-projected salinity changes having a relatively small contribution to steric change in a density-weighted space (comparing Figure 6.10 (a) with Figure 6.10 (c)).

Figure 6.10 (c) shows a decrease in steric height arising from deepening of more saline waters centred on SAMW in the Southern Hemisphere (27.0 kg m^{-3}) and the NPIW density range in the Northern Hemisphere ($\sim$26.8 kg m^{-3}). However this contribution of $N'\beta S_z$ is relatively minor with most of the displacement-driven density change in Figure 6.10 (e) coming from $N'\alpha\theta_z$.

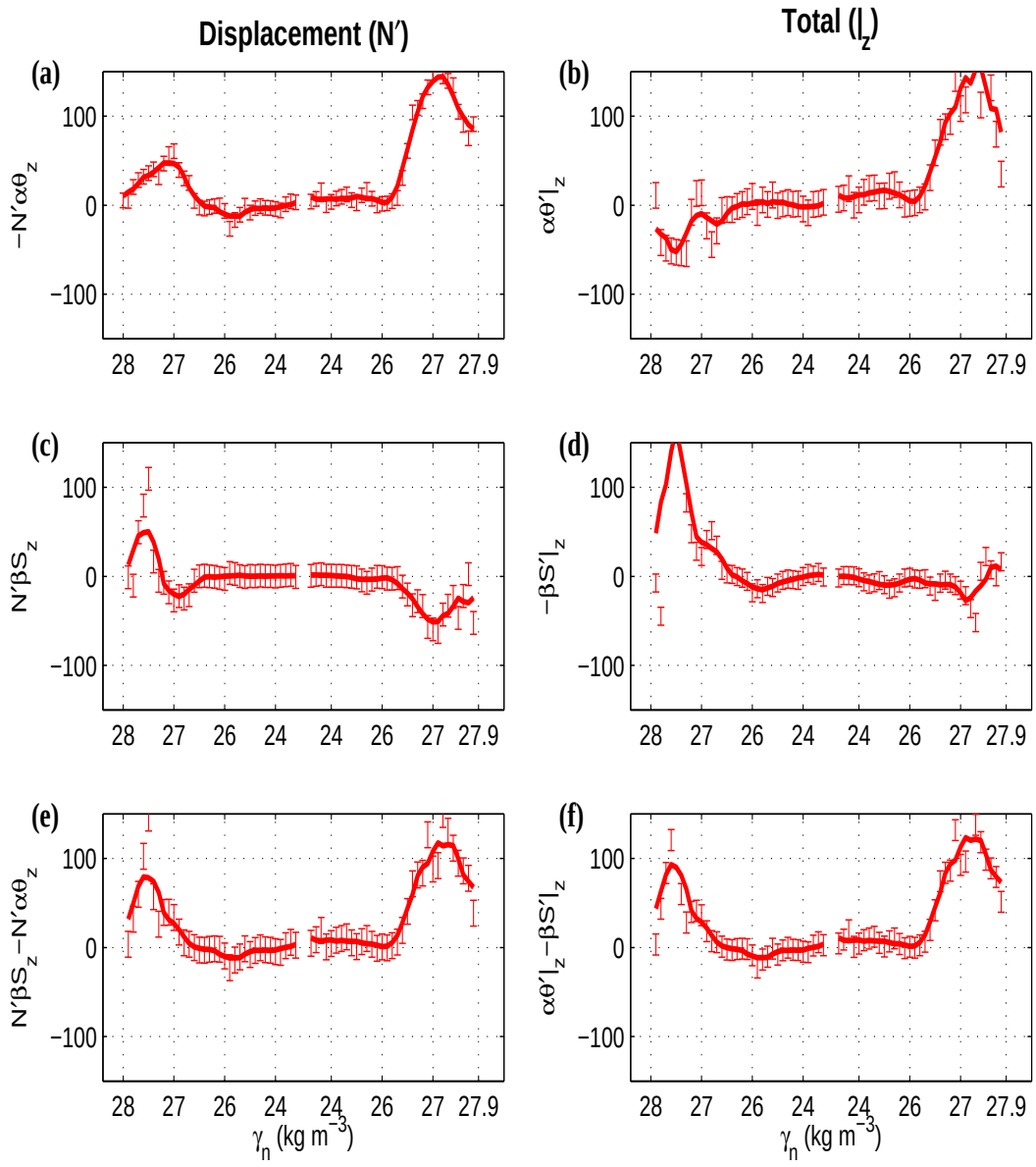

Figure 6.10: Zonal back-projections of contribution to global sea level change (1970-1992 in mm) from the changes from each density layer, where the sea level change comes from **(a)** $N'\alpha\theta_z$, **(b)** $\alpha\theta'|_z$, **(c)** $N'\beta S_z$, **(d)** $\beta S'|_z$, **(e)** -($N'\alpha\theta_z$-$N'\beta S_z$) (Equation 6.4), and **(f)** -($\beta S'|_z$-$\alpha\theta'|_z$) (Equation 6.3). Error bars are given to one standard deviation. Note that the horizontal axis splits in the centre and increases both to the right and left, reflecting the latitudinal density variations.

The large contribution of along-isopycnal changes can be seen by examining the differences between the steric sea-level change from displacement (Figure 6.10 (a,c)), and the integrated change on pressure surfaces (Figure 6.10 (b,d)). In particular the freshening in the Southern Hemisphere mode, intermediate, and deep water isopycnals (26.0-28.0 kg m^{-3}) show through clearly by appearing as a sea-surface rise ($\beta S'|_z$=$\beta S'|_n$-$N'\beta S_z$: Figure 6.10 (d)), which is not reflected in the isopycnal displacement term alone ($N'\alpha\theta_z$: Figure 6.10 (c)). By contrast in the Northern Hemisphere the 26.3-27.9 kg m^{-3} density surfaces have had a large temperature-driven contribution to sea-level rise (Figure 6.10 (b)). In this case the fact that there is no corresponding large halosteric rise of the opposite sign in Figure 6.10 (d) on these surfaces, means that the pattern in Figure 6.10 (b) is caused largely by vertical displacement of isopycnals.

Note again that the total steric sea-level change (Figure 6.10 (f)), the $\alpha\theta'|_n$ and $\beta S'|_n$ terms that contribute to the patterns shown in Figures 6.10 (b) and 6.10 (d) respectively, are density-compensating and cancel out. For this reason, it is only the displacement of isopycnals that contribute to sea-level change, and hence Figures 6.10 (e) and 6.10 (f) are identical.

The *total* sea level change (combining $\alpha\theta'|_z$ and $\beta S'|_z$) from each density layer is also shown in physical space in Figure 6.11 (a) (by latitude instead of density as shown in Figure 6.10 (f)). Essentially Figure 6.11 (a) takes the contributions to sea level from each density layer (ie. the changes in density: Figure 6.11 (c)), and projects and plots it at the outcrop region.

Note that the zonally back-projected pattern of surface height change (Figure 6.11 (a)) is not the pattern of height change that would be observed at the surface of the ocean, but instead more accurately reflects ocean circulation and emphasises the relatively large contributions of those water masses whose origins are in the mid to high-latitudes. The more conventional *geographic* (actual) pattern of steric sea-surface height change has been described in Chapter 3, and is shown from 0-2000 dbar in Figure 6.11 (b). The main difference between the two projections is that Figure 6.11 (a) shows where heat and freshwater changes *enter* the ocean, and Figure 6.11 (b) shows where it is *stored*.

From 1970-1992 the largest back-projected rises in sea-surface height came from

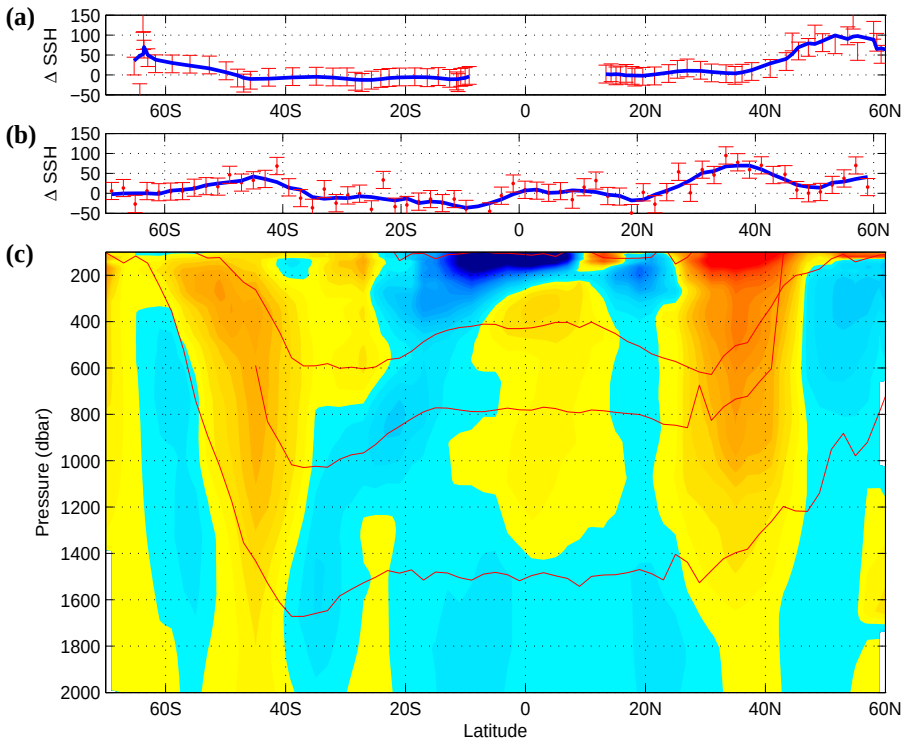

Figure 6.11: Zonally averaged steric changes from ∼1970-1992. **(a)** Back-projected steric sea-level change in mm (as in Figure 6.10 (f)). **(b)** Vertically integrated steric sea-level change (0-2000 dbar). Error bars are calculated used methods described in Chapter 2.5. **(c)** Density change ($\alpha\theta'|_z$-$\beta S'|_z$) where red represents a decrease in density (expansion of water), and blue is a density increase (contraction). The darker the colour, the greater the expansion (red) or contraction (blue). In (c) the units are dimensionless but represent the expansion contribution of the water column.

the density layers that outcrop in the high-latitude Northern Hemisphere, and are approximately 100 mm (4.5 mm yr^{-1}). Although these along-layer averages are an unorthodox reference frame, the best way to visualise it is that if all the heat and freshwater fluxes that entered into the ocean at this latitude (approximately 50°N-60°N) were stored vertically, then a rise of 100 mm would be seen.

In the Southern Hemisphere a significant proportion of the globally averaged sea level rise enters the ocean south of the Polar Front (approximately 50°S: 26.8 kg m^{-3}), at a maximum of around 50 mm at 65°S (2.3 mm yr^{-1}). The changing surface conditions in the Southern Hemisphere subtropical gyres and low-latitude layers have resulted in a net decrease in steric sea-surface height.

Integrating temperature and salinity changes vertically and weighting by area, reveals a globally averaged change of 5.1 mm (0-2000 dbar). As a consistency check, this steric sea-level rise compares reasonably well with the area-weighted along-isopycnal sea-level rise of 4.4 mm. The differences between these two estimates occur because the along density layer integrals of sea level rise does not quite have the same footprint over all latitudes as the global estimate from the fixed reference depth level.

The main result from the density layer estimate of sea-level rise (Figure 6.11 (a)) is the importance of the high-latitudes in contributing to steric sea-level rise. This is despite the relatively small surface area of these regions, and reflects the importance of these high-latitudes in renewing the deep waters of the entire ocean.

6.5 Summary and discussion

This chapter set out to understand the ambiguity associated with the use of neutral density surfaces as a reference frame for diagnosing climate change signals in the ocean. Adopting techniques developed by Bindoff and McDougall (1994), the water mass change was separated from isopycnal movement, with a formal analysis method being used to identify different pure subduction scenarios to the observed interior changes (1970-1992). Finally the use of the novel 'zonal back-projection' technique enabled the relative importance of different density surfaces to global steric sea-level change to be diagnosed.

As with the temperature and salinity observations in earlier chapters, there were clear globally coherent patterns that emerged. Across most water masses the changes on pressure surfaces due to downward displacement of density surfaces were of a similar magnitude to the actual along-isopycnal changes advected from the ocean surface. Importantly, both terms (ie. $N'\alpha\theta_z$ and $\alpha\theta'|_n$ respectively) have distinct spatial patterns. Water mass changes have been discussed at length in previous chapters, with along-isopycnal changes being strongest around intermediate waters, the upper-thermocline, recently ventilated NADW, and in the Southern Ocean. There were two main regions of deepening isopycnals that led to significant changes in the upper 1500 dbar. These regions were centred around 40°N and 40°S and caused significant temperature decreases in density from the vertical temperature gradient. There was comparatively little density contribution in these two regions associated with isopycnal movement through the vertical salinity gradient.

The total combined water mass and vertical displacement temperature changes on pressure surfaces (Figure 6.3 (a)) look very similar to the global zonal averages estimated by conventional methods (Levitus et al. (2005a): Chapter 1, Figure 1.3). Here it is shown that much of the observed change on pressure surfaces is due not to surface anomalies being advected along density surfaces, but in some latitudes and regions is the result of vertical isopycnal displacement with little water mass change. Such isopycnal movement can be a product of either the addition (or removal) of lighter overlying water, or as the result of changing surface winds. Vertical displacement of density surfaces has been shown previously to be the dominant contribution to isobaric changes in the North Atlantic Ocean (Bryden et al., 1996; Arbic and Owens, 2001). However here it is also shown to occur on global scales, particularly in waters that are distance from their source regions and in regions with high decadal variability.

In density space these density changes were dominated by vertical temperature gradients rather than salinity, and integrating the changes along density surface shows the largest steric sea-level rises occur in isopycnals that outcrop in the high-latitudes of both hemispheres. Interestingly there are steric sea-level decreases resulting from density surfaces that outcrop in the low and mid-latitudes. While they make up a significant proportion of the World Ocean, the low and mid-latitudes contributions do not overwhelm the sea level rise from high-latitudes and an overall steric sea level rise of 4.4 mm yr^{-1} results. This is equivalent to a rise of 0.2 mm yr^{-1} from

1970-1992, although excludes changes in the upper 100 m.

The use of zonal back-projections implies a highly idealised model that assumes spreading along the length of density surface in the study period and no diapycnal temperature or salinity fluxes. However, despite it's simplicity, it does emphasise the strong influence that the high-latitude regions, particularly the Southern Ocean and the North Atlantic, have on both global heat and freshwater budgets, and on global water mass change. Note that despite the despite the large volumes of the ocean that these deeper density layers occupy, they communicate with the atmosphere through a relatively small area.

The Pure Freshening subduction scenario (ie. no heave or warming), plays only a small part in the density decreases observed in the upper few hundred metres of the water column. However deeper in the water column, it does have a more significant role in the density changes in SAMW and NPIW. Elsewhere the implication is that while there are clear and coherent salinity changes in isopycnal layers (which have been attributed to changes in the hydrological cycle in Chapters 3 and 4), these have relatively little contribution to the density decreases, and hence steric sea-level change across much of the globe. The Pure Heave and Pure Warming subduction mechanisms are hard to distinguish, as across much of the ocean they have equal skill in explaining the observed changes.

In the least-squares formal analysis there is no weighting applied to the six observed quantities that are used to estimate the proportion of variance explained by each of the pure subduction processes. By doing so there is an implicit assumption that there is equal confidence in both the displacement and the along-isopycnal observations. In fact there is greater variance and hence larger error bars in the displacement terms (Figures 6.8-6.9 (c-d)), than in the corresponding changes *along* neutral density surfaces (Figures 6.8-6.9 (a-b)). Including this uncertainty in the least-squares analysis of subduction processes would result in a similar general pattern of change, although would downweight the variance explained by a Pure Heave subduction scenario and increase the variance explained by Pure Warming and Pure Freshening.

The pattern of change in the Southern Ocean is indicative of a southward shift of the Southern Hemisphere subtropical gyres and the ACC. This type of shift has

been well documented in recent literature (Alory et al., 2007; Gille, 2007; Rintoul and England, 2002) and tends to be attributed to increased westerly winds. This model implies increasing Ekman pumping, and hence deepening isopycnals and an associated southward shift of isopycnals. Both the observations in previous chapters and in climate models, demonstrate that such physical changes have been occurring.

This chapter uses formal analysis to separate out the potential explanations and reveals that such a wind-driven Pure Heave mechanism can explain some of the temperature and salinity changes observed in the Southern Ocean. However the formal analysis presented shows that Pure Warming also provides an equally plausible explanation, is more consistent with the observation of significant water mass change, and results in a similar southward shift of density surfaces. Weighting the observed variability in the formal analysis would strengthen the case for a Pure Warming explanation of the observed density perturbations in the Southern Ocean.

Chapter 7 Conclusion and scope for future work

7.1 Conclusion

The oceans are an integral part of the global climate system, acting as a reservoir for 97% of the world's water and having a heat capacity a thousand times greater than the atmosphere (Levitus et al., 2005a). It therefore follows that documenting and interpreting the physical changes in the oceans are essential to understanding the global climate change story. Here three high-quality quality-controlled datasets were combined to present ocean temperature, salinity, and oxygen changes on density surfaces for the first time on a global scale. Density surfaces are a more natural reference frame than pressure surfaces as they more accurately follow the paths of water masses, and are more easily used to separate the changes due to processes such as winds, mesoscale eddies, and Rossby waves, from those changes caused by air-sea interaction.

Comparing observations between the 1970-1992 and the 1992-2005 periods revealed statistically significant patterns of change on global and ocean-basin scales. In particular the following key features were evident along neutral density surfaces.

- A warming and salinity increase in water above and around the shallow salinity-maximum.
- A cooling and freshening in thermocline waters and salinity-minimum waters in both hemispheres.
- Around the deep salinity-maximum density surfaces there was relatively little water property change away from ventilation regions. Near ventilation and source regions there was strong warming and salinity increases in the North Atlantic and Southern Oceans.
- A statistically significant, and approximately symmetrical, deepening of intermediate level density surfaces (300-1500 dbar) in both hemispheres poleward of 40°.

- A near-global decrease in oxygen concentration in the upper-3000 dbar (1970-1992), with a total oxygen loss of $12.9 \pm 2.5 \times 10^{14}$ mol at an average of 1.82 ± 0.92 μmol l^{-1} ($\sim$1% of the mean ocean oxygen content).
- Less than 15% of this global decrease in oxygen concentration can be explained by the observed increased surface temperature; however there is a correlation between increased surface stratification and oxygen decreases near key water mass ventilation regions.
- On a global scale, changes in temperature, salinity, and isopycnal displacement were generally consistent between the 1970-1992 and the 1992-2005 periods.
- Regional variability on shorter time scales was evident in the subpolar North Atlantic waters (100-2000 dbar), and in the South Indian Ocean Mode Waters (ie. NAO and SAM signals). The spatial patterns of change in the equatorial Pacific Ocean show an ENSO-type signature in both time periods.

The salinity changes on density layers observed within the ocean were back-projected to estimate the changes in surface fluxes. Statistically significant apparent freshwater inputs poleward of 40° in both hemispheres ($\sim$100 mm yr^{-1}) were estimated ($\sim$1970-1992). Decreases in apparent precipitation-minus-evaporation were found in the low latitudes ($\sim$10 mm yr^{-1}). Apparent surface heat fluxes were estimated from temperature changes and showed a symmetrical pattern of global change in both hemispheres, with apparent heat flux increases in the high-latitudes, relatively small decreases in subtropical gyres, and a slight increase at the equator (Figure 7.1: red line).

The importance of the high-latitudes to the global freshwater, heat, and oxygen budgets is clearly demonstrated in Figure 7.1, where a disproportionately large amount of the total freshwater, heat, and oxygen change occurs in those density surfaces that outcrop poleward of 40°. This is illustrated in the Southern Ocean, where despite covering less than 25% of the global ocean surface area, the density layers that outcrop in this region account for 57% of the freshwater change and for 39% of the total oxygen losses ($\sim$1970-1992). North of 40°N similar cumulative surface fluxes are inferred from the ocean changes in a latitude range that represents only 11% of the total World Ocean surface area (60% of the apparent freshwater flux changes and 45% of the oxygen flux change). Equatorward of 40° these results suggest that the low-latitudes have contributed a smaller part to the global budgets of temperature, salinity, and oxygen change due to the relatively small volumes of

density layers.

Using a neutral density surface reference frame allowed the changes on pressure surfaces to be separated into displacement and along-isopycnal components. In the upper-1500 dbar of the North Atlantic Ocean, the vertical displacement of density surfaces is the dominant mechanism for the observed changes, and is the primary cause of the large temperature increases on pressure surfaces in the Southern Ocean (700-1100 dbar).

Using a least squared analysis technique (Bindoff and McDougall, 1994), the movement of density surfaces and change along density surfaces is tested against Pure Warming, Pure Freshening, and Pure Heave subduction scenarios. Despite there being clear patterns of water mass change, a Pure Freshening subduction mechanism explains relatively little of the observed variance in density change away from key mode and intermediate formation regions. Pure Warming and Pure Heave provide better explanations for the observed changes, with the two subduction mechanisms explaining the change in density-weighted space with equal skill across much of the globe.

These observed changes in the ocean interior are consistent with models of rising greenhouse gases in the atmosphere on a global scale over the past 50 years. The IPCC coupled ocean-atmosphere models show an enhancement of the hydrological cycle, resulting in an ocean freshening in the high-latitudes and more saline waters originating from the inter-tropical convergence zones. In a warming earth, these changes in the distribution of freshwater are coupled with a southward shift and strengthening of the high-latitude circumpolar winds in both hemispheres. In the oceans these changes have a signature of a poleward displacement and deepening of density surfaces.

In this model, one consequence of the warming and freshening in the high-latitudes is an increased stratification of the upper-ocean. This increased stratification in the key water mass formation and upwelling regions reduces the exchange between the mixed-layer and the ocean interior, decreasing the flushing time of water masses and allowing more time for oxygen consumption resulting in a global decrease of oxygen as observed.

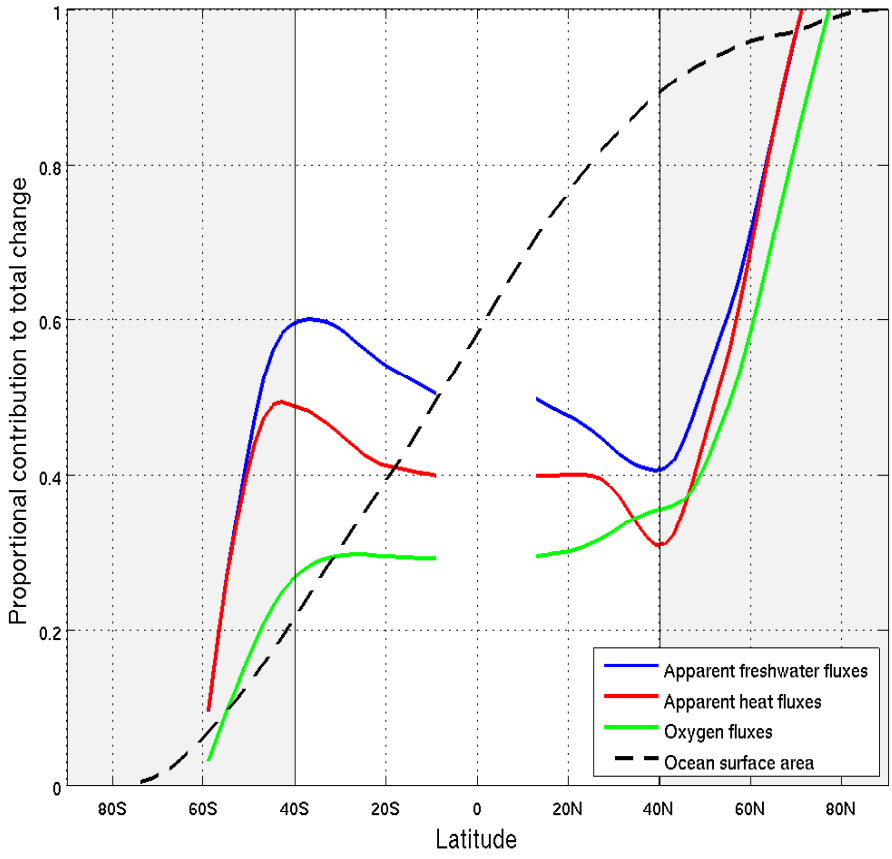

Figure 7.1: The cumulative proportional contribution of each latitude band to the total flux change (1970-1992). Each flux was taken from its density layer outcropping region (back-projected along zonally averaged density layers), and linearly interpolated to regular spaced latitudes. From south to north, the cumulative distribution of *changes* in fluxes was divided by the *sum of all surface fluxes* (which was positive for apparent heat and freshwater and negative for oxygen fluxes). Given that none of the density layers used in this analysis outcropped poleward of 60° or between 10°S and 12°N, these regions were omitted. The cumulative proportion of ocean surface area (fixed in time) at each latitude is shown by a black dashed line. As an example, approximately 55% of the total global freshwater increase has entered the ocean south of 40°S, despite this area only being 22% of the total global ocean surface area. There were freshwater losses (∼15%) in the mid and low-latitudes, while 60% of the net freshwater increase entered north of 40°N. This figure highlights the importance of the high-latitude processes in understanding decadal-scale climate change.

While in Chapter 5 the winds were not seen as being the dominant mechanism for oxygen change, when coupled with warming (ie. the addition of lighter water at the surface or along density surfaces), they can explain the deepening and poleward movement of isopycnals in most ocean basins. The freshwater redistribution is believed to have a relatively small contribution to these *density* decreases on pressure surfaces, despite being a strong component of mode and intermediate water mass changes. Steric sea level reflects this deepening, with large high-latitude rises and decreases in the low-latitudes, dominated by strong interannual variability (ENSO) in the Pacific Ocean where the water masses have relatively short flushing times. On a global scale however, this interannual variability from ENSO is relatively small when compared with the underlying trend, as the properties of the deep water masses that make up a large volume of the World's Oceans are set in the high-latitude regions of both hemispheres.

7.2 Scope for future work

Using a density-based coordinate system, this thesis has focused on the *diagnosis* of ocean water property changes, with some largely qualitative discussion of possible explanations for the observed changes. There is large scope for future work to build on these physical relationships that have been identified, with a more quantitative analysis of the physical links between the variables discussed in Chapters 3 to 6 (ie. sea-surface height, stratification, oxygen, circulation pathways and renewal rates). The lack of historical observations in the Southern Hemisphere frequently means that such analyses can only be synoptic in nature. However in future years, studies could make use of the comprehensive spatial coverage that the evolving Argo dataset is providing. The introduction of a temporal component into a quantitative analysis of the relationships between various ocean parameters is likely to require the synthesis of models and observations in a similar fashion to some of the reanalysis products that are available (ie. Bluelink, SODA (Carton et al., 2000), ECCO (Stammer et al., 1999)).

There are two main benefits to using such models. The first is that individual ocean parameters can be isolated and a number of different scenarios can be run (ie. hypothesis testing). This allows the relative magnitude and sensitivity to change of each component of the ocean system to be examined, and would allow a better understanding of the sources of the net global ocean freshening. In addition, models

would be of use in identifying the contribution of wind-driven Ekman fluxes to interior water property changes, the extent to which stratification affects renewal rates (and hence oxygen concentration levels), and to more accurately identify circulation pathways and flushing times of individual water masses along density surfaces. This would enable more quantitative relationships to be developed based both on theory and on the actual physical observations. Given that our conceptual model is built on the premise of little diapycnal mixing, it would also be of interest to test this assumption by identifying how diffusion varies across different ocean basins and density layers.

The second main benefit of combining observed data with coupled ocean-atmosphere computer models, is that the observations could be used to test the robustness of model outputs and potentially inspire more confidence in projections of future climate. While many IPCC-class models already do project future climate and ocean changes, the use of a density coordinate system and the introduction of oxygen as a parameter are not common. These two features are valuable tools that improve our understanding of ocean circulation and the renewal of water masses, as well as emphasising the importance to the high-latitude regions to the long-term changes in the global ocean system.

The benefits of examining changes in oxygen concentration levels are only just beginning to be recognised in the scientific literature; however a lack of modern observations hampers any up to date analysis of changes on a global scale. Recently there have been a small number of Argo floats with oxygen sensors deployed, and it is expected that in the next decade reduced costs, better reliability, and a greater awareness of the role of oxygen will increase this number significantly. Once this occurs, then oceanographers will rapidly be provided with a high-quality global oxygen atlas to compare with historical observations. By integrating oxygen observations with other biological tracers (ie. nitrate, phosphate), and examining the Redfield ratios, the biological and physical components of the oxygen signal could be separated.

Conclusion

The techniques of mapping data from different time periods to a common grid point and comparing them on neutral density surfaces, has been shown in this thesis to be a plausible and a reasonably robust tool. The logical extension of this is to apply the same technique to other spatially distributed ocean tracers (ie. dissolved organic carbon, CFC's: Sabine et al. (2004)) in order to identify key regions of sequestration and outgassing. While poor spatial coverage may make this difficult for some tracers, it again may require an integration of these observations with models in order to better understand how changes in the ocean interior relate to atmospheric variability. It is only through diagnosing changes in individual components, attributing these to atmospheric forcing, and quantifying the numerous physical relationships in the complex ocean-atmospheric system, that we can hope to truly understand the implications of future climate change scenarios.

References

Allen, M. and Ingram, W. (2002). Constraints on future changes in climate and the hydrological cycle. *Nature*, 419:224–232.

Alory, G., Wijffels, S., and Meyers, G. (2007). Observed temperature trends in the Indian Ocean over 1960-1999 and associated mechanisms. *Geophysical Research Letters*, 34(2).

Andreev, A. and Watanabe, S. (2002). Temporal changes in dissolved oxygen of the intermediate water in the subarctic North Pacific. *Geophysical Research Letters*, 29(14).

Antonov, J., Levitus, S., and Boyer, T. (2002). Steric sea level variations during 1957–1994: Importance of salinity. *Journal of Geophysical Research*, 107(C12):8013–8020.

Antonov, J., Levitus, S., and Boyer, T. (2005). Thermosteric sea level rise, 1955–2003. *Geophysical Research Letters*, 32(12).

Aoki, S. (1997). Trends and interannual variability of surface layer temperature in the Indian Sector of the Southern Ocean observed by Japanese Antarctic research expeditions. *Journal of Oceanography*, 53(6):623–631.

Aoki, S., Bindoff, N., and Church, J. (2005). Interdecadal water mass changes in the Southern Ocean between 30°E and 160°E. *Geophysical Research Letters*, 32(7).

Arbic, B. and Owens, W. (2001). Climatic warming of Atlantic intermediate waters. *Journal of Climate.*, 14(20):4091–4108.

Banks, H. and Bindoff, N. (2003). Comparison of observed temperature and salinity changes in the Indo-Pacific with results from the coupled climate model HadCM3: Processes and mechanisms. *Journal of Climate.*, 16(1):156–166.

Bindoff, N. and Church, J. (1992). Warming of the water column in the southwest Pacific Ocean. *Nature*, 357(6373):59–62.

Bindoff, N. and McDougall, T. (1994). Diagnosing climate change and ocean ventilation using hydrographic data. *Journal of Physical Oceanography*, 24(6):1137–1152.

Bindoff, N. and McDougall, T. (2000). Decadal changes along an Indian Ocean section at 32°S and their interpretation. *Journal of Physical Oceanography*, 30(6):1207–1222.

Bindoff, N., Willebrand, J., Artale, V., Cazenave, A., Gregory, J., Gulev, S., Hanawa, K., Le Quéré, C., Levitus, S., Nojiri, Y., Shum, C., Talley, L., and Unnikrishnan, A. (2007). *Observations: Oceanic climate change and sea level,* in *Climate change 2007: The physical science basis. Contribution of working group I to the fourth assessment report of the Intergovernmental Panel on Climate Change*, pages 385–432. Cambridge University Press.

Boyer, T., Levitus, S., Antonov, J., Locarnini, R., and Garcia, H. (2005). Linear trends in salinity for the World Ocean, 1955–1998. *Geophysical Research Letters*, 32(1).

Boyer, T., Levitus, S., Antonov, J., Locarnini, R., Mishonov, A., Garcia, H., and Josey, S. (2007). Changes in freshwater content in the North Atlantic Ocean 1955-2006. *Geophysical Research Letters*, 34(16).

Bryden, H., Griffiths, M., Lavin, A., Millard, R., Parrilla, G., and Smethie, W. (1996). Decadal changes in water mass characteristics at 24°N in the subtropical North Atlantic Ocean. *Journal of Climate.*, 9(12):3162–3186.

Bryden, H., McDonagh, E., and King, B. (2003). Changes in ocean water mass properties: Oscillations or trends? *Science*, 300(5628):2086–2088.

Cai, W. (2006). Antarctic ozone depletion causes an intensification of the Southern Ocean super-gyre circulation. *Geophysical Research Letters*, 33(3).

Cai, W. and Cowan, T. (2007). Trends in Southern Hemisphere circulation in IPCC AR4 models over 1950–99: Ozone depletion versus greenhouse forcing. *Journal of Climate*, 20(4):681–693.

Carton, J., Chepurin, G., and Cao, X. (2000). A Simple Ocean Data Assimilation Analysis of the Global Upper Ocean 1950–95. Part II: Results. *Journal of Physical Oceanography*, 30(2):311–326.

Cazenave, A. and Nerem, R. (2004). Present-day sea level change: Observations and causes. *Reviews of Geophysics*, 42(3).

Church, J. and White, N. (2006). A 20th century acceleration in global sea-level rise. *Geophysical Research Letters*, 33(1).

Church, J., White, N., and Arblaster, J. (2005). Significant decadal-scale impact of volcanic eruptions on sea level and ocean heat content. *Nature*, 438(7064):74–77.

Curry, R. (2002). HydroBase2: a database and tools for climatological analysis. *http://www.whoi.edu/science/PO/hydrobase*.

Curry, R., Dickson, B., and Yashayaev, L. (2003). A change in the freshwater balance of the Atlantic Ocean over the past four decades. *Nature*, 426:826–829.

Curry, R. and Mauritzen, C. (2005). Dilution of the Northern North Atlantic Ocean in recent decades. *Nature*, 308:1772–1774.

Deser, C., Alexander, M., and Timlin, M. (1996). Upper-ocean thermal variations in the North Pacific during 1970–1991. *Journal of Climate.*, 9(8):1840–1855.

Deutsch, C., Emerson, S., and Thompson, L. (2005). Fingerprints of climate change in North Pacific oxygen. *Geophysical Research Letters*, 32(16).

Downes, S., Bindoff, N., and Rintoul, S. (2008). IN PREPARATION: Impacts of climate change on the subduction of mode and intermediate water masses in the Southern Ocean.

Emerson, S., Watanabe, Y., Ono, T., and Mecking, S. (2004). Temporal trends in apparent oxygen utilization in the upper pycnocline of the North Pacific: 1980–2000. *Journal of Oceanography*, 60(1):139–147.

Fyfe, J. and Saenko, O. (2006). Simulated changes in the extratropical Southern Hemisphere winds and currents. *Geophysical Research Letters*, 33(6).

Garcia, H., Boyer, T., Levitus, S., Locarnini, R., and Antonov, J. (2005a). Climatological annual cycle of upper ocean oxygen content anomaly. *Geophysical Research Letters*, 32(5).

Garcia, H., Boyer, T., Levitus, S., Locarnini, R., and Antonov, J. (2005b). On the variability of dissolved oxygen and apparent oxygen utilization content for the upper world ocean: 1955 to 1998. *Geophysical Research Letters*, 32(9).

Gille, S. (2002). Warming of the Southern Ocean since the 1950s. *Science*, 295(5558):1275–1277.

Gille, S. (2007). In press: Decadal-scale temperature trends in the Southern Hemisphere Ocean.

Godfrey, J., Johnson, G., McPhaden, M., Reverdin, G., and Wijffels, S. (2001). The tropical ocean circulation. *Ocean Circulation and Climate*, pages 215–245.

Gordon, H. et al. (2002). *The CSIRO Mk3 Climate System Model*. CSIRO Atmospheric Research.

Gouretski, V. and Koltermann, K. (2007). How much is the ocean really warming? *Geophysical Research Letters*, 34(1).

Gregg, W., Conkright, M., Ginoux, P., OReilly, J., and Casey, N. (2003). Ocean primary production and climate: Global decadal changes. *Geophysical Research Letters*, 30(15).

Gregory, J., Church, J., Boer, G., Dixon, K., Flato, G., Jackett, D., Lowe, J., O'Farrell, S., Roeckner, E., Russell, G., et al. (2001). Comparison of results from

several AOGCMs for global and regional sea-level change 1900-2100. *Climate Dynamics*, 18(3):225–240.

Hanawa, K. and Talley, L. (2001). *Mode waters,* in *Ocean circulation and climate*, pages 373–386. Academic Press.

Hatun, H., Sando, A., Drange, H., Hansen, B., and Valdimarsson, H. (2005). Influence of the Atlantic subpolar gyre on the thermohaline circulation. *Science*, 309(5742):1841–1844.

Held, I. and Soden, B. (2006). Robust responses of the hydrological cycle to global warming. *Journal of Climate.*, 19(21):5686–5699.

Holbrook, N. and Bindoff, N. (1997). Interannual and decadal temperature variability in the Southwest Pacific Ocean between 1955 and 1988. *Journal of Climate.*, 10(5):1035–1049.

Ishii, M., Kimoto, M., Sakamoto, K., and Iwasaki, S. (2006). Steric sea level changes estimated from historical ocean subsurface temperature and salinity analyses. *Journal of Oceanography*, 62(2):155–170.

Ivchenko, V., Wells, N., and Aleynik, D. (2006). Anomaly of heat content in the northern Atlantic in the last 7 years: Is the ocean warming or cooling? *Geophysical Research Letters*, 33(22).

Jackett, D. and McDougall, T. (1997). A neutral density variable for the Worlds oceans. *Journal of Physical Oceanography*, 27(2):237–263.

Johnson, G. and Gruber, N. (2007). Decadal water mass variations along 20°W in the Northeastern Atlantic Ocean. *Progress in Oceanography*, 73(3-4):277–295.

Johnson, G. and Orsi, A. (1997). Southwest Pacific Ocean water-mass changes between 1968/69 and 1990/91. *Journal of Climate.*, 10(2):306–316.

Joyce, T., Pickart, R., and Millard, R. (1999). Long-term hydrographic changes at 52° and 66° W in the North Atlantic Subtropical Gyre and Caribbean. *Deep-Sea Research, Part II*, 46:245–278.

Kalnay, E., Kanamitsu, M., Kistler, R., Collins, W., Deaven, D., Gandin, L., Iredell, M., Saha, S., White, G., Woollen, J., et al. (1996). The NCEP/NCAR 40-Year Reanalysis Project. *Bulletin of the American Meteorological Society*, 77(3):437–471.

Kara, A., Rochford, P., and Hurlburt, H. (2003). Mixed layer depth variability over the global ocean. *Journal of Geophysical Research*, 108(C3).

Keeling, R. and Garcia, H. (2002). The change in oceanic O_2 inventory associated with recent global warming. *Proceedings of the National Academy of Sciences*, 99(12):7848.

Leadbetter, S., Williams, R., McDonagh, E., and King, B. (2007). A twenty year reversal in water mass trends in the subtropical North Atlantic. *Geophysical Research Letters*, 34(12).

Ledwell, J., Watson, A., and Law, C. (1993). Evidence for slow mixing across the pycnocline from an open-ocean tracer-release experiment. *Nature*, 364(6439):701–703.

Levitus, S. (1999). World Ocean Atlas 1998. *Ocean Climate Laboratory, National Oceanographic Data Center, CD-ROM and Documentation*.

Levitus, S., Antonov, J., and Boyer, T. (2005a). Warming of the world ocean, 1955–2003. *Geophysical Research Letters*, 32(2).

Levitus, S., Antonov, J., Boyer, T., Garcia, H., and Locarnini, R. (2005b). Linear trends of zonally averaged thermosteric, halosteric, and total steric sea level for individual ocean basins and the world ocean,(1955–1959)–(1994–1998). *Geophysical Research Letters*, 32(16).

Lombard, A., Cazenave, A., Le Traon, P., Guinehut, S., and Cabanes, C. (2006). Perspectives on present-day sea level change: a tribute to Christian le Provost. *Ocean Dynamics*, 56(5):445–451.

Lukas, R. (2001). Freshening of the upper thermocline in the North Pacific subtropical gyre associated with decadal changes of rainfall. *Geophysical Research Letters*, 28(18).

Marshall, J., Nurser, A., and Williams, R. (1993). Inferring the subduction rate and period over the North Atlantic. *Journal of Physical Oceanography*, 23(7):1315–1329.

Matear, R. and Hirst, A. (2003). Long-term changes in dissolved oxygen concentrations in the ocean caused by protracted global warming. *Global Biogeochemical Cycles*, 17(4).

Matear, R., Hirst, A., and McNeil, B. (2000). Changes in dissolved oxygen in the Southern Ocean with climate change. *Geochemistry, Geophysics and Geosystems*, 1(11).

McCartney, M. (1977). *Subantarctic Mode Water,* in *A voyage of discovery*, pages 103–119. Pergamon Press.

McDonagh, E., Bryden, H., King, B., Sanders, R., Cunningham, S., and Marsh, R. (2005). Decadal changes in the South Indian Ocean thermocline. *Journal of Climate*, 18(10):1575–1590.

McDougall, T. (1987). Neutral surfaces. *Journal of Physical Oceanography*, 17(11):1950–1964.

Mecking, S., Warner, M., and Bullister, J. (2006). Temporal changes in pCFC-12 ages and AOU along two hydrographic sections in the eastern subtropical North Pacific. *Deep-Sea Research. Part 1. Oceanographic research papers*, 53(1):169–187.

Meehl, G., Stocker, T., Collins, W., Friedlingstein, P., Gaye, A., Gregory, J., Kitoh, A., Knutti, R., Murphy, J., Noda, A., Raper, S., Watterson, I., Weaver, A., and Zhao, Z.-C. (2007). *Global climate projections,* in *Climate change 2007: The physical science basis. Contribution of working group I to the fourth assessment report of the Intergovernmental Panel on Climate Change*, pages 747–846. Cambridge University Press.

Murray, R., Bindoff, N., and Reason, C. (2007). Modeling decadal changes on the Indian Ocean Section I5 at 32°S. *Journal of Climate.*, 20(13):3106–3130.

Nakanowatari, T., Ohshima, K., and Wakatsuchi, M. (2007). Warming and oxygen decrease of intermediate water in the northwestern North Pacific, originating from the Sea of Okhotsk, 1955-2004. *Geophysical Research Letters*, 34(4).

Nurser, A. and Marshall, J. (1991). On the Relationship between subduction rates and diabatic forcing of the mixed layer. *Journal of Physical Oceanography*, 21(12):1793–1802.

O'Dwyer, J. and Williams, R. (1997). The climatological distribution of potential vorticity over the abyssal ocean. *Journal of Physical Oceanography*, 27(11):2488–2506.

Ono, T., Midorikawa, T., Watanabe, Y., Tadokoro, K., and Saino, T. (2001). Temporal increases of phosphate and apparent oxygen utilization in the subsurface waters of western subarctic Pacific from 1968 to 1998. *Geophysical Research Letters*, 28(17).

Randall, D., Woodand, R., Bony, S., Colman, R., Fichefet, T., Fyfe, J., Kattsov, V., Pitman, A., Shukla, J., Srinivasan, J., Stouffer, R., Sumi, A., and Taylor, K. (2007). *Climate models and their evaluation,* in *Climate change 2007: The physical science basis. Contribution of working group I to the fourth assessment report of the Intergovernmental Panel on Climate Change*, pages 589–662. Cambridge University Press.

Rayner, N., Parker, D., Horton, E., Folland, C., Alexander, L., Rowell, D., Kent, E., and Kaplan, A. (2003). Global analyses of sea surface temperature, sea ice, and night marine air temperature since the late nineteenth century. *Journal of Geophysical Research*, 108(D14).

Read, J. and Gould, W. (1992). Cooling and freshening of the subpolar North Atlantic Ocean since the 1960s. *Nature*, 360(6399):55–57.

Rintoul, S. and England, M. (2002). Ekman transport dominates local air–sea fluxes in driving variability of Subantarctic Mode Water. *Journal of Physical Oceanography*, 32(5):1308–1321.

Rintoul, S., Hughes, C., and Olbers, D. (2001). The Antarctic Circumpolar Current system. *Ocean Circulation and Climate*, pages 271–302.

Sabine, C., Feely, R., Gruber, N., Key, R., Lee, K., Bullister, J., Wanninkhof, R., Wong, C., Wallace, D., Tilbrook, B., et al. (2004). The oceanic sink for anthropogenic CO_2. *Science*, 305(5682):367–371.

Sallée, J., Wienders, N., Speer, K., and Morrow, R. (2006). Formation of Subantarctic Mode Water in the southeastern Indian Ocean. *Ocean Dynamics*, 56(5):525–542.

Santoso, A. and England, M. (2004). Antarctic Intermediate Water circulation and variability in a coupled climate model. *Journal of Physical Oceanography*, 34(10):2160–2179.

Sarmiento, J. and Gruber, N. (2006). *Ocean Biogeochemical Dynamics*. Princeton University Press.

Schiermeier, Q. (2007). Artefacts in ocean data hide rising temperatures. *Nature*, 447(7140):8–9.

Schmitz, W. (1996). *On the world ocean circulation. Volume II, the Pacific and Indian Oceans–a global update*. Woods Hole Oceanographic Institution.

Stammer, D., Davis, R., Fu, L., Fukomori, I., Giering, R., Lee, T., Marotzke, J., Marshall, J., Menemnlis, D., Niiler, P., et al. (1999). The consortium for Estimating the Circulation and Climate of the Ocean (ECCO)–Science goals and task plan. *The ECCO Consortium, Report*.

Stark, S., Wood, R., and Banks, H. (2006). Reevaluating the causes of observed changes in Indian Ocean water masses. *Journal of Climate.*, 19(16):4075–4086.

Suga, T., Hanawa, K., and Toba, Y. (1989). Subtropical Mode Water in the 137°E Section. *Journal of Physical Oceanography*, 19(10):1605–1618.

Talley, L. (1993). Distribution and formation of North Pacific Intermediate Water. *Journal of Physical Oceanography*, 23(3):517–537.

Talley, L. (1999). Some aspects of ocean heat transport by the shallow, intermediate and deep overturning circulations. *Mechanisms of Global Climate Change at Millenial Time Scales, Geophysical Monograph*, pages 1–22.

Talley, L. (2007). *Hydrographic Atlas of the World Ocean Circulation Experiment (WOCE). Volume 2: Pacific Ocean.* International WOCE Project Office, Southampton, U.K.

Thompson, D. and Solomon, S. (2002). Interpretation of recent Southern Hemisphere climate change. *Science*, 296(5569):895–899.

Tomczak, M. and Godfrey, J. (1994). *Regional Oceanography: An Introduction.* Pergamon Press, Oxford.

Trenberth, K., Jones, P., Ambenje, P., Bojariu, R., Easterling, D., Tank, A. K., Parker, D., Rahimzadeh, F., Renwick, J., Rusticucci, M., Soden, B., and Zhai, P. (2007). *Observations: Surface and atmospheric climate change,* in *Climate change 2007: The physical science basis. Contribution of working group I to the fourth assessment report of the Intergovernmental Panel on Climate Change*, pages 235–336. Cambridge University Press.

Wadhams, P. and Munk, W. (2004). Ocean freshening, sea level rising, sea ice melting. *Geophysical Research Letters*, 31(11).

Weiss, R. (1970). The Solubility of Nitrogen, Oxygen and Argon in Water and Seawater. *Deep-Sea Research*, 17:721–735.

Wentz, F., Ricciardulli, L., Hilburn, K., and Mears, C. (2007). How much more rain will global warming bring? *Science*, 317(5835).

Wijffels, S., Willis, J., Domingues, C., Barker, P., White, N., Gronell, A., Ridgway, K., and Church, J. (2007). Changing expendable bathythermograph fall-rates and their impact on estimates of thermosteric sea level rise. *Journal of Climate*, IN PRESS.

Willis, J., Lyman, J., Johnson, G., and Gilson, J. (2007). Correction to"Recent cooling of the upper ocean". *Geophysical Research Letters*, 34(16).

Willis, J., Roemmich, D., and Cornuelle, B. (2004). Interannual variability in upper ocean heat content, temperature, and thermosteric expansion on global scales. *Journal of Geophysical Research*, 109(C12).

Wong, A. (1999). *Water mass changes in the North and South Pacific Oceans between the 1960s and 1985-94*. PhD thesis, University of Tasmania, 249pp.

Wong, A., Bindoff, N., and Church, J. (1999). Large-scale freshening of intermediate waters in the Pacific and Indian Oceans. *Nature*, 400(6743):440.

Wong, A., Bindoff, N., and Church, J. (2001). Freshwater and heat changes in the North and South Pacific Oceans between the 1960s and 1985-94. *Journal of Climate.*, 14(7):1613–1633.

Wong, A. P. (2005). Subantarctic Mode Water and Antarctic Intermediate Water in the South Indian Ocean based on profiling float data 2000-2004. *Journal of Marine Research*, 63:789–812.

Zhang, Z., Zwiers, F., Hegerl, G., Lambert, F., Gillett, N., Solomon, S., Stott, P., and Nozawa, T. (2007). Detection of human influence on twentieth-century precipitation trends. *Nature*, 448(7152):461–465.